STATE ESTIMATION IN SYSTEMS MODELLED BY ORDINARY DIFFERENTIAL EQUATIONS AND PARTIAL DIFFERENTIAL EQUATIONS

A Thesis Submitted to

Delhi Technological University

for the Award of Degree of

Doctor of Philosophy

In

Electronics and Communication Engineering

By

Rahul Bansal

(Enrollment No.: 2K14/Ph.D/EC/09)

Under the Supervision of

Dr. Sudipta Majumdar

Assistant Professor

Department of Electronics and Communication Engineering

Delhi Technological University (Formerly DCE)

Bawana Road, Delhi-110042, India.

August, 2019

DECLARATION

I declare that the research work reported in this thesis entitled "**State Estimation in Systems Modelled by Ordinary Differential Equations and Partial Differential Equations**" for the award of the degree of *Doctor of Philosophy in Electronics and Communication Engineering* has been carried out by me under the supervision of *Dr. Sudipta Majumdar*, Department of Electronics and Communication Engineering, Delhi Technological University, Delhi, India.

The research work embodied in this thesis, except where otherwise indicated, is my original research. This thesis has not been submitted by me earlier in part or full to any other University or Institute for the award of any degree or diploma. This thesis does not contain other person's data, graphs or other information, unless specifically acknowledged.

Date :

(Rahul Bansal)
Enrollment no.: 2K14/Ph.D/EC/09
Department of ECE
Delhi Technological University,
Delhi-110042, India

DELHI TECHNOLOGICAL UNIVERSITY

(Formerly Delhi College of Engineering)

Shahbad Daulatpur, Bawana Road, Delhi-110042, India

CERTIFICATE

This is to certify that the research work embodied in the thesis entitled **"State Estimation in Systems Modelled by Ordinary Differential Equations and Partial Differential Equations"** submitted by **Mr. Rahul Bansal** with enrollment number **(2K14/Ph.D/EC/09)** is the result of his original research carried out in the Department of Electronics and Communication Engineering, Delhi Technological University, Delhi, for the award of **Doctor of Philosophy** under the supervision of **Dr. Sudipta Majumdar**.

It is further certified that this work is original and has not been submitted in part or fully to any other University or Institute for the award of any degree or diploma.

This is to certify that the above statement made by the candidate is correct to the best of our knowledge.

(Dr. Sudipta Majumdar)
Supervisor
Department of ECE
Delhi Technological University,
Delhi-110042, India

(Dr. N. S. Raghava)
Professor & Head
Department of ECE
Delhi Technological University,
Delhi-110042, India

ACKNOWLEDGEMENTS

First and foremost I wish to express my sincere gratitude to my supervisor Dr. Sudipta Majumdar, Department of Electronics and Communication Engineering, Delhi Technological University (DTU), Delhi for her inspiring guidance and support during my research work, and for giving me the freedom to explore my own ideas. It is indeed a great pleasure for me to work under her supervision. I appreciate all her contributions of time and ideas to make my Ph.D. experience productive and stimulating. The joy and enthusiasm she has for her research was contagious and motivational for me.

Secondly, I wish to thank Prof. Harish Parthasarthy, Department of Electronics and Communication Engineering, Netaji Subhas University of Technology, Delhi for his everlasting support and guidance in my Ph. D.

I sincerely thank Prof. N. S. Raghava, Professor and Head, Department of ECE, DTU for providing me the necessary facilities and valuable suggestions during the progress of the work. I would like to thank Professor S. Indu for continuous support throughout my Ph.D.

I want to acknowledge Mr. Amit Gautam for continuous support and encouragement during my Ph.D.

I gratefully acknowledge the academic branch and administration of DTU for providing the environment and facilities to carry out my research work. I also express my thanks to office staff of Department of ECE for all kinds of support.

I would like to thank Dr. Sandeep Kumar, Dr. P K Verma, Dr. Ambrish Devanshu for valuable discussions on the subject matter. I want to acknowledge Ashish Kumar, Tej Singh, Akhilesh Verma, Dr. Abhishek Kumar, Ram Pratap, Mr. Manoj Kumar, Rehan, Kartik, Ankit, Dr. N. Jain and Dr. K. Gurumurthy for their constant support and encouragement. I express my thanks to all research scholars of the Department of ECE.

I wish to record my profound gratitude to my parents who have provided me all kinds of support and help for my academic achievements, and for their constant love and care. I would like to express my thanks to my brother, sisters, brothers-in-laws and sister-in-law and other family members for their heartiest cooperation and affection.

I want to express my thanks to all of them who have not been mentioned here but supported, encouraged and inspired me during my Ph.D. work.

I gratefully acknowledge the Council for Scientific and Industrial Research (CSIR), Government of India, for providing fellowship (Junior research fellowship (JRF) and senior research fellowship (SRF)) that made my Ph.D. work possible.

Last but not the least, I thank the almighty God for showing me the right path to complete this Ph.D. thesis.

Date : **(Rahul Bansal)**

Place : Delhi, India.

Dedicated to My Parents

Subhash Bansal

&

Beena Bansal

Contents

Declaration i

Certificate page iii

Acknowledgements v

Abstract xi

List of figures xiii

List of tables xv

1 Introduction 1

1.1 A Brief Contextual Review of State Estimation 3
1.2 Perturbation Method 5
1.3 Wavelet Transform 6
1.4 Recursive Least Squares Algorithm 8
1.5 Kronecker Product 9
1.6 Organization of the Thesis 9
1.7 List of Publications 10

2 Perturbation Based Nonlinear Modelling of Analog Circuits 13

2.1 Cross Coupled Oscillator Circuit Analysis Using Perturbation Method . 15
2.1.1 Nonlinear Modelling of Cross Coupled Oscillator 15
2.1.2 Simulation Results for Cross Coupled Oscillator Circuit 25
2.2 Differential Amplifier Circuit Analysis Using Perturbation Method 27
2.2.1 Nonlinear Modelling of Differential Amplifier Circuit 27
2.2.2 Simulation Results for Differential Amplifier Circuit 31
2.3 Ebers-Moll Modelled Differential Amplifier Circuit Analysis Using Perturbation Method 33
2.3.1 Nonlinear Modelling of Ebers-Moll Modelled Differential Amplifier Circuit 33
2.3.2 Simulation Results for Ebers-Moll Model Based Differential Amplifier Circuit 41

2.4 MOSFET Circuit Analysis Using Perturbation Method 43
2.4.1 Nonlinear Modelling of MOSFET Circuit 43
2.4.2 Simulation Results for MOSFET Circuit 49

3 Extended Kalman Filter Based State Estimation of Analog Circuits 51
3.1 State Estimation of MOSFET Circuit 53
3.1.1 MOSFET Circuit Analysis 54
3.1.2 Applying EKF to MOSFET Circuit 57
3.1.3 Simulation Results for MOSFET Circuit 60
3.2 State Estimation of Differential Amplifier Circuit 65
3.2.1 State Space Model of Differential Amplifier Circuit 65
3.2.2 Applying EKF to Differential Amplifier Circuit 67
3.2.3 Simulation Results for Differential Amplifier Circuit 70

4 Extended Kalman Filter Based Nonlinear System Identification Described in Terms of Kronecker Product 75
4.1 Modelling of MOSFET Circuit Dynamics Using Kronecker Product . . . 78
4.2 System Representation Using Kronecker Product Based Wavelet Transform Method 82
4.3 Applying EKF to MOSFET Circuit 86
4.4 Simulation Results 88

5 Stochastic Filtering in Electromagnetics 97
5.1 Sate Space Representation of Maxwell's Equation 99
5.2 State Space Modelling of Hertzian Dipole Antenna 104
5.3 Applying KF to Hertzian Dipole 106
5.4 Simulation Results 109

6 Conclusions and Future Scope 117
6.1 Conclusions 117
6.2 Scope for Future Work 119

Bibliography 121

Appendix 134

Abstract

This thesis documents our investigation of state estimation in systems modelled by ordinary differential equations (ODE's) and partial differential equations (PDE's). The complete study can be classified as an investigation of two related problems. The first problem is to obtain the precise mathematical model that presents accurately the dynamics of the nonlinear system. Generally, a system is described using a set of differential equations. By solving these equations, we obtain the input-output relation of a system. But, nonlinear system presents difficulties in obtaining the input-output relation. For this nonlinear representation, three different approaches have been used in this thesis. They are :- (i) Approximate input-output relation using perturbation technique. (ii) Implementation of Kronecker product to represent dynamics of a nonlinear system. (iii) Kronecker based wavelet representation of a system. After obtaining the input-output relation of a nonlinear system, we have to implement the estimation algorithm. So, the second problem is to choose the state estimation method that provides real-time estimation, simplicity, less computational complexity and compression. For state estimation, we implemented following two methods:- (i) Kalman filter (KF) and Extended Kalman filter (EKF). (ii) Block processing estimation based on wavelet transform.

At first, we used perturbation theory to derive the closed form nonlinear relation of following circuits:-
(i) Bipolar junction transistor (BJT) based cross coupled oscillator circuit.
(ii) BJT differential amplifier (DA) circuit.
(iii) Metal oxide semiconductor field effect transistor (MOSFET) circuit.
In these, we computed the distortion occurring due to the use of linear part only, which show the importance of nonlinear expression. The second problem deals with the estimation of following two circuits:-
(i) BJT based DA.

(ii) MOSFET circuit.
The EKF method has been used for estimation purpose. The simulation results have been compared with the recursive least squares (RLS) method for different noisy signals. The root mean square error (RMSE) computation presents the superiority of the EKF method as compared to the RLS method.

As a third problem, we estimated the output voltage of MOSFET using EKF by modeling the nonlinear system dynamics using Kronecker product. The proposed method has been compared with Kronecker based wavelet transform (WT) representation of the system and estimation using least mean square (LMS). The proposed method has the following advantages:- (i) It can be used for any mode of transistor operation. (ii) It can also be used for large amplitude input signal. (iii) The method presents the real-time estimation. (iv) Use of Kronecker product presents more accurate representation of the system.

As a fourth problem, we estimated the electric and magnetic fields of Hertzian antenna using KF and compared the results with RLS estimator. The proposed method uses the Kronecker product for compact representation of discretized field in the form of vectors and partial differential operators in the form of matrices. Simulation results show that the KF presents better results than the RLS.

List of Figures

2.1 Cross coupled oscillator circuit. 16
2.2 Cross coupled output voltage. 26
2.3 Differential amplifier circuit. 27
2.4 Differential amplifier output voltage. 32
2.5 Differential amplifier circuit diagram. 34
2.6 Ebers-Moll modelled differential amplifier output at input frequency 1000 Hz and peak to peak input 2 mV. 42
2.7 MOSFET and its EKV equivalent circuit. 43
2.8 MOSFET output voltage for sinusoidal input with peak to peak value 20mV. 50

3.1 MOSFET and its EKV equivalent circuit. 53
3.2 Estimation without noise in conduction mode. 61
3.3 Estimated output voltage for noisy input in conduction mode. White Gaussian noise of zero mean and 0.25 variance is used. 62
3.4 Estimation without noise in saturation mode. 62
3.5 Estimated output voltage for noisy input in saturation mode. White Gaussian noise of zero mean and 0.25 variance is used. 62
3.6 RMSE of estimated voltage in using (i) RLS, (ii) EKF. 63
3.7 Residual of estimated voltage in using (i) RLS, (ii) EKF. 63
3.8 Differential amplifier circuit. 65
3.9 Differential amplifier output for sinusoidal input. (a). Noiseless DA input voltage. (b). Estimated DA output voltage for noiseless input. 71
3.10 DA output for noisy input. White Gaussian noise of zero mean and 0.01 variance is used. Peak to peak differential input voltage is 2mV. (a): Noisy DA input voltage. (b). Estimated DA output voltage for noisy input. 72
3.11 : DA output for noisy input. White Gaussian noise of zero mean and 0.1 variance is used. Peak to peak differential input voltage is 2mV. (a): Noisy DA input voltage. (b). Estimated DA output voltage for noisy input. 72

4.1 MOSFET and its EKV equivalent circuit. 78
4.2 Darlington pair circuit using MOSFET. 82

4.3 Output voltage estimation for noisy input (white Gaussian noise of zero mean and 0.001 variance) using (i) EKF on Kronecker based system representation (ii) LMS on WT based system representation. Input frequency is 1000 Hz. 89
4.4 Output voltage estimation for noisy input (white Gaussian noise of zero mean and 0.001 variance) using (i) EKF on Kronecker based system representation (ii) LMS on WT based system representation. Input frequency is 1000 Hz. W=2μm, L=2μm. 90
4.5 Output voltage estimation for noisy input (white Gaussian noise of zero mean and 0.001 variance) using (i) EKF on Kronecker based system representation (ii) LMS on WT based system representation. Input frequency is 1000 Hz. W=20μm, L=20μm. 90
4.6 Output voltage estimation for noisy input (white Gaussian noise of zero mean and 0.001 variance) using (i) EKF on Kronecker based system representation (ii) LMS on WT based system representation. Input frequency is 1000 Hz. W=10μm, L=20μm. 91
4.7 Output voltage estimation for noisy input (white Gaussian noise of zero mean and 0.001 variance) using (i) EKF on Kronecker based system representation (ii) LMS on WT based system representation. Input frequency is 1000 Hz. W=10μm, L=2μm. 91

5.1 Hertzian dipole antenna. 105
5.2 Electric field intensity (E_r) for noisy driving source (white Gaussian noise of zero mean and 0.00025 variance) for near-field. 110
5.3 Electric field intensity (E_θ) for noisy driving source (white Gaussian noise of zero mean and 0.00025 variance) for near-field. 110
5.4 Magnetic field intensity (H_ϕ) for noisy driving source (white Gaussian noise of zero mean and 0.00025 variance) for near-field. 110
5.5 Electric field intensity (E_r) for noisy driving source (white Gaussian noise of zero mean and 0.00025 variance) for far-field. 111
5.6 Electric field intensity (E_θ) for noisy driving source (white Gaussian noise of zero mean and 0.00025 variance)for far-field. 111
5.7 Magnetic field intensity (H_ϕ) for noisy driving source (white Gaussian noise of zero mean and 0.00025 variance) for far-field. 111
5.8 (a): Estimated E-field using KF for near field. (b): Estimated E-field using RLS for near field. 112
5.9 (a): Estimated H-field using KF for near field. (b): Estimated H-field using RLS for near field. 112
5.10 (a): Estimated E-field using KF for far field. (b): Estimated E-field using RLS for far field. 112
5.11 (a): Estimated H-field using KF for far field. (b): Estimated H-field using RLS for far field. 113

List of Tables

2.1 Distortion error for different capacitors and inductors in BJT cross coupled oscillator. . . . 25
2.2 Differential Gain and Percentage Distortion . . . 33
2.3 Distortion error percentage for Ebers-Moll modelled differential amplifier. 41
2.4 Percentage distortion when different voltage amplitude and frequency is given at input of MOSFET circuit. . . . 49

3.1 RMSE of Output voltage estimation in conduction mode using EKF and RLS. . . . 61
3.2 RMSE of output voltage estimation in saturation mode using EKF and RLS. . . . 63
3.3 Residual mean and variance of output estimation in conduction mode using EKF and RLS. . . . 64
3.4 Residual mean and variance of output estimation in saturation mode using EKF and RLS. . . . 64
3.5 RMSE of output estimation using EKF and RLS for peak to peak differential input of 2mV. . . . 71

4.1 RMSE of output voltage estimation using EKF and wavelet transform method when peak to peak MOSFET input is 20mV for practical data. . 92
4.2 RMSE of output voltage estimation using EKF and wavelet transform method when peak to peak MOSFET input is 20mV. . . . 92
4.3 Computational burden for EKF algorithm. . . . 95
4.4 Computational burden for WT method. . . . 95

5.1 RMSE of electric field (E_r) estimation using KF for near-field. . . . 113
5.2 RMSE of electric field (E_θ) estimation using KF for near-field. . . . 113
5.3 RMSE of magnetic field (H_ϕ) estimation using KF for near-field. . . . 113
5.4 RMSE of electric field (E_r) estimation using RLS for near-field. . . . 114
5.5 RMSE of electric field (E_θ) estimation using RLS for near-field. . . . 114
5.6 RMSE of magnetic field (H_ϕ) estimation using RLS for near-field. . . . 114
5.7 RMSE of electric field (E_r) estimation using KF for far-field. . . . 114
5.8 RMSE of electric field (E_θ) estimation using KF for far-field. . . . 114
5.9 RMSE of magnetic field (H_ϕ) estimation using KF for far-field. . . . 115
5.10 RMSE of electric field (E_r) estimation using RLS for far-field. . . . 115

5.11 RMSE of electric field (E_θ) estimation using RLS for far-field. 115
5.12 RMSE of magnetic field (H_ϕ) estimation using RLS for far-field. 115

Chapter 1

Introduction

This thesis documents our investigation of state estimation in systems modelled by ordinary differential equations (ODE's) and partial differential equations (PDE's). The complete study can be classified as an investigation of two related problems. The first problem is to obtain the precise mathematical model that presents the dynamics of the nonlinear system accurately. Generally, a system is described using a set of differential equations. By solving these equations, we obtain the input-output relation of a system. But, nonlinear system presents difficulties in obtaining the input-output relation. For this nonlinear representation, three different approaches have been used in this thesis. They are :-

(i) Approximate input-output relation using perturbation technique.

(ii) Implementation of Kronecker product to represent dynamics of a nonlinear system.

(iii) Kronecker based wavelet representation of a system.

After obtaining the input-output relation of a nonlinear system, we have to implement the estimation algorithm. So, the second problem is to choose the state estimation method that provides real-time estimation, simplicity, less computational complexity and compression. For state estimation, we implemented following two methods:-

(i) Kalman filter (KF) and Extended Kalman filter (EKF).

(ii) Block processing estimation based on wavelet transform (WT).

We modelled the input as an Ornstein - Uhlenbeck (O.U.) process to account the both, white noise and Brownian process. The formal derivation of Brownian motion is

white noise. But, to deal with the white noise in dynamical system, perturbed by noise, we used Îto calculus rather than white noise calculus. The Kushner Kollainpur nonlinear filter is a real-time filter but, of infinite dimensional. So, impossible to implement in a computer. It is derived by Îto calculus combined with Bayes' rule, recombined with conditional density. To get over infinite dimensionality, we expand the Kushner Kollainpur equation around the conditional mean, retained up to quadratic order in states estimation errors. In this way, we get finite dimensional filter EKF, which gives the joint evaluation of conditional mean and conditional error covariance. We compared EKF with block processing estimates based on WT. Here, we take an advantage of the fact that over different time slots, minimum and maximum frequencies are different. So, we adjust the resolution in each block in such a way, so that we do not have to use all the wavelet coefficients to get reasonable estimates. The minimum and maximum indices are different by minimum and maximum frequencies within each time slot. The final outcome of the wavelet based estimate is that although it is block processing and not the real-time processing based estimation, but we are able to estimate using lesser data storage i.e. having compression. EKF is a real-time estimation and has been compared with WT based block processing as regards, complexity, real-time estimation and compression as all the samples are not used for estimation.

Above discussed methods have been implemented for state estimation of linear and nonlinear systems. We implemented the perturbation theory on the following nonliear circuits described by ODE's:-

(i) Bipolar junction transistor (BJT) based cross coupled oscillator (CCO) circuit,

(ii) BJT based differential amplifier (DA) circuit,

(iii) Metal oxide semiconductor field effect transistor (MOSFET) circuit.

and Kronecker based nonlinear representation on the circuit.

Further we implemented the EKF estimation of the following two representations of the circuit:-

(i) MOSFET using Enz-Krummenacher-Vittoz (EKV) model.

(ii) Kronecker based representation of MOSFET.

We also used KF for estimation purpose in Hertzian antenna electric and magnetic field. For this, system is described by PDE's.

1.1 A Brief Contextual Review of State Estimation

State estimation is important for various control applications [1] [2], robotics [3] [4] etc. The purpose of state estimation is to adjust the model parameters in such a way so that they are closer to observed values by minimizing the errors that affect the model parameters. The measured data usually contain noise due to device inaccuracy, electrical and environmental disturbances. Also, the device parameter values given in the manufacturer data sheet may introduce errors as they are measured under standard conditions. Thus, the data sheet values are not the same as those measured under real environmental conditions. Since, the device states changes with the environmental conditions, it requires online estimation of device states.

The batch, discrete time estimation problem formulation is as follows:-

$$\text{Motion model:} \quad \mathbf{x}_k = \mathbf{A}_{k-1}\mathbf{x}_{k-1} + \mathbf{v}_k + \mathbf{w}_k, \qquad k = 1, ..., K \tag{1.1}$$

$$\text{Observation model:} \quad \mathbf{y}_k = \mathbf{C}_k\mathbf{x}_k + \mathbf{n}_k, \qquad k = 0, ..., K \tag{1.2}$$

where k represents discrete time index.

$$\begin{aligned}
\text{System state:} \quad & \mathbf{x}_k \in \mathbb{R}^N \\
\text{Initial state:} \quad & \mathbf{x}_0 \in \mathbb{R}^N \sim \mathcal{N}(\check{\mathbf{x}}_0, \check{\mathbf{P}}_0) \\
\text{Input:} \quad & \mathbf{v}_k \in \mathbb{R}^N \\
\text{Process noise:} \quad & \mathbf{w}_k \in \mathbb{R}^N \sim \mathcal{N}(0, \mathbf{Q}_k) \\
\text{Measurement:} \quad & \mathbf{y}_k \in \mathbb{R}^N \\
\text{Measurement noise:} \quad & \mathbf{n}_k \in \mathbb{R}^N \sim \mathcal{N}(0, \mathbf{R}_k)
\end{aligned}$$

All the above variables are random excluding $\mathbf{v}_k$, which is deterministic. Here, it is assumed that the noise variables and initial state information are uncorrelated with one another. $\mathbf{A}_k \in \mathbb{R}^{N\times N}$ is known as the transition matrix and $\mathbf{C}_k \in \mathbb{R}^{M\times N}$ is known as the observation matrix.

Using the above defined models, the state estimation is defined as:-

The problem of state estimation is to provide an estimate $\hat{\boldsymbol{x}}_k$ of the true state of a system, at one or more time step k, given the knowledge of initial state $\check{\boldsymbol{x}}_0$, a sequence of measurements $\boldsymbol{y}_{0:k,meas}$, a sequence of inputs, $\boldsymbol{v}_{1:k}$, as well as knowledge of the system's dynamics and observation models.

The batch linear Gaussian estimation problem is important as the batch solution for computing state estimates uses all the measurements in the estimation of all the states at once, hence the term 'batch' [5]. But, the disadvantage of the batch method is that it can not be used in real time, as one can not use future measurements to estimate past states. It uses all the data in the estimate of every state. This requires recursive state estimation and the Kalman filter (KF) is the classical solution to this.

The general state estimation problem can be formulated as follows:-

Suppose $\mathbf{x}(t)$ represents a "state", a vector-valued function of a parameter t, $\mathbf{z}(t)$ represents the observational data. It is also vector function of t. $\theta(t)$ represents additive observation errors. $\mathbf{f}[\mathbf{x}(t), t]$ representing a function describing the dependence of observations on the state, when there were no observation errors. Representing $\mathbf{z}(t)$ as

$$\mathbf{z}(t) = \mathbf{f}[\mathbf{x}(t), t] + \theta(t) \tag{1.3}$$

In general state formulation, **z**, **f**, θ are vector-valued as it may contain various observational data. The parameter $'t'$ is time. In general, $'t'$ may represent some other parameter also and can be represented by a vector t.

In linear case, **f** depends linearly on the **x**. The problem is to work on the observational data $\mathbf{z}(t)$ to estimate the state or functionals of the state. There are two different cases:-

(i) x may be viewed as a deterministic function of t and presents a set of unknown initial parameters. Then, state estimation problem becomes a parameter estimation problem of these parameters. In the "state equation" terms, the deterministic function is the solution of the state equation and unknown initial parameters represent the initial condition. This corresponds to "no system noise" in state equation.

(ii) x may be viewed as a stochastic process, then it will have a covariance function $\mathbf{X}(t, t')$. This case corresponds to the presence of "system noise".

State estimation is also important for monitoring applications, industrial processes as there are many disturbing components that affects the process control. In the power systems context, state estimation has been classified as static state estimation (SSE) and dynamic state estimation (DSE). Weighted least square (WLS) method is an example of SSE method [6] - [8]. KF method [9] [10], H_∞ filter [11] [12], particle filter (PF) [13] - [16], adaptive filter [17], maximum-likelihood method [18] - [20],

Ensemble-Kalman filter [21] - [23], EKF [24] - [28] are various DSE methods. Wu [7] presented a review of decoupled, stable and robust estimators used for power system state estimation. Different methods have been proposed in literature for systems described by differential equation. In [29], Raissi *et al.* proposed the prediction correction approach based method for state estimation of systems described by nonlinear differential equations, where the prediction step is improved by using a more accurate interval computation of the solution of the ordinary differential equation. In [30], Zhang *et al.* presented the state estimation for systems described by the continuous, linear n-dimensional ordinary differential equation. The solution proposed is based on optimal filtering theory for Îto-Volterra systems. In [31], Mandela *et al.* proposed a modified EKF method for state estimation of constrained nonlinear differential algebraic equation. This method has the advantage of using measurement of both algebraic and differential states. It is a recursive approach that includes constraints also. In [32], Mobed *et al.* proposed a modified EKF that handles the uncertainties in both differential and algebraic equations and equality constraints.

1.2 Perturbation Method

Perturbation theory is used to model as a small deformation of a system that is exactly solvable. It is implemented on a system that can not be solved exactly. It uses the mathematical method of approximation to obtain the solution of a deformed system. It is the method that continuously improves the previously obtained approximate solution to a problem. In this way, the method allows to implement the computational efficiency of idealized systems to more realistic problems. Also, it presents the analytic insight into complex problems. The method is implemented by adding a small term 'ε' to exactly solvable problem as

$$A = A_0 + \varepsilon A_1 + \varepsilon^2 A_2 + ... \tag{1.4}$$

where A_0 is the known solution to the exactly solvable problem and A_1, A_2,... are nonlinear terms. Use of only linear model for nonlinear system presents error between the actual response and linear approximation, so nonlinear model is important. Nonlinear closed form input output relation is also important for design and simulation of complex circuits as transfer of physical description into mathematical form is required for simulation.

Perturbation theory is widely used for different applications. Buonomo and Schiavo [33] used perturbation method for periodic response of forced nonlinear circuit and also considered the harmonic distortion. Majumdar and Parthasarathy [34] implemented perturbation technique to Ebers-Moll modelled transistor amplifier circuit. This method has been used to derive the closed form Volterra series. Rathee and Parthasarathy [35] proposed perturbation-based Fourier series model for representation of nonlinear distortion in circuits. This method has the advantage of simple implementation. Rathee and Parthasarathy [36] used perturbation method to decompose the driving force and circuit state into linear and nonlinear components. Further, the nonlinear circuit is represented by a nonlinear differential equation, in which the fluctuations are modelled using Îto stochastic differential equations. The results obtained in this way are compared with perturbation based deterministic differential equations. This comparison presents the noise component. Dang *et al.* [37] used perturbation method for space variance of range envelope in synthetic aperture radar. In [38], perturbation method is implemented on 64-PSK.

1.3 Wavelet Transform

WT is used in various applications [39] - [41] due to its time frequency localization characteristics. Compact support, vanishing moments of higher order, dilation relation, smoothness, generator of an orthonormal basis of function spaces $L^2(R)$ are some of the characteristics of WT. Time frequency localization characteristics of the WT makes it important tool for signal analysis.

The main characteristic of the mother wavelet is given by

$$\int_{-\infty}^{\infty} \psi(t)dt = 0. \tag{1.5}$$

This implies that it is oscillatory and has zero mean value. Also, this function needs to satisfy the admissibility condition

$$\int_{-\infty}^{\infty} \frac{|\hat{\psi}(\omega)|^2}{|\omega|} d\omega = 0. \tag{1.6}$$

The admissibility condition allows the reconstruction of the original signal using inverse WT.

There are two different types of wavelets:- (i) Continuous wavelet transform (CWT),

(ii) Discrete wavelet transform (DWT).

The CWT maps a function $f(t)$ onto time scale space by

$$W_f < a, b > = \int_{-\infty}^{\infty} \psi_{a,b}(t)\, f(t) dt \tag{1.7}$$

$$= < \psi_{a,b}(t), f(t) > \tag{1.8}$$

The CWT uses the translations and dilations of a prototype or mother function $\psi(t)$. CWT is described by the following equation

$$X(a, b) = \frac{1}{|a|^{\frac{1}{2}}} \int_{-\infty}^{\infty} x(t) \psi^* \left(\frac{t-b}{a} \right) dt, \qquad a > 0,\ b \in \mathbb{R} \tag{1.9}$$

where $\psi(t)$ is the mother wavelet. a is the scaling parameter. b is the translation parameter. $*$ denotes the complex conjugate. $a > 1$ gives dilated wavelet. $a < 1$ gives contracted wavelet. $\frac{1}{|a|^{\frac{1}{2}}}$ is the energy normalization factor. Wavelets are mathematical functions that decompose the data into different frequency components and then analyze each component with a resolution matched to its scale.

In DWT, scaling and translation parameters are discretized, $a = 2^j$, $b = 2^j\, k$. So the DWT is

$$\psi_{j,k}(t) = 2^{\frac{-j}{2}} \psi(2^{-j} t - k), \qquad j, k \in \mathbb{Z} \tag{1.10}$$

The orthonormal wavelets satisfy the condition:-

$$\int_{-\infty}^{\infty} \psi_{j,\,k}(t) \psi_{j',\,k'}(t) dt = \begin{cases} 1, & \text{if } j = j' \text{ and } k = k'; \\ 0, & \text{Otherwise.} \end{cases} \tag{1.11}$$

There are very effective techniques of construction of the mother wavelet function ψ from the "scaling sequence". Depending on the choice of the scaling sequence, we have Daubechies wavelet, Haar wavelet, Shannon wavelet etc. having specific properties required for specific kinds of applications. Daubechies wavelets are example of orthogonal wavelets. These are DWT. In this way, time series data analysis using WT presents scale and position information. The scaling and wavelet functions of Daubechies wavelets have longer supports, which offers improved capability of these transformations. These transformations offer powerful tool for various signal processing such as compression, noise removal, image enhancement etc.

1.4 Recursive Least Squares Algorithm

The recursive least square (RLS) is an adaptive filtering. It obtains the filter coefficients in recursive manner. It uses the minimization of weighted least square cost function criteria to obtain the filter weights by considering the input signal as the deterministic signal. It has wide spread application in engineering including signal processing and communication. Various form of this algorithm also used in literature for parameter estimation and system identification purpose. The two classes of least square methods are:-

(i) Iterative method for offline identification.

(ii) Recursive methods for online identification.

The least squares have applications in control and function fitting, estimation and system identification. The RLS filter is used in different applications [42] - [45].

RLS computes the state recursively and gives the optimal solution in the mean squared sense [46]. In the RLS algorithm, the past errors are rounded-off and present state computations are propagated to the future instant which results in error accumulation. Consider the desired signal $\mathbf{d}_k$ and optimum solution $\mathbf{W}_k = [W_1 \ W_2 ... W_{M-1}]^T$. The desired signal is given by

$$\mathbf{d}_k = \mathbf{y}_k^T \mathbf{W}_k + \mathbf{w}_k^{(R)} \tag{1.12}$$

where $\mathbf{y}_k = [y_k ... y_{k-M+1}]^T$ is the observation vector, $\mathbf{w}_k^{(R)}$ is the zero mean white Gaussian noise. The aim of the RLS algorithm is to estimate $\mathbf{W}_k$ such that sum of weighted mean square error $\sum_{j=1}^{k} \lambda^{k-j} [\mathbf{d}_j - \mathbf{W}_k \mathbf{y}_j^T]^2$ is minimized. Here λ is forgetting factor. Consider the correlation matrix $\mathbf{C}_k = \sum_{i=1}^{k} \lambda^{k-i} \mathbf{y}(i)\mathbf{y}^T(i) = \lambda \mathbf{C}_{k-1} + \mathbf{y}(i)\mathbf{y}^T(i)$. $\mathbf{P}_k^{(R)}$ is the inverse correlation matrix given by $\mathbf{P}_k^{(R)} = \mathbf{C}_k^{-1}$. The steps involved in RLS algorithm are

$$\zeta_k = \mathbf{d}_k - \mathbf{y}_k^T \mathbf{W}_k \tag{1.13}$$

$$\mathbf{K}_k^{(R)} = \frac{\mathbf{P}_{k-1}^{(R)} \mathbf{y}_k}{1 + \mathbf{y}_k^T \mathbf{P}_{k-1}^{(R)} \mathbf{y}_k} \tag{1.14}$$

$$\mathbf{W}_k = \mathbf{W}_{k-1} + \mathbf{K}_k^{(R)} \zeta_k. \tag{1.15}$$

$$\lambda_k = 1 - \frac{\left(1 - \mathbf{y}_k^T \mathbf{K}_k^{(R)}\right) \zeta_k^2}{\chi} \tag{1.16}$$

$$\mathbf{P}_k^{(R)} = \lambda_k^{-1}\mathbf{P}_{k-1}^{(R)} - \lambda_k^{-1}\mathbf{K}_k^{(R)}\mathbf{y}_k^T\mathbf{P}_{k-1}^{(R)} \tag{1.17}$$

where ζ is the estimation error, $\mathbf{K}_k^{(R)}$ is the RLS gain. χ is constant value. The variable forgetting factor is used to stabilize $\mathbf{P}_k^{(R)}$ as it is sensitive to any disturbance that causes the increase in estimation error. This algorithm can be easily derived using the so called matrix inversion lemma.

1.5 Kronecker Product

The Kronecker product of two matrices $A\,(p \times q)$ and $B\,(m \times n)$ is denoted by $A \otimes B$ [47] [48] and is a $pm \times qn$ matrix is given by

$$A \otimes B = \begin{bmatrix} a_{11}B & a_{12}B & \dots & a_{1q}B \\ a_{21}B & a_{22}B & \dots & a_{2q}B \\ \vdots & \vdots & \ddots & \vdots \\ a_{p1}B & a_{p2}B & \dots & a_{pq}B \end{bmatrix}. \tag{1.18}$$

Let I_n be the identity matrix of size $n \times n$, the Kronecker product satisfies following properties

(i) $I_n \otimes A = diag[A, A, \dots A]$.

(ii) $(k\,A) \otimes B = A \otimes (k\,B) = k\,(A \otimes B)$, where k is the constant value.

(iii) $(A \otimes B)^T = A^T \otimes B^T$, where T denotes the transpose of matrix.

(iv) $(A \otimes B)(C \otimes D) = AC \otimes BD$.

(v) If X is a matrix and $Vec\,(X)$ denotes the column vector obtained by arranging all the columns of X serially one below the other, then $Vec(AXB) = (B^T \otimes A)Vec(X)$. This identity is useful in manipulating parameters/data which are in matrix rather than in vector form.

1.6 Organization of the Thesis

The organization of the problems investigated in the thesis is as follows:-

Chapter 2 deals with the implementation of perturbation theory to derive the linear and nonlinear closed form expressions of the following three circuits:-

(i) BJT based CCO circuit.
(ii) BJT based DA circuit.
(iii) MOSFET circuit.

It also presents the computation of the distortion occurring due to linear part only.

Chapter 3 presents the state estimation of the following nonlinear circuits using EKF:-
(i) BJT based DA circuit.
(ii) MOSFET circuit.
We present the brief description of few recent methods of state estimation and compare estimation using EKF with that using RLS method.

In **Chapter 4**, we present the formulation of nonlinear circuit dynamics modelling using Kronecker product and the estimation using EKF. Also, we compared the state estimation with WT based representation of the nonlinear circuit using Kronecker product and estimation using least mean square (LMS). The advantages of both the methods are presented. We present the numerical computation of both the methods. This chapter also discusses few recent methods used for state estimation and their disadvantages.

Chapter 5 presents the stochastic filtering in electromagnetics. This chapter deals with the formulation of electric and magnetic field estimation using KF and discrete set of measurements. The formulation uses the Kronecker product for compact representation of discretized field in the form of vectors and partial differential operators in the form of matrices. It compares the KF based field estimation with the RLS based field estimation.

Finally, some concluding remarks are presented in **Chapter 6** and some future work direction is also presented.

1.7 List of Publications

1. **Bansal R**, Majumdar S, Parthasarthy H. Extended Kalman filter based nonlinear system identification described in terms of Kronecker product. International Journal of Electronics and Communications (AEU), vol. 108, pp. 107-117, 2019.

2. **Bansal R**, Majumdar S, Extended Kalman filter based state estimation of MOSFET circuit, COMPEL - The International Journal For Computation And Mathe-

matics In Electrical And Electronic Engineering, https://doi.org/10.1108/COMPEL-09-2018-0367, 2019.

3. **Bansal R**, Majumdar S. Nonlinear modelling and simulation of cross coupled oscillator, Journal of Advanced Research in Dynamical and Control Systems, vol. 9, issue 11, pp. 35-45, 2017.

4. **Bansal R**, Majumdar S, Perturbation based modelling of differential amplifier circuit. International Journal of Electronics and Communication Engineering. 12(4), 331-336, 2018.

5. **Bansal R**, Majumdar S, Nonlinear analysis differential amplifier circuit, IEEE WiSPNET-2017, pp. 770-776, 2017.

6. **Bansal R**, Majumdar S, Perturbation based nonlinear analysis of MOSFET circuit. IEEE ICPEICES-2018). 2018

Papers communicated to international journals are:-

1. **Bansal R**, Majumdar S, State estimation of differential amplifier circuit using extended Kalman filter.

2. **Bansal R**, Majumdar S, Parthasarthy H, Stochastic filtering in electromagnetics.

Chapter 2

Perturbation Based Nonlinear Modelling of Analog Circuits

This chapter[1] presents the modelling of following circuits using perturbation theory:-

(i) Cross coupled oscillator (CCO) circuit.

(ii) Bipolar junction transistor (BJT) differential amplifier (DA) circuit.

(iii) MOSFET circuit.

Generally, nonlinear circuit components are approximated by linear model for different applications. But, use of linear model causes signal distortion, which affect the performance of the nonlinear circuit component. This requires nonlinear closed form expression of circuit components. The nonlinearity of amplifier can not be neglected as little change in input may affect output significantly. Differential circuits and device topologies are also useful in wireless system applications as compared to single ended architectures, as they are immune to electromagnetic coupling and have improved even order linearity. Also, inherently available voltage swing in amplifier is useful for integrated circuits that has to cope up with very low supply voltages. One of

[1]The result of this chapter is based on the following research papers (i) Bansal R, Majumdar S. Nonlinear modelling and simulation of cross coupled oscillator, J Adv Research Dynamical Control Syst, vol. 9, issue 11, pp. 35-45, 2017, (ii) Bansal R, Majumdar S, Perturbation based modelling of differential amplifier circuit. Int J Electron Commun Eng. 2018;12(4), 331-336, (iii) Bansal R, Majumdar S, Nonlinear analysis differential amplifier circuit, IEEE WiSPNET-2017, pp. 770-776, 2017, (iv) Bansal R, Majumdar S, Perturbation based nonlinear analysis of MOSFET circuit. IEEE (ICPEICES-2018). 2018.

the most important consideration in the design of amplifier is the harmonic distortion resulting from the nonlinear components of the circuits. Amplifier circuits are usually analyzed using the approximate linear model of nonlinear components, which leads to small discrepancies between the actual response and the approximated linear one. Also, many applications of amplifier require linear response. As two signals are input to amplifier containing BJT (nonlinear device), it may create intermodulation power. These intermodulation effects may cause interference to the desired signal. In practice, the degree of balance of a differential circuit depends on matching of circuit components. High degree balance of a differential amplifier requires the identical performance and electrical properties of two transistors comprising the amplifier circuit. But, due to semiconductor fabrication limitations, this matching is difficult, which causes even order nonlinearity. This nonlinearity degrades the system performance that uses differential amplifier. This requires the mathematical expressions of nonlinearity of differential amplifier. Nonlinear circuit analysis can be done using different methods [49] - [58].

Kuntman [49] used the Ebers-Moll model of the transistor to obtain the optimum source resistance of the amplifier circuit. To obtain the nonlinear nodal solution, Newton Raphson method has been used. Fong and Meyer [50] presented the Volterra model of common emitter amplifier and differential pair transconductance using large signal model. Song *et al.* [51] used Volterra model together with memory polynomial model for compensation of nonlinear distortion of a power amplifier.

Though Volterra series is the extension of linear system theory, but large number of parameters related with the Volterra series limits the practical application of this model having modest memory. Also, Volterra series has the disadvantage that modelling using this requires immoderate computations as the determination of unknown coefficients increases exponentially with degree of nonlinearity and the Volterra filter length. The perturbation theory has the advantage of simple implementation as the method is applied by continuously improving the previously obtained approximate solution of a problem. It is implemented by a small deformation of a system that is exactly solvable. Wu *et al.* [52] used the perturbation technique to get the amount of asymmetry and nonuniformity during the transfer from differential to common mode in a differential circuit. Afifi and Dusseaux [53] implemented perturbation method on scattering of electromagnetic wave to obtain the coherent and incoherent intensities. Mishra and Yadava [54] studied the effect of internal and external noise perturbations

in chaotic Colpitts oscillator. Liu *et al.* [55] presented a robust Kalman filter in which a random perturbation is taken into account. These random perturbations of parameters have been considered in state and measurement matrices, which are known as state dependent multiplicative noises. Thuan and Huong [56] studied the effect of nonlinear perturbations on stability and passivity of delayed switched systems, as the instability of system leads in poor performance of the dynamic system. Buonomo and Schiavo [57] derived the nonlinear distortion in analog circuits using perturbation theory that use single and two tone input signal. Wang *et al.* [58] presented perturbation projection vector modelling of an oscillator which is based on memristor and used it for pattern recognition. Wang *et al.* [61] studied the effect of nonlinear perturbation. Lakshmanan *et al.* [62] presented the effect of nonlinear perturbation on uncertain systems.

Nonlinear modelling of CCO using Ebers-Moll model of the BJT together with perturbation method has been presented in Section 2.1.1. To observe the effect of nonlinear expression, simulation results have been presented in Section 2.1.2. Section 2.2.1 presents the mathematical derivation of linear and nonlinear expressions of DA circuit by retaining the quadratic terms of BJT Ebers-Moll model and perturbation method. The derived expressions have been plotted in MATLAB software and shown in Section 2.2.2. Mathematical derivation closed form linear and nonlinear expression of MOSFET using EKV model of MOSFET and perturbation has been presented in Section 2.4.1. These also make use of Kirchhoff's laws. MATLAB simulations of these derived expressions have been shown in Section 2.4.2. Also the distortion calculation due to consideration of linear term only is shown is Table 2.4.

2.1 Cross Coupled Oscillator Circuit Analysis Using Perturbation Method

2.1.1 Nonlinear Modelling of Cross Coupled Oscillator

Figure 2.1 shows BJT CCO with common emitter (CE) configuration in which collector of first transistor Q_1 is coupled with the base of other transistor Q_2. Applying Kirchhoff laws to the circuit as shown in Figure 2.1, we have

$$v_{C_1} + Z_1 I_{C_1} = V_{CC} \tag{2.1}$$

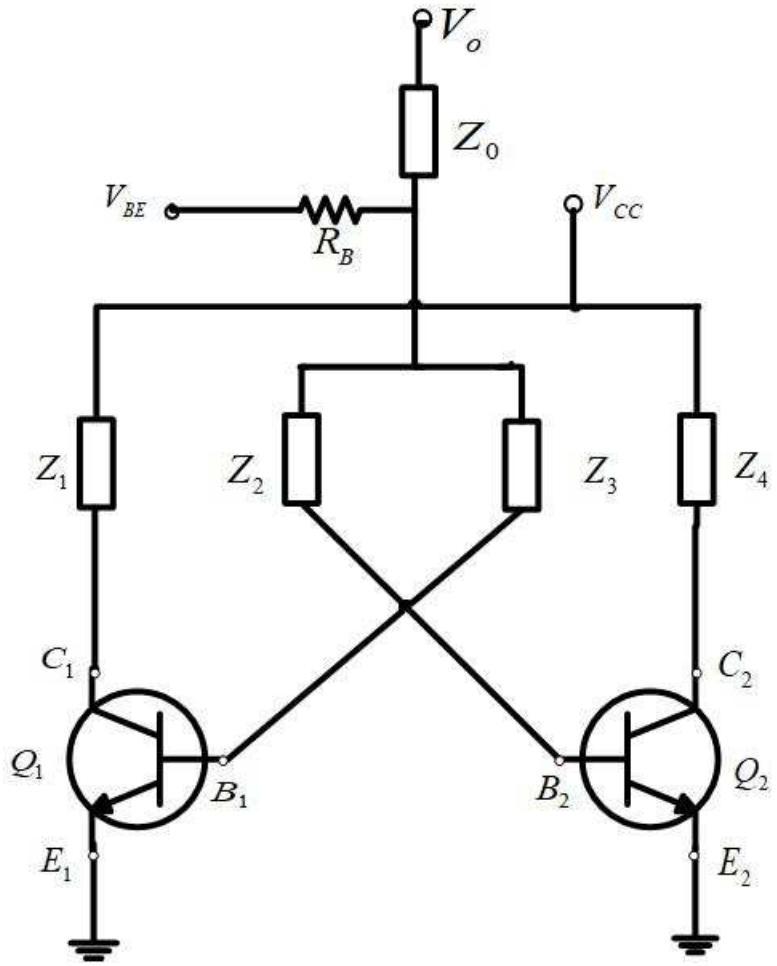

Figure 2.1: Cross coupled oscillator circuit.

$$v_{C_2} + Z_2 I_{C_2} = V_{CC} \tag{2.2}$$

$$-v_o + Z_O(I_{B_1} + I_{B_2}) + I_{B_2} Z_2 + v_{B_2} = 0 \tag{2.3}$$

$$-v_o + Z_O(I_{B_1} + I_{B_2}) + I_{B_2} Z_3 + v_{B_1} = 0 \tag{2.4}$$

$$I_{C_1}\left(1 + \frac{1}{\beta_1}\right) - I_{E_1} = 0 \tag{2.5}$$

where v_{B_1}, v_{C_1}, v_{E_1}, v_{B_2} and v_{C_2} are state variables. Equations (2.1)-(2.5) are obtained by Kirchhoff's voltage law and Kirchhoff's current law. Replacing the transistor circuit by Ebers-Moll model [34] [59] [60], the collector current I_C and the emitter current I_E can be written as

$$I_C = \alpha_F I_{ES}\left[exp\frac{v_{BE}}{V_T} - 1\right] - I_{CS}\left[exp\frac{v_{BC}}{V_T} - 1\right] \tag{2.6}$$

$$I_E = -I_{ES}\left[exp\frac{v_{BE}}{V_T} - 1\right] + \alpha_R I_{CS}\left[exp\frac{v_{BC}}{V_T} - 1\right] \tag{2.7}$$

I_{CS} and I_{ES} are reverse saturation currents at the collector and emitter junctions respectively. V_T is the thermal voltage. $V_T = \frac{\bar{k}T}{q}$ where $\bar{k}$ is Boltzmann constant in Joules per degree Kelvin, q is the magnitude of charge of an electron and T is the temperature in Kelvin. α_F and α_R are current gains in normal and inverted operation respectively. Now, separating the linear and nonlinear parts in the collector and emitter currents of both the transistors and relating only upto quadratic order in the expansion of the exponentials, we have

$$\begin{aligned} I_{C_1} =& a_{11}v_{B_1}^{(0)} + a_{12}v_{C_1}^{(0)} + a_{13}v_{E_1}^{(0)} + \varepsilon f_1(v_{B_1}^{(0)}, v_{C_1}^{(0)}, v_{E_1}^{(0)}, v_{B_2}^{(0)}, v_{C_2}^{(0)}, v_{E_2}^{(0)}) \\ =& a_{11}v_{B_1}^{(0)} + a_{12}v_{C_1}^{(0)} + a_{13}v_{E_1}^{(0)} + \varepsilon(b_{11}v_{B_1}^{2(0)} + b_{12}v_{C_1}^{2(0)} + b_{13}v_{E_1}^{2(0)} + b_{14}v_{B_1}^{(0)}v_{E_1}^{(0)} + b_{15}v_{B_1}^{(0)}v_{C_1}^{(0)}) \end{aligned} \tag{2.8}$$

$$\begin{aligned} I_{C_2} =& a_{21}v_{B_2}^{(0)} + a_{22}v_{C_2}^{(0)} + a_{23}v_{E_2}^{(0)} + \varepsilon f_2(v_{B_1}^{(0)}, v_{C_1}^{(0)}, v_{E_1}^{(0)}, v_{B_2}^{(0)}, v_{C_2}^{(0)}, v_{E_2}^{(0)}) \\ =& a_{21}v_{B_2}^{(0)} + a_{22}v_{C_2}^{(0)} + a_{23}v_{E_2}^{(0)} + \varepsilon(b_{21}v_{B_2}^{2(0)} + b_{22}v_{C_2}^{2(0)} + b_{23}v_{E_2}^{2(0)} + b_{24}v_{B_2}^{(0)}v_{E_2}^{(0)} + b_{25}v_{B_2}^{(0)}v_{C_2}^{(0)}) \end{aligned} \tag{2.9}$$

$$\begin{aligned} I_{E_1} =& c_{11}v_{B_1}^{(0)} + c_{12}v_{C_1}^{(0)} + c_{13}v_{E_1}^{(0)} + \varepsilon g_1(v_{B_1}^{(0)}, v_{C_1}^{(0)}, v_{E_1}^{(0)}, v_{B_2}^{(0)}, v_{C_2}^{(0)}, v_{E_2}^{(0)}) \\ =& c_{11}v_{B_1}^{(0)} + c_{12}v_{C_1}^{(0)} + c_{13}v_{E_1}^{(0)} + \varepsilon(d_{11}v_{B_1}^{2(0)} + d_{12}v_{C_1}^{2(0)} + d_{13}v_{E_1}^{2(0)} + d_{14}v_{B_1}^{(0)}v_{E_1}^{(0)} + d_{15}v_{B_1}^{(0)}v_{C_1}^{(0)}) \end{aligned} \tag{2.10}$$

where f_1, f_2 and g_1 are quadratic functions of arguments. The small signal equivalent circuit model of the transistor is given by the linear terms of I_C and I_E, whereas the nonlinear terms give the corrections, when the voltage amplitude is large. The a's, b's, c's and d's are

$$\begin{aligned} &a_{11} = \tfrac{\alpha_{F_1}I_{ES_1} - I_{CS_1}}{V_T}, && a_{12} = \tfrac{I_{CS_1}}{V_T}, && a_{13} = -\tfrac{\alpha_{F_1}I_{ES_1}}{V_T}, && a_{21} = \tfrac{\alpha_{F_2}I_{ES_2} - I_{CS_2}}{V_T} \\ &a_{22} = \tfrac{I_{CS_2}}{V_T}, && a_{23} = -\tfrac{\alpha_{F_2}I_{ES_2}}{V_T}, && b_{11} = \tfrac{\alpha_{F_1}I_{ES_1}}{2V_T^2} - \tfrac{I_{CS_1}}{2V_T^2}, && b_{12} = -\tfrac{I_{CS_1}}{2V_T^2}, \\ &b_{21} = \tfrac{\alpha_{F_2}I_{ES_2}}{2V_T^2} - \tfrac{I_{CS_2}}{2V_T^2}, && b_{13} = \tfrac{\alpha_{F_1}I_{ES_1}}{2V_T^2}, && b_{22} = -\tfrac{I_{CS_2}}{2V_T^2}, && b_{23} = \tfrac{\alpha_{F_2}I_{ES_2}}{2V_T^2} \\ &c_{11} = \tfrac{\alpha_{R_1}I_{CS_1} - I_{ES_1}}{V_T}, && c_{12} = -\tfrac{\alpha_{R_1}I_{CS_1}}{V_T}, && c_{21} = \tfrac{\alpha_{R_2}I_{CS_2} - I_{ES_2}}{V_T}, && c_{13} = \tfrac{I_{ES_1}}{V_T} \\ &b_{24} = -\tfrac{\alpha_{R_2}I_{ES_2}}{V_T^2}, && b_{25} = \tfrac{I_{ES_2}}{V_T^2}, && d_{11} = \tfrac{\alpha_{R_1}I_{CS_1}}{2V_T^2} - \tfrac{I_{ES_1}}{2V_T^2}, && b_{14} = -\tfrac{\alpha_{F_1}I_{ES_1}}{V_T^2}, \\ &b_{15} = \tfrac{I_{CS_1}}{V_T^2}, && c_{22} = -\tfrac{\alpha_{R_2}I_{CS_2}}{V_T}, && c_{23} = \tfrac{I_{ES_2}}{V_T}, && d_{15} = -\tfrac{\alpha_{R_1}I_{CS_1}}{V_T^2} \\ &d_{12} = \tfrac{\alpha_{R_1}I_{CS_1}}{2V_T^2}, && d_{13} = -\tfrac{I_{ES_1}}{2V_T^2}, && d_{14} = \tfrac{I_{ES_1}}{V_T^2}. \end{aligned}$$

We have attached a perturbation tag ε to the nonlinear part which signifies the fac-

t that the nonlinear contribution to the circuit dynamics is small as compared to the linear contribution. The perturbation method involves expanding the solution to the nonlinear state algebraic equations in powers of ε and after substituting this expansion into the equations, we equate equal powers of ε on both sides. It then turns onto that the n^{th} order term in the perturbation expansion of the state that satisfies a linear differential algebraic equation driven by nonlinear functions of the lower order terms which have been already determined. We carry out one procedure only for $\varepsilon^n, n = 0, 1,$ as this much gives satisfactory good approximation for the nonlinear effects.

Now applying perturbation method to the voltage parameters, we have

$$v_o = v_o^{(0)} + \varepsilon v_o^{(1)} \tag{2.11}$$

$$v_{B_1} = v_{B_1}^{(0)} + \varepsilon v_{B_1}^{(1)} \tag{2.12}$$

$$v_{C_1} = v_{C_1}^{(0)} + \varepsilon v_{C_1}^{(1)} \tag{2.13}$$

$$v_{E_1} = v_{E_1}^{(0)} + \varepsilon v_{E_1}^{(1)} \tag{2.14}$$

$$v_{B_2} = v_{B_2}^{(0)} + \varepsilon v_{B_2}^{(1)} \tag{2.15}$$

$$v_{C_2} = v_{C_2}^{(0)} + \varepsilon v_{C_2}^{(1)} \tag{2.16}$$

Substituting values of v_o, v_{B_1}, v_{C_1}, v_{E_1}, v_{B_2} and v_{C_2} from (2.11)-(2.16) into (2.1)-(2.5), we get

$$\begin{aligned}&(v_{C_1}^{(0)} + \varepsilon v_{C_1}^{(1)}) + Z_1\{a_{11}v_{B_1}^{(0)} + a_{12}v_{C_1}^{(0)} + a_{13}v_{E_1}^{(0)} + \varepsilon(b_{11}v_{B_1}^{2(0)} + b_{12}v_{C_1}^{2(0)} + b_{13}v_{E_1}^{2(0)} \\ &+ b_{14}v_{B_1}^{(0)}v_{E_1}^{(0)} + b_{15}v_{B_1}^{(0)}v_{C_1}^{(0)})\} = V_{CC}\end{aligned} \tag{2.17}$$

$$\begin{aligned}&(v_{C_2}^{(0)} + \varepsilon v_{C_1}^{(2)}) + Z_4\{a_{21}v_{B_2}^{(0)} + a_{22}v_{C_2}^{(0)} + a_{23}v_{E_2}^{(0)} + \varepsilon(b_{21}v_{B_2}^{2(0)} + b_{22}v_{C_2}^{2(0)} + b_{23}v_{E_2}^{2(0)} \\ &+ b_{24}v_{B_2}^{(0)}v_{E_2}^{(0)} + b_{25}v_{B_2}^{(0)}v_{C_2}^{(0)})\} = V_{CC}\end{aligned} \tag{2.18}$$

$$\begin{aligned}&-(v_o^{(0)} + \varepsilon v_o^{(1)}) + \left(\frac{Z_o}{\beta_1}\right)\{a_{11}v_{B_1}^{(0)} + a_{12}v_{C_1}^{(0)} + a_{13}v_{E_1}^{(0)} + \varepsilon(b_{11}v_{B_1}^{2(0)} + b_{12}v_{C_1}^{2(0)} \\ &+ b_{13}v_{E_1}^{2(0)} + b_{14}v_{B_1}^{(0)}v_{E_1}^{(0)} + b_{15}v_{B_1}^{(0)}v_{C_1}^{(0)})\} + \left(\frac{Z_o + Z_2}{\beta_2}\right)\{a_{21}v_{B_2}^{(0)} + a_{22}v_{C_2}^{(0)} + a_{23}v_{E_2}^{(0)} \\ &+ \varepsilon(b_{21}v_{B_2}^{2(0)} + b_{22}v_{C_2}^{2(0)} + b_{23}v_{E_2}^{2(0)} + b_{24}v_{B_2}^{(0)}v_{E_2}^{(0)} + b_{25}v_{B_2}^{(0)}v_{C_2}^{(0)})\} + v_{B_1}^{(0)} + \varepsilon v_{B_1}^{(1)} = 0\end{aligned} \tag{2.19}$$

$$-(v_o^{(0)}+\varepsilon v_o^{(1)})+\left(\frac{Z_o+Z_3}{\beta_1}\right)\{a_{11}v_{B_1}^{(0)}+a_{12}v_{C_1}^{(0)}+a_{13}v_{E_1}^{(0)}+\varepsilon(b_{11}v_{B_1}^{2(0)}+b_{12}v_{C_1}^{2(0)}$$
$$+b_{13}v_{E_1}^{2(0)}+b_{14}v_{B_1}^{(0)}v_{E_1}^{(0)}+b_{15}v_{B_1}^{(0)}v_{C_1}^{(0)})\}+\left(\frac{Z_o}{\beta_2}\right)\{a_{21}v_{B_2}^{(0)}+a_{22}v_{C_2}^{(0)}+a_{23}v_{E_2}^{(0)}$$
$$+\varepsilon(b_{21}v_{B_2}^{2(0)}+b_{22}v_{C_2}^{2(0)}+b_{23}v_{E_2}^{2(0)}+b_{24}v_{B_2}^{(0)}v_{E_2}^{(0)}+b_{25}v_{B_2}^{(0)}v_{C_2}^{(0)})\}+v_{B_2}^{(0)}+\varepsilon v_{B_2}^{(1)}=0 \quad (2.20)$$

$$\left(1+\frac{1}{\beta_1}\right)[a_{11}v_{B_1}^{(0)}+a_{12}v_{C_1}^{(0)}+a_{13}v_{E_1}^{(0)}+\varepsilon(b_{11}v_{B_1}^{2(0)}+b_{12}v_{C_1}^{2(0)}+b_{13}v_{E_1}^{2(0)}+b_{14}v_{B_1}^{(0)}v_{E_1}^{(0)}$$
$$+b_{15}v_{B_1}^{(0)}v_{C_1}^{(0)})]-[c_{11}v_{B_1}^{(0)}+c_{12}v_{C_1}^{(0)}+c_{13}v_{E_1}^{(0)}+\varepsilon(d_{11}v_{B_1}^{2(0)}+d_{12}v_{C_1}^{2(0)}+d_{13}v_{E_1}^{2(0)}+d_{14}v_{B_1}^{(0)}v_{E_1}^{(0)}$$
$$+d_{15}v_{B_1}^{(0)}v_{C_1}^{(0)})]=0 \quad (2.21)$$

Zeroth order expressions or linear expressions are obtained by comparing the coefficients of $\varepsilon^{(0)}$ terms in equations (2.17)-(2.21).

$$v_{B_1}^{(0)}(a_{11}Z_1)+v_{C_1}^{(0)}(1+a_{12}Z_1)=V_{CC} \quad (2.22)$$

$$v_{B_2}^{(0)}(a_{21}Z_4)+v_{C_2}^{(0)}(1+a_{22}Z_4)=V_{CC} \quad (2.23)$$

$$-v_o^{(0)}+v_{B_1}^{(0)}\left(\frac{a_{11}Z_o}{\beta_1}\right)+v_{C_1}^{(0)}\left(\frac{a_{12}Z_o}{\beta_1}\right)+v_{B_2}^{(0)}\left(1+\frac{a_{21}(Z_o+Z_2)}{\beta_2}\right)+v_{C_2}^{(0)}\left(\frac{a_{22}(Z_o+Z_2)}{\beta_2}\right)=0 \quad (2.24)$$

$$-v_o^{(0)}+v_{B_1}^{(0)}\left(1+\frac{a_{11}(Z_o+Z_3)}{\beta_1}\right)+v_{C_1}^{(0)}\left(\frac{a_{12}(Z_o+Z_3)}{\beta_1}\right)+v_{B_2}^{(0)}\left(\frac{a_{21}Z_o}{\beta_2}\right)+v_{C_2}^{(0)}\left(\frac{a_{22}Z_o}{\beta_2}\right)=0 \quad (2.25)$$

$$v_{B_1}^{(0)}\left(\left(1+\frac{1}{\beta_1}\right)a_{11}-c_{11}\right)+v_{C_1}^{(0)}\left(\left(1+\frac{1}{\beta_1}\right)a_{12}-c_{12}\right)+v_{E_1}^{(0)}\left(\left(1+\frac{1}{\beta_1}\right)a_{13}-c_{13}\right)=0. \quad (2.26)$$

Representing the unperturbed state vector as

$$X_0(s)=\begin{bmatrix}v_o^{(0)} & v_{B_1}^{(0)} & v_{C_1}^{(0)} & v_{B_2}^{(0)} & v_{C_2}^{(0)}\end{bmatrix}^T$$

These equations have been solved by using Laplace transform.

$$A(s)X_0(s)=B(s)V_{CC}$$

$$X_0(s)=A^{-1}(s)B(s)V_{CC} \quad (2.27)$$

where $A(s)$ and $B(s)$ are

$$A = \begin{bmatrix} 0 & a_{11}Z_1 & 1+a_{12}Z_1 & 0 & 0 \\ 0 & 0 & 0 & a_{21}Z_4 & 1+a_{22}Z_4 \\ -1 & \left(\frac{a_{11}Z_o}{\beta_1}\right) & \left(\frac{a_{12}Z_o}{\beta_1}\right) & \left(1+\frac{a_{21}(Z_o+Z_2)}{\beta_2}\right) & \left(\frac{a_{22}(Z_o+Z_2)}{\beta_2}\right) \\ -1 & \left(1+\frac{a_{11}(Z_o+Z_3)}{\beta_1}\right) & \left(\frac{a_{22}(Z_o+Z_3)}{\beta_1}\right) & \left(\frac{a_{21}Z_o}{\beta_2}\right) & \left(\frac{a_{22}Z_o}{\beta_2}\right) \\ 0 & \left(1+\frac{1}{\beta_1}\right)a_{11}-c_{11} & \left(1+\frac{1}{\beta_1}\right)a_{12}-c_{12} & 0 & 0 \end{bmatrix}.$$

$B(s) = [1 \quad 1 \quad 0 \quad 0 \quad 0]^T$.

Take $\Phi_1(t) = v_o^{(0)}(t)$, $\Phi_2(t) = v_{B_1}^{(0)}(t)$, $\Phi_3(t) = v_{C_1}^{(0)}(t)$, $\Phi_4(t) = v_{B_2}^{(0)}(t)$, $\Phi_5(t) = v_{C_2}^{(0)}(t)$.

Therefore,

$$\Phi_1(s) = \frac{A_{11}+A_{21}}{|A|}V_{CC} \tag{2.28}$$

$$\Phi_2(s) = \frac{A_{12}+A_{22}}{|A|}V_{CC} \tag{2.29}$$

$$\Phi_3(s) = \frac{A_{13}+A_{23}}{|A|}V_{CC} \tag{2.30}$$

$$\Phi_4(s) = \frac{A_{14}+A_{24}}{|A|}V_{CC} \tag{2.31}$$

$$\Phi_5(s) = \frac{A_{15}+A_{25}}{|A|}V_{CC} \tag{2.32}$$

where $|A|$ is the determinant of matrix $A_{11}, A_{12}...A_{55}$ are the cofactors of matrix A. The

linear expression is

$$\begin{aligned} v_o(t) =& k_8 u(t) + k_{44}\left[\frac{b}{a^2+b^2}\left(-\frac{b}{a^2+b^2}e^{-at}cos(bt) - \frac{a}{a^2+b^2}e^{-at}sin(bt)\right)\right]V_{CC}u(t) \\ & - k_{44}\left[\frac{a}{a^2+b^2}\left(\frac{b}{a^2+b^2}e^{-at}sin(bt) - \frac{a}{a^2+b^2}e^{-at}cos(bt)\right)\right]V_{CC}u(t) \\ & + \frac{k_{44}(k_{43}-a)}{b}\left[\frac{-b}{a^2+b^2}\left(\frac{b}{a^2+b^2}e^{-at}sin(bt) - \frac{a}{a^2+b^2}e^{-at}cos(bt)\right)\right]V_{CC}u(t) \\ & - \frac{k_{44}(k_{43}-a)}{b}\left[\frac{a}{a^2+b^2}\left(-\frac{b}{a^2+b^2}e^{-at}cos(bt) - \frac{a}{a^2+b^2}e^{-at}sin(bt)\right)\right]V_{CC}u(t) \end{aligned} \tag{2.33}$$

Now, we compare the coefficients of $\varepsilon^{(1)}$ in equations (2.17)-(2.21) to obtain nonlinear expressions.

Representing the perturbed state vector as

$$X_1(s) = \begin{bmatrix} v_o^{(1)} & v_{B_1}^{(1)} & v_{C_1}^{(1)} & v_{B_2}^{(1)} & v_{C_2}^{(1)} \end{bmatrix}^T$$

$$A(s)X_1(s) = I_i(s)Z(s) \tag{2.34}$$

where *i*=1, 2, 3, $Z(s) = [U_{11}, U_{12}, U_{21}]$, $X_1(s) = L[x_1(t)]$

$$I_1(s) = [-1 \quad 0 \quad -1 \quad -1 \quad -1]^T$$

$$I_2(s) = [0 \quad -1 \quad -1 \quad -1 \quad 0]^T$$

$$I_3(s) = [0 \quad 0 \quad 0 \quad 0 \quad 1]^T$$

Here, L denotes the Laplace transform operator. The first order nonlinear operator is expressed as

$$U_{11}(s) = L[u_{11}(t)] = L[f_1(v_{B_1}^{(0)}, v_{C_1}^{(0)}, v_{E_1}^{(0)}, v_{B_2}^{(0)}, v_{C_2}^{(0)}, v_{E_2}^{(0)})] \tag{2.35}$$

$$U_{12}(s) = L[u_{12}(t)] = L[f_2(v_{B_1}^{(0)}, v_{C_1}^{(0)}, v_{E_1}^{(0)}, v_{B_2}^{(0)}, v_{C_2}^{(0)}, v_{E_2}^{(0)})] \tag{2.36}$$

$$U_{21}(s) = L[u_{21}(t)] = L[g_1(v_{B_1}^{(0)}, v_{C_1}^{(0)}, v_{E_1}^{(0)}, v_{B_2}^{(0)}, v_{C_2}^{(0)}, v_{E_2}^{(0)})] \tag{2.37}$$

$$u_{11}(t) = f_1(v_{B_1}^{(0)}, v_{C_1}^{(0)}, v_{E_1}^{(0)}, v_{B_2}^{(0)}, v_{C_2}^{(0)}, v_{E_2}^{(0)}) = (b_{11}v_{B_1}^{2(0)} + b_{12}v_{C_1}^{2(0)} + b_{13}v_{B_1}^{(0)}v_{C_1}^{(0)}) \tag{2.38}$$

$$u_{12}(t) = f_2(v_{B_1}^{(0)}, v_{C_1}^{(0)}, v_{E_1}^{(0)}, v_{B_2}^{(0)}, v_{C_2}^{(0)}, v_{E_2}^{(0)}) = (b_{21}v_{B_2}^{2(0)} + b_{22}v_{C_2}^{2(0)} + b_{23}v_{B_2}^{(0)}v_{C_2}^{(0)}) \tag{2.39}$$

$$u_{21}(t) = g_1(v_{B_1}^{(0)}, v_{C_1}^{(0)}, v_{E_1}^{(0)}, v_{B_2}^{(0)}, v_{C_2}^{(0)}, v_{E_2}^{(0)}) = (d_{11}v_{B_1}^{2(0)} + d_{12}v_{C_1}^{2(0)} + d_{13}v_{B_1}^{(0)}v_{C_1}^{(0)}) \tag{2.40}$$

The nonlinear expression output for the CCO is

$$v_o^{(1)}(s) = -\frac{A_{11}+A_{31}+A_{41}+A_{51}}{|A|}U_{11}(s) - \frac{A_{21}+A_{31}+A_{41}}{|A|}U_{11}(s) + \frac{A_{51}}{|A|}U_{11}(s). \tag{2.41}$$

Now, using Z_2, Z_3 as capacitors C_2, C_3 and Z_1, Z_4 as inductors L_1, L_4 and impedance Z_0 as output capacitance C_0, we have

$$\begin{aligned} v_o^{(1)}(s) =& \frac{s^8(k_{46}-k_{25}) + s^7(k_{47}-k_{26}) + s^6(k_{48}-k_{27}) + s^5(k_{49}-k_{28})}{s^4((s+a)^2+b^2)^3} \\ &+ \frac{s^4(k_{50}-k_{29}) + s^3(k_{51}-k_{30}) + s^2(k_{52}-k_{31}) + s^1(k_{53}-k_{32}) + (k_{54}-k_{33})}{s^4((s+a)^2+b^2)^3} \\ &- \frac{s^7k_{38} + s^6k_{39} + s^5k_{40} + s^4k_{41} + s^3k_{42} + s^2k_{43} + s^1k_{44} + k_{45}}{s^3((s+a)^2+b^2)^3} \end{aligned} \tag{2.42}$$

where

$k_0 = k_{\beta_1} + \frac{a_{21}a_{22}L_4k_{\beta_1}}{C_o\beta_2} - \frac{a_{11}a_{21}L_1k_{\beta_2}}{C_2\beta_2}$,

$k_1 = L_4a_{22}k_{\beta_1} - L_4a_{21}k_{\beta_1} - L_4a_{22}a_{21}k_{\beta_1} - L_1a_{11}k_{\beta_2} + \frac{a_{21}a_{22}a_{12}L_1L_4k_{\beta_1}}{C_o\beta_2}$,

$k_2 = L_4L_1a_{22}a_{12}k_{\beta_1} - L_1L_4a_{21}^2k_{\beta_1} - L_1L_4a_{22}a_{11}k_{\beta_2}$,

$k_3 = -L_1L_4^2a_{21}^2a_{22}k_{\beta_1}$,

$k_4 = \frac{a_{21}k_{\beta_1}}{C_o\beta_2} + \frac{a_{21}k_{\beta_1}}{C_2\beta_2}$,

$k_5 = -\frac{a_{21}a_{12}k_{\beta_1}}{C_o^2\beta_1\beta_2} - \frac{a_{21}a_{11}k_{\beta_2}}{C_oC_3\beta_1\beta_2} - \frac{a_{21}a_{11}k_{\beta_2}}{C_oC_2\beta_1\beta_2} - \frac{a_{21}a_{11}k_{\beta_2}}{C_2C_3\beta_1\beta_2} + \frac{a_{21}a_{12}k_{\beta_2}}{\beta_1\beta_2}\left(\frac{1}{C_o}+\frac{1}{C_2}\right)\left(\frac{1}{C_o}+\frac{1}{C_3}\right)$,

$k_6 = \left(\frac{a_{21}a_{22}L_4k_{\beta_1}}{C_o^2\beta_1\beta_2} - \frac{a_{21}a_{22}L_4k_{\beta_1}}{\beta_1\beta_2}\left(\frac{1}{C_o}+\frac{1}{C_2}\right)\left(\frac{1}{C_o}+\frac{1}{C_3}\right) - \frac{a_{11}k_{\beta_2}}{C_3\beta_1} - \frac{a_{21}k_{\beta_2}}{C_o\beta_2} - \frac{a_{21}k_{\beta_2}}{C_2\beta_2} - \frac{a_{12}k_{\beta_2}}{\beta_1}\left(\frac{1}{C_o}+\frac{1}{C_3}\right) + \frac{a_{21}k_{\beta_2}}{C_o\beta_2} - \frac{a_{22}k_{\beta_1}}{C_o\beta_2}\right)$,

$$k_7 = \frac{a_{12}a_{22}L_1k_{\beta_1}}{C_o\beta_2} - \frac{a_{11}a_{22}L_1k_{\beta_2}}{C_o\beta_2} - k_{\beta_2} - \frac{a_{11}a_{22}L_4k_{\beta_2}}{\beta_1}\left(\frac{1}{C_o}+\frac{1}{C_2}\right)\left(\frac{1}{C_o}+\frac{1}{C_3}\right),$$

$$k_8 = -L_4a_{22}k_{\beta_2},\ k_9 = -\frac{a_{21}k_{\beta_2}}{C_2\beta_2},\ k_{10} = -L_4a_{22}k_{\beta_2}$$

$$k_{11} = \frac{2a_{21}k_{\beta_2}}{C_o\beta_2} + \frac{a_{21}k_{\beta_1}}{C_2\beta_2}\ k_{12} = 1,\ k_{13} = L_4a_{22}k_{\beta_1},\ k_{14} = \frac{a_{11}k_{\beta_2}}{C_3\beta_1} - \frac{a_{12}k_{\beta_1}}{C_3\beta_1} - \frac{a_{22}k_{\beta_1}}{C_2\beta_2},$$

$$k_{15} = \frac{a_{11}a_{22}L_4p_2}{C_2\beta_2} - \frac{a_{12}a_{22}L_4k_{\beta_1}}{\beta_1}\left(\frac{1}{C_2}+\frac{1}{C_2}\right),$$

$$k_{16} = L_4a_{22}k_{\beta_2},$$

$$k_{17} = \frac{a_{21}k_{\beta_1}}{C_2\beta_2},$$

$$k_{18} = \frac{a_{11}a_{21}L_4p_2}{C_3\beta_1} - \frac{a_{12}a_{21}L_4k_{\beta_1}}{C_3\beta_1} - \frac{a_{11}a_{21}L_1k_{\beta_2}}{C_2\beta_2} + k_{\beta_1} + \frac{a_{12}a_{21}L_1k_{\beta_1}}{C_2\beta_2},$$

$$k_{19} = L_4a_{21}k_{\beta_1} - L_1a_{11}k_{\beta_2} + L_1a_{12}k_{\beta_1},$$

$$k_{20} = -\frac{a_{21}a_{12}k_{\beta_1}}{\beta_1\beta_2}\left(\frac{1}{C_o}+\frac{1}{C_2}\right)\left(\frac{1}{C_o}+\frac{1}{C_3}\right) + \frac{a_{21}a_{11}k_{\beta_2}}{\beta_1\beta_2}\left(\frac{1}{C_o}+\frac{1}{C_2}\right)\left(\frac{1}{C_o}+\frac{1}{C_3}\right) + \frac{a_{21}a_{11}}{\beta_1\beta_2}\left(\frac{1}{C_o}+\frac{1}{C_2}\right)$$
$$\times\left(\frac{1}{C_o}+\frac{1}{C_3}\right) - \frac{a_{21}a_{11}}{C_o^2\beta_1\beta_2},$$

$$k_{21} = \frac{a_{22}a_{12}L_4k_{\beta_1}}{C_o^2\beta_1\beta_2} - \frac{a_{22}a_{21}a_{12}L_4k_{\beta_1}}{C_o^2\beta_1\beta_2} - \frac{a_{22}a_{21}a_{12}L_4k_{\beta_1}}{\beta_1\beta_2}\left(\frac{1}{C_o}+\frac{1}{C_2}\right)\left(\frac{1}{C_o}+\frac{1}{C_3}\right) - \frac{a_{11}k_{\beta_2}}{C_3\beta_1} - \frac{a_{21}k_{\beta_2}}{C_o\beta_2}$$
$$-\frac{a_{21}k_{\beta_2}}{C_2\beta_2} + \frac{a_{12}k_{\beta_2}}{\beta_1}\left(\frac{1}{C_o}+\frac{1}{C_3}\right) + \frac{a_{22}k_{\beta_1}}{C_o\beta_2} + \frac{a_{21}k_{\beta_1}}{C_o\beta_2} + \frac{(a_{22}-a_{11})a_{21}a_{12}(L_1+L_4)k_{\beta_1}}{\beta_1\beta_2}\left(\frac{1}{C_o}+\frac{1}{C_2}\right)\left(\frac{1}{C_o}+\frac{1}{C_3}\right)$$
$$+\frac{a_{21}}{\beta_2}\left(\frac{1}{C_o}+\frac{1}{C_2}\right) + \frac{a_{11}}{\beta_1}\left(\frac{1}{C_o}+\frac{1}{C_3}\right),$$

$$k_{22} = 1 - k_{\beta_2} - \frac{a_{11}a_{22}L_4k_{\beta_2}}{\beta_1}\left(\frac{1}{C_o}+\frac{1}{C_3}\right) - \frac{a_{12}a_{22}L_1k_{\beta_1}}{C_o\beta_2} - \frac{a_{11}a_{22}L_1k_{\beta_2}}{C_o\beta_2} + \frac{(a_{12}-a_{11})a_{21}L_1k_{\beta_2}}{C_o\beta_2}$$
$$+\frac{a_{11}a_{12}L_1k_{\beta_2}}{\beta_2}\left(\frac{1}{C_o}+\frac{1}{C_2}\right) + \frac{a_{21}a_{12}L_1}{\beta_2}\left(\frac{1}{C_o}+\frac{1}{C_2}\right) + \frac{a_{11}a_{12}L_4}{\beta_1}\left(\frac{1}{C_o}+\frac{1}{C_3}\right),$$

$$k_{23} = L_4a_{22}k_{\beta_2} + L_1a_{11}k_{\beta_2} + L_1a_{12} + L_4a_{22},$$

$$k_{24} = (a_{12}-a_{11})a_{22}L_1L_4k_{\beta_2},$$

$$k_{25} = b_{11}k_{24}k_{10}^2 + b_{12}k_{24}k_{13}^2 + b_{13}k_{24}k_{10}k_{13}$$

$$k_{26} = b_{11}k_{23}k_{10}^2 + 2b_{12}k_{24}k_{12}k_{13} + b_{12}k_{23}k_{13}^2 + b_{13}k_{24}k_{10}k_{12} + b_{13}k_{23}k_{10}k_{13}$$

$$k_{27} = b_{11}k_{22}k_{10}^2 + 2b_{11}k_{24}k_9k_{10} + b_{12}k_{24}k_{12}^2 + 2b_{12}k_{24}k_{13}k_{11} + 2b_{12}k_{23}k_{13}k_{12} + b_{12}k_{22}k_{13}^2$$
$$+b_{13}k_{24}k_9k_{13} + b_{13}k_{24}k_{10}k_{11} + b_{13}k_{22}k_{10}k_{13},$$

$$k_{28} = b_{11}k_{21}k_{10}^2 + 2b_{11}k_{23}k_9k_{10} + b_{12}k_{23}k_{12}^2 + 2b_{12}k_{24}k_{12}k_{11} + 2b_{12}k_{23}k_{13}k_{11} + 2b_{12}k_{22}k_{13}k_{12}$$
$$+b_{12}k_{21}k_{13}^2 + b_{13}k_{24}k_9k_{12} + b_{13}k_{23}k_9k_{13} + b_{13}k_{23}k_{10}k_{11} + b_{13}k_{22}k_{10}k_{12} + b_{13}k_{21}k_{10}k_{13},$$

$$k_{29} = b_{11}k_{20}k_{10}^2 + 2b_{11}k_{21}k_9k_{10} + b_{11}k_{24}k_9^2 + b_{12}k_{24}k_{11}^2 + b_{12}k_{22}k_{12}^2 + 2b_{12}k_{23}k_{12}k_{11} + 2b_{12}k_{22}k_{13}k_{11}$$
$$+2b_{12}k_{21}k_{13}k_{12} + b_{12}k_{20}k_{13}^2 + b_{13}k_{24}k_9k_{11} + b_{13}k_{23}k_9k_{12} + b_{13}k_{22}k_{10}k_{11} + b_{13}k_{22}k_9k_{13}$$
$$+b_{13}k_{21}k_{10}k_{12} + b_{13}k_{20}k_{10}k_{13},$$

$$k_{30} = b_{11}k_{20}k_{10}^2 + 2b_{11}k_{21}k_9k_{10} + b_{11}k_{23}k_9^2 + b_{12}k_{23}k_{11}^2 + b_{12}k_{21}k_{12}^2 + 2b_{12}k_{22}k_{12}k_{11} + 2b_{12}k_{21}k_{13}k_{11}$$
$$+2b_{12}k_{20}k_{13}k_{12} + b_{13}k_{23}k_9k_{11} + b_{13}k_{22}k_9k_{12} + b_{13}k_{21}k_{10}k_{11} + b_{13}k_{21}k_9k_{13} + b_{13}k_{20}k_{10}k_{12},$$

$$k_{31} = b_{11}k_{22}k_9^2 + 2b_{11}k_{20}k_9k_{10} + b_{12}k_{22}k_{11}^2 + 2b_{12}k_{21}k_{12}k_{11} + b_{12}k_{20}k_{12}^2 + 2b_{12}k_{20}k_{13}k_{11}$$
$$+b_{13}k_{22}k_9k_{11} + b_{13}k_{21}k_9k_{12} + b_{13}k_{20}k_{13}k_{12} + b_{13}k_{20}k_{10}k_{11},$$

$$k_{32} = b_{11}k_{21}k_9^2 + b_{12}k_{21}k_{11}^2 + 2b_{12}k_{20}k_{12}k_{11} + b_{13}k_{21}k_9k_{11} + b_{13}k_{20}k_9k_{12},$$

$$k_{33} = b_{11}k_{20}k_9^2 + b_{12}k_{20}k_{11}^2 + b_{13}k_{20}k_9k_{11},$$

$$k_{34} = -a_{11}a_{22}L_1L_4k_{\beta_2},$$

$$k_{35} = a_{11}L_1k_{\beta_2},$$

$$k_{36} = \frac{a_{12}a_{22}L_1k_{\beta_1}}{C_o\beta_2} - \frac{a_{11}a_{22}L_1p_2}{C_o\beta_2} + \frac{a_{12}a_{21}L_1p_2}{C_o\beta_2} - \frac{a_{11}a_{21}L_1p_2}{C_o\beta_2} + \frac{a_{11}a_{12}L_1p_2}{C_o\beta_2} + \frac{a_{11}a_{21}L_1p_2}{C_2\beta_2},$$

$$k_{37} = \frac{a_{22}k_{\beta_1}}{C_o\beta_2} + \frac{a_{21}k_{\beta_1}}{C_o\beta_2},$$

$$k_{38} = a_{12}a_{22}L_1L_4,$$

$$k_{39} = a_{21}L_1 + a_{22}L_4,$$

$$k_{40} = 1 + \frac{a_{21}a_{12}L_1}{\beta_2}\left(\frac{1}{C_o} + \frac{1}{C_2}\right) + \frac{a_{11}a_{22}L_4}{\beta_1}\left(\frac{1}{C_o} + \frac{1}{C_3}\right),$$

$$k_{41} = -\frac{a_{21}(a_{11}-a_{22})a_{12}(L_1+L_4)}{\beta_1\beta_2}\left(\frac{1}{C_o} + \frac{1}{C_3}\right)\left(\frac{1}{C_o} + \frac{1}{C_2}\right),$$

$$k_{42} = -\frac{a_{11}a_{21}}{C_o^2\beta_1\beta_2} + \frac{a_{11}a_{21}}{C_o^2\beta_1\beta_2}\left(\frac{1}{C_o} + \frac{1}{C_3}\right)\left(\frac{1}{C_o} + \frac{1}{C_2}\right),$$

$$k_{46} = d_{11}k_{38}k_{10}^2 + d_{12}k_{38}k_{13}^2 + d_{13}k_{38}k_{10}k_{13}$$

$$k_{47} = d_{11}k_{39}k_{10}^2 + 2d_{12}k_{38}k_{12}k_{13} + d_{12}k_{39}k_{13}^2 + d_{13}k_{38}k_{10}k_{12} + d_{13}k_{39}k_{10}k_{13}$$

$$\begin{aligned} k_{48} = {} & d_{11}k_{40}k_{10}^2 + 2d_{11}k_{38}k_9k_{10} + d_{12}k_{38}k_{12}^2 + 2d_{12}k_{38}k_{13}k_{11} + 2d_{12}k_{39}k_{13}k_{12} + d_{12}k_{40}k_{13}^2 \\ & + d_{13}k_{38}k_9k_{13} + d_{13}k_{38}k_{10}k_{11} + d_{13}k_{40}k_{10}k_{13}, \end{aligned}$$

$$\begin{aligned} k_{49} = {} & d_{11}k_{41}k_{10}^2 + 2d_{11}k_{39}k_9k_{10} + d_{12}k_{39}k_{12}^2 + 2d_{12}k_{38}k_{12}k_{11} + 2d_{12}k_{39}k_{13}k_{11} + 2d_{12}k_{40}k_{13}k_{12} \\ & + d_{12}k_{41}k_{13}^2 + d_{13}k_{38}k_9k_{12} + d_{13}k_{39}k_9k_{13} + d_{13}k_{39}k_{10}k_{11} + d_{13}k_{40}k_{10}k_{12} + d_{13}k_{41}k_{10}k_{13}, \end{aligned}$$

$$\begin{aligned} k_{50} = {} & d_{11}k_{42}k_{10}^2 + 2d_{11}k_{41}k_9k_{10} + d_{11}k_{38}k_9^2 + d_{12}k_{38}k_{11}^2 + d_{12}k_{40}k_{12}^2 + 2d_{12}k_{39}k_{12}k_{11} \\ & + 2d_{12}k_{41}k_{13}k_{12} + d_{12}k_{42}k_{13}^2 + d_{13}k_{38}k_9k_{11} + b_{13}k_{39}k_9k_{12} + d_{13}k_{40}k_{10}k_{11} + d_{13}k_{40}k_9k_{13} \\ & + d_{13}k_{41}k_{10}k_{12} + d_{13}k_{42}k_{10}k_{13} + 2d_{12}k_{40}k_{13}k_{11}, \end{aligned}$$

$$\begin{aligned} k_{51} = {} & d_{11}k_{42}k_{10}^2 + 2d_{11}k_{41}k_9k_{10} + d_{11}k_{39}k_9^2 + d_{12}k_{39}k_{11}^2 + d_{12}k_{41}k_{12}^2 + 2d_{12}k_{40}k_{12}k_{11} + 2d_{12}k_{41}k_{13}k_{11} \\ & + 2d_{12}k_{42}k_{13}k_{12} + d_{13}k_{39}k_9k_{11} + d_{13}k_{40}k_9k_{12} + b_{13}k_{41}k_{10}k_{11} + d_{13}k_{41}k_9k_{13} + d_{13}k_{42}k_{10}k_{12}, \end{aligned}$$

$$\begin{aligned} k_{52} = {} & d_{11}k_{40}k_9^2 + 2d_{11}k_{42}k_9k_{10} + d_{12}k_{40}k_{11}^2 + 2d_{12}k_{41}k_{12}k_{11} + d_{12}k_{42}k_{12}^2 + 2d_{12}k_{42}k_{13}k_{11} \\ & + d_{13}k_{41}k_9k_{12} + d_{13}k_{42}k_{13}k_{12} + d_{13}k_{42}k_{10}k_{11} + d_{13}k_{40}k_9k_{11}, \end{aligned}$$

$$k_{53} = d_{11}k_{41}k_9^2 + d_{12}k_{41}k_{11}^2 + 2d_{12}k_{42}k_{12}k_{11} + d_{13}k_{41}k_9k_{11} + d_{13}k_{42}k_9k_{12},$$

$$k_{54} = d_{11}k_{42}k_9^2 + d_{12}k_{42}k_{11}^2 + d_{13}k_{42}k_9k_{11},$$

$$k_{55} = b_{21}k_{34}k_{16}^2 + b_{22}k_{34}k_{19}^2 + b_{23}k_{34}k_{16}k_{19},$$

$$\begin{aligned} k_{56} = {} & b_{21}k_{35}k_{16}^2 + 2b_{21}k_{34}k_{16}k_{15} + b_{22}k_{35}k_{19}^2 + 2b_{22}k_{34}k_{18}k_{19} + b_{23}k_{34}k_{18}k_{16} + b_{23}k_{34}k_{15}k_{19} \\ & + b_{23}k_{35}k_{16}k_{19}, \end{aligned}$$

$$\begin{aligned} k_{57} = {} & b_{21}k_{36}k_{16}^2 + b_{21}k_{34}k_{15}^2 + 2b_{21}k_{34}k_{16}k_{14} + 2b_{21}k_{35}k_{16}k_{15} + 2b_{22}k_{34}k_{17}k_{19} + b_{22}k_{34}k_{18}^2 \\ & + b_{22}k_{36}k_{19}^2 + b_{23}k_{34}k_{17}k_{16} + b_{23}k_{34}k_{15}k_{18} + b_{23}k_{34}k_{14}k_{19} + b_{23}k_{35}k_{16}k_{18} + b_{23}k_{35}k_{15}k_{19} \\ & + b_{23}k_{36}k_{16}k_{19} + 2b_{22}k_{35}k_{17}k_{19}, \end{aligned}$$

$$\begin{aligned} k_{58} = {} & b_{21}k_{35}k_{15}^2 + 2b_{21}k_{34}k_{15}k_{14} + 2b_{21}k_{35}k_{16}k_{14} + 2b_{21}k_{36}k_{16}k_{15} + 2b_{21}k_{37}k_{16}^2 + b_{22}k_{35}k_{18}^2 \\ & + 2b_{22}k_{34}k_{17}k_{18} + 2b_{22}k_{35}k_{17}k_{19} + 2b_{22}k_{36}k_{18}k_{19} + b_{22}k_{37}k_{19}^2 + b_{23}k_{34}k_{15}k_{17} \\ & + b_{23}k_{34}k_{14}k_{18} + b_{23}k_{35}k_{16}k_{17} + b_{23}k_{35}k_{15}k_{18} + b_{23}k_{35}k_{14}k_{19} + b_{23}k_{36}k_{16}k_{18} \\ & + b_{23}k_{36}k_{15}k_{19} + b_{23}k_{37}k_{16}k_{19}, \end{aligned}$$

$$\begin{aligned} k_{59} = {} & b_{21}k_{34}k_{14}^2 + 2b_{21}k_{35}k_{15}k_{14} + b_{21}k_{36}k_{15}^2 + 2b_{21}k_{36}k_{16}k_{14} + 2b_{21}k_{37}k_{16}k_{15} + b_{22}k_{34}k_{17}^2 \\ & + b_{22}k_{36}k_{18}^2 + 2b_{22}k_{35}k_{17}k_{18} + 2b_{22}k_{36}k_{17}k_{19} + 2b_{22}k_{37}k_{19}k_{18} + b_{23}k_{34}k_{14}k_{17} + b_{23}k_{35}k_{15}k_{17} \end{aligned}$$

$$+b_{23}k_{35}k_{14}k_{18}+b_{23}k_{36}k_{16}k_{17}+b_{23}k_{36}k_{15}k_{18}+b_{23}k_{36}k_{14}k_{19}+b_{23}k_{37}k_{16}k_{18}+b_{23}k_{37}k_{15}k_{19},$$

$$k_{60}=b_{21}k_{35}k_{14}^2+2b_{21}k_{36}k_{15}k_{14}+2b_{21}k_{37}k_{16}k_{14}+b_{21}k_{37}k_{15}^2+b_{22}k_{35}k_{17}^2+2b_{22}k_{36}k_{15}k_{18}$$
$$+2b_{22}k_{37}k_{19}k_{17}+2b_{22}k_{37}k_{18}^2+b_{23}k_{35}k_{14}k_{17}+b_{23}k_{36}k_{15}k_{17}+b_{23}k_{36}k_{14}k_{18}+b_{23}k_{37}k_{16}k_{17}$$
$$+b_{23}k_{37}k_{15}k_{18}+b_{23}k_{37}k_{14}k_{19},$$

$$k_{61}=b_{21}k_{36}k_{14}^2+2b_{21}k_{37}k_{15}k_{14}+b_{22}k_{36}k_{17}^2+2b_{22}k_{37}k_{18}k_{17}+b_{23}k_{36}k_{14}k_{17}+b_{23}k_{37}k_{15}k_{17}$$
$$+b_{23}k_{37}k_{14}k_{19},$$

$$k_{62}=b_{21}k_{37}k_{14}^2+b_{22}k_{37}k_{17}^2+b_{23}k_{37}k_{14}k_{17},$$

$$k_{\beta_1}=\left(1+\tfrac{1}{\beta_1}\right)a_{11}-c_{11},$$

$$k_{\beta_2}=\left(1+\tfrac{1}{\beta_1}\right)a_{12}-c_{12}.$$

2.1.2 Simulation Results for Cross Coupled Oscillator Circuit

The linear and nonlinear output voltages have been plotted in MATLAB. Figure 2.2(a) shows linear output, whereas nonlinear output is presented in Figure 2.2(b). The simulated result shows the deviation of the nonlinear output from the linear output. Mathematically, the percentage distortion due to only linear term has been calculated using following expression.

$$\text{Percentage distortion}=\frac{v_0-v_0^{(0)}}{v_0}\times 100\% \tag{2.43}$$

where v_o represents the sum of linear and nonlinear output voltage. $v_o^{(0)}$ denotes only linear output voltage.

Table 2.1: Distortion error for different capacitors and inductors in BJT cross coupled oscillator.

$L_1(nH)$	$L_4(nH)$	$C_2(pF)$	$C_4(pF)$	Percentage distortion
6000	7000	1000	5	0.333%
600	700	0.5	0.1	0.428%

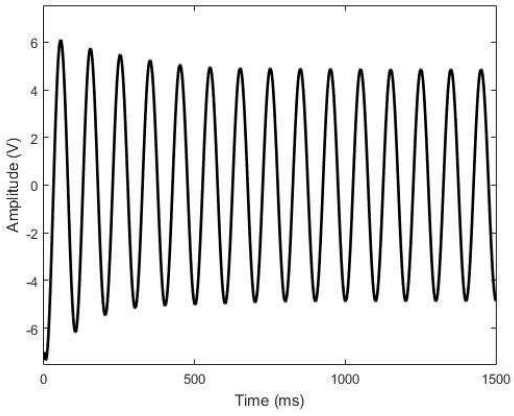

(a) Linear output.

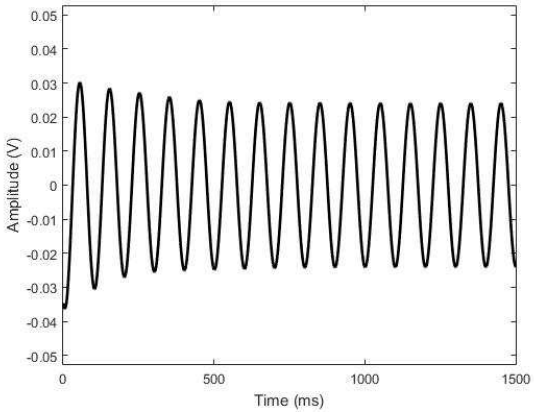

(b) First order nonlinear output

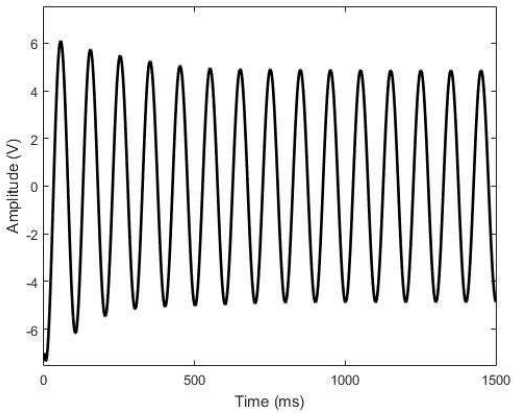

(c) zero and first order nonlinear output.

Figure 2.2: Cross coupled output voltage.

2.2 Differential Amplifier Circuit Analysis Using Perturbation Method

2.2.1 Nonlinear Modelling of Differential Amplifier Circuit

BJT DA circuit is shown in Figure 2.3. It has transistors Q_1 and Q_2. Applying Kirchhoff's voltage law (KVL) and Kirchhoff's current law (KCL) to DA circuit, we have

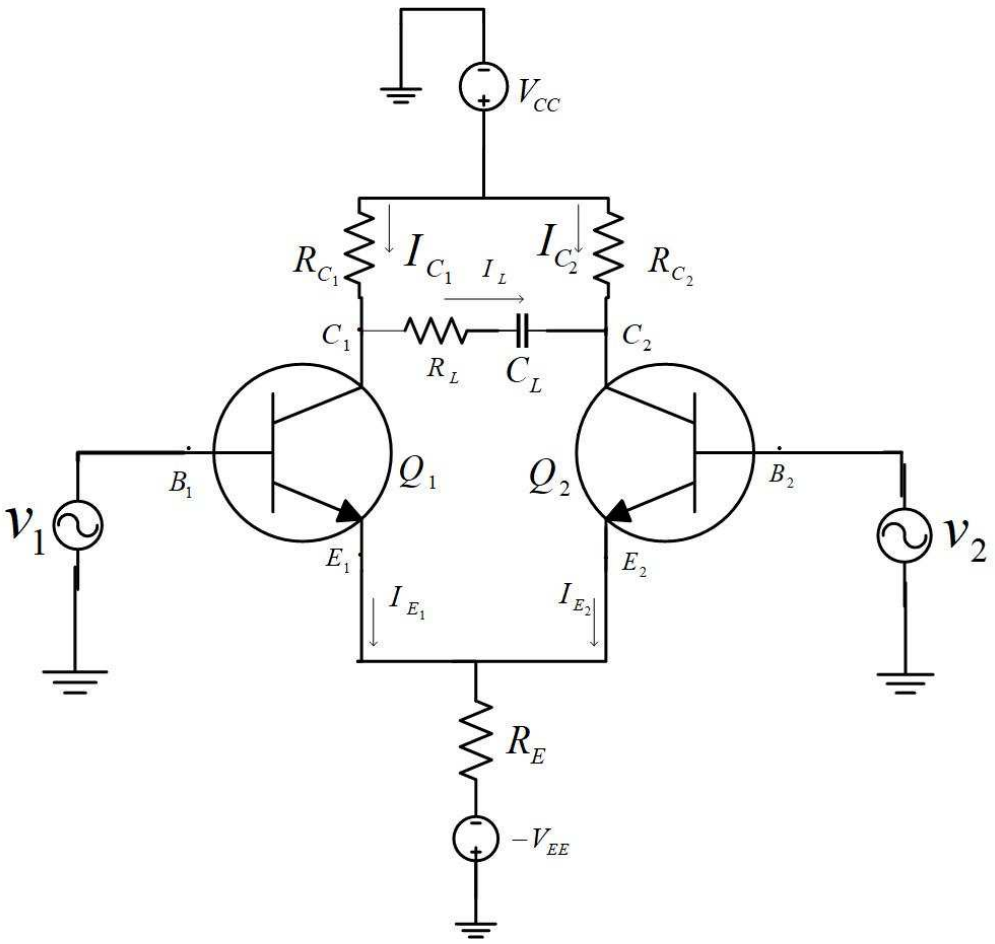

Figure 2.3: Differential amplifier circuit.

$$\frac{V_{EE}+v_E}{R_E}+(I_{E_1}+I_{E_2})=0 \tag{2.44}$$

$$i_L R_L+\frac{1}{C_L}\int i_L dt = v_{C_1}-v_{C_2} \tag{2.45}$$

$$\frac{V_{CC}-v_{C_1}}{R_{C_1}}-I_L-I_{C_1}=0 \tag{2.46}$$

$$\frac{V_{CC}-v_{C_2}}{R_{C_2}}+I_L-I_{C_2}=0 \tag{2.47}$$

From the circuit, we have, $v_{BE_1}=v_1-v_E$, $v_{BE_2}=v_2-v_E$, $v_{BC_1}=v_1-v_{C_1}$, $v_{BC_2}=v_2-v_{C_2}$, where v_{C_1}, v_{C_2}, v_E and q_L are the state vectors. Also, $\int i_L dt=q_L$, where q_L is the charge at load. The collector current and emitter current for the transistors Q_1 i.e. I_{C_1}, I_{E_1} are

$$I_{C_1}=\beta_1 I_0\left[e^{\left(\frac{v_{BE_1}}{V_T}\right)}-1\right] \tag{2.48}$$

$$I_{E_1}=\frac{I_0}{1-\alpha_1}\left[e^{\left(\frac{v_{BE_1}}{V_T}\right)}-1\right] \tag{2.49}$$

Similarly, the collector currents and emitter current for the transistors Q_2 i.e. I_{C_2}, I_{E_2} are

$$I_{C_2}=\beta_2 I_0\left[e^{\left(\frac{v_{BE_2}}{V_T}\right)}-1\right] \tag{2.50}$$

$$I_{E_2}=\frac{I_0}{1-\alpha_2}\left[e^{\left(\frac{v_{BE_2}}{V_T}\right)}-1\right] \tag{2.51}$$

Expanding equations (2.48)-(2.51) in Taylor series expansion, we get

$$I_{C_1}=\beta_1 I_0\left(\frac{v_1-v_E}{V_T}\right)+\frac{\beta_1 I_0}{2}\left(\frac{v_1-v_E}{V_T}\right)^2+\text{Higher order terms} \tag{2.52}$$

$$I_{E_1}=\frac{I_0}{1-\alpha_1}\left(\frac{v_1-v_E}{V_T}\right)+\frac{I_0}{2(1-\alpha_1)}\left(\frac{v_1-v_E}{V_T}\right)^2+\text{Higher order terms} \tag{2.53}$$

$$I_{C_2}=\beta_2 I_0\left(\frac{v_2-v_E}{V_T}\right)+\frac{\beta_2 I_0}{2}\left(\frac{v_2-v_E}{V_T}\right)^2+\text{Higher order terms} \tag{2.54}$$

$$I_{E_2}=\frac{I_0}{1-\alpha_2}\left(\frac{v_2-v_E}{V_T}\right)+\frac{I_0}{2(1-\alpha_2)}\left(\frac{v_2-v_E}{V_T}\right)^2+\text{Higher order terms} \tag{2.55}$$

Then, from equations (2.44)-(2.47) and neglecting the higher order terms in equations (2.52)-(2.55), we have

$$\begin{aligned}&\frac{V_{EE}+v_E}{R_E}+\frac{I_0}{1-\alpha_1}\left(\frac{v_1-v_E}{V_T}\right)+\frac{I_0}{2(1-\alpha_1)}\left(\frac{v_1-v_E}{V_T}\right)^2\\&+\frac{I_0}{1-\alpha_2}\left(\frac{v_2-v_E}{V_T}\right)+\frac{I_0}{2(1-\alpha_2)}\left(\frac{v_2-v_E}{V_T}\right)^2=0\end{aligned} \tag{2.56}$$

$$R_L\frac{dq_L}{dt}+\frac{q_L}{C_L}-v_{C_1}+v_{C_2}=0 \tag{2.57}$$

$$\frac{V_{CC}-v_{C_1}}{R_{C_1}}-\frac{dq_L}{dt}-\beta_1 I_0\left(\frac{v_1-v_E}{V_T}\right)+\frac{\beta_1 I_0}{2}\left(\frac{v_1-v_E}{V_T}\right)^2=0 \tag{2.58}$$

$$\frac{V_{CC}-v_{C_2}}{R_{C_2}}+\frac{dq_L}{dt}-\beta_2 I_0\left(\frac{v_2-v_E}{V_T}\right)+\frac{\beta_2 I_0}{2}\left(\frac{v_2-v_E}{V_T}\right)^2=0 \tag{2.59}$$

Now, applying perturbation to state variables as: $v_{C_1}=v_{C_1}^{(0)}+\varepsilon v_{C_1}^{(1)}$, $v_{C_2}=v_{C_2}^{(0)}+\varepsilon v_{C_2}^{(1)}$, $v_E=v_E^{(0)}+\varepsilon v_E^{(1)}$ and $q_L=q_L^{(0)}+\varepsilon q_L^{(1)}$

Applying perturbation method to equations (2.56)-(2.59) and rearranging the equations, we have

$$\begin{aligned}(v_E^{(0)}+\varepsilon v_E^{(1)})\left(\frac{1}{R_E}-\frac{I_0}{V_T(1-\alpha_1)}-\frac{I_0}{V_T(1-\alpha_2)}\right)&=-\frac{V_{EE}}{R_E}-\frac{v_1 I_0}{V_T(1-\alpha_1)}-\frac{v_2 I_0}{V_T(1-\alpha_2)}\\&-(v_1-v_E)^2\frac{I_0}{2V_T^2(1-\alpha_1)}-(v_2-v_E)^2\frac{I_0}{2V_T^2(1-\alpha_2)}\end{aligned} \tag{2.60}$$

$$(v_{C_1}^{(0)}+\varepsilon v_{C_1}^{(1)})+(q_L^{(0)}+\varepsilon q_L^{(1)})\left(R_L\frac{d}{dt}+\frac{1}{C_L}\right)+(v_{C_2}^{(0)}+\varepsilon v_{C_2}^{(1)})=0 \tag{2.61}$$

$$\begin{aligned}&(v_{C_1}^{(0)}+\varepsilon v_{C_1}^{(1)}))\left(\frac{1}{R_{C_1}}\right)+(q_L^{(0)}+\varepsilon q_L^{(1)})\left(\frac{d}{dt}\right)+(v_E^{(0)}+\varepsilon v_E^{(1)})\times\left(-\frac{\beta_1 I_0}{V_T}\right)\\&=\frac{V_{CC}}{R_{C_1}}+v_1\left(-\frac{\beta_1 I_0}{V_T}\right)+(v_1-v_E)^2\left(-\frac{\beta_1 I_0}{2V_T^2}\right)\end{aligned} \tag{2.62}$$

$$\begin{aligned}&(v_{C_2}^{(0)}+\varepsilon v_{C_2}^{(1)}))\left(\frac{1}{R_{C_2}}\right)+(q_L^{(0)}+\varepsilon q_L^{(1)})\left(-\frac{d}{dt}\right)+(v_E^{(0)}+\varepsilon v_E^{(1)})\times\left(-\frac{\beta_2 I_0}{V_T}\right)\\&=\frac{V_{CC}}{R_{C_2}}+v_2\left(-\frac{\beta_2 I_0}{V_T}\right)+(v_2-v_E)^2\left(-\frac{\beta_2 I_0}{2V_T^2}\right).\end{aligned} \tag{2.63}$$

Linear terms are obtained by comparing the coefficients of $\varepsilon^{(0)}$ in equations (2.60)-(2.63). They are:

$$v_E^{(0)}\left(\frac{1}{R_E}-\frac{I_0}{V_T(1-\alpha_1)}-\frac{I_0}{V_T(1-\alpha_2)}\right)=-\frac{V_{EE}}{R_E}-\frac{v_1 I_0}{V_T(1-\alpha_1)}-\frac{v_2 I_0}{V_T(1-\alpha_2)} \tag{2.64}$$

$$v_{C_1}^{(0)}+q_L^{(0)}\left(R_L\frac{d}{dt}+\frac{1}{C_L}\right)+v_{C_2}^{(0)}=0 \tag{2.65}$$

$$v_{C_1}^{(0)}\left(\frac{1}{R_{C_1}}\right)+q_L^{(0)}\left(\frac{d}{dt}\right)+v_E^{(0)}\left(-\frac{\beta_1 I_0}{V_T}\right)=\frac{V_{CC}}{R_{C_1}}+v_1\left(-\frac{\beta_1 I_0}{V_T}\right) \tag{2.66}$$

$$v_{C_2}^{(0)}\left(\frac{1}{R_{C_2}}\right)+q_L^{(0)}\left(-\frac{d}{dt}\right)+v_E^{(0)}\left(-\frac{\beta_2 I_0}{V_T}\right)=\frac{V_{CC}}{R_{C_2}}+v_2\left(-\frac{\beta_2 I_0}{V_T}\right) \tag{2.67}$$

$$A(s)X_0(s)=B_1(s)v_1(s)+B_2(s)v_2(s)+C_1(s)V_{EE}+C_2(s)V_{CC} \tag{2.68}$$

$$X_0(s)=\begin{bmatrix} v_{C_1}^{(0)} & v_{C_2}^{(0)} & v_E^{(0)} & q_L^{(0)} \end{bmatrix} \tag{2.69}$$

$$A=\begin{bmatrix} 0 & 0 & \left\{\frac{1}{R_E}-\frac{I_0}{V_T(1-\alpha_1)}-\frac{I_0}{V_T(1-\alpha_2)}\right\} & 0 \\ \frac{1}{R_{C_1}} & 0 & -\frac{\beta_1 I_0}{V_T} & \frac{d}{dt} \\ 0 & \frac{1}{R_{C_2}} & -\frac{\beta_2 I_0}{V_T} & -\frac{d}{dt} \\ -1 & 1 & 0 & R_L\frac{d}{dt}+\frac{1}{C_L} \end{bmatrix} \tag{2.70}$$

$$B_1(s)=\begin{bmatrix} -\frac{I_0}{V_T(1-\alpha_1)} & -\frac{\beta_1 I_0}{V_T} & 0 & 0 \end{bmatrix} \tag{2.71}$$

$$B_2(s)=\begin{bmatrix} -\frac{I_0}{V_T(1-\alpha_2)} & 0-\frac{\beta_2 I_0}{V_T} & 0 \end{bmatrix} \tag{2.72}$$

$$C_1(s)=\begin{bmatrix} -\frac{1}{R_E} & 0 & 0 & 0 \end{bmatrix} \tag{2.73}$$

$$C_2(s)=\begin{bmatrix} 0 & \frac{1}{R_{C_1}} & \frac{1}{R_{C_2}} & 0 \end{bmatrix} \tag{2.74}$$

$$v_{C_1}^{(0)}=\left\{-\frac{I_0}{V_T(1-\alpha_1)}\times\frac{A_{11}}{|A|}-\frac{\beta_1 I_0}{V_T}\times\frac{A_{21}}{|A|}\right\}*v_1(t)+\left\{-\frac{I_0}{V_T(1-\alpha_2)}\times\frac{A_{11}}{|A|}-\frac{\beta_2 I_0}{V_T}\times\frac{A_{31}}{|A|}\right\}$$
$$*v_2(t)-\frac{1}{R_E}\times\frac{A_{11}}{|A|}V_{EE}+\left(\frac{1}{R_{C_1}}\times\frac{A_{21}}{|A|}+\frac{1}{R_{C_2}}\times\frac{A_{31}}{|A|}\right)V_{CC} \tag{2.75}$$

$$v_{C_2}^{(0)}=\left\{-\frac{I_0}{V_T(1-\alpha_1)}\times\frac{A_{12}}{|A|}-\frac{\beta_1 I_0}{V_T}\times\frac{A_{22}}{|A|}\right\}*v_1(t)+\left\{-\frac{I_0}{V_T(1-\alpha_2)}\times\frac{A_{12}}{|A|}-\frac{\beta_2 I_0}{V_T}\times\frac{A_{32}}{|A|}\right\}$$
$$*v_2(t)-\frac{1}{R_E}\times\frac{A_{12}}{|A|}V_{EE}+\left(\frac{1}{R_{C_1}}\times\frac{A_{22}}{|A|}+\frac{1}{R_{C_2}}\times\frac{A_{32}}{|A|}\right)V_{CC} \tag{2.76}$$

$$v_E^{(0)}=\left\{-\frac{I_0}{V_T(1-\alpha_1)}\times\frac{A_{13}}{|A|}-\frac{\beta_1 I_0}{V_T}\times\frac{A_{23}}{|A|}\right\}*v_1(t)+\left\{-\frac{I_0}{V_T(1-\alpha_2)}\times\frac{A_{13}}{|A|}-\frac{\beta_2 I_0}{V_T}\times\frac{A_{33}}{|A|}\right\}$$
$$*v_2(t)-\frac{1}{R_E}\times\frac{A_{13}}{|A|}V_{EE}+\left(\frac{1}{R_{C_1}}\times\frac{A_{23}}{|A|}+\frac{1}{R_{C_2}}\times\frac{A_{33}}{|A|}\right)V_{CC} \tag{2.77}$$

$$q_L^{(0)} = \left\{ -\frac{I_0}{V_T(1-\alpha_1)} \times \frac{A_{14}}{|A|} - \frac{\beta_1 I_0}{V_T} \times \frac{A_{24}}{|A|} \right\} * v_1(t) + \left\{ -\frac{I_0}{V_T(1-\alpha_2)} \times \frac{A_{14}}{|A|} - \frac{\beta_2 I_0}{V_T} \times \frac{A_{34}}{|A|} \right\} * v_2(t) - \frac{1}{R_E} \times \frac{A_{14}}{|A|} V_{EE} + \left(\frac{1}{R_{C_1}} \times \frac{A_{24}}{|A|} + \frac{1}{R_{C_2}} \times \frac{A_{34}}{|A|} \right) V_{CC} \tag{2.78}$$

To obtain first order nonlinear terms, we compare coefficients of $\varepsilon^{(1)}$ in equations (2.60)-(2.63). We have

$$v_E^{(1)} \left(\frac{1}{R_E} - \frac{I_0}{V_T(1-\alpha_1)} - \frac{I_0}{V_T(1-\alpha_2)} \right) = -\frac{(v_1 - v_E^{(0)})^2 I_0}{2V_T^2(1-\alpha_1)} - \frac{(v_2 - v_E^{(0)})^2 I_0}{2V_T^2(1-\alpha_2)} \tag{2.79}$$

$$v_{C_1}^{(1)} + q_L^{(1)} \left(R_L \frac{d}{dt} + \frac{1}{C_L} \right) + v_{C_2}^{(1)} = 0 \tag{2.80}$$

$$v_{C_1}^{(1)} \left(\frac{1}{R_{C_1}} \right) + q_L^{(1)} \left(\frac{d}{dt} \right) + v_E^{(1)} \left(-\frac{\beta_1 I_0}{V_T} \right) = -(v_1 - v_E^{(0)})^2 \left(\frac{\beta_1 I_0}{2V_T^2} \right) \tag{2.81}$$

$$v_{C_2}^{(1)} \left(\frac{1}{R_{C_2}} \right) + q_L^{(1)} \left(-\frac{d}{dt} \right) + v_E^{(1)} \left(-\frac{\beta_2 I_0}{V_T} \right) = -(v_2 - v_E^{(0)})^2 \left(\frac{\beta_2 I_0}{2V_T^2} \right) \tag{2.82}$$

$$X_1(s) = \begin{bmatrix} v_{C_1}^{(1)} & v_{C_2}^{(1)} & v_E^{(1)} & q_L^{(1)} \end{bmatrix} \tag{2.83}$$

$$v_{C_1}^{(1)} = \left\{ -\frac{I_0}{2V_T^2(1-\alpha_1)} \times \frac{A_{11}}{|A|} - \frac{\beta_1 I_0}{2V_T^2} \times \frac{A_{21}}{|A|} \right\} * (v_1 - v_E^{(0)})^2 + \left\{ -\frac{I_0}{2V_T^2(1-\alpha_2)} \times \frac{A_{11}}{|A|} - \frac{\beta_2 I_0}{2V_T^2} \times \frac{A_{31}}{|A|} \right\} * (v_2 - v_E^{(0)})^2 \tag{2.84}$$

$$v_{C_2}^{(1)} = \left\{ -\frac{I_0}{2V_T^2(1-\alpha_1)} \times \frac{A_{12}}{|A|} - \frac{\beta_1 I_0}{2V_T^2} \times \frac{A_{22}}{|A|} \right\} * (v_1 - v_E^{(0)})^2 + \left\{ -\frac{I_0}{2V_T^2(1-\alpha_2)} \times \frac{A_{12}}{|A|} - \frac{\beta_2 I_0}{2V_T^2} \times \frac{A_{32}}{|A|} \right\} * (v_2 - v_E^{(0)})^2 \tag{2.85}$$

2.2.2 Simulation Results for Differential Amplifier Circuit

Nonlinear equations derived for BJT DA have been implemented in MATLAB. Circuit element values used in simulations are: $V_{CC} = 12V$,$V_{EE} = -12V$, $R_{C_1} = 8k\Omega$, $R_{C_2} = 8k\Omega$, $R_E = 0.08k\Omega$, $R_L = 10k\Omega$, $C_L = 10\mu C$ and sampling time is 10μsec. Linear and first order nonlinear terms have been plotted for different amplitudes and input frequencies. Table 2.2 shows the percentage error due to linear term only for different input amplitudes and frequencies. Percentage distortion has been calculated using the expression as given in equation (2.43).

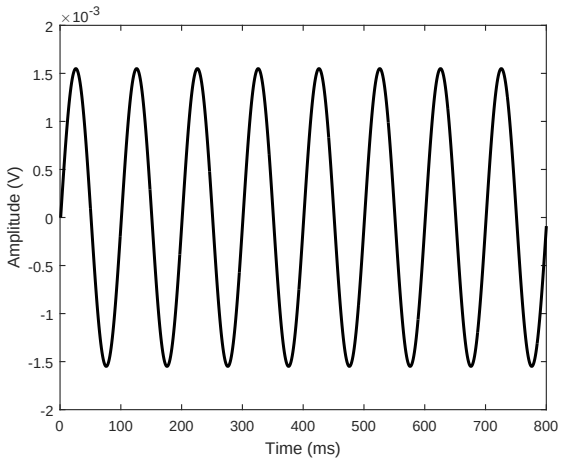

(a) Differential input to DA circuit.

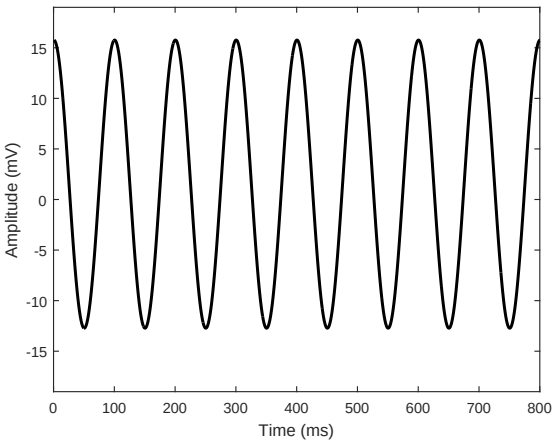

(b) Linear differential output voltage.

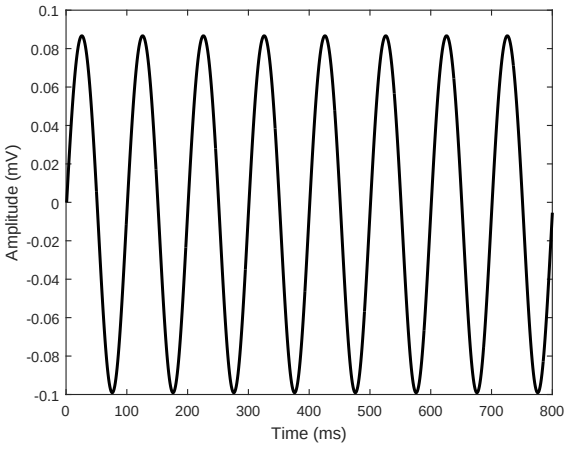

(c) First order nonlinear differential output voltage.

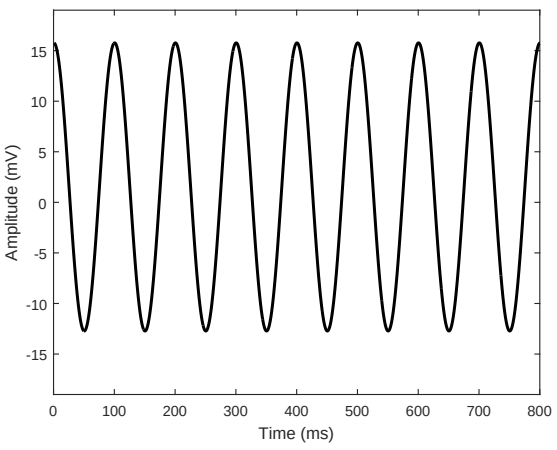

(d) Linear and nonlinear differential output voltage.

Figure 2.4: Differential amplifier output voltage.

Table 2.2: Differential Gain and Percentage Distortion

S. No.	Input at Q_1 (V)	Input at Q_2 (V)	V_{PP}, Peak to peak differential input (mV)	Frequency (Hz)	Gain (dB)	Percentage distortion
1.	1	1.001	2	100	23.49	0.642%
2.	1	1.0015	3	100	23.49	0.643%
3.	1	1.001	2	1000	23.50	0.644%
4.	1	1.0015	3	1000	23.50	0.650%
5.	1	1.001	2	10000	23.50	0.658%
6.	1	1.0015	3	10000	23.51	0.660%

2.3 Ebers-Moll Modelled Differential Amplifier Circuit Analysis Using Perturbation Method

2.3.1 Nonlinear Modelling of Ebers-Moll Modelled Differential Amplifier Circuit

After setting up the KVL and KCL equations for a BJT transistor circuit, we make second degree approximations to the Ebers-Moll exponential function and then use perturbation theory for nonlinear differential equation to obtain approximate solution to the state equations.

Following equations have been obtained for the differential amplifier circuit shown in Figure 2.5 by implementing Kirchhoff's laws.

$$v_{BE_1} + R_E(I_{E_1} + I_{E_2}) = v_1 + V_{EE} \tag{2.86}$$

$$v_{BE_2} + R_E(I_{E_1} + I_{E_2}) = v_2 + V_{EE} \tag{2.87}$$

$$v_{C_1} + R_{C_1} I_{C_1} = V_{CC} \tag{2.88}$$

$$v_{C_2} + R_{C_2} I_{C_2} = V_{CC} \tag{2.89}$$

$$I_{C_1}\left(1 + \frac{1}{\beta_1}\right) - I_{E_1} = 0 \tag{2.90}$$

$$I_{C_2}\left(1 + \frac{1}{\beta_2}\right) - I_{E_2} = 0 \tag{2.91}$$

where v_{B_1}, v_{C_1}, v_{E_1}, v_{B_2}, v_{C_2} and v_{E_2} are state variables. Equations (2.86)-(2.89) are obtained by KVL and equations (2.90)-(2.91) are obtained by KCL. Replacing transistor

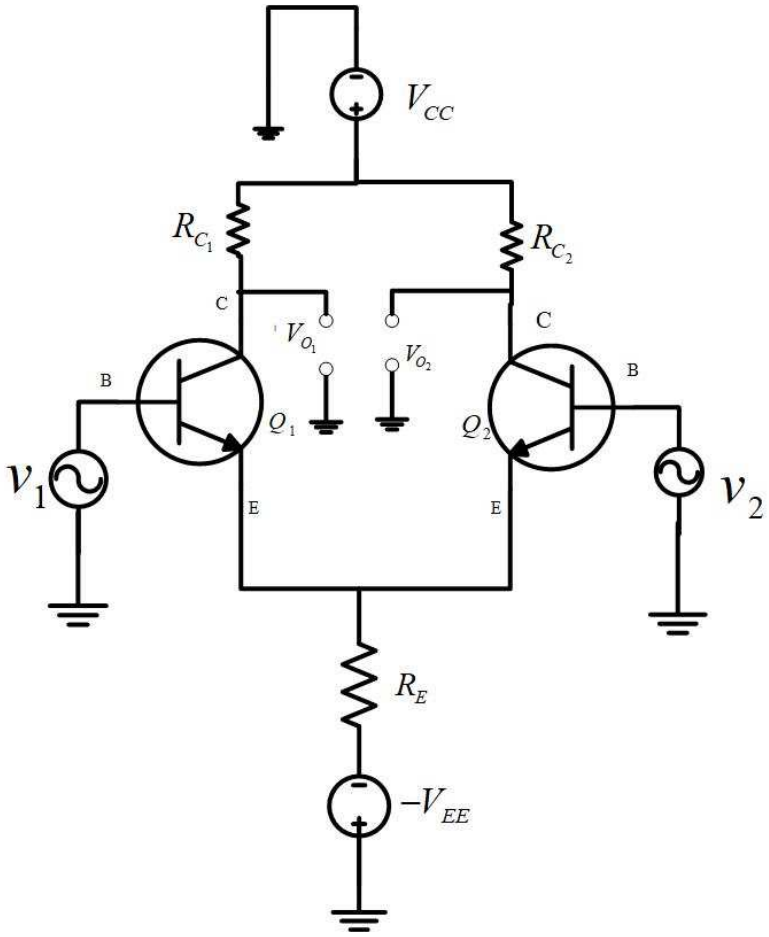

Figure 2.5: Differential amplifier circuit diagram.

circuit by Ebers-Moll model, the collector current I_C and the emitter current I_E can be written as

$$I_C = \alpha_F I_{ES}\left[exp\frac{v_{BE}}{V_T} - 1\right] - I_{CS}\left[exp\frac{v_{BC}}{V_T} - 1\right] \tag{2.92}$$

$$I_E = -I_{ES}\left[exp\frac{v_{BE}}{V_T} - 1\right] + \alpha_R I_{CS}\left[exp\frac{v_{BC}}{V_T} - 1\right] \tag{2.93}$$

I_{CS} and I_{ES} are reverse saturation currents at the collector and emitter junctions respectively. V_T is the thermal voltage. α_F and α_R are current gains in normal and inverted operation respectively. By separating the linear and nonlinear parts in above mentioned I_C and I_E expressions for two transistors Q_1 and Q_2, we have

$$\begin{aligned} I_{C_1} &= p_{11}v_{B_1}^{(0)} + p_{12}v_{C_1}^{(0)} + p_{13}v_{E_1}^{(0)} + \varepsilon f_1(v_{B_1}^{(0)}, v_{C_1}^{(0)}, v_{E_1}^{(0)} \\ &= p_{11}v_{B_1}^{(0)} + p_{12}v_{C_1}^{(0)} + p_{13}v_{E_1}^{(0)} + \varepsilon(q_{11}v_{B_1}^{2(0)} + q_{12}v_{C_1}^{2(0)} + q_{13}v_{E_1}^{2(0)} + q_{14}v_{B_1}^{(0)}v_{E_1}^{(0)} + q_{15}v_{B_1}^{(0)}v_{C_1}^{(0)}) \end{aligned} \tag{2.94}$$

$$I_{C_2} = p_{21}v_{B_2}^{(0)} + p_{22}v_{C_2}^{(0)} + p_{23}v_{E_2}^{(0)} + \varepsilon f_2(v_{B_2}^{(0)}, v_{C_2}^{(0)}, v_{E_2}^{(0)}) \tag{2.95}$$
$$= p_{21}v_{B_2}^{(0)} + p_{22}v_{C_2}^{(0)} + p_{23}v_{E_2}^{(0)} + \varepsilon(q_{21}v_{B_2}^{2(0)} + q_{22}v_{C_2}^{2(0)} + q_{23}v_{E_2}^{2(0)} + q_{24}v_{B_2}^{(0)}v_{E_2}^{(0)} + q_{25}v_{B_2}^{(0)}v_{C_2}^{(0)})$$

$$I_{E_1} = r_{11}v_{B_1}^{(0)} + r_{12}v_{C_1}^{(0)} + r_{13}v_{E_1}^{(0)} + \varepsilon g_1(v_{B_1}^{(0)}, v_{C_1}^{(0)}, v_{E_1}^{(0)}) \tag{2.96}$$
$$= r_{11}v_{B_1}^{(0)} + r_{12}v_{C_1}^{(0)} + r_{13}v_{E_1}^{(0)} + \varepsilon(s_{11}v_{B_1}^{2(0)} + s_{12}v_{C_1}^{2(0)} + s_{13}v_{E_1}^{2(0)} + s_{14}v_{B_1}^{(0)}v_{E_1}^{(0)} + s_{15}v_{B_1}^{(0)}v_{C_1}^{(0)})$$

$$I_{E_2} = r_{21}v_{B_2}^{(0)} + r_{22}v_{C_2}^{(0)} + r_{23}v_{E_2}^{(0)} + \varepsilon g_2(v_{B_2}^{(0)}, v_{C_2}^{(0)}, v_{E_2}^{(0)}) \tag{2.97}$$
$$= r_{21}v_{B_2}^{(0)} + r_{22}v_{C_2}^{(0)} + r_{23}v_{E_2}^{(0)} + \varepsilon(s_{21}v_{B_2}^{2(0)} + s_{22}v_{C_2}^{2(0)} + s_{23}v_{E_2}^{2(0)} + s_{24}v_{B_2}^{(0)}v_{E_2}^{(0)} + s_{25}v_{B_2}^{(0)}v_{C_2}^{(0)})$$

where f_1, f_2, g_1 and g_2 are quadratic functions of arguments. The p's, q's, r's and s's are

$$p_{11} = \frac{\alpha_{F_1}I_{ES_1}}{V_T} - \frac{I_{CS_1}}{V_T}, \quad p_{12} = \frac{I_{CS_1}}{V_T}, \quad p_{13} = -\frac{\alpha_{F_1}I_{ES_1}}{V_T}, \quad d_{12} = \frac{\alpha_{R_1}I_{CS_1}}{2V_T^2}$$
$$p_{21} = \frac{\alpha_{F_2}I_{ES_2}}{V_T} - \frac{I_{CS_2}}{V_T}, \quad p_{22} = \frac{I_{CS_2}}{V_T}, \quad p_{23} = -\frac{\alpha_{F_2}I_{ES_2}}{V_T}, \quad s_{13} = -\frac{I_{ES_1}}{2V_T^2},$$
$$q_{11} = \frac{\alpha_{F_1}I_{ES_1}}{2V_T^2} - \frac{I_{CS_1}}{2V_T^2}, \quad q_{12} = -\frac{I_{CS_1}}{2V_T^2}, \quad q_{13} = \frac{\alpha_{F_1}I_{ES_1}}{2V_T^2}, \quad s_{14} = \frac{I_{ES_1}}{V_T^2},$$
$$q_{21} = \frac{\alpha_{F_2}I_{ES_2}}{2V_T^2} - \frac{I_{CS_2}}{2V_T^2}, \quad q_{22} = -\frac{I_{CS_2}}{2V_T^2}, \quad q_{23} = \frac{\alpha_{F_2}I_{ES_2}}{2V_T^2}, \quad s_{15} = -\frac{\alpha_{R_1}I_{CS_1}}{V_T^2}$$
$$r_{11} = \frac{\alpha_{R_1}I_{CS_1}}{V_T} - \frac{I_{ES_1}}{V_T}, \quad r_{12} = -\frac{\alpha_{R_1}I_{CS_1}}{V_T}, \quad r_{13} = \frac{I_{ES_1}}{V_T}, \quad s_{22} = \frac{\alpha_{R_2}I_{CS_2}}{2V_T^2},$$
$$r_{21} = \frac{\alpha_{R_2}I_{CS_2}}{V_T} - \frac{I_{ES_2}}{V_T}, \quad q_{24} = -\frac{\alpha_{R_2}I_{ES_2}}{V_T^2}, \quad q_{25} = \frac{I_{ES_2}}{V_T^2}, \quad s_{23} = -\frac{I_{ES_2}}{2V_T^2},$$
$$s_{11} = \frac{\alpha_{R_1}I_{CS_1}}{2V_T^2} - \frac{I_{ES_1}}{2V_T^2}, \quad q_{14} = -\frac{\alpha_{F_1}I_{ES_1}}{V_T^2}, \quad q_{15} = \frac{I_{CS_1}}{V_T^2}, \quad s_{24} = \frac{I_{ES_2}}{V_T^2}$$
$$d_{21} = \frac{\alpha_{R_2}I_{CS_2}}{2V_T^2} - \frac{I_{ES_2}}{2V_T^2}, \quad r_{22} = -\frac{\alpha_{R_2}I_{CS_2}}{V_T}, \quad r_{23} = \frac{I_{ES_2}}{V_T}, \quad s_{25} = -\frac{\alpha_{R_2}I_{CS_2}}{V_T^2}.$$

Substituting the values of I_C, I_E and applying perturbation method, we have

$$v_{B_1} = v_{B_1}^{(0)} + \varepsilon v_{B_1}^{(1)} \tag{2.98}$$
$$v_{C_1} = v_{C_1}^{(0)} + \varepsilon v_{C_1}^{(1)} \tag{2.99}$$
$$v_{E_1} = v_{E_1}^{(0)} + \varepsilon v_{E_1}^{(1)} \tag{2.100}$$
$$v_{B_2} = v_{B_2}^{(0)} + \varepsilon v_{B_2}^{(1)} \tag{2.101}$$
$$v_{C_2} = v_{C_2}^{(0)} + \varepsilon v_{C_2}^{(1)} \tag{2.102}$$
$$v_{E_2} = v_{E_2}^{(0)} + \varepsilon v_{E_2}^{(1)} \tag{2.103}$$

where, $v_B^{(0)}$, $v_C^{(0)}$ and $v_E^{(0)}$ are the linear components of Ebers-Moll model and $v_B^{(1)}$, $v_C^{(1)}$ and $v_E^{(1)}$ are the nonlinear components of the Ebers-Moll model. Substituting these

expressions into the equations (2.86) - (2.91) of the amplifier circuit, we get

$$[v_{B_1}^{(0)}+\varepsilon v_{B_1}^{(1)}]-[v_{E_1}^{(0)}+\varepsilon v_{E_1}^{(1)}]+R_E[r_{11}v_{B_1}^{(0)}+r_{12}v_{C_1}^{(0)}+r_{13}v_{E_1}^{(0)}+\varepsilon(s_{11}v_{B_1}^{2(0)}+s_{12}v_{C_1}^{2(0)}+s_{13}v_{E_1}^{2(0)} +s_{14}v_{B_1}^{(0)}v_{E_1}^{(0)}+s_{15}v_{B_1}^{(0)}v_{C_1}^{(0)})]+[r_{21}v_{B_2}^{(0)}+r_{22}v_{C_2}^{(0)}+r_{23}v_{E_2}^{(0)}+\varepsilon(s_{21}v_{B_2}^{2(0)}+s_{22}v_{C_2}^{2(0)}+s_{23}v_{E_2}^{2(0)} +s_{24}v_{B_2}^{(0)}v_{E_2}^{(0)}+s_{25}v_{B_2}^{(0)}v_{C_2}^{(0)})]=v_1+V_{EE} \tag{2.104}$$

$$[v_{B_2}^{(0)}+\varepsilon v_{B_2}^{(1)}]-[v_{E_2}^{(0)}+\varepsilon v_{E_2}^{(1)}]+R_E[r_{11}v_{B_1}^{(0)}+r_{12}v_{C_1}^{(0)}+r_{13}v_{E_1}^{(0)}+\varepsilon(s_{11}v_{B_1}^{2(0)}+s_{12}v_{C_1}^{2(0)}+s_{13}v_{E_1}^{2(0)} +s_{14}v_{B_1}^{(0)}v_{E_1}^{(0)}+s_{15}v_{B_1}^{(0)}v_{C_1}^{(0)})]+[r_{21}v_{B_2}^{(0)}+r_{22}v_{C_2}^{(0)}+r_{23}v_{E_2}^{(0)}+\varepsilon(s_{21}v_{B_2}^{2(0)}+s_{22}v_{C_2}^{2(0)}+s_{23}v_{E_2}^{2(0)} +s_{24}v_{B_2}^{(0)}v_{E_2}^{(0)}+s_{25}v_{B_2}^{(0)}v_{C_2}^{(0)})]=v_2+V_{EE} \tag{2.105}$$

$$[v_{C_1}^{(0)}+\varepsilon v_{C_1}^{(1)}]+R_{C_1}[p_{11}v_{B_1}^{(0)}+p_{12}v_{C_1}^{(0)}+p_{13}v_{E_1}^{(0)}+\varepsilon(q_{11}v_{B_1}^{2(0)}+q_{12}v_{C_1}^{2(0)}+q_{13}v_{E_1}^{2(0)}+q_{14}v_{B_1}^{(0)}v_{E_1}^{(0)} +q_{15}v_{B_1}^{(0)}v_{C_1}^{(0)})]=V_{CC} \tag{2.106}$$

$$[v_{C_2}^{(0)}+\varepsilon v_{C_2}^{(1)}]+R_{C_2}[p_{21}v_{B_2}^{(0)}+p_{22}v_{C_2}^{(0)}+p_{23}v_{E_2}^{(0)}+\varepsilon(q_{21}v_{B_2}^{2(0)}+q_{22}v_{C_2}^{2(0)}+q_{23}v_{E_2}^{2(0)}+q_{24}v_{B_2}^{(0)}v_{E_2}^{(0)} +q_{25}v_{B_2}^{(0)}v_{C_2}^{(0)})]=V_{CC} \tag{2.107}$$

$$\left(1+\frac{1}{\beta_1}\right)[p_{11}v_{B_1}^{(0)}+p_{12}v_{C_1}^{(0)}+p_{13}v_{E_1}^{(0)}+\varepsilon(q_{11}v_{B_1}^{2(0)}+q_{12}v_{C_1}^{2(0)}+q_{13}v_{E_1}^{2(0)}+q_{14}v_{B_1}^{(0)}v_{E_1}^{(0)} +q_{15}v_{B_1}^{(0)}v_{C_1}^{(0)})]-[r_{11}v_{B_1}^{(0)}+r_{12}v_{C_1}^{(0)}+r_{13}v_{E_1}^{(0)}+\varepsilon(s_{11}v_{B_1}^{2(0)}+s_{12}v_{C_1}^{2(0)}+s_{13}v_{E_1}^{2(0)}+s_{14}v_{B_1}^{(0)}v_{E_1}^{(0)} +s_{15}v_{B_1}^{(0)}v_{C_1}^{(0)})]=0 \tag{2.108}$$

$$\left(1+\frac{1}{\beta_2}\right)[p_{21}v_{B_2}^{(0)}+p_{22}v_{C_2}^{(0)}+p_{23}v_{E_2}^{(0)}+\varepsilon(q_{21}v_{B_2}^{2(0)}+q_{22}v_{C_2}^{2(0)}+q_{23}v_{E_2}^{2(0)}+q_{24}v_{B_2}^{(0)}v_{E_2}^{(0)} +q_{25}v_{B_2}^{(0)}v_{C_2}^{(0)})]-[r_{21}v_{B_2}^{(0)}+r_{22}v_{C_2}^{(0)}+r_{23}v_{E_2}^{(0)}+\varepsilon(s_{21}v_{B_2}^{2(0)}+s_{22}v_{C_2}^{2(0)}+s_{23}v_{E_2}^{2(0)}+s_{24}v_{B_2}^{(0)}v_{E_2}^{(0)} +s_{25}v_{B_2}^{(0)}v_{C_2}^{(0)})]=0. \tag{2.109}$$

To obtain the linear expression, we compare the coefficients of $\varepsilon^{(0)}$ in equations (2.104)-(2.109), we get

$$v_{B_1}^{(0)}[1+R_Er_{11}]+v_{C_1}^{(0)}[R_Er_{12}]+v_{E_1}^{(0)}[-1+R_Er_{13}]+v_{B_2}^{(0)}[R_Er_{21}]+v_{C_2}^{(0)}[R_Er_{22}]+v_{E_2}^{(0)}[R_Er_{23}] =v_1+V_{EE} \tag{2.110}$$

$$v_{B_1}^{(0)}[R_E r_{11}] + v_{C_1}^{(0)}[R_E r_{12}] + v_{E_1}^{(0)}[R_E r_{13}] + v_{B_2}^{(0)}[1 + R_E r_{21}] + v_{C_2}^{(0)}[R_E r_{22}] + v_{E_2}^{(0)}[-1 + R_E c_{23}]$$
$$= v_2 + V_{EE} \tag{2.111}$$

$$v_{B_1}^{(0)}[R_{C_1} p_{11}] + v_{C_1}^{(0)}[1 + R_{C_1} p_{12}] + v_{E_1}^{(0)}[R_{C_1} p_{13}] = V_{CC} \tag{2.112}$$

$$v_{B_2}^{(0)}[R_{C_2} p_{21}] + v_{C_2}^{(0)}[1 + R_{C_2} p_{22}] + v_{E_2}^{(0)}[R_{C_2} p_{23}] = V_{CC} \tag{2.113}$$

$$v_{B_1}^{(0)}\left[\left(1 + \frac{1}{\beta_1}\right) p_{11} - r_{11}\right] + v_{C_1}^{(0)}\left[\left(1 + \frac{1}{\beta_1}\right) a_{12} - r_{12}\right] + v_{E_1}^{(0)}\left[\left(1 + \frac{1}{\beta_1}\right) p_{13} - r_{13}\right] = 0 \tag{2.114}$$

$$v_{B_2}^{(0)}\left[\left(1 + \frac{1}{\beta_2}\right) p_{21} - r_{21}\right] + v_{C_2}^{(0)}\left[\left(1 + \frac{1}{\beta_2}\right) p_{22} - r_{22}\right] + v_{E_2}^{(0)}\left[\left(1 + \frac{1}{\beta_2}\right) p_{23} - r_{23}\right] = 0. \tag{2.115}$$

Representing the unperturbed state vector as

$$X_0(s) = [v_{B_1}^{(0)}, v_{C_1}^{(0)}, v_{E_1}^{(0)}, v_{B_2}^{(0)}, v_{C_2}^{(0)}, v_{E_2}^{(0)}]^T$$

Using Laplace transform, we have

$$A(s)X_0(s) = B_1(s)v_1(s) + B_2(s)v_2(s) + D(s)V_{EE} + E(s)V_{CC}$$

where A(s) is a matrix-valued function of the complex variable s and $B_1(s)$, $B_2(s)$, $D(s)$ and $E(s)$ are vector-valued functions of the complex variable s. The solution is given by

$$X_0(s) = A^{-1}(s)B_1(s)v_1(s) + A^{-1}(s)B_2(s)v_2(s) + A^{-1}(s)D(s)V_{EE} + A^{-1}(s)E(s)V_{CC} \tag{2.116}$$

where matrix A is

$$A = \begin{bmatrix} x_{11} & x_{12} & x_{13} & x_{14} & x_{15} & x_{16} \\ x_{21} & x_{22} & x_{23} & x_{24} & x_{25} & x_{26} \\ x_{31} & x_{32} & x_{33} & x_{34} & x_{35} & x_{36} \\ x_{41} & x_{42} & x_{43} & x_{44} & x_{45} & x_{46} \\ x_{51} & x_{52} & x_{53} & x_{54} & x_{55} & x_{56} \\ x_{61} & x_{62} & x_{63} & x_{64} & x_{65} & x_{66} \end{bmatrix}.$$

where

$x_{11} = 1 + R_E r_{11}$, $x_{12} = R_E r_{12}$, $x_{13} = -1 + R_E r_{13}$, $x_{14} = R_E r_{21}$, $x_{15} = R_E r_{22}$,
$x_{16} = R_E r_{23}$, $x_{21} = R_E r_{11}$, $x_{22} = R_E r_{12}$, $x_{23} = R_{C_1} p_{13}$, $x_{24} = 1 + R_E r_{21}$,
$x_{25} = R_E r_{22}$, $x_{26} = -1 + R_E r_{23}$, $x_{31} = R_{C_1} p_{11}$, $x_{32} = 1 + R_{C_1} p_{12}$, $x_{33} = R_{C_1} p_{13}$

$x_{34}=0,\quad x_{35}=0,\quad x_{36}=0,\quad x_{41}=0,\quad x_{42}=0,$
$x_{43}=0,\quad x_{44}=R_{C_2}p_{21},\quad x_{45}=1+R_{C_2}a_{22},\quad x_{46}=R_{C_2}p_{23},\quad x_{51}=x_1p_{11}-r_{11},$
$x_{52}=x_1p_{12}-r_{12}, x_{53}=x_1p_{13}-r_{13}, x_{54}=0, x_{55}=0, x_{66}=0, x_{61}=0, x_{62}=0, x_{63}=0$
$x_{64}=\left(1+\frac{1}{\beta_2}\right)p_{21}-r_{21}, x_{65}=\left(1+\frac{1}{\beta_2}\right)p_{22}-r_{22}, x_{66}=\left(1+\frac{1}{\beta_2}\right)p_{23}-r_{23}$

$$B_1(s)=[1\quad 0\quad 0\quad 0\quad 0\quad 0]^T$$

$$B_2(s)=[0\quad 1\quad 0\quad 0\quad 0\quad 0]^T$$

$$D(s)=[1\quad 1\quad 0\quad 0\quad 0\quad 0]^T$$

$$E(s)=[0\quad 0\quad 1\quad 1\quad 0\quad 0]^T$$

The expression for $v_{B_1}^{(0)}$, $v_{C_1}^{(0)}$, $v_{E_1}^{(0)}$, $v_{B_2}^{(0)}$, $v_{C_2}^{(0)}$, $v_{E_2}^{(0)}$ are given by

$$v_{B_1}^{(0)}(t)=h_1^{(1)}*v_1(t)+g_1^{(1)}*v_2(t)+\Phi_1(t)+\Psi_1(t) \tag{2.117}$$
$$v_{C_1}^{(0)}(t)=h_2^{(1)}*v_1(t)+g_2^{(1)}*v_2(t)+\Phi_2(t)+\Psi_2(t) \tag{2.118}$$
$$v_{E_1}^{(0)}(t)=h_3^{(1)}*v_1(t)+g_3^{(1)}*v_2(t)+\Phi_3(t)+\Psi_3(t) \tag{2.119}$$
$$v_{B_2}^{(0)}(t)=h_4^{(1)}*v_1(t)+g_4^{(1)}*v_2(t)+\Phi_4(t)+\Psi_4(t) \tag{2.120}$$
$$v_{C_2}^{(0)}(t)=h_5^{(1)}*v_1(t)+g_5^{(1)}*v_2(t)+\Phi_5(t)+\Psi_5(t) \tag{2.121}$$
$$v_{E_2}^{(0)}(t)=h_6^{(1)}*v_1(t)+g_6^{(1)}*v_2(t)+\Phi_6(t)+\Psi_6(t) \tag{2.122}$$

where $*$ is convolution operator. The expressions for $H_1^{(1)}(s)$, $H_2^{(1)}(s)$, $H_3^{(1)}(s)$, $H_4^{(1)}(s)$, $H_5^{(1)}(s)$ and $H_6^{(1)}(s)$ are

$H_1^{(1)}(s)=\frac{A_{11}}{|A|}$, $H_2^{(1)}(s)=\frac{A_{12}}{|A|}$, $H_3^{(1)}(s)=\frac{A_{13}}{|A|}$, $H_4^{(1)}(t)=\frac{A_{14}}{|A|}$, $H_5^{(1)}(s)=\frac{A_{15}}{|A|}$, $H_6^{(1)}(s)=\frac{A_{16}}{|A|}$

The expressions for $G_1^{(1)}(s)$, $G_2^{(1)}(s)$, $G_3^{(1)}(s)$, $G_4^{(1)}(s)$, $G_5^{(1)}(s)$ and $G_6^{(1)}(s)$ are

$G_1^{(1)}(s)=\frac{A_{21}}{|A|}$, $G_2^{(1)}(s)=\frac{A_{22}}{|A|}$, $G_3^{(1)}(s)=\frac{A_{23}}{|A|}$, $G_4^{(1)}(s)=\frac{A_{24}}{|A|}$, $G_5^{(1)}(s)=\frac{A_{25}}{|A|}$, $G_6^{(1)}(s)=\frac{A_{26}}{|A|}$

where $|A|$ is Determinant of matrix A.

The expressions for $\Phi_1(s)$, $\Phi_2(s)$, $\Phi_3(s)$, $\Phi_4(t)$, $\Phi_5(s)$ and $\Phi_6(s)$ are

$\Phi_1(s)=\frac{A_{11}+A_{21}}{|A|}V_{EE}$, $\Phi_2(s)=\frac{A_{12}+A_{22}}{|A|}V_{EE}$, $\Phi_3(s)=\frac{A_{13}+A_{23}}{|A|}V_{EE}$, $\Phi_4(s)=\frac{A_{14}+A_{24}}{|A|}V_{EE}$,
$\Phi_5(s)=\frac{A_{15}+A_{25}}{|A|}V_{EE}$, $\Phi_6(s)=\frac{A_{16}+A_{26}}{|A|}V_{EE}$

And the expressions for $\Psi_1(s)$, $\Psi_2(s)$, $\Psi_3(s)$, $\Psi_4(s)$, $\Psi_5(s)$ and $\Psi_6(s)$ are

$\Psi_1(s)=\frac{A_{31}+A_{41}}{|A|}V_{CC}$, $\Psi_2(s)=\frac{A_{32}+A_{42}}{|A|}V_{CC}$, $\Psi_3(s)=\frac{A_{33}+A_{43}}{|A|}V_{CC}$, $\Psi_4(s)=\frac{A_{34}+A_{44}}{|A|}V_{CC}$,
$\Psi_5(s)=\frac{A_{35}+A_{45}}{|A|}V_{CC}$, $\Psi_6(s)=\frac{A_{36}+A_{46}}{|A|}V_{CC}$

The impulse response of the small signal model equivalent are

$$v_{B_1}^{(0)}(t) = n_1\delta(t) * v_1(t) + n_2\delta(t) * v_2(t) + n_3\delta(t)V_{EE} + n_4\delta(t)V_{CC} \tag{2.123}$$

$$v_{C_1}^{(0)}(t) = n_5\delta(t) * v_1(t) + n_6\delta(t) * v_2(t) + n_7\delta(t)V_{EE} + n_8\delta(t)V_{CC} \tag{2.124}$$

$$v_{E_1}^{(0)}(t) = n_9\delta(t) * v_1(t) + n_{10}\delta(t) * v_2(t) + n_{11}\delta(t)V_{EE} + n_{12}\delta(t)V_{CC} \tag{2.125}$$

$$v_{B_2}^{(0)}(t) = n_{13}\delta(t) * v_1(t) + n_{14}\delta(t) * v_2(t) + n_{15}\delta(t)V_{EE} + n_{16}\delta(t)V_{CC} \tag{2.126}$$

$$v_{C_2}^{(0)}(t) = n_{17}\delta(t) * v_1(t) + n_{18}\delta(t) * v_2(t) + n_{19}\delta(t)V_{EE} + n_{20}\delta(t)V_{CC} \tag{2.127}$$

$$v_{E_2}^{(0)}(t) = n_{21}\delta(t) * v_1(t) + n_{22}\delta(t) * v_2(t) + n_{23}\delta(t)V_{EE} + n_{24}\delta(t)V_{CC} \tag{2.128}$$

where

$n_1 = \frac{A_{11}}{|A|}$, $n_2 = \frac{A_{21}}{|A|}$, $n_3 = \frac{A_{11}+A_{21}}{|A|}$, $n_4 = \frac{A_{31}+A_{41}}{|A|}$

$n_5 = \frac{A_{12}}{|A|}$, $n_6 = \frac{A_{22}}{|A|}$, $n_7 = \frac{A_{12}+A_{22}}{|A|}$, $n_8 = \frac{A_{32}+A_{42}}{|A|}$

$n_9 = \frac{A_{13}}{|A|}$, $n_{10} = \frac{A_{23}}{|A|}$, $n_{11} = \frac{A_{13}+A_{23}}{|A|}$, $n_{12} = \frac{A_{33}+A_{43}}{|A|}$

$n_{13} = \frac{A_{14}}{|A|}$, $n_{14} = \frac{A_{24}}{|A|}$, $n_{17} = \frac{A_{14}+A_{24}}{|A|}$, $n_{16} = \frac{A_{34}+A_{44}}{|A|}$

$n_{17} = \frac{A_{15}}{|A|}$, $n_{18} = \frac{A_{25}}{|A|}$, $n_{19} = \frac{A_{15}+A_{25}}{|A|}$, $n_{20} = \frac{A_{35}+A_{45}}{|A|}$

$n_{21} = \frac{A_{16}}{|A|}$, $n_{22} = \frac{A_{26}}{|A|}$, $n_{23} = \frac{A_{16}+A_{26}}{|A|}$, $n_{24} = \frac{A_{36}+A_{46}}{|A|}$.

The nonlinear expressions are obtained by comparing the coefficients of $\varepsilon^{(1)}$ in equations (2.104)-(2.109).

$$A(s)X_1(s) = I_i(s)Z(s)$$

where i=1, 2, 3, 4 , $Z(s) = [U_{11}, U_{12}, U_{21}, U_{22}]$, $X_1(s) = L[x_1(t)]$,

$$X_1(s) = [v_{B_1}^{(1)}, v_{C_1}^{(1)}, v_{E_1}^{(1)}, v_{B_2}^{(1)}, v_{C_2}^{(1)}, v_{E_2}^{(1)}]^T$$

$$I_1(s) = [0, 0, -R_{C_1}, 0, -x_1, 0]^T$$

$$I_2(s) = [0, 0, 0, -R_{C_2}, 0, -x_2]^T$$

$$I_3(s) = [-R_E, -R_E, 0, 0, 1, 0]^T$$

$$I_4(s) = [-R_E, -R_E, 0, 0, 0, 1]^T$$

Here, L represents the Laplace transform operator. These first order state vectors have been written in terms of zeroth order state vectors to solve the nonlinear equations.

$$U_{11}(s) = L[u_{11}(t)] = L[f_1(v_{B_1}^{(0)}, v_{C_1}^{(0)}, v_{E_1}^{(0)}, v_{B_2}^{(0)}, v_{C_2}^{(0)}, v_{E_2}^{(0)})]$$

$$U_{12}(s) = L[u_{12}(t)] = L[f_2(v_{B_1}^{(0)}, v_{C_1}^{(0)}, v_{E_1}^{(0)}, v_{B_2}^{(0)}, v_{C_2}^{(0)}, v_{E_2}^{(0)})]$$

$$U_{21}(s) = L[u_{21}(t)] = L[g_1(v_{B_1}^{(0)}, v_{C_1}^{(0)}, v_{E_1}^{(0)}, v_{B_2}^{(0)}, v_{C_2}^{(0)}, v_{E_2}^{(0)})]$$

$$U_{22}(s) = L[u_{22}(t)] = L[g_2(v_{B_1}^{(0)}, v_{C_1}^{(0)}, v_{E_1}^{(0)}, v_{B_2}^{(0)}, v_{C_2}^{(0)}, v_{E_2}^{(0)})]$$

or

$$\begin{aligned} u_{11}(t) &= f_1(v_{B_1}^{(0)}, v_{C_1}^{(0)}, v_{E_1}^{(0)}, v_{B_2}^{(0)}, v_{C_2}^{(0)}, v_{E_2}^{(0)}) \\ &= (q_{11}v_{B_1}^{2(0)} + q_{12}v_{C_1}^{2(0)} + q_{13}v_{E_1}^{2(0)} + q_{14}v_{B_1}^{(0)}v_{E_1}^{(0)} + q_{15}v_{B_1}^{(0)}v_{C_1}^{(0)}) \end{aligned} \tag{2.129}$$

$$\begin{aligned} u_{12}(t) &= f_2(v_{B_1}^{(0)}, v_{C_1}^{(0)}, v_{E_1}^{(0)}, v_{B_2}^{(0)}, v_{C_2}^{(0)}, v_{E_2}^{(0)}) \\ &= (q_{21}v_{B_2}^{2(0)} + q_{22}v_{C_2}^{2(0)} + q_{23}v_{E_2}^{2(0)} + q_{24}v_{B_2}^{(0)}v_{E_2}^{(0)} + q_{25}v_{B_2}^{(0)}v_{C_2}^{(0)}) \end{aligned} \tag{2.130}$$

$$\begin{aligned} u_{21}(t) &= g_1(v_{B_1}^{(0)}, v_{C_1}^{(0)}, v_{E_1}^{(0)}, v_{B_2}^{(0)}, v_{C_2}^{(0)}, v_{E_2}^{(0)}) \\ &= (s_{11}v_{B_1}^{2(0)} + s_{12}v_{C_1}^{2(0)} + s_{13}v_{E_1}^{2(0)} + s_{14}v_{B_1}^{(0)}v_{E_1}^{(0)} + s_{15}v_{B_1}^{(0)}v_{C_1}^{(0)}) \end{aligned} \tag{2.131}$$

$$\begin{aligned} u_{22}(t) &= g_2(v_{B_1}^{(0)}, v_{C_1}^{(0)}, v_{E_1}^{(0)}, v_{B_2}^{(0)}, v_{C_2}^{(0)}, v_{E_2}^{(0)}) \\ &= (s_{21}v_{B_2}^{2(0)} + s_{22}v_{C_2}^{2(0)} + s_{23}v_{E_2}^{2(0)} + s_{24}v_{B_2}^{(0)}v_{E_2}^{(0)} + s_{25}v_{B_2}^{(0)}v_{C_2}^{(0)}) \end{aligned} \tag{2.132}$$

$$\begin{aligned} v_{C_1}^{(1)}(s) = &- \frac{R_{c_1}A_{32} + \left(1 + \frac{1}{\beta_1}\right)A_{52}}{|A|}U_{11}(s) - \left(\frac{R_{c_2}A_{42}}{|A|} + \frac{\left(1 + \frac{1}{\beta_2}\right)A_{62}}{|A|}\right)U_{12}(s) \\ &- \frac{R_EA_{12} + R_EA_{22} - A_{52}}{|A|} \times U_{21}(s) - \frac{R_EA_{12} + R_EA_{22} - A_{62}}{|A|}U_{22}(s) \end{aligned} \tag{2.133}$$

$$\begin{aligned} v_{C_2}^{(1)}(s) = &- \frac{R_{c_1}A_{35} + \left(1 + \frac{1}{\beta_1}\right)A_{55}}{|A|}U_{11}(s) - \frac{R_{c_2}A_{45}}{|A|}U_{12}(s) - \frac{\left(1 + \frac{1}{\beta_2}\right)A_{65}}{|A|}U_{12}(s) \\ &- \frac{R_EA_{15} + R_EA_{25} - A_{55}}{|A|} \times U_{21}(s) - \frac{R_EA_{15} + R_EA_{25} - A_{65}}{|A|}U_{22}(s). \end{aligned} \tag{2.134}$$

Thus the nonlinear output voltage expressions are:

$$v_{C_1}^{(1)}(t) = n_{25}\delta(t) * u_{11}(t) + n_{26}\delta(t) * u_{12}(t) + n_{27}\delta(t) * u_{21}(t) + n_{28}\delta(t) * u_{22}(t) \tag{2.135}$$

$$v_{C_2}^{(1)}(t) = n_{29}\delta(t) * u_{11}(t) + n_{30}\delta(t) * u_{12}(t) + n_{31}\delta(t) * u_{21}(t) + n_{32}\delta(t) * u_{22}(t) \quad (2.136)$$

where

$$n_{25} = -\frac{R_E A_{12} + R_E A_{22} - A_{52}}{|A|},\ n_{26} = -\frac{R_{c_1} A_{32} + \left(1 + \frac{1}{\beta_1}\right) A_{52}}{|A|},\ n_{27} = -\frac{R_{c_2} A_{42} + \left(1 + \frac{1}{\beta_2}\right) A_{62}}{|A|},$$
$$n_{31} = -\frac{R_E A_{15} + R_E A_{25} - A_{55}}{|A|},\ n_{30} = -\frac{R_{c_2} A_{45} + \left(1 + \frac{1}{\beta_2}\right) A_{65}}{|A|},\ n_{29} = -\frac{R_{c_1} A_{35} + \left(1 + \frac{1}{\beta_1}\right) A_{55}}{|A|},$$
$$n_{28} = -\frac{R_E A_{12} + R_E A_{22} - A_{62}}{|A|},\ n_{32} = -\frac{R_E A_{15} + R_E A_{25} - A_{65}}{|A|}.$$

It should be remarked here that we have approximated the exponential nonlinearity in the Ebers-Moll model by linear quadratic functions. This is a good enough approximation as our experiments show, provided the voltage swings are high to prevent linearization from giving good results, but not too high to require cubic approximation.

2.3.2 Simulation Results for Ebers-Moll Model Based Differential Amplifier Circuit

The zeroth and first order output voltages have been plotted for different input voltages and frequencies in MATLAB (Figure 2.6). The percentage distortion due to linear term only has been calculated using expression (2.43). Table 2.3 shows the percentage error distortion.

Table 2.3: Distortion error percentage for Ebers-Moll modelled differential amplifier.

S. No.	Input at Q_1 (V)	Input at Q_2 (V)	V_{PP}, Peak to peak differential input (mV)	Frequency (KHz)	Percentage distortion
1.	1	1.001	2	1	0.3516%
2.	1	1.0015	3	1	0.3518%
3.	1	1.001	2	1	0.3540%
4.	1	1.0015	3	10	0.3565%
5.	1	1.001	2	10	0.3566%
6.	1	1.0015	3	10	0.3568%

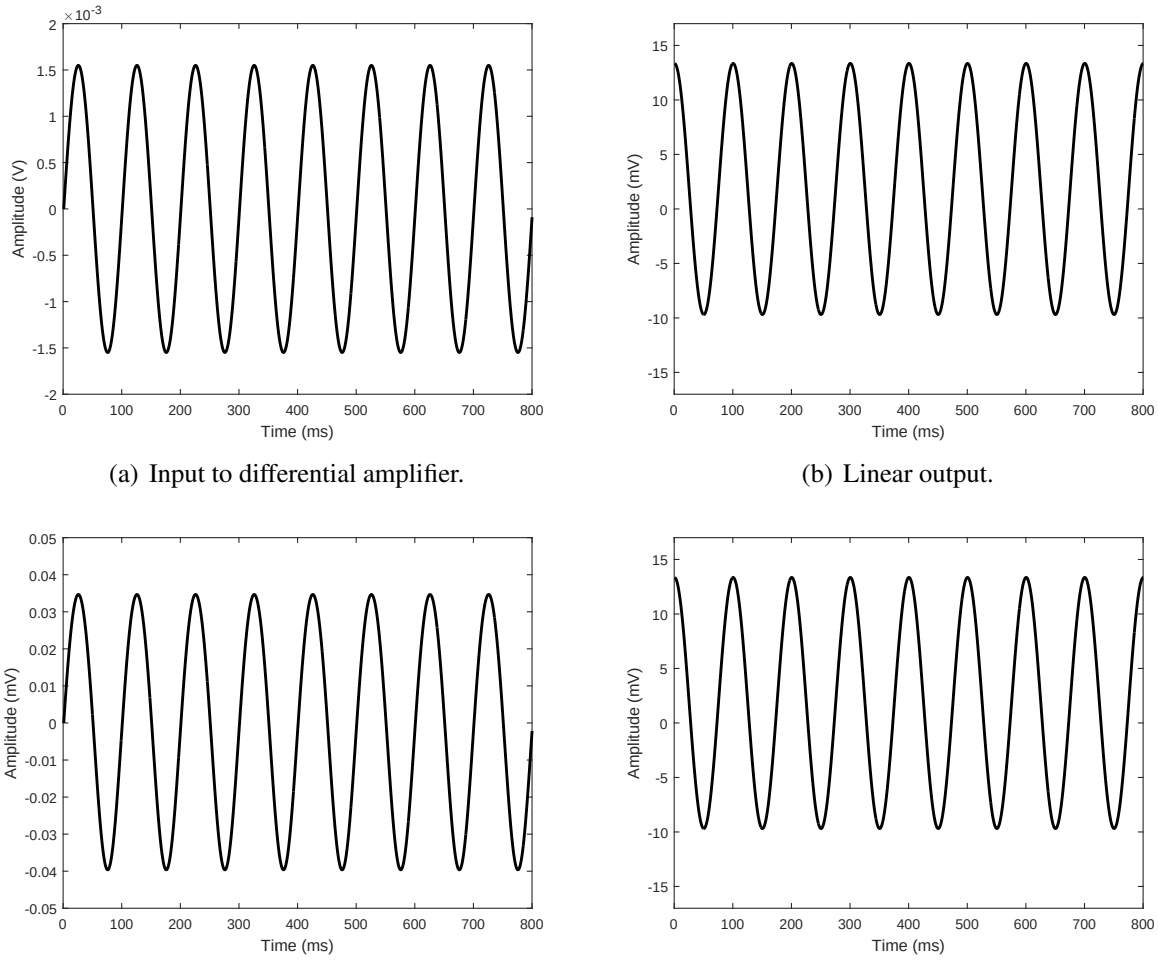

(a) Input to differential amplifier.

(b) Linear output.

(c) First order nonlinear output.

(d) Zero and first order output.

Figure 2.6: Ebers-Moll modelled differential amplifier output at input frequency 1000 Hz and peak to peak input 2 mV.

2.4 MOSFET Circuit Analysis Using Perturbation Method

2.4.1 Nonlinear Modelling of MOSFET Circuit

MOSFET circuit is shown in Figure 2.7(a). MOSFET equivalent EKV model is shown in Figure 2.7(b). Applying Kirchhoff's voltage law (KVL) and Kirchhoff's current law (KCL) and replacing the MOS transistor by EKV model [63] [64], we have:

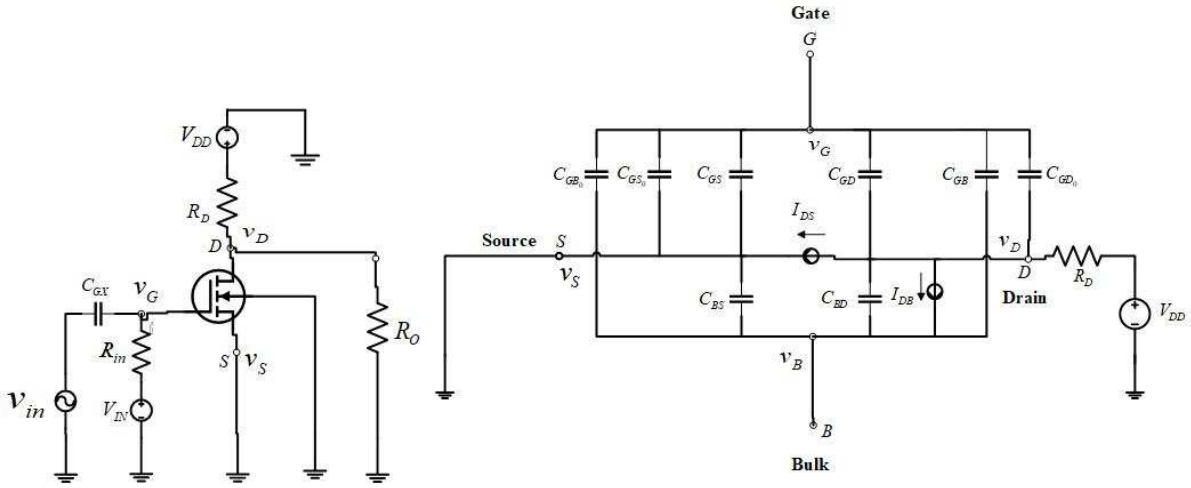

(a) MOSFET circuit diagram (b) EKV equivalent circuit for MOSFET.

Figure 2.7: MOSFET and its EKV equivalent circuit.

$$(C_{GS}+C_{GS_0})\left(\frac{dv_S(t)}{dt}-\frac{dv_G(t)}{dt}\right)+(C_{GD}+C_{GD_0})\times\left(\frac{dv_D(t)}{dt}-\frac{dv_G(t)}{dt}\right)+(C_{GB}+C_{GB_0})$$
$$\times\left(\frac{dv_B(t)}{dt}-\frac{dv_G(t)}{dt}\right)=0 \tag{2.137}$$

$$(C_{GD}+C_{GD_0})\left(\frac{dv_G(t)}{dt}-\frac{dv_D(t)}{dt}\right)+C_{BD}\left(\frac{dv_B(t)}{dt}-\frac{dv_D(t)}{dt}\right)=I_{DS}+I_{DB} \tag{2.138}$$

$$(C_{GS}+C_{GS_0})\left(\frac{dv_G(t)}{dt}-\frac{dv_S(t)}{dt}\right)+C_{BS}\left(\frac{dv_B(t)}{dt}-\frac{dv_S(t)}{dt}\right)=-I_{DS} \tag{2.139}$$

$$C_{GX}\left(\frac{dv_{in}}{dt}-\frac{dv_G(t)}{dt}\right)+\frac{V_{IN}-v_G(t)}{R_{in}}=0 \tag{2.140}$$

where $v_G(t)$, $v_S(t)$, $v_D(t)$ and $v_B(t)$ are the state variables. C_{GD}, C_{GS} and C_{GB} are the drain to channel capacitance, source to channel capacitance and base to channel

capacitance respectively. C_{OX} is oxide capacitance. Drain current I_D is

$$I_D = I_{DS} + I_{DB} \tag{2.141}$$

As $I_{DB} \cong 0$, therefore $I_D \cong I_{DS}$. From the EKV model of weak inversion, we have

$$I_D = I_{DS} = I_0 \frac{W}{L} e^{\frac{v_{GB}-V_{T_0}}{\eta U_T}} \left(e^{-\frac{v_{SB}}{U_T}} - e^{-\frac{v_{DB}}{U_T}} \right) \tag{2.142}$$

where $\frac{W}{L}$ is the aspect ratio, V_{T_0} and U_T are the equilibrium threshold voltage and thermal voltage respectively. I_0 is unary specific current. η is subthreshold slope factor.

Expanding (2.142) using Taylor series and retaining up to quadratic terms, we have

$$\begin{aligned} I_D = & \frac{I_0 W}{U_T L} \left\{ (v_D - v_S) \left(1 - \frac{V_{T_0}}{\eta U_T} + \frac{V_{T_0}^2}{2\eta^2 U_T^2} - \frac{1}{6} \frac{V_{T_0}^3}{\eta^3 U_T^3} \right) \right\} + \frac{I_0 W}{2 U_T^2 L} \left\{ \left(v_S^2 - v_D^2 \right. \right. \\ & \left. \left. -2(v_S v_B - v_D v_B) - v_D v_S + v_S v_D \right) \times \left(1 - \frac{V_{T_0}}{\eta U_T} + \frac{V_{T_0}^2}{2\eta^2 U_T^2} - \frac{1}{6} \frac{V_{T_0}^3}{\eta^3 U_T^3} \right) \right\} \\ & + \frac{I_0 W}{U_T L} \left\{ (v_G v_D - v_B v_D - v_G v_S + v_B v_S) \times \left(\frac{1}{\eta U_T} - \frac{V_{T_0}}{\eta^2 U_T^2} + \frac{3 V_{T_0}^2}{\eta^3 U_T^3} \right) \right\}. \end{aligned} \tag{2.143}$$

Using $C_{GS} + C_{GS_0} = C_S$, $C_{GD} + C_{GD_0} = C_D$ and $C_{GB} + C_{GB_0} = C_B$ and separating linear and first order nonlinear terms of state variables as:

$$v_G(t) = v_G^{(0)}(t) + \varepsilon v_G^{(1)}(t) \tag{2.144}$$

$$v_D(t) = v_D^{(0)}(t) + \varepsilon v_D^{(1)}(t) \tag{2.145}$$

$$v_S(t) = v_S^{(0)}(t) + \varepsilon v_S^{(1)}(t) \tag{2.146}$$

$$v_B(t) = v_B^{(0)}(t) + \varepsilon v_B^{(1)}(t) \tag{2.147}$$

where linear state variables are $v_G^{(0)}(t)$, $v_D^{(0)}(t)$, $v_S^{(0)}(t)$, $v_B^{(0)}(t)$ and first order nonlinear terms of state variables are $v_G^{(1)}(t)$, $v_D^{(1)}(t)$, $v_S^{(1)}(t)$, $v_B^{(1)}(t)$. Thus from (2.137)-(2.140) and (2.143)-(2.147), we have

$$\left\{ v_G^{(0)}(t) + \varepsilon v_G^{(1)}(t) \right\} \left(\frac{d}{dt} + \frac{1}{R_{in} C_{GX}} \right) = \frac{V_{IN}}{R_{in} C_{GX}} + v_{in}^{'} \tag{2.148}$$

$$C_D\frac{d\{v_G^{(0)}(t)+\varepsilon v_G^{(1)}(t)\}}{dt}+\{v_D^{(0)}(t)+\varepsilon v_D^{(1)}(t)\}\left(-C_D\frac{d}{dt}-C_{BD}\frac{d}{dt}-M_1\right)+M_1\{v_S^{(0)}(t)$$
$$+\varepsilon v_S^{(1)}(t)\}+C_{BD}\frac{d\{v_B^{(0)}(t)\}}{dt}+C_{BD}\frac{d\{\varepsilon v_B^{(1)}(t)\}}{dt}=M_1v_T\{v_S^{2(0)}(t)-v_D^{2(0)}(t)-2v_S^{(0)}v_B^{(0)}$$
$$+2v_D^{(0)}(t)v_B^{(0)}(t)\}+M_2\{v_G^{(0)}(t)v_D^{(0)}(t)-v_B^{(0)}(t)v_D^{(0)}(t)-v_G^{(0)}(t)v_S^{(0)}(t)+v_B(t)v_S(t)\} \quad (2.149)$$

$$C_S\frac{d\{v_G^{(0)}(t)+\varepsilon v_G^{(1)}(t)\}}{dt}+\{v_S^{(0)}(t)+\varepsilon v_S^{(1)}(t)\}\left(-C_S\frac{d}{dt}-C_{BS}\frac{d}{dt}-M_1\right)+M_1\{v_D^{(0)}(t)$$
$$+\varepsilon v_D^{(1)}(t)\}+C_{BS}\frac{d\{v_B^{(0)}(t)\}}{dt}+C_{BS}\frac{d\{\varepsilon v_B^{(1)}(t)\}}{dt}=-M_1v_T\{v_S^{2(0)}(t)-v_D^{2(0)}(t)-2v_Sv_B$$
$$+2v_D(t)v_B(t)\}-M_2\{v_G^{(0)}(t)v_D^{(0)}(t)-v_B^{(0)}(t)v_D^{(0)}(t)-v_G^{(0)}(t)v_S^{(0)}(t)+v_B^{(0)}(t)v_S^{(0)}(t)\} \quad (2.150)$$

$$\{v_G^{(0)}(t)+\varepsilon v_G^{(1)}(t)\}(-C_G-C_D-C_B)+C_D\{v_D^{(0)}+\varepsilon v_D^{(1)}\}+C_S\{v_S^{(0)}(t)+\varepsilon v_S^{(1)}(t)\}$$
$$+C_B\{v_B^{(0)}(t)+\varepsilon v_B^{(1)}(t)\}=0 \quad (2.151)$$

where

$$M_1=\frac{I_0}{U_T}\frac{W}{L}\left(1-\frac{V_{T_0}}{\eta U_T}+\frac{V_{T_0}^2}{2\eta^2U_T^2}-\frac{1}{6}\frac{V_{T_0}^3}{\eta^3U_T^3}\right)$$

$$M_2=\frac{I_0}{U_T}\frac{W}{L}\left(\frac{1}{\eta U_T}-\frac{V_{T_0}}{\eta^2U_T^2}+\frac{V_{T_0}^2}{2\eta^3U_T^3}\right)$$

and $v_{in}^{'}=\frac{dv_{in}}{dt}$.

Comparing $\varepsilon^{(0)}$ terms in (2.148)-(2.151) to obtain zeroth order terms

$$v_G^{(0)}(t)\left(\frac{d}{dt}+\frac{1}{R_{in}C_{GX}}\right)=\frac{V_{IN}}{R_{in}C_{GX}}+v_{in}^{'} \quad (2.152)$$

$$C_D\frac{dv_G^{(0)}(t)}{dt}+v_D^{(0)}(t)\left(-C_D\frac{d}{dt}-C_{BD}\frac{d}{dt}-M_1\right)+M_1v_S^{(0)}(t)+C_{BD}\frac{dv_B^{(0)}(t)}{dt}=0 \quad (2.153)$$

$$C_S\frac{dv_G^{(0)}(t)}{dt}+v_S^{(0)}(t)\left(-C_S\frac{d}{dt}-C_{BS}\frac{d}{dt}-M_1\right)+M_1v_D^{(0)}(t)+C_{BS}\frac{dv_B^{(0)}(t)}{dt}=0 \quad (2.154)$$

$$v_G^{(0)}(t)(-C_G - C_D - C_B) + C_D v_D^{(0)}(t) + C_S v_S^{(0)}(t) + C_B v_B^{(0)}(t) = 0 \tag{2.155}$$

Laplace transformed equation is

$$\mathbf{A}_1(s)\mathbf{x}^{(0)}(s) = \mathbf{B}_1(s)u_1(s) \tag{2.156}$$

where s is complex variable and $u_1 = \left(\frac{V_{IN}}{R_{in}C_{GX}} + v_{in}^{'}\right)$. State vector $\mathbf{x}^{(0)}(s)$ is

$$\mathbf{x}^{(0)}(s) = \begin{bmatrix} v_G^{(0)}(s) & v_D^{(0)}(s) & v_S^{(0)}(s) & v_B^{(0)}(s) \end{bmatrix}^T,$$

Where $\mathbf{A}_1(s)$ is

$$\mathbf{A}_1(s) = \begin{bmatrix} A_{1a} & 0 & 0 & 0 \\ sC_D & A_{1b} & M_1 & sC_{BD} \\ sC_S & M_1 & A_{1c} & sC_{BS} \\ A_{1d} & C_D & C_S & C_B \end{bmatrix}, \tag{2.157}$$

where
$A_{1a} = \left(s + \frac{1}{R_{in}C_{GX}}\right), \qquad A_{1_b} = (-sC_D - sC_{BD} - M_1),$
$A_{1c} = (-sC_S - sC_{BS} - M_1), \quad A_{1d} = -C_G - C_D - C_B$
where $\mathbf{B}_1(s)$ is

$$\mathbf{B}_1(s) = \begin{bmatrix} 1 & 0 & 0 & 0 \end{bmatrix}^T$$

Solution of (2.156) is given by

$$\mathbf{x}^{(0)}(s) = \mathbf{A}_1^{-1}(s)\mathbf{B}_1(s)u_1(s) \tag{2.158}$$

Impulse responses of linear model are

$$v_G{}^{(0)}(t) = \frac{A_{11}}{|\mathbf{A}_1|} * u_1(t) \tag{2.159}$$

$$v_D{}^{(0)}(t) = \frac{A_{12}}{|\mathbf{A}_1|} * u_1(t) \tag{2.160}$$

$$v_S{}^{(0)}(t) = \frac{A_{13}}{|\mathbf{A}_1|} * u_1(t) \tag{2.161}$$

$$v_B{}^{(0)}(t) = \frac{A_{14}}{|\mathbf{A}_1|} * u_1(t) \tag{2.162}$$

where $*$ is convolution operator. $A_{11}, A_{12}...A_{44}$ are the cofactors of matrix $\mathbf{A}_1$ and $|\mathbf{A}_1|$ is the determinant of matrix $\mathbf{A}_1$.

$$v_G{}^{(0)}(t) = e^{-\frac{1}{R_{in}C_{GX}}t}u(t) * u_1(t) \tag{2.163}$$

$$v_D{}^{(0)}(t) = \left[\frac{M_5}{M_3}m_1 e^{-\frac{1}{R_{in}C_{GX}}t}u(t) + \frac{M_5}{M_3}m_2 e^{-\frac{M_1M_4}{M_3}t}u(t)\right] * u_1(t) \tag{2.164}$$

$$v_S{}^{(0)}(t) = \left[\frac{M_7}{M_3}m_3 e^{-\frac{1}{R_{in}C_{GX}}t}u(t) + \frac{M_7}{M_3}m_4 e^{-\frac{M_1M_4}{M_3}t}u(t)\right] * u_1(t) \tag{2.165}$$

$$v_B{}^{(0)}(t) = \left[\frac{M_9}{M_3}m_5 e^{-\frac{1}{R_{in}C_{GX}}t}u(t) + \frac{M_9}{M_3}m_6 e^{-\frac{M_1M_4}{M_3}t}u(t)\right] * u_1(t) \tag{2.166}$$

where

$$\begin{aligned}
M_3 &= (C_DC_BC_S + C_DC_BC_{BS} + C_SC_BC_{BS} + C_DC_{BD}C_{BS} + C_DC_SC_{BS} + C_SC_{BD}C_{BS})\\
M_4 &= \{C_BC_D + C_BC_{BD} + C_BC_S + C_BC_{BS} + C_SC_{BS} + C_DC_{BS} + C_SC_{BD} + C_DC_{BD}\}\\
M_5 &= \left\{C_DC_BC_S + C_DC_BC_{BS} + C_DC_SC_{BS} + C_{BD}(C_S + C_{BS})(C_S + C_D + C_{BD}) - C_S^2C_{BD}\right\}\\
M_6 &= \{C_DC_B + C_SC_B + C_SC_{BS} + C_BC_{BS} + C_DC_{BS} + C_{BD}(C_S + C_D + C_{BD})\}\\
M_7 &= \left\{-C_D^2B_S + (C_D + C_{BD})(C_SC_B + C_SC_{BS} + C_BC_{BS} + C_DC_{BS}) + C_SC_DC_{BD}\right\}\\
M_8 &= (C_BC_D + C_BC_S + C_SC_{BS} + C_BC_{BS} + C_DC_{BS} + C_SC_{BD} + C_BC_{BD} + C_DC_{BD})\\
M_9 &= (C_SC_DC_{BS} + C_SC_{BD}C_{BS} + C_SC_DC_{BD} + C_DC_{BD}C_{BS} + C_SC_BC_D + C_BC_DC_{BS}\\
&\quad + C_SC_{BD}C_B + C_BC_{BD}C_{BS})\\
M_{10} &= \{C_SC_{BD} + C_SC_{BS} + C_DC_{BD} + C_DC_{BS} + C_DC_B + C_BC_{BD} + C_SC_B + C_BC_{BS}\}
\end{aligned}$$

$$m_1 = \frac{\left(-\frac{1}{R_{in}C_{GX}} + \frac{k_1k_6}{k_5}\right)}{\left(-\frac{1}{R_{in}C_{GX}} + \frac{k_1k_4}{k_3}\right)}, \qquad m_2 = \frac{\left(-\frac{k_1k_4}{k_3} + \frac{k_1k_6}{k_5}\right)}{\left(\frac{1}{R_{in}C_{GX}} - \frac{k_1k_4}{k_3}\right)}, \qquad m_3 = \frac{\left(-\frac{1}{R_{in}C_{GX}} + \frac{k_1k_8}{k_7}\right)}{\left(-\frac{1}{R_{in}C_{GX}} + \frac{k_1k_4}{k_3}\right)},$$
$$m_4 = \frac{\left(-\frac{k_1k_4}{k_3} + \frac{k_1k_8}{k_7}\right)}{\left(\frac{1}{R_{in}C_{GX}} - \frac{k_1k_4}{k_3}\right)}, \qquad m_5 = \frac{\left(-\frac{1}{R_{in}C_{GX}} + \frac{k_1k_{10}}{k_9}\right)}{\left(-\frac{1}{R_{in}C_{GX}} + \frac{k_1k_4}{k_3}\right)}, \qquad m_6 = \frac{\left(-\frac{k_1k_4}{k_3} + \frac{k_1k_{10}}{k_9}\right)}{\left(\frac{1}{R_{in}C_{GX}} - \frac{k_1k_4}{k_3}\right)}.$$

Comparing $\varepsilon^{(1)}$ terms in (2.148)-(2.151) to obtain first order nonlinear terms, we have

$$v_G^{(1)}(t)\left(\frac{d}{dt} + \frac{1}{R_{in}C_{GX}}\right) = 0 \tag{2.167}$$

$$C_D\frac{dv_G^{(1)}(t)}{dt}+v_D^{(1)}(t)\left(-C_D\frac{d}{dt}-C_{BD}\frac{d}{dt}-M_1\right)+M_1v_S^{(1)}+C_{BD}\frac{dv_B^{(1)}(t)}{dt}=M_1v_T\{v_S^{2(0)}(t)$$
$$-v_D^{2(0)}(t)-2v_S^{(0)}v_B^{(0)}+2v_D^{(0)}(t)v_B^{(0)}(t)\}+M_2\{v_G^{(0)}(t)v_D^{(0)}(t)-v_B^{(0)}(t)v_D^{(0)}(t)-v_G^{(0)}(t)v_S^{(0)}(t)$$
$$+v_B^{(0)}(t)v_S^{(0)}(t)\} \tag{2.168}$$

$$C_S\frac{dv_G^{(1)}(t)}{dt}+v_S^{(1)}(t)\left(-C_S\frac{d}{dt}-C_{BS}\frac{d}{dt}-M_1\right)+M_1v_D^{(1)}=C_{BS}\frac{dv_B^{(1)}(t)}{dt}-M_1v_T\{v_S^{2(0)}(t)$$
$$-v_D^{2(0)}(t)-2v_S^{(0)}v_B^{(0)}+2v_D^{(0)}(t)v_B^{(0)}(t)\}-M_2\{v_G^{(0)}(t)v_D^{(0)}(t)-v_B^{(0)}(t)v_D^{(0)}(t)-v_G^{(0)}(t)v_S^{(0)}(t)$$
$$+v_B^{(0)}(t)v_S^{(0)}(t)\} \tag{2.169}$$

$$v_G^{(1)}(t)(-C_G-C_D-C_B)+C_Dv_D^{(1)}(t)+C_Sv_S^{(1)}(t)+C_Bv_B^{(1)}(t)=0. \tag{2.170}$$

Laplace transformed equation is

$$\mathbf{A}_2(s)\mathbf{x}^{(1)}(s)=\mathbf{B}_2(s)u_2(s). \tag{2.171}$$

State vector $\mathbf{x}^{(1)}(s)$ is

$$\mathbf{x}^{(1)}(s)=\begin{bmatrix} v_G^{(1)}(s) & v_D^{(1)}(s) & v_S^{(1)}(s) & v_B^{(1)}(s)\end{bmatrix}^T$$

where $\mathbf{A}_2(s)$ is

$$\mathbf{A}_2(s)=\begin{bmatrix} A_{2a} & 0 & 0 & 0\\ sC_D & A_{2b} & M_1 & sC_{BD}\\ sC_S & M_1 & A_{2c} & sC_{BS}\\ A_{2d} & C_D & C_S & C_B\end{bmatrix}, \tag{2.172}$$

where

$A_{2a}=\left(s+\frac{1}{R_{in}C_{GX}}\right)$, $A_{2b}=(-sC_D-sC_{BD}-M_1)$,
$A_{2c}=(-sC_S-sC_{BS}-M_1)$, $A_{2d}=-C_G-C_D-C_B$
and $\mathbf{B}_2(s)$ is

$$\mathbf{B}_2(s)=\begin{bmatrix} 0 & 1 & -1 & 0\end{bmatrix}^T$$

Solution of (2.171) is

$$\mathbf{x}^{(1)}(s) = \mathbf{A}_2^{-1}(s)\mathbf{B}_2(s)u_2(s). \tag{2.173}$$

The first order nonlinear output is

$$v_D{}^{(1)}(t) = \frac{A_{22}}{|\mathbf{A}_2|} * u_2(t) - \frac{A_{32}}{|\mathbf{A}_2|} * u_2(t) = -\frac{M_{11}}{M_3} e^{-\frac{M_1 M_4}{M_3} t} * u_2(t) \tag{2.174}$$

where

$$u_2(t) = M_1 v_T \{v_S^{2(0)}(t) - v_D^{2(0)}(t) - 2v_S^{(0)}(t)v_B^{(0)}(t) + 2v_D^{(0)}\} \times v_B^{(0)}(t) - M_2\{v_G^{(0)}(t)v_D^{(0)}(t) - v_B^{(0)}(t)v_D^{(0)}(t) - v_G^{(0)}(t)v_S^{(0)}(t) + v_B^{(0)}(t)v_S^{(0)}(t)\}$$

$M_{11} = C_B C_S + C_B C_{BS} + C_S C_{BS} + C_B C_{BD}$.

2.4.2 Simulation Results for MOSFET Circuit

The linear and nonlinear expressions derived have been simulated in MATLAB for different input amplitude values and different frequencies. Parameters used for simulations are: $U_T = 0.0256V$, $V_{T_0} = 0.5V$, $R_{in} = 5k\Omega$, $C_{GX} = 6.0 \times 10^{-10}$, $C_S = 0.5 \times 10^{-9}F$, $C_D = 1.0 \times 10^{-9}F$, $C_B = 1.5 \times 10^{-10}F$, $C_{BS} = 1 \times 10^{-11}F$, $C_{BD} = 1.15 \times 10^{-9}F$, $I_0 = 1.0 \times 10^{-9}A$ and $\eta = 1$. Figure 2.8 shows linear and nonlinear output voltage for $20mV$ peak to peak input. Table 2.4 shows the percentage distortion error due to use of linear term only. Percentage distortion is calculated using (2.43).

Table 2.4: Percentage distortion when different voltage amplitude and frequency is given at input of MOSFET circuit.

S. No.	Input voltage (V)	Input frequency	Percentage distortion
1.	0.010	100	0.062%
2.	0.010	1000	0.063%
3.	0.010	10000	0.066%
4.	0.025	100	0.067%
5.	0.025	1000	0.068%
6.	0.025	10000	0.071%

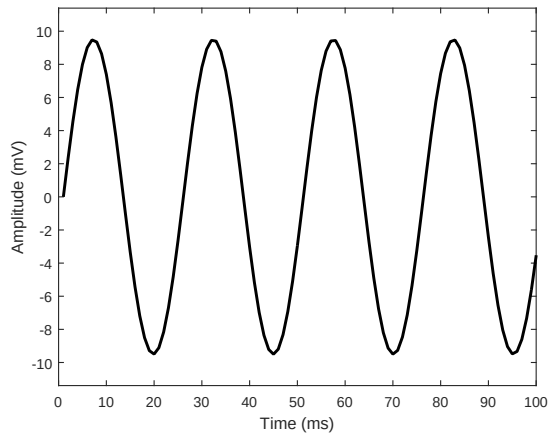

(a) Input to MOSFET circuit.

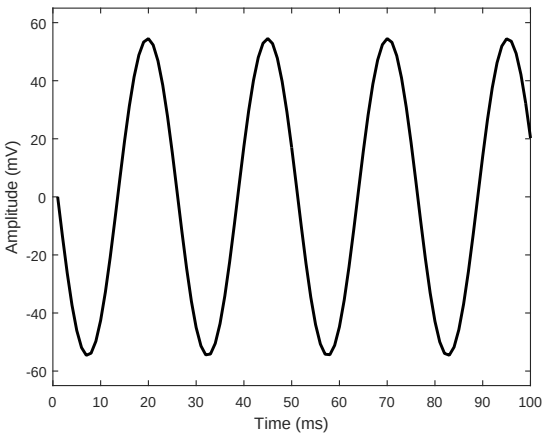

(b) Zeroth order output voltage.

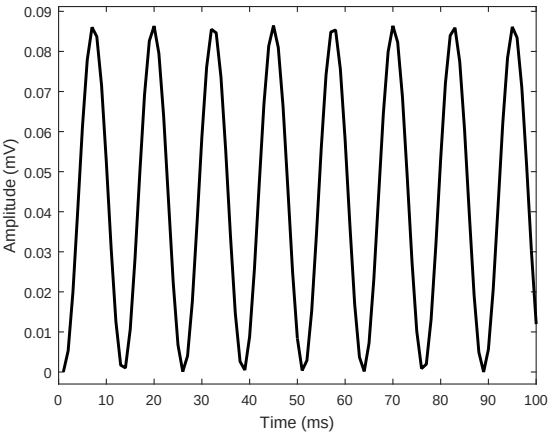

(c) First order output voltage.

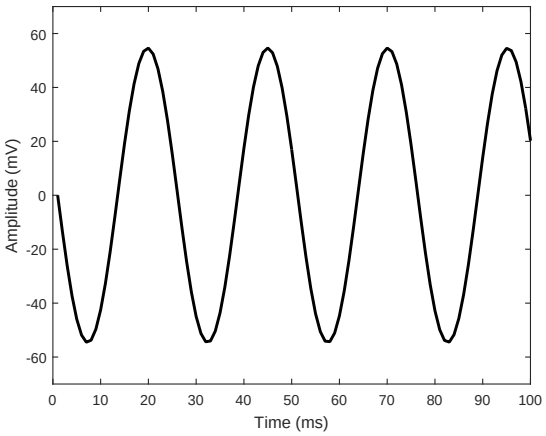

(d) Zeroth and first order output voltage.

Figure 2.8: MOSFET output voltage for sinusoidal input with peak to peak value 20mV.

Chapter 3

Extended Kalman Filter Based State Estimation of Analog Circuits

---

This chapter[1] presents the implementation of extended Kalman filter (EKF) for estimation of output voltage of following two circuits:-

(i) MOSFET circuit.

(ii) Bipolar junction transistor (BJT) differential amplifier (DA) circuit.

Kirchhoff's current law (KCL) and Enz-Krummenacher-Vittoz (EKV) model of MOSFET have been used to obtain the state space model of the MOSFET circuit as the maximal precision of simulation needs modelling of electronic circuit in terms of circuit components and device parameters. Ebers-Moll model, KCL and Kirchhoff's voltage law (KVL) have been used to obtain the state space model of BJT DA circuit. The proposed method has been compared with the recursive least squares (RLS) method [46]. Simulation results illustrate the better accuracy of estimation using EKF as compared to the RLS method.

Various methods have been used for state estimation. Kamas and Sanders [65] used the Lyapunov function-based state estimation method for power electronic circuits. Beadle and Djuric [66] presented weighted Bayesian bootstrap filter for state

[1]This chapter comprises the content which is based on research article (i) Extended Kalman filter based state estimation of MOSFET circuit, COMPEL, doi.org/10.1108/COMPEL09-2018-0367, 2019. (ii) Bansal R, Majumdar S. State estimation of differential amplifier circuit using EKF. (Communicated).

estimation of nonlinear model. This filter has the advantage that it is not limited by linear or Gaussian noise assumption. Chen *et al.* [67] proposed weighted least absolute value state estimation together with transformations for state estimation of the power system. Yu *et al.* [68] proposed an adaptive Kalman filter (KF) for dynamic harmonic state estimation. This filter has the advantage that it does not require the knowledge of the noise covariance matrix which is essential for KF. Kyriakides *et al.* [69] proposed the Huber function technique which is used for power application. Zhao *et al.* [70] presented forecasting aided state estimation for power system, which is based on generalized maximum likelihood estimator in which spatial and temporal correlations are also considered. In this way, it presents more accurate results. This method has the advantage of good efficiency and robustness. Rana *et al.* [71] proposed distributed dynamic state estimation for microgrids. The main advantage of the method is that it requires small iterations for good estimation. Kong *et al.* [72] proposed three stage estimation method for AC-DC distribution networks. The method has the advantage of smaller computational complexity as compared to the centralized state estimation method and it has better accuracy as compared to other conventional methods. Sutivong *et al.* [73] proposed the state estimation of Gaussian channels which are state dependent. The method uses power sharing to obtain the optimal solution. Zhao *et al.* [74] presented state estimation method for false data injection attack on power system. They used vector relaxing error for state estimation. Netto and Mil [75] proposed Kalman filter for state estimation of power system, which is based on generalized maximum likelihood (GM) Koopman operator. This method has the advantage of data driven and model independent approach. Zhao [76] presented for extended Kalman filter for dynamic estimation that considers model uncertainties also. Zheng *et al.* [77] proposed distributed robust bilinear method for state estimation of power system. The method has the advantage of compressing the bad measurements. Yu *et al.* [78] proposed an filter based approach that estimates static and dynamic states of power system. Wang *et al.* [79] developed integrated state estimation and control method for management of battery used for power grid systems. Cao *et al.* [80] proposed state estimation for cyber physical systems, where the performance of estimation depends on the quality of wireless communication. This method has the better performance as compared to the estimation based on random mechanism. Li *et al.* [81] proposed state estimation of frequency traffic which uses ensemble learning framework to macroscopic traffic flow model. Farnoosh *et al.* [82] presented parameter estimation of RL circuit using the least squares and Bayesian approach. The EKF

has several advantages [83] - [88]. Hu and Gallacher [87] presented the parameter estimation of ring vibratory gyroscope using EKF. Paschero *et al.* [88] proposed the multi cell EKF for state of charge estimation of an energy storage system.

The output voltage estimation i.e. state estimation of MOSFET is proposed using EKF in Section 3.1.2. The EKF described in appendix Section A.2 has been used in this section. The estimation using EKF requires the state space modelling of the circuit which has been derived for two different modes of MOSFET. They are conduction mode and saturation mode. The derivation of state space representation uses KCL and EKV model of the transistor. The EKV model is shown in Figure 3.1 (b). The estimation using EKF has been compared with RLS method and PSPICE simulated values in Section 3.1.3. The Section 3.2.1 deals with the derivation of state space representation of DA circuit. This representation is used for state estimation the circuit using EKF in Section 3.2.2. Finally, some general remarks have been discussed at the end of Section 3.2.3. The innovation process and the effect of small measurement noise are discussed in this section.

3.1 State Estimation of MOSFET Circuit

The MOSFET circuit is shown in Figure 3.1(a). The EKV model of the MOSFET circuit is shown in Figure 3.1(b). Applying KCL to the circuit, we have

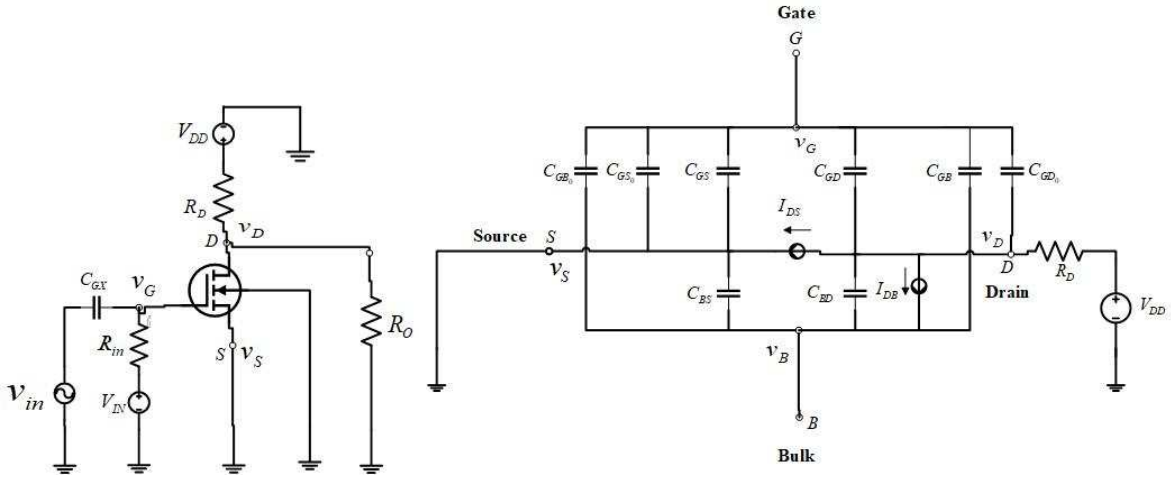

(a) MOSFET circuit diagram (b) EKV equivalent circuit for MOSFET.

Figure 3.1: MOSFET and its EKV equivalent circuit.

$$(C_{GS}+C_{GS_0})\left(\frac{dv_S}{dt}-\frac{dv_G}{dt}\right)+(C_{GD}+C_{GD_0})\left(\frac{dv_D}{dt}-\frac{dv_G}{dt}\right)$$
$$+(C_{GB}+C_{GB_0})\times\left(\frac{dv_B}{dt}-\frac{dv_G}{dt}\right)=0 \tag{3.1}$$

$$(C_{GD}+C_{GD_0})\left(\frac{dv_G}{dt}-\frac{dv_D}{dt}\right)+C_{BD}\left(\frac{dv_B}{dt}-\frac{dv_D}{dt}\right)=I_{DS}+I_{DB} \tag{3.2}$$

$$(C_{GS}+C_{GS_0})\left(\frac{dv_G}{dt}-\frac{dv_S}{dt}\right)+C_{BS}\left(\frac{dv_B}{dt}-\frac{dv_S}{dt}\right)=-I_{DS} \tag{3.3}$$

$$C_{GX}\left(\frac{dv_{in}}{dt}-\frac{dv_G}{dt}\right)+\frac{V_{IN}-v_G}{R_{in}}=0 \tag{3.4}$$

where v_G, v_D, v_S and v_B are the state variables. C_{GD}, C_{GS} and C_{GB} are the drain to channel capacitance, source to channel capacitance and base to channel capacitance respectively. C_{OX} is oxide capacitance. Drain current I_D is

$$I_D=I_{DS}+I_{DB} \tag{3.5}$$

As $I_{DB}\cong 0$, therefore $I_D\cong I_{DS}$.

3.1.1 MOSFET Circuit Analysis

(i) Conduction Mode:-

From the EKV model of weak inversion, we have

$$I_D=I_{DS}=I_0\frac{W}{L}e^{\frac{v_{GB}-V_{T_0}}{\eta U_T}}\left(e^{-\frac{v_{SB}}{U_T}}-e^{-\frac{v_{DB}}{U_T}}\right) \tag{3.6}$$

where W is the width and L is the length of the MOSFET channel, $\frac{W}{L}$ is the aspect ratio, V_{T_0} and U_T are the the equilibrium threshold voltage and thermal voltage respectively. I_0 is the unary specific current. η is the subthreshold slope factor. Expanding (3.6) using Maclaurin series and retaining up to quadratic terms, as computation of higher order terms leads to increase in complexity. Expansion up to quadratic terms give more accurate results than the use of linear term only. Though higher order terms present more accurate result, but the gist of the nonlinearity can be obtained using

the second order terms only.

$$I_D = \frac{I_0 W}{U_T L}\left\{(v_D - v_S)\left(1 - \frac{V_{T_0}}{\eta U_T} + \frac{V_{T_0}^2}{2\eta^2 U_T^2} - \frac{1}{6}\frac{V_{T_0}^3}{\eta^3 U_T^3}\right)\right\} + \frac{I_0 W}{2U_T^2 L}\left\{\left(v_S^2 - v_D^2 - 2(v_S v_B - v_D v_B) - v_D v_S + v_S v_D\right) \times \left(1 - \frac{V_{T_0}}{\eta U_T} + \frac{V_{T_0}^2}{2\eta^2 U_T^2} - \frac{1}{6}\frac{V_{T_0}^3}{\eta^3 U_T^3}\right)\right\} + \frac{I_0 W}{U_T L}\left\{(v_G v_D - v_B v_D - v_G v_S + v_B v_S) \times \left(\frac{1}{\eta U_T} - \frac{V_{T_0}}{\eta^2 U_T^2} + \frac{3V_{T_0}^2}{\eta^3 U_T^3}\right)\right\}. \tag{3.7}$$

Using $C_{GS} + C_{GS_0} = C_S$, $C_{GD} + C_{GD_0} = C_D$ and $C_{GB} + C_{GB_0} = C_B$, we have

$$\frac{dv_G}{dt} = -\frac{v_G}{R_{in}C_{GX}} + \frac{V_{IN}}{R_{in}C_{GX}} + v_{in}^{'} \tag{3.8}$$

$$\frac{dv_B}{dt} = -\frac{p_2 v_G}{R_{in}C_{GX}} + p_1 p_7 (v_D - v_S) - \frac{p_1 p_7}{U_T} v_S v_B + \frac{p_1 p_7}{U_T} v_D v_B - \frac{p_1 p_7}{2U_T} v_D v_S + \frac{p_1 p_7}{2U_T} v_S v_D + p_1 p_8 (v_G v_D - v_G v_S + v_B v_S - v_B v_D) + \frac{p_1 p_7}{2U_T} v_S^2 - \frac{p_1 p_7}{2U_T} v_D^2 + k_2 \left(\frac{V_{IN}}{R_{in}C_{GX}} + v_{in}^{'}\right) \tag{3.9}$$

$$\frac{dv_S}{dt} = -\frac{p_4 v_G}{R_{in}C_{GX}} + p_3 p_7 (v_D - v_S) - \frac{p_3 k_7}{U_T} v_S v_B + \frac{p_3 k_7}{U_T} v_D v_B - \frac{p_3 p_7}{2U_T} v_D v_S + \frac{p_3 p_7}{2U_T} v_S v_D + p_3 p_8 (v_G v_D - v_G v_S + v_B v_S - v_B v_D) + \frac{p_3 p_7}{2U_T} v_S^2 - \frac{p_3 k_7}{2U_T} v_D^2 + p_4 \left(\frac{V_{IN}}{R_{in}C_{GX}} + v_{in}^{'}\right) \tag{3.10}$$

$$\frac{dv_D}{dt} = -\frac{p_6 v_G}{R_{in}C_{GX}} + p_5 p_7 (v_D - v_S) - \frac{p_5 p_7}{U_T} v_S v_B + \frac{p_5 p_7}{U_T} v_D v_B - \frac{p_5 p_7}{2U_T} v_D v_S + \frac{p_5 p_7}{2U_T} v_S v_D + p_5 p_8 (v_G v_D - v_G v_S + v_B v_S - v_B v_D) + \frac{p_5 p_7}{2U_T} v_S^2 - \frac{p_5 p_7}{2U_T} v_D^2 + p_6 \left(\frac{V_{IN}}{R_{in}C_{GX}} + v_{in}^{'}\right) \tag{3.11}$$

where

$p_1 = \frac{C_D(C_S+C_{BS})(C_S C_{BS}+C_S C_{BD})}{C_S C_{BS}(C_{BD}C_S(-C_S-C_{BS})+C_S C_{BS}(-C_D-C_{BD}))} - \frac{1}{C_{BS}}$,

$p_2 = \left[\frac{C_D(C_S+C_{BS})\{-C_S C_D C_{BS} - C_S C_{BD}(C_S+C_{BS})\}}{C_S C_{BS}\{C_S C_{BD}(-C_S-C_{BS})+C_S C_{BS}(-C_D-C_{BD})\}} + \frac{C_D(C_S+C_{BS})\{-C_{BD}(C_S+C_D+C_B)(C_S+C_{BS})\}}{C_S C_{BS}\{C_S C_{BD}(-C_S-C_{BS})+C_S C_{BS}(-C_D-C_{BD})\}} + \frac{(C_S+C_B+C_D)(C_S+C_{BS})}{C_S C_{BS}} - \frac{C_S}{C_{BS}}\right]$,

$p_3 = \frac{C_D(C_{BS}+C_{BD})}{\{C_S C_{BD}(C_S+C_{BS})+C_S C_{BS}(C_S+C_{BD})\}}$,

$p_4 = \left[\frac{C_D}{C_S}\left\{\frac{C_S C_D C_{BS} - C_S^2 C_{BD} + C_{BD}(C_S+C_{BS})(C_S+C_D+C_B)}{C_D C_{BD}(C_S+C_{BS})+C_S C_{BS}(C_D+C_{BD})}\right\} + \frac{C_S+C_D+C_B}{C_S}\right]$,

$p_5 = \frac{C_S(C_{BS}+C_{BD})}{C_D C_{BD}(-C_S-C_{BS})+C_S C_{BS}(-C_D-C_{BD})}$,
$p_6 = \frac{-C_S C_D C_{BS}+C_S^2 C_{BD}+C_{BD}(-C_S-C_{BS})(C_S+C_D+C_B)}{C_D C_{BD}(-C_S-C_{BS})+C_S C_{BS}(-C_D-C_{BD})}$,
$p_7 = \frac{I_0}{U_T}\frac{W}{L}\left(1-\frac{V_{T_0}}{\eta U_T}+\frac{V_{T_0}^2}{2\eta^2 U_T^2}-\frac{1}{6}\frac{V_{T_0}^3}{\eta^3 U_T^3}\right)$,
$p_8 = \frac{I_0}{U_T}\frac{W}{L}\left(\frac{1}{\eta U_T}-\frac{V_{T_0}}{\eta^2 U_T^2}+\frac{V_{T_0}^2}{2\eta^3 U_T^3}\right)$,
$v_{in}^{'} = \frac{d}{dt}v_{in}$.

(ii) Saturation Mode:-

The drain current in saturation mode of weak inversion is given by

$$I_D = I_{DS} = \frac{W}{L} I_0 e^{\frac{v_{GS}-V_{T_0}}{U_T}} \tag{3.12}$$

Expansion of (3.12) using Maclaurin series up to quadratic terms gives

$$I_D = I_{DS} = \frac{W}{L} I_0 \left[\left(1-\frac{V_{T_0}}{U_T}+\frac{V_{T_0}^2}{U_T^2}\right)+(v_G-v_S)\left(\frac{1}{U_T}-\frac{V_{T_0}}{U_T^2}\right)+\frac{v_G^2}{2U_T^2}+\frac{v_S^2}{2U_T^2}-\frac{v_G v_S}{U_T^2}\right]. \tag{3.13}$$

So, the dynamical equations of the circuit in saturation region are

$$\frac{dv_G}{dt} = -\frac{v_G}{R_{in}C_{GX}}+\frac{V_{IN}}{R_{in}C_{GX}}+v_{in}^{'} \tag{3.14}$$

$$\frac{dv_B}{dt} = -\frac{p_2 v_G}{R_{in}C_{GX}}+p_1 p_9 (v_G-v_S)+\frac{p_1 W I_0}{2LU_T^2}\left(v_G^2+v_S^2-2v_G v_S\right)+p_1 p_{10}+p_2\left(\frac{V_{IN}}{R_{in}C_{GX}}+v_{in}^{'}\right) \tag{3.15}$$

$$\frac{dv_S}{dt} = -\frac{p_4 v_G}{R_{in}C_{GX}}+p_3 p_9 (v_G-v_S)+\frac{p_3 W I_0}{2LU_T^2}\left(v_G^2+v_S^2-2v_G v_S\right)+p_3 p_{10}+p_4\left(\frac{V_{IN}}{R_{in}C_{GX}}+v_{in}^{'}\right) \tag{3.16}$$

$$\frac{dv_D}{dt} = -\frac{p_6 v_G}{R_{in}C_{GX}}+p_5 p_9 (v_G-v_S)+\frac{p_5 W I_0}{2LU_T^2}\left(v_G^2+v_S^2-2v_G v_S\right)+p_5 p_{10}+p_6\left(\frac{V_{IN}}{R_{in}C_{GX}}+v_{in}^{'}\right) \tag{3.17}$$

where
$p_9 = \frac{I_0 W}{L}\left(\frac{1}{U_T}-\frac{V_{T_0}}{U_T^2}\right)$,
$p_{10} = \frac{I_0 W}{L}\left(1-\frac{V_{T_0}}{U_T}+\frac{V_{T_0}^2}{U_T^2}\right)$.

Euler-Maruyama method has been used to obtain discrete time state space equation using $t_k - t_{k-1} = T_S$ such that

$$\mathbf{F}_k = e^{\mathbf{F}(t_k-t_{k-1})} \approx I+\mathbf{F}T_S \tag{3.18}$$

$$\mathbf{B}_k = \int_{t_{k-1}}^{t_k} e^{\mathbf{F}(t_k-\tau)}\mathbf{B}d\tau \approx \mathbf{B}T_S. \tag{3.19}$$

where T_s is the sampling time [89].

3.1.2 Applying EKF to MOSFET Circuit

The MOSFET output voltage has been estimated using EKF. We estimated the drain voltage of EKV modelled MOSFET circuit. Discrete time state space equations are

$$\mathbf{x}_k = \mathbf{f}_{k-1}(\mathbf{x}_{k-1}, \mathbf{u}_{k-1}, \mathbf{v}_{k-1}) \tag{3.20}$$

$$\mathbf{y}_k = \mathbf{h}_k(\mathbf{x}_k, \mathbf{w}_k) \tag{3.21}$$

(i) Conduction Mode:-

Equation (3.20) in conduction mode is represented by

$$\mathbf{x}_k^{(c)} = \mathbf{F}_{k-1}^{(c)}\mathbf{x}_{k-1}^{(c)} + \mathbf{B}_{k-1}^{(c)}\mathbf{u}_{k-1} \tag{3.22}$$

where

$$\mathbf{x}_k^{(c)} = \begin{bmatrix} v_G & v_B & v_S & v_D \end{bmatrix}^T.$$

$$\mathbf{F}_{k-1}^{(c)} = \frac{\partial f_{k-1}^{(c)}(\hat{\mathbf{x}}_{k-1|k-1}, \mathbf{u}_{k-1})}{\partial \mathbf{x}_{k-1}^{(c)}} \tag{3.23}$$

$$= \begin{bmatrix} F_{11}^c & F_{12}^c & F_{13}^c & F_{14}^c \\ F_{21}^c & F_{22}^c & F_{23}^c & F_{24}^c \\ F_{31}^c & F_{32}^c & F_{33}^c & F_{34}^c \\ F_{41}^c & F_{42}^c & F_{43}^c & F_{44}^c \end{bmatrix}. \tag{3.24}$$

where

$F_{11}^c = 1 - \frac{T_s}{R_{in}C_{GX}}$, $F_{21}^c = -\frac{p_2T_s}{R_{in}C_{GX}} + T_sp_1p_8(v_D - v_S)$,
$F_{23}^c = -p_1p_7T_s + \frac{p_1p_7T_s}{U_T}\left(\frac{v_D}{2} + v_S\right)$, $F_{22}^c = 1 + p_1p_8T_s(-v_D + v_S)$,
$F_{24}^c = p_1p_7T_s + \frac{p_1p_7T_s}{U_T}\left(v_B - v_D - \frac{v_S}{2}\right)$, $F_{31}^c = -\frac{p_4T_s}{R_{in}C_{GX}} + T_sp_3p_8(v_D - v_S)$,
$F_{32}^c = p_3p_8T_s(-v_D + v_S)$, $F_{33}^c = 1 - p_3p_7T_s + \frac{p_3p_7T_s}{U_T}\left(\frac{v_D}{2} + v_S\right)$,
$F_{34}^c = p_3p_7T_s + \frac{p_3p_7T_s}{U_T}\left(v_B - v_D - \frac{v_S}{2}\right)$, $F_{41}^c = -\frac{p_6T_s}{R_{in}C_{GX}} + T_sp_5p_8(v_D - v_S)$,
$F_{42}^c = p_5p_8T_s(-v_D + v_S)$, $F_{43}^c = -p_5p_7T_s + \frac{p_5p_7T_s}{U_T}\left(\frac{v_D}{2} + v_S\right)$,
$F_{44}^c = 1 + p_5p_7T_s + \frac{p_5p_7T_s}{U_T}\left(v_B - v_D - \frac{v_S}{2}\right)$,

$F_{12}^c = 0$, $F_{13}^c = 0$, $F_{14}^c = 0$,

$$\mathbf{B}_{k-1}^{(c)} = \frac{\partial \mathbf{f}_{k-1}^{(c)}(\hat{\mathbf{x}}^{(c)}{}_{k-1|k-1}, \mathbf{u}_{k-1})}{\partial \mathbf{u}_{k-1}} \tag{3.25}$$

$$= \begin{bmatrix} T_s & p_2 T_s & p_4 T_s & p_6 T_s \end{bmatrix}^T \tag{3.26}$$

where $\mathbf{u} = \left(\frac{V_{IN}}{R_{in} C_{GX}} + v_{in}^{'}\right)$.

Measurement model in conduction mode is

$$\mathbf{y}_k^{(c)} = \mathbf{H}_k^{(c)} \mathbf{x}_k^{(c)} \tag{3.27}$$

where

$$\mathbf{H}_k^{(c)} = \frac{\partial h_k^{(c)}(f_{k-1}^{(c)}(\hat{\mathbf{x}}^{(c)}{}_{k-1|k-1}))}{\partial \mathbf{x}_k^{(c)}} \tag{3.28}$$

$$= \begin{bmatrix} 0 & 0 & 0 & 1 \end{bmatrix}. \tag{3.29}$$

The state space representation of the circuit in the conduction mode is

$$\begin{bmatrix} v_{G_k} \\ v_{B_k} \\ v_{S_k} \\ v_{D_k} \end{bmatrix} = \begin{bmatrix} F_{11}^c & F_{12}^c & F_{13}^c & F_{14}^c \\ F_{21}^c & F_{22}^c & F_{23}^c & F_{24}^c \\ F_{31}^c & F_{32}^c & F_{33}^c & F_{34}^c \\ F_{41}^c & F_{42}^c & F_{43}^c & F_{44}^c \end{bmatrix} \begin{bmatrix} v_{G_{k-1}} \\ v_{B_{k-1}} \\ v_{S_{k-1}} \\ v_{D_{k-1}} \end{bmatrix} + \begin{bmatrix} T_s \\ p_2 T_s \\ p_4 T_s \\ p_6 T_s \end{bmatrix} \left(\frac{V_{IN}}{R_{in} C_{GX}} + v_{in}^{'}\right) \tag{3.30}$$

(ii) Saturation Mode:-

Equation (3.20) in saturation mode is represented as:

$$\mathbf{x}_k^{(s)} = \mathbf{F}_{k-1}^{(s)} \mathbf{x}_{k-1}^{(s)} + \mathbf{B}_{k-1}^{(s)} \mathbf{u}_{k-1} + \mathbf{C}_{k-1}^{(s)} \tag{3.31}$$

where

$$\mathbf{x}_k^{(s)} = \begin{bmatrix} v_G & v_B & v_S & v_D \end{bmatrix}^T.$$

$$\mathbf{F}_{k-1}^{(s)} = \begin{bmatrix} F_{11}^s & F_{12}^s & F_{13}^s & F_{14}^s \\ F_{21}^s & F_{22}^s & F_{23}^s & F_{24}^s \\ F_{31}^s & F_{32}^s & F_{33}^s & F_{34}^s \\ F_{41}^s & F_{42}^s & F_{43}^s & F_{44}^s \end{bmatrix} \tag{3.32}$$

where

$F^s_{11} = 1 - \frac{T_s}{R_{in}C_{GX}}$, $F^s_{12} = 0$, $F^s_{13} = 0$, $F^s_{14} = 0$,

$F^s_{21} = p_1 p_9 T_s - \frac{p_2 T_s}{R_{in}C_{GX}} + \frac{p_1 T_s W I_0}{L U_T^2}(v_G - v_S)$, $F^s_{22} = 1$,

$F^s_{23} = -p_1 p_9 T_s + \frac{p_1 T_s W I_0}{L U_T^2} v_S$, $F^s_{24} = 0$,

$F^s_{31} = p_3 p_9 T_s - \frac{p_4 T_s}{R_{in}C_{GX}} + \frac{p_3 T_s W I_0}{L U_T^2}(v_G - v_S)$, $F^s_{32} = 0$,

$F^s_{33} = 1 - p_3 p_9 T_s + \frac{p_3 T_s W I_0}{L U_T^2} v_S$, $F^s_{34} = 0$,

$F^s_{41} = p_5 p_9 T_s - \frac{p_6 T_s}{R_{in}C_{GX}} + \frac{p_5 T_s W I_0}{L U_T^2}(v_G - v_S)$, $F^s_{42} = 0$,

$F^s_{43} = -p_5 k_9 T_s + \frac{p_5 T_s W I_0}{L U_T^2} v_S$, $F^s_{44} = 1$,

$$\mathbf{B}^{(s)}_{k-1} = \begin{bmatrix} T_s & p_2 T_s & p_4 T_s & p_6 T_s \end{bmatrix}^T \tag{3.33}$$

$$\mathbf{C}^{(s)}_{k-1} = \begin{bmatrix} 0 & p_1 p_{10} T_s & p_3 p_{10} T_s & p_5 p_{10} T_s \end{bmatrix}^T. \tag{3.34}$$

Measurement model in saturation mode is

$$\mathbf{y}^{(s)}_k = \mathbf{H}^{(s)}_k \mathbf{x}^{(s)}_k \tag{3.35}$$

where

$$\mathbf{H}^{(s)}_k = \begin{bmatrix} 0 & 0 & 0 & 1 \end{bmatrix}. \tag{3.36}$$

The state space representation of the circuit in the saturation mode is

$$\begin{bmatrix} v_{G_k} \\ v_{B_k} \\ v_{S_k} \\ v_{D_k} \end{bmatrix} = \begin{bmatrix} F^s_{11} & F^s_{12} & F^s_{13} & F^s_{14} \\ F^s_{21} & F^s_{22} & F^s_{23} & F^s_{24} \\ F^s_{31} & F^s_{32} & F^s_{33} & F^s_{34} \\ F^s_{41} & F^s_{42} & F^s_{43} & F^s_{44} \end{bmatrix} \begin{bmatrix} v_{G_{k-1}} \\ v_{B_{k-1}} \\ v_{S_{k-1}} \\ v_{D_{k-1}} \end{bmatrix} + \begin{bmatrix} T_s \\ p_2 T_s \\ p_4 T_s \\ p_6 T_s \end{bmatrix} \left(\frac{V_{IN}}{R_{in}C_{GX}} + v'_{in} \right) + \begin{bmatrix} 0 \\ p_1 p_{10} T_s \\ p_3 p_{10} T_s \\ p_5 p_{10} T_s \end{bmatrix}. \tag{3.37}$$

The process noise $\mathbf{v}_k$ and and the measurement noise $\mathbf{w}_k$ are added to (3.22) and (3.27) respectively to apply EKF algorithm in conduction mode. We have

$$\mathbf{x}^{(c)}_k = \mathbf{F}^{(c)}_{k-1} \mathbf{x}^{(c)}_{k-1} + \mathbf{B}^{(c)}_{k-1} \mathbf{u}_{k-1} + \mathbf{v}_{k-1} \tag{3.38}$$

$$\mathbf{y}^{(c)}_k = \mathbf{H}^{(c)}_k \mathbf{x}^{(c)}_k + \mathbf{w}_k \tag{3.39}$$

Similarly, process noise $\mathbf{v}_k$ and measurement noise $\mathbf{w}_k$ are added to ((3.31) and (3.35) respectively to apply EKF algorithm in saturation mode as:

$$\mathbf{x}_k^{(s)} = \mathbf{F}_{k-1}^{(s)}\mathbf{x}_{k-1}^{(s)} + \mathbf{B}_{k-1}^{(s)}\mathbf{u}_{k-1} + \mathbf{C}_{k-1}^{(s)} + \mathbf{v}_{k-1} \tag{3.40}$$

$$\mathbf{y}_k^{(s)} = \mathbf{H}_k^{(s)}\mathbf{x}_k^{(s)} + \mathbf{w}_k \tag{3.41}$$

The EKF method described in appendix section A.2 has been applied to MOSFET circuit shown in Figure 3.1. After initialization, iterative process between the time update and measurement update have been used.

3.1.3 Simulation Results for MOSFET Circuit

Simulations have been performed in MATLAB software. The parameters used for simulations are: $U_T = 0.0256V$, $V_{T_0} = 0.5V$, $R_{in} = 3\,k\Omega$, $C_{GX} = 1.0 \times 10^{-11}$, $C_S = 1.5 \times 10^{-10}F$, $C_D = 1.5 \times 10^{-10}F$, $C_B = 4 \times 10^{-10}F$, $C_{BS} = 0.99 \times 10^{-11}F$, $C_{BD} = 1.0 \times 10^{-11}F$, $I_0 = 1.0 \times 10^{-9}A$ and $\eta = 1$. The sampling frequency is taken as the ten times of input frequency. The output voltage estimation using EKF method has been compared with the RLS method and PSPICE simulated values. PSPICE simulated values have been considered as actual value. Simulations have been performed for two different scenarios: - (i) noiseless input signal (ii) noisy input signal. Gaussian noise with zero mean and different variance have been used for noisy input signal. Initial values assigned to covariances are: $\mathbf{Q}_k = \mathrm{diag}\,[0.0025\ \ 0.002\ \ 0.002\ \ 0.002]$ and $\mathbf{R}_k = 0.01$. As the EKF performance depends on proper selection of covariance matrices, $\mathbf{Q}_k$, $\mathbf{R}_k$ and $P(0)$ have been selected by trial and error method.

We simulated the output estimation in the weak inversion for two different modes of transistor (i) the conduction mode, (ii) the saturation mode. Figure 3.2 and Figure 3.3 show the output voltage estimation for noiseless and noisy input respectively in conduction mode. Figure 3.4 and Figure 3.5 show the output voltage estimation in saturation mode for noiseless and noisy input respectively. These figures compare the EKF estimated output voltage with the RLS method and actual values. The EKF presents better estimation as compared to RLS as measurement noise is taken into account by the EKF method. Table 3.1 and Table 3.2 show the root mean square error (RMSE) comparison in conduction and saturation mode, respectively, using EKF and

RLS method.

$$RMSE = \sqrt{\frac{1}{N}\sum_{k=1}^{N} e_k^2} \tag{3.42}$$

where e_k is the difference between actual value and estimated value. N is the total number of samples used. Table 3.3 and Table 3.4 show the residual mean comparison using RLS and EKF method in conduction and saturation mode respectively. Figure 3.6 and Figure 3.7 show the estimation error for conduction and saturation mode, respectively.

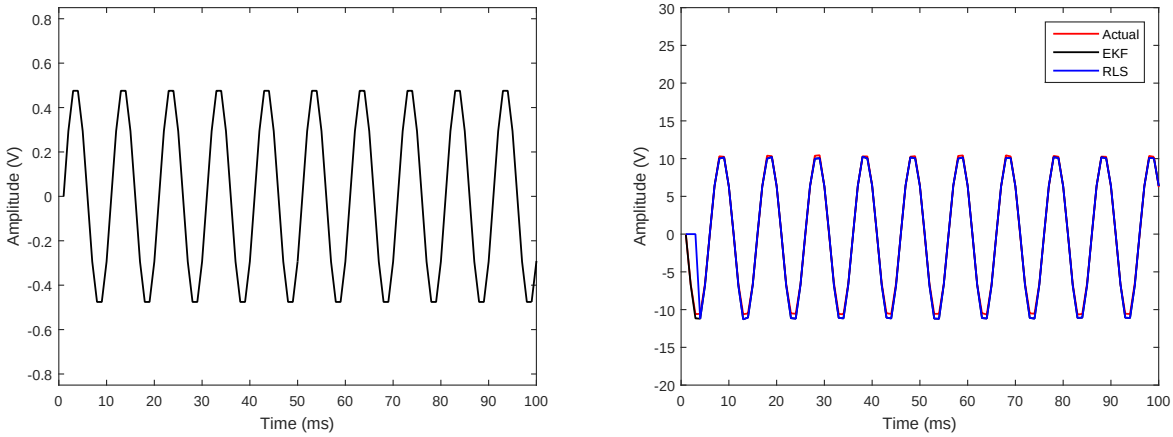

(a) Noiseless input to MOSFET. (b) Estimated MOSFET output voltage for noiseless input.

Figure 3.2: Estimation without noise in conduction mode.

Table 3.1: RMSE of Output voltage estimation in conduction mode using EKF and RLS.

S. No.	Gaussian noise at input source	Input frequency (Hz)	EKF RMSE	RLS RMSE
1.	$\mu = 0, \sigma = 0.25$	100	0.3242	0.6223
2.	$\mu = 0, \sigma = 0.25$	1000	0.3242	0.6241
3.	$\mu = 0, \sigma = 0.25$	10000	0.3243	0.6260
4.	$\mu = 0, \sigma = 0.10$	100	0.2707	0.5353
5.	$\mu = 0, \sigma = 0.10$	1000	0.2708	0.5364
6.	$\mu = 0, \sigma = 0.10$	10000	0.2710	0.5365

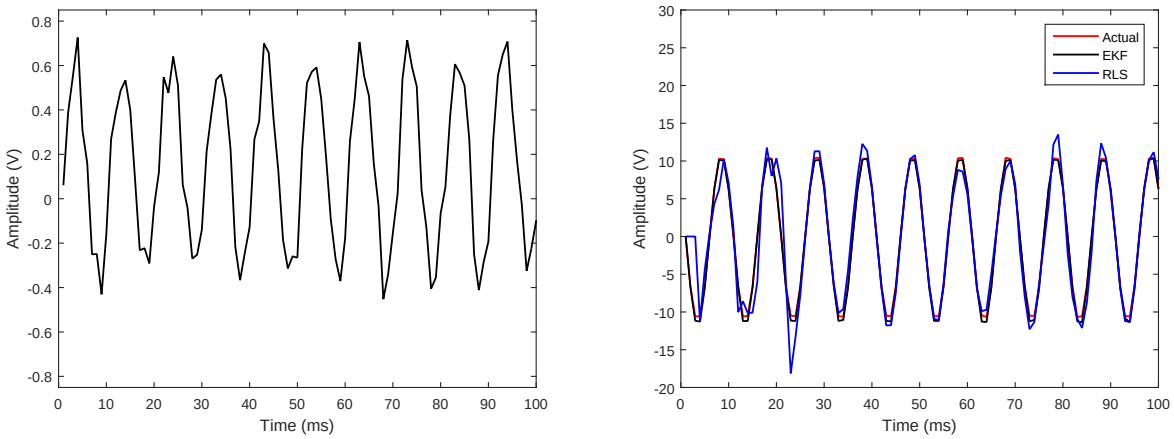

(a) Noisy input to MOSFET. (b) Estimated MOSFET output voltage for noisy input.

Figure 3.3: Estimated output voltage for noisy input in conduction mode. White Gaussian noise of zero mean and 0.25 variance is used.

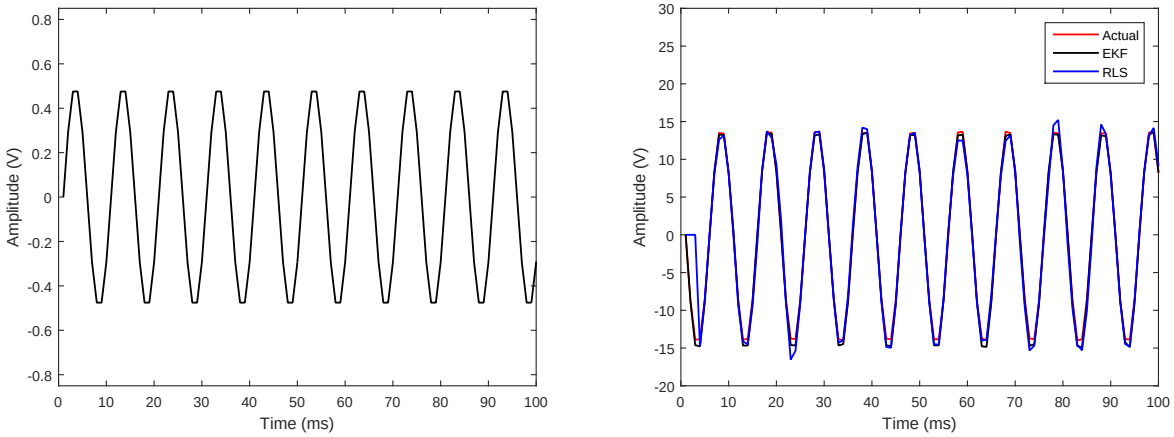

(a) Noiseless input to MOSFET. (b) Estimated MOSFET output voltage for noiseless input.

Figure 3.4: Estimation without noise in saturation mode.

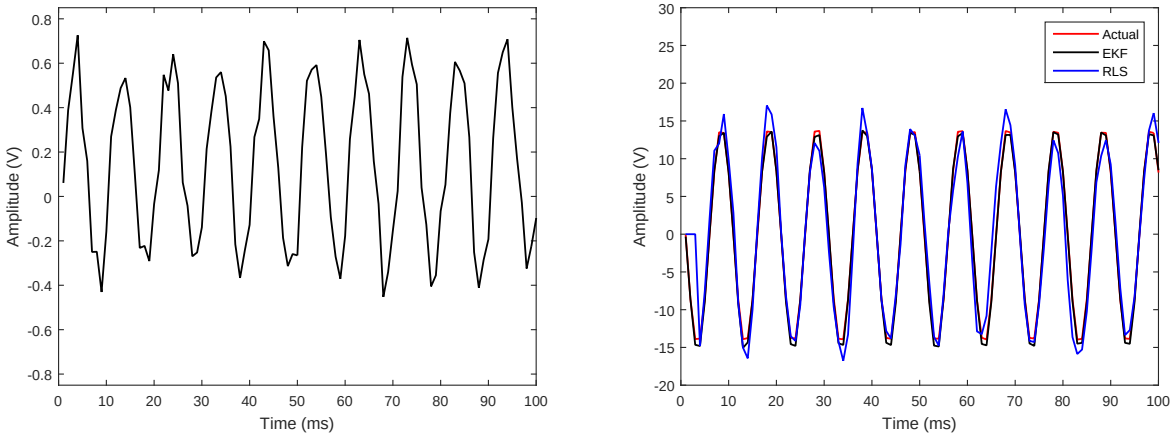

(a) Noisy input to MOSFET. (b) Estimated MOSFET output voltage for noisy input.

Figure 3.5: Estimated output voltage for noisy input in saturation mode. White Gaussian noise of zero mean and 0.25 variance is used.

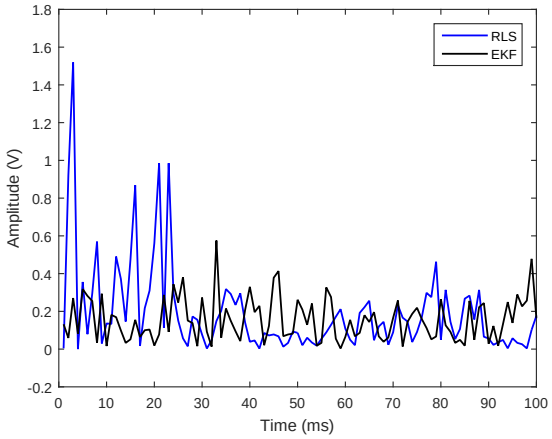

(a) RMSE in conduction mode.

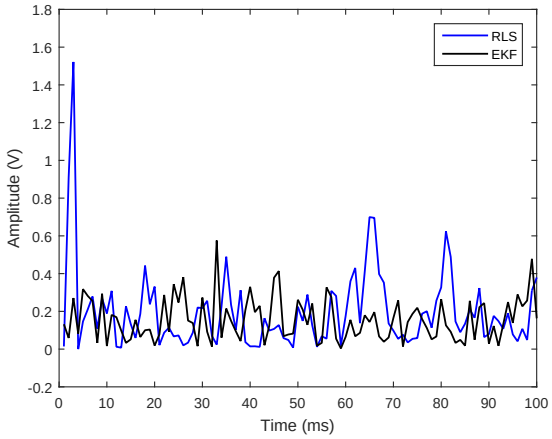

(b) RMSE in saturation mode.

Figure 3.6: RMSE of estimated voltage in using (i) RLS, (ii) EKF.

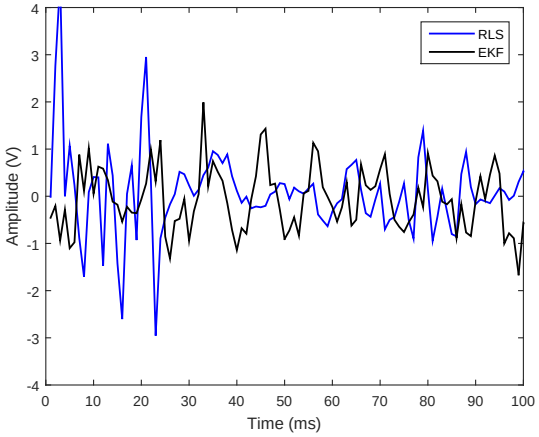

(a) Residual in conduction mode.

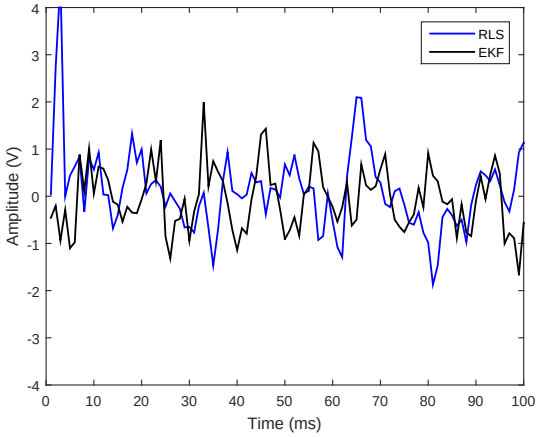

(b) Residual in saturation mode

Figure 3.7: Residual of estimated voltage in using (i) RLS, (ii) EKF.

Table 3.2: RMSE of output voltage estimation in saturation mode using EKF and RLS.

S. No.	Gaussian noise at input source	Input frequency (Hz)	EKF RMSE	RLS RMSE
1.	$\mu = 0, \sigma = 0.25$	100	0.4024	0.6043
2.	$\mu = 0, \sigma = 0.25$	1000	0.4028	0.6044
3.	$\mu = 0, \sigma = 0.25$	10000	0.4031	0.6048
4.	$\mu = 0, \sigma = 0.10$	100	0.3460	0.6144
5.	$\mu = 0, \sigma = 0.10$	1000	0.3461	0.6144
6.	$\mu = 0, \sigma = 0.10$	10000	0.3461	0.6145

Table 3.3: Residual mean and variance of output estimation in conduction mode using EKF and RLS.

S. No.	Gaussian noise at input source	Input frequency (Hz)	EKF Residual mean	RLS Residual mean	EKF Residual variance	RLS Residual variance
1.	$\mu = 0, \sigma = 0.25$	100	0.0643	0.4410	0.3742	1.0429
2.	$\mu = 0, \sigma = 0.25$	1000	0.0643	0.4411	0.3744	1.0586
3.	$\mu = 0, \sigma = 0.25$	10000	0.0645	0.4412	0.3744	1.0646
4.	$\mu = 0, \sigma = 0.10$	100	0.0619	0.4184	0.3611	1.0243
5.	$\mu = 0, \sigma = 0.10$	1000	0.0622	0.4235	0.3614	1.0365
6.	$\mu = 0, \sigma = 0.10$	10000	0.0625	0.4251	0.3620	1.0358

Table 3.4: Residual mean and variance of output estimation in saturation mode using EKF and RLS.

S. No.	Gaussian noise at input source	Input frequency (Hz)	EKF Residual mean	RLS Residual mean	EKF Residual variance	RLS Residual variance
1.	$\mu = 0, \sigma = 0.25$	100	0.0506	0.4373	0.3456	1.0229
2.	$\mu = 0, \sigma = 0.25$	1000	0.0507	0.4374	0.3459	1.0286
3.	$\mu = 0, \sigma = 0.25$	10000	0.0510	0.4382	0.3460	1.0346
4.	$\mu = 0, \sigma = 0.10$	100	0.0422	0.3995	0.3436	0.9414
5.	$\mu = 0, \sigma = 0.10$	1000	0.0423	0.3996	0.3438	0.9454
6.	$\mu = 0, \sigma = 0.10$	10000	0.0423	0.4016	0.3441	0.9586

3.2 State Estimation of Differential Amplifier Circuit

3.2.1 State Space Model of Differential Amplifier Circuit

Figure 3.8 shows the differential amplifier circuit diagram, which consists of two BJTs Q_1 and Q_2. By applying KVL and KCL, we have

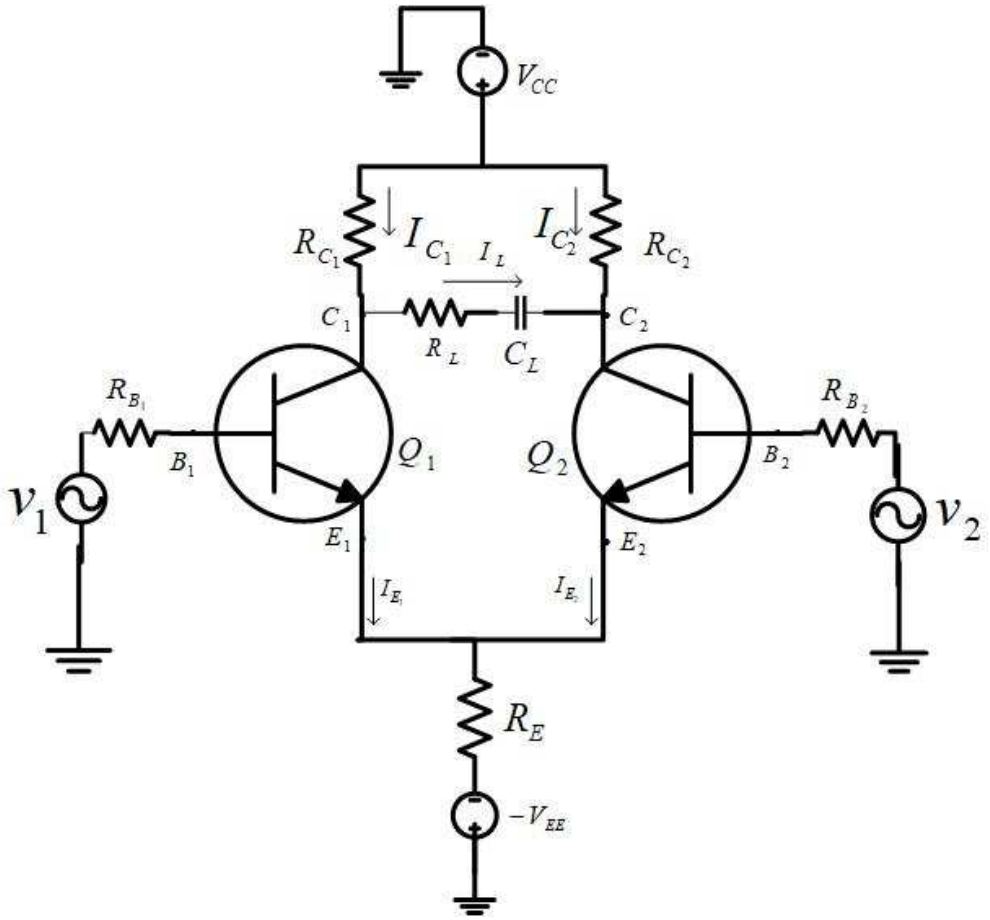

Figure 3.8: Differential amplifier circuit.

$$i_L R_L + \frac{1}{C_L}\int i_L dt = v_{C_1} - v_{C_2} \tag{3.43}$$

$$\frac{V_{EE} + v_E}{R_E} + (I_{E_1} + I_{E_2}) = 0 \tag{3.44}$$

$$\frac{V_{CC} - v_{C_1}}{R_{C_1}} = i_L + I_{C_1} \tag{3.45}$$

$$\frac{V_{CC} - v_{C_2}}{R_{C_2}} = -i_L + I_{C_2} \tag{3.46}$$

where v_{C_1}, v_{C_2}, v_E and q_L are the state variables. Using $q_L = \int i_L dt$, we have

$$R_L \frac{dq_L}{dt} + \frac{q_L}{C_L} = v_{C_1} - v_{C_2} \tag{3.47}$$

where q_L is the charge at load R_L. Replacing Q_1 and Q_2 with Ebers-Moll model, we have

$$I_{C_1} = \alpha_{F_1} I_{ES_1} \left[exp \frac{v_{BE_1}}{V_T} - 1 \right] - I_{CS_1} \left[exp \frac{v_{BC_1}}{V_T} - 1 \right] \tag{3.48}$$

$$I_{C_2} = \alpha_{F_2} I_{ES_2} \left[exp \frac{v_{BE_2}}{V_T} - 1 \right] - I_{CS_2} \left[exp \frac{v_{BC_2}}{V_T} - 1 \right] \tag{3.49}$$

$$I_{E_1} = -I_{ES_1} \left[exp \frac{v_{BE_1}}{V_T} - 1 \right] + \alpha_{R_1} I_{CS_1} \left[exp \frac{v_{BC_1}}{V_T} - 1 \right] \tag{3.50}$$

$$I_{E_2} = -I_{ES_2} \left[exp \frac{v_{BE_2}}{V_T} - 1 \right] + \alpha_{R_2} I_{CS_2} \left[exp \frac{v_{BC_2}}{V_T} - 1 \right] \tag{3.51}$$

I_{CS_1}, I_{CS_2} are the reverse saturation currents at the collector junction of Q_1 and Q_2 respectively. I_{ES_1} and I_{ES_2} are the reverse saturation currents at the emitter junction of Q_1 and Q_2 respectively. V_T is the thermal voltage. α_{F_1}, α_{F_2} and α_{R_1}, α_{R_2} are current gains of two transistors in forward and reverse mode respectively.

Solving for $\frac{dv_E}{dt}$, $\frac{dq_L}{dt}$, $\frac{dv_{C_1}}{dt}$ and $\frac{dv_{C_2}}{dt}$, we have

$$\begin{aligned}
\frac{dv_E(t)}{dt} = & \left[\left\{ \frac{r_8}{r_7} - \frac{r_5}{r_7} \left(1 + \frac{r_2}{r_1} \right) \right\} \times \frac{1}{V_T} \left\{ -\frac{r_2 r_5}{r_1 r_7} - \frac{r_4 r_6}{r_3 r_7} \right\} v_1^{'} + \left\{ \frac{r_9}{r_7} - \frac{r_6}{r_7} \left(1 + \frac{r_4}{r_3} \right) \right\} \right. \\
& \left. \times \frac{1}{V_T} \left\{ -\frac{r_2 r_5}{r_1 r_7} - \frac{r_4 r_6}{r_3 r_7} \right\} v_2^{'} \right] v_E + \left[- \left\{ \left(1 + \frac{r_2 r_5}{r_1 r_7} + \frac{r_4 r_6}{r_3 r_7} \right) \left(1 + \frac{r_2}{r_1} \right) \left(\frac{r_5}{V_T} + \frac{I_{CS_1}}{V_T^2} \right) \right. \right. \\
& \left. + \frac{r_2}{r_1 r_7} \left(r_8 - \frac{r_5}{r_1} (r_1 + r_2) \right) \left(\frac{r_5}{V_T} + \frac{I_{CS_1}}{V_T^2} \right) \right\} \frac{v_1^{'}}{r_7} + \left\{ \frac{r_2}{r_1 r_7} \left(r_9 - \frac{r_6}{r_3} (r_3 + r_4) \right) \right. \\
& \left. \times \left(\frac{r_5}{V_T} + \frac{I_{CS_1}}{V_T^2} \right) \right\} \frac{v_2^{'}}{r_7} \Bigg] v_{C_1} + \left[\left\{ - \left(1 + \frac{r_2 r_5}{r_1 r_7} + \frac{r_4 r_6}{r_3 r_7} \right) \left(1 + \frac{r_4}{r_3} \right) \left(\frac{r_6}{V_T} + \frac{I_{CS_2}}{V_T^2} \right) \right. \right. \\
& \left. + \frac{r_4}{r_3 r_7} \left(r_9 - \frac{r_6}{r_3} (r_3 + r_4) \right) \left(\frac{r_5}{V_T} + \frac{I_{CS_1}}{V_T^2} \right) \right\} \frac{v_2^{'}}{r_7} + \left\{ \frac{r_4}{r_3 r_7} \left(r_8 - \frac{r_5}{r_1} (r_1 + r_2) \right) \right. \\
& \left. \times \left(\frac{r_6}{V_T} + \frac{I_{CS_2}}{V_T^2} \right) \right\} \frac{v_1^{'}}{r_7} \Bigg] v_{C_2} + \left[\left\{ 1 + \frac{r_2 r_5}{r_1 r_7} + \frac{r_4 r_6}{r_3 r_7} \right\} \times \left\{ \frac{r_8}{r_7} - \frac{r_5}{r_7} \left(1 + \frac{r_2}{r_1} \right) \right\} \right] v_1^{'} \\
& + \left[\left\{ 1 + \frac{r_2 r_5}{r_1 r_7} + \frac{r_4 r_6}{r_3 r_7} \right\} \times \left\{ \frac{r_9}{r_7} - \frac{r_6}{r_7} \left(1 + \frac{r_4}{r_3} \right) \right\} \right] v_2^{'}
\end{aligned} \tag{3.52}$$

$$\frac{dq_L}{dt} = -\frac{q_L}{R_L C_L} + \frac{v_{C_1} - v_{C_2}}{R_L} \tag{3.53}$$

$$\begin{aligned}\frac{dv_{C_1}}{dt} =& \frac{r_2}{r_1 V_T}\left[\left\{1+\frac{r_2 r_5}{r_1 r_7}+\frac{r_4 r_6}{r_3 r_7}\right\}\left\{\frac{r_8}{r_7}-\frac{r_5}{r_7}\left(1+\frac{r_2}{r_1}\right)\right\}v_1^{'}+\left(1+\frac{r_2 r_5}{r_1 r_7}+\frac{r_4 r_6}{r_3 r_7}\right)\right.\\ &\left.\times\left\{\frac{r_9}{r_7}-\frac{r_6}{r_7}\left(1+\frac{r_4}{r_3}\right)\right\}v_2^{'}\right]v_E+\left[\left(1+\frac{r_2}{r_1 V_T}\right)-\frac{r_2}{r_1 V_T}\left\{1+\frac{r_2 r_5}{r_1 r_7}+\frac{r_4 r_6}{r_3 r_7}\right\}\right.\\ &\left.\times\left\{\frac{r_8}{r_7}-\frac{r_5}{r_7}\left(1+\frac{r_2}{r_1}\right)\right\}v_1^{'}+\frac{r_2}{r_1 V_T}\left\{1+\frac{r_2 r_5}{r_1 r_7}+\frac{r_4 r_6}{r_3 r_7}\right\}\times\left\{\frac{r_9}{r_7}-\frac{r_6}{r_7}\left(1+\frac{r_4}{r_3}\right)\right\}v_2^{'}\right]\\ &\times v_{C_1}+\left[\left(1+\frac{r_2}{r_1}\right)-\frac{r_2}{r_1}\left\{1+\frac{r_2 r_5}{r_1 r_7}+\frac{r_4 r_6}{r_3 r_7}\right\}\times\left\{\frac{r_8}{r_7}-\frac{r_5}{r_7}\left(1+\frac{r_2}{r_1}\right)\right\}\right]v_1^{'}\\ &-\frac{r_2}{r_1 V_T}\left[\left\{1+\frac{r_2 r_5}{r_1 r_7}+\frac{r_4 r_6}{r_3 r_7}\right\}\times\left\{\frac{r_9}{r_7}-\frac{r_6}{r_7}\left(1+\frac{r_4}{r_3}\right)\right\}\right]v_2^{'} \end{aligned} \tag{3.54}$$

$$\begin{aligned}\frac{dv_{C_2}}{dt} =& \frac{r_4}{r_3 V_T}\left[\left\{1+\frac{r_2 r_5}{r_1 r_7}+\frac{r_4 r_6}{r_3 r_7}\right\}\left\{\frac{r_8}{r_7}-\frac{r_5}{r_7}\left(1+\frac{r_2}{r_1}\right)\right\}v_1^{'}+\left(1+\frac{r_2 r_5}{r_1 r_7}+\frac{r_4 r_6}{r_3 r_7}\right)\right.\\ &\left.\times\left\{\frac{r_9}{r_7}-\frac{r_6}{r_7}\left(1+\frac{r_4}{r_3}\right)\right\}v_2^{'}\right]v_E+\left[\left(1+\frac{r_4}{r_3 V_T}\right)-\frac{r_4}{r_3 V_T}\left\{1+\frac{r_2 r_5}{r_1 r_7}+\frac{r_4 r_6}{r_3 r_7}\right\}\right.\\ &\left.\times\left\{\frac{r_8}{r_7}-\frac{r_5}{r_7}\left(1+\frac{r_2}{r_1}\right)\right\}v_1^{'}+\frac{r_2}{r_1 V_T}\left\{1+\frac{r_2 r_5}{r_1 r_7}+\frac{r_4 r_6}{r_3 r_7}\right\}\times\left\{\frac{r_9}{r_7}-\frac{r_6}{r_7}\left(1+\frac{r_4}{r_3}\right)\right\}v_2^{'}\right]\\ &\times v_{C_2}-\frac{r_4}{r_3 V_T}\left[\left\{1+\frac{r_2 r_5}{r_1 r_7}+\frac{r_4 r_6}{r_3 r_7}\right\}\times\left\{\frac{r_9}{r_7}-\frac{r_6}{r_7}\left(1+\frac{r_4}{r_3}\right)\right\}\right]v_1^{'}\\ &+\left[\left(1+\frac{r_4}{r_3}\right)-\frac{r_2}{r_1}\left\{1+\frac{r_2 r_5}{r_1 r_7}+\frac{r_4 r_6}{r_3 r_7}\right\}\times\left\{\frac{r_8}{r_7}-\frac{r_5}{r_7}\left(1+\frac{r_2}{r_1}\right)\right\}\right]v_2^{'} \end{aligned} \tag{3.55}$$

$$y = v_{C_1} - v_{C_2} \tag{3.56}$$

where

$r_1 = \frac{\alpha_{R_1} I_{CS_1}\left(1+\frac{1}{\beta_1}\right)}{V_T}+\frac{I_{CS_1}}{V_T}$, $r_2 = -\frac{\alpha_{F_1} I_{ES_1}\left(1+\frac{1}{\beta_1}\right)}{V_T}-\frac{I_{ES_1}}{V_T}$, $r_3 = \frac{\alpha_{R_2} I_{CS_2}\left(1+\frac{1}{\beta_2}\right)}{V_T}+\frac{I_{CS_2}}{V_T}$,

$r_4 = -\frac{\alpha_{F_2} I_{ES_2}\left(1+\frac{1}{\beta_2}\right)}{V_T}-\frac{I_{ES_2}}{V_T}$, $r_5 = \frac{1}{R_{C_1}}+\frac{I_{CS_1}}{V_T}$, $r_6 = \frac{1}{R_{C_2}}+\frac{I_{CS_2}}{V_T}$,

$r_7 = -\frac{\alpha_{F_1} I_{ES_1}}{V_T}-\frac{\alpha_{F_2} I_{ES_2}}{V_T}$, $r_8 = -\frac{\alpha_{F_1} I_{ES_1}}{V_T}+\frac{I_{CS_1}}{V_T}$, $r_9 = -\frac{\alpha_{F_2} I_{ES_2}}{V_T}+\frac{I_{CS_2}}{V_T}$,

and $v_1^{'} = \frac{d}{dt}v_1$, $v_2^{'} = \frac{d}{dt}v_2$

3.2.2 Applying EKF to Differential Amplifier Circuit

The EKF algorithm can be applied for parameter estimation by using the unknown parameters as extended state variables. We estimate the collector voltage of both the transistors. Discrete time state space equations (3.52)-(3.56) are

$$\mathbf{x}_k = \mathbf{f}_{k-1}(\mathbf{x}_{k-1}, \mathbf{u}_{k-1}) \tag{3.57}$$

$$\mathbf{y}_k = \mathbf{h}_k(\mathbf{x}_k) \tag{3.58}$$

The state model is

$$\mathbf{x}_k = \mathbf{F}_{k-1}\mathbf{x}_{k-1} + \mathbf{B}_{k-1}^{(1)}\mathbf{u}_1 + \mathbf{B}_{k-1}^{(2)}\mathbf{u}_2 \tag{3.59}$$

where

$$\mathbf{x}_k = \begin{bmatrix} v_{E_k} & q_{L_k} & v_{C_{1_k}} & v_{C_{2_k}} \end{bmatrix}^T \tag{3.60}$$

$$\mathbf{F}_{k-1} = \frac{\partial \mathbf{f}_{k-1}(\hat{\mathbf{x}}_{k-1}, \mathbf{u}_{k-1})}{\partial \mathbf{x}_{k-1}} \tag{3.61}$$

$$= \begin{bmatrix} F_{11} & F_{12} & F_{13} & F_{14} \\ F_{21} & F_{22} & F_{23} & F_{24} \\ F_{31} & F_{32} & F_{33} & F_{34} \\ F_{41} & F_{42} & F_{43} & F_{44} \end{bmatrix} \tag{3.62}$$

where

$$F_{11} = \left[\left\{\frac{r_8}{r_7} - \frac{r_5}{r_7}\left(1+\frac{r_2}{r_1}\right)\right\}\frac{1}{V_T}\left\{-\frac{r_2r_5}{r_1r_7} - \frac{r_4r_6}{r_3r_7}\right\}v_1' + \left\{\frac{r_9}{r_7} - \frac{r_6}{r_7}\left(1+\frac{r_4}{r_3}\right)\right\}\frac{1}{V_T}\left\{-\frac{r_2r_5}{r_1r_7} - \frac{r_4r_6}{r_3r_7}\right\}v_2'\right],$$

$$F_{13} = \left[-\left\{\left(1+\frac{r_2r_5}{r_1r_7} + \frac{r_4r_6}{r_3r_7}\right)\left(1+\frac{r_2}{r_1}\right)\left(\frac{r_5}{V_T} + \frac{I_{CS_1}}{V_T^2}\right)\frac{r_2}{r_1r_7}\left(r_8 - \frac{r_5}{r_1}(r_1+r_2)\right)\left(\frac{r_5}{V_T} + \frac{I_{CS_1}}{V_T^2}\right)\right\}\frac{v_1'}{r_7}\right.$$
$$\left. + \left\{\frac{r_2}{r_1r_7}\left(r_9 - \frac{r_6}{r_3}(r_3+r_4)\right)\left(\frac{r_5}{V_T} + \frac{I_{CS_1}}{V_T^2}\right)\right\}\frac{v_2'}{r_7}\right],$$

$$F_{14} = \left[\left\{-\left(1+\frac{r_2r_5}{r_1r_7} + \frac{r_4r_6}{r_3r_7}\right)\left(1+\frac{r_4}{r_3}\right)\left(\frac{r_6}{V_T} + \frac{I_{CS_2}}{V_T^2}\right) + \frac{r_4}{r_3r_7}\left(r_9 - \frac{r_6}{r_3}(r_3+r_4)\right)\left(\frac{r_5}{V_T} + \frac{I_{CS_1}}{V_T^2}\right)\right\}\frac{v_2'}{r_7}\right.$$
$$\left. + \left\{\frac{r_4}{r_3r_7}\left(r_8 - \frac{r_5}{r_1}(r_1+r_2)\right)\left(\frac{r_6}{V_T} + \frac{I_{CS_2}}{V_T^2}\right)\right\}\frac{v_1'}{r_7}\right],$$

$$F_{31} = \frac{r_2}{r_1V_T}\left[\left\{1+\frac{r_2r_5}{r_1r_7} + \frac{r_4r_6}{r_3r_7}\right\}\left\{\frac{r_8}{r_7} - \frac{r_5}{r_7}\left(1+\frac{r_2}{r_1}\right)\right\}v_1' + \left(1+\frac{r_2r_5}{r_1r_7} + \frac{r_4r_6}{r_3r_7}\right)\left\{\frac{r_9}{r_7} - \frac{r_6}{r_7}\left(1+\frac{r_4}{r_3}\right)\right\}v_2'\right],$$

$$F_{33} = \left[\left(1+\frac{r_2}{r_1V_T}\right) - \frac{r_2}{r_1V_T}\left\{1+\frac{r_2r_5}{r_1r_7} + \frac{r_4r_6}{r_3r_7}\right\} \times \left\{\frac{r_8}{r_7} - \frac{r_5}{r_7}\left(1+\frac{r_2}{r_1}\right)\right\}v_1'\frac{r_2}{r_1V_T} + \left\{1+\frac{r_2r_5}{r_1r_7} + \frac{r_4r_6}{r_3r_7}\right\}\right.$$
$$\left. \times \left\{\frac{r_9}{r_7} - \frac{r_6}{r_7}\left(1+\frac{r_4}{r_3}\right)\right\}v_2'\right],$$

$$F_{41} = \frac{r_4}{r_3V_T}\left[\left\{1+\frac{r_2r_5}{r_1r_7} + \frac{r_4r_6}{r_3r_7}\right\}\left\{\frac{r_8}{r_7} - \frac{r_5}{r_7}\left(1+\frac{r_2}{r_1}\right)\right\}v_1' + \left(1+\frac{r_2r_5}{r_1r_7} + \frac{r_4r_6}{r_3r_7}\right)\left\{\frac{r_9}{r_7} - \frac{r_6}{r_7}\left(1+\frac{r_4}{r_3}\right)\right\}v_2'\right],$$

$$F_{44} = \left[\left(1+\frac{r_4}{r_3V_T}\right) - \frac{r_4}{r_3V_T}\left\{1+\frac{r_2r_5}{r_1r_7} + \frac{r_4r_6}{r_3r_7}\right\}\left\{\frac{r_8}{r_7} - \frac{r_5}{r_7}\left(1+\frac{r_2}{r_1}\right)\right\}v_1'\frac{k_2}{r_1V_T} + \left\{1+\frac{r_2r_5}{r_1r_7} + \frac{r_4r_6}{r_3r_7}\right\}\right.$$
$$\left. \times \left\{\frac{r_9}{r_7} - \frac{r_6}{r_7}\left(1+\frac{r_4}{r_3}\right)\right\}v_2'\right],$$

$$F_{12} = 0, \quad F_{32} = 0, \quad F_{42} = 0$$

$$\mathbf{B}_{k-1}^{(1)} = \frac{\partial \mathbf{f}_{k-1}(\hat{\mathbf{x}}_{k-1}, \mathbf{u}_{k-1})}{\partial \mathbf{u}_1} \tag{3.63}$$

$$= \begin{bmatrix} B_1 & B_2 & B_3 & B_4 \end{bmatrix}^T \tag{3.64}$$

$$\mathbf{B}_{k-1}^{(2)} = \frac{\partial \mathbf{f}_{k-1}(\hat{\mathbf{x}}_{k-1}, \mathbf{u}_{k-1})}{\partial \mathbf{u}_2} \tag{3.65}$$

$$= \begin{bmatrix} B_5 & B_6 & B_7 & B_8 \end{bmatrix}^T \tag{3.66}$$

where

$B_1 = T_s \left[\left\{ 1 + \frac{r_2 r_5}{r_1 r_7} + \frac{r_4 r_6}{r_3 r_7} \right\} \times \left\{ \frac{r_8}{r_7} - \frac{r_5}{r_7} \left(1 + \frac{r_2}{r_1} \right) \right\} \right],$

$B_3 = T_s \left[\left(1 + \frac{r_2}{r_1} \right) - \frac{r_2}{r_1} \left\{ 1 + \frac{r_2 r_5}{r_1 r_7} + \frac{r_4 r_6}{r_3 r_7} \right\} \times \left\{ \frac{r_8}{r_7} - \frac{r_5}{r_7} \left(1 + \frac{r_2}{r_1} \right) \right\} \right],$

$B_4 = -\frac{r_4 T_s}{r_3 V_T} \left[\left\{ 1 + \frac{r_2 r_5}{r_1 r_7} + \frac{r_4 r_6}{r_3 r_7} \right\} \times \left\{ \frac{r_9}{r_7} - \frac{r_6}{r_7} \left(1 + \frac{r_4}{r_3} \right) \right\} \right],$

$B_5 = T_s \left[\left\{ 1 + \frac{r_2 r_5}{r_1 r_7} + \frac{r_4 r_6}{r_3 r_7} \right\} \times \left\{ \frac{r_9}{r_7} - \frac{r_6}{r_7} \left(1 + \frac{r_4}{r_3} \right) \right\} \right],$

$B_7 = -\frac{r_2 T_s}{r_1 V_T} \left[\left\{ 1 + \frac{r_2 r_5}{r_1 r_7} + \frac{r_4 r_6}{r_3 r_7} \right\} \times \left\{ \frac{r_9}{r_7} - \frac{r_6}{r_7} \left(1 + \frac{r_4}{r_3} \right) \right\} \right],$

$B_8 = T_s \left[\left(1 + \frac{r_4}{r_3} \right) - \frac{r_2}{r_1} \left\{ 1 + \frac{r_2 r_5}{r_1 r_7} + \frac{r_4 r_6}{r_3 r_7} \right\} \times \left\{ \frac{r_8}{r_7} - \frac{r_5}{r_7} \left(1 + \frac{r_2}{r_1} \right) \right\} \right],$

$B_2 = 0, \quad B_6 = 0.$

T_s is sampling time.

The measurement model is

$$\mathbf{y}_k = \mathbf{H}_k \mathbf{x}_k \tag{3.67}$$

$$\mathbf{H}_k = \frac{\partial \mathbf{h}_k(\mathbf{f}_{k-1}(\hat{\mathbf{x}}_{k-1}))}{\partial \mathbf{x}_k} \tag{3.68}$$

$$= \begin{bmatrix} 0 & 0 & 1 & -1 \end{bmatrix}. \tag{3.69}$$

The extended state space model is:

$$\begin{bmatrix} \mathbf{x}_k \\ \theta_k \end{bmatrix} = \begin{bmatrix} \mathbf{F}_{k-1} & 0 \\ 0 & 1 \end{bmatrix} \begin{bmatrix} \mathbf{x}_{k-1} \\ \theta_{k-1} \end{bmatrix} + \begin{bmatrix} \mathbf{B}_{k-1} \\ 0 \end{bmatrix} \mathbf{v}_i + \begin{bmatrix} v_{x_{k-1}} \\ v_{\theta_{k-1}} \end{bmatrix} \tag{3.70}$$

$$\mathbf{y}_k = \mathbf{H}_k \mathbf{x}_k + w_k \tag{3.71}$$

where

$$\mathbf{x}_k = \begin{bmatrix} v_{E_k} & q_{L_k} \end{bmatrix}^T$$

and $\theta_k = [v_{C1_k}, v_{C2_k}]$. The discrete time state space equation for proposed BJT DA circuit is:

$$\begin{bmatrix} v_{E_k} \\ q_{L_k} \\ v_{C1_k} \\ v_{C2_k} \end{bmatrix} = \begin{bmatrix} F_{11} & F_{12} & F_{13} & F_{14} \\ F_{21} & F_{22} & F_{23} & F_{24} \\ F_{31} & F_{32} & F_{33} & F_{34} \\ F_{41} & F_{42} & F_{43} & F_{44} \end{bmatrix} \begin{bmatrix} v_{E_{k-1}} \\ q_{L_{k-1}} \\ v_{C1_{k-1}} \\ v_{C2_{k-1}} \end{bmatrix} + \begin{bmatrix} B_1 \\ B_2 \\ B_3 \\ B_4 \end{bmatrix} v_1' + \begin{bmatrix} B_5 \\ B_6 \\ B_7 \\ B_8 \end{bmatrix} v_2'$$

$$\mathbf{y}_k = v_{C1_k} - v_{C2_k} \tag{3.72}$$

where

$$\mathbf{x}_k = \begin{bmatrix} v_{E_k} & q_{L_k} & v_{C1_k} & v_{C2_k} \end{bmatrix}^T \tag{3.73}$$

$$\mathbf{F}_{k-1} = \begin{bmatrix} F_{11} & F_{12} & F_{13} & F_{14} \\ F_{21} & F_{22} & F_{23} & F_{24} \\ F_{31} & F_{32} & F_{33} & F_{34} \\ F_{41} & F_{42} & F_{43} & F_{44} \end{bmatrix} \tag{3.74}$$

$$\mathbf{B}_{k-1}^{(1)} = \begin{bmatrix} B_1 & B_2 & B_3 & B_4 \end{bmatrix}^T \tag{3.75}$$

$$\mathbf{B}_{k-1}^{(2)} = \begin{bmatrix} B_5 & B_6 & B_7 & B_8 \end{bmatrix}^T \tag{3.76}$$

$$\mathbf{H}_k = \begin{bmatrix} 0 & 0 & 1 & -1 \end{bmatrix} \tag{3.77}$$

3.2.3 Simulation Results for Differential Amplifier Circuit

The estimation of collector voltages of BJT DA has been performed in MATLAB using EKF. The EKF estimated values have been compared with the RLS estimated method and PSPICE simulated values. PSPICE simulated values have been considered as the actual value. Peak to peak differential input voltage is 2mV. Parameters used in simulation are: $R_{C_1} = 8k\Omega$, $R_{C_2} = 8k\Omega$, $R_E = 0.10k\Omega$, $R_L = 10k\Omega$, $C_L = 10\mu F$. Input signal frequency is 1 kHz. Sampling time is 0.0001 seconds. Figure 3.9 to Figure 3.11 show the estimation for noiseless and noisy input using EKF and RLS method and compares with PSPICE simulated values. The white Gaussian noise with zero mean and different variances have been used as noisy input for estimation purpose. $\mathbf{Q}_k$= diag $[0.01\ 0.01\ 0.01\ 0.01]$ and $\mathbf{R}_k$=0.1. $\mathbf{Q}_k$ and $\mathbf{R}_k$ have been selected by trial and error method. Table 3.5 presents the root mean square error (RMSE) of EKF and RLS methods for noisy inputs. EKF method has smaller RMSE value as compared to RLS method.

Table 3.5: RMSE of output estimation using EKF and RLS for peak to peak differential input of 2mV.

S. No.	Gaussian noise at input source	Input frequency (Hz)	EKF RMSE	RLS RMSE
1.	$\mu = 0, \sigma = 0.005$	100	0.00034	0.00040
2.	$\mu = 0, \sigma = 0.010$	1000	0.00037	0.00045
3.	$\mu = 0, \sigma = 0.025$	10000	0.00043	0.00048
4.	$\mu = 0, \sigma = 0.050$	100	0.00051	0.00085
5.	$\mu = 0, \sigma = 0.100$	1000	0.00054	0.00093

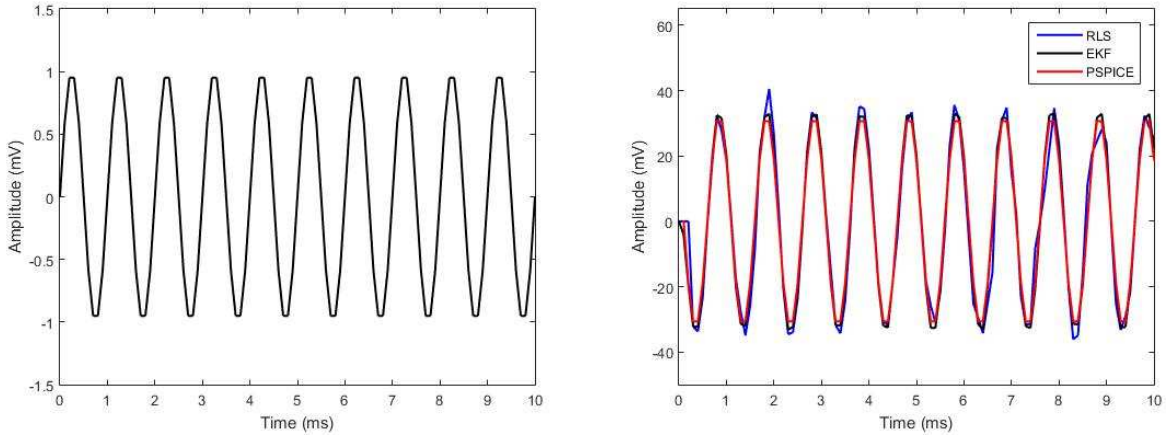

(a) (b)

Figure 3.9: Differential amplifier output for sinusoidal input. (a). Noiseless DA input voltage. (b). Estimated DA output voltage for noiseless input.

General Remarks

(i) Considering $\mathbf{w}[n]$ as independent and identically distributed (i.i.d.), $\mathbf{w} \sim N(0, I)$ and $\mathbf{v}[n]$ as i.i.d., $\mathbf{v} \sim N(0, I)$, we have

$$\mathbb{E}(d\mathbf{w}(t)\, d\mathbf{w}(t)^T) = dt\, I \tag{3.78}$$

$$\mathbb{E}(d\mathbf{v}(t)\, d\mathbf{v}(t)^T) = dt\, I \tag{3.79}$$

where $\mathbb{E}$ represents the expectation value. Now replacing dt by Δ, we have

$$\mathbb{E}(\sqrt{\Delta}\mathbf{w}[n+1]\, \sqrt{\Delta}\mathbf{w}[n+1]^T) = \Delta I. \tag{3.80}$$

The factor of $\sqrt{\Delta}$ comes because by Itô formulae. Similarly, we have for $\mathbf{v}(t)$.

$$\mathbf{x}[n+1] = (I + \mathbf{f}\Delta)\mathbf{x}[n] + \sqrt{\Delta}\,\mathbf{v}[n+1] \tag{3.81}$$

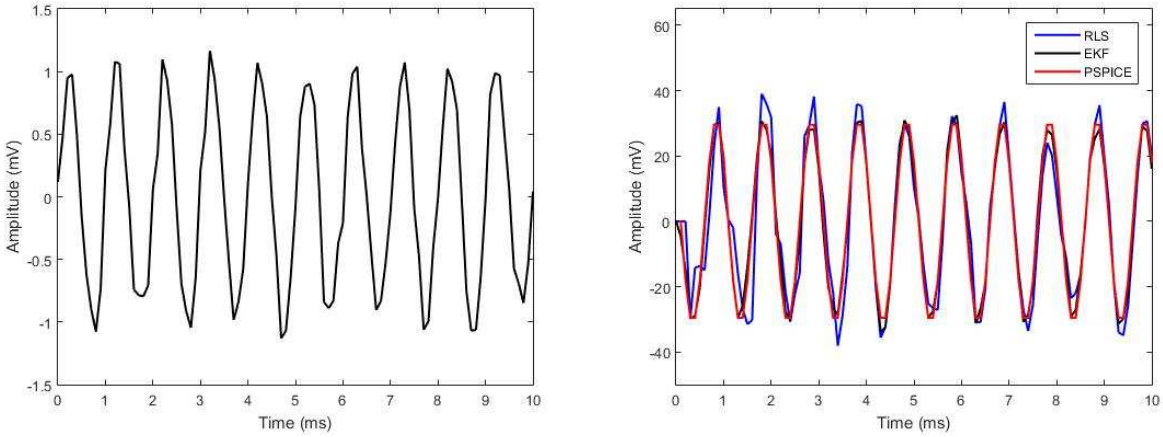

(a) (b)

Figure 3.10: DA output for noisy input. White Gaussian noise of zero mean and 0.01 variance is used. Peak to peak differential input voltage is 2mV. (a): Noisy DA input voltage. (b). Estimated DA output voltage for noisy input.

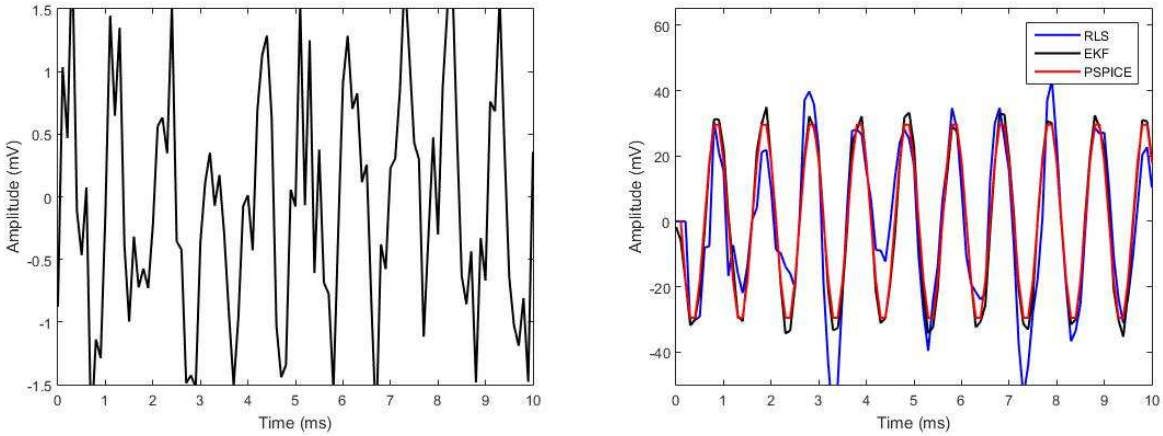

(a) (b)

Figure 3.11: : DA output for noisy input. White Gaussian noise of zero mean and 0.1 variance is used. Peak to peak differential input voltage is 2mV. (a): Noisy DA input voltage. (b). Estimated DA output voltage for noisy input.

$$\mathbf{y}[n+1] = \mathbf{y}[n] + \mathbf{h}(\mathbf{x}[n])\,\Delta + \sqrt{\Delta}\,\mathbf{w}[n+1] \tag{3.82}$$

$$\hat{\mathbf{x}}[n+1] - \hat{\mathbf{x}}[n] = \mathbf{f}(\hat{\mathbf{x}}[n])\Delta + P[n]\mathbf{R}^{-1}h'(\hat{\mathbf{x}}[n])^T(\mathbf{y}[n+1] - \mathbf{y}[n] - \mathbf{h}(\hat{\mathbf{x}}[n])\Delta) \tag{3.83}$$

The difference between measured and estimated output is known as the innovation process and is represented by $i[n]$.

$$\begin{aligned} i[n] &= \mathbf{y}[n+1] - \mathbf{y}[n] - \mathbf{h}(\hat{\mathbf{x}}[n])\Delta \\ &= \mathbf{h}(\mathbf{x}[n+1]) + \sqrt{\Delta}\mathbf{w}[n+1] - \mathbf{h}'(\hat{\mathbf{x}}[n])\Delta \\ &= \mathbf{h}(\mathbf{x}[n])\Delta - \mathbf{h}(\hat{\mathbf{x}}[n])\Delta + \sqrt{\Delta}\mathbf{w}[n+1] \\ &\approx \Delta\mathbf{h}'(\hat{\mathbf{x}}[n])e[n] + \sqrt{\Delta}\mathbf{w}[n+1] \end{aligned} \tag{3.84}$$

$$e[n] = \mathbf{x}[n] - \hat{\mathbf{x}}[n] \tag{3.85}$$

$$\mathbb{E}(i[n]i[n]^T) = \Delta^2 E(\mathbf{h}'(\hat{\mathbf{x}}[n])P_{n|n}\mathbf{h}'(\hat{\mathbf{x}}[n])) + \Delta I \tag{3.86}$$

$$\mathbb{E}(i[n]i[n+r]^T) = 0, \quad r \geq 1. \tag{3.87}$$

So, it is white non-Gaussian process.

(ii) Though it seems that large measurement noise will cause bad estimates, but above EKF equations imply that if the variance of measurement noise is very small as compared to some matrix norm, $\mathbf{R}^{-1}$ will be very large and will cause instability.

Chapter 4

Extended Kalman Filter Based Nonlinear System Identification Described in Terms of Kronecker Product

---

This Chapter[1] presents the implementation of extended Kalman filter (EKF) on MOSFET for output voltage estimation. For this, the nonlinear system dynamics has been modelled using Kronecker product. To obtain the state space model of the circuit, Enz-Krummenacher-Vittoz (EKV) model of the MOSFET and Kirchhoff's current law (KCL) have been used. This method has been compared with the wavelet transform (WT) representation of the system using Kronecker product, where the least mean square (LMS) has been implemented for state estimation. Simulation results validate the superiority of EKF method on Kronecker representation of the system.

Major contributions of the proposed work are (i) EKF in literature has been applied mostly to control problems as in robotics, but very little of EKF has been applied to nonlinear electronic circuit. (ii) Usually parameter estimation in circuits is based on block processing algorithms and not on real time algorithms. (iii) Applying WT to nonlinear dynamical system described by the circuit, by transforming the dynamical state equations using Kronecker product (tensor product) into a form, where the gradient

[1]This chapter consists the results of research article "Bansal R, Majumdar S, Parthasarthy H. Extended Kalman filter based nonlinear system identification described in terms of kronecker product, AEU-Int J Electron C, 108, pp. 107-117, 2019".

algorithm can be applied. For block processing algorithm, we use wavelets which take into account resolution/scaling properties of the circuit signals over different time slots. This enables us to store lesser data i. e. achieve compression during estimation process. (iv) Comparing real time EKF for state estimation with WT based parameter estimation by representing the dynamical system using the Kronecker product enables easy approach to both the methods. Wavelet based parameter estimation is usually applied to linear models. Here, we applied to a nonlinear model by representing the dynamics of the nonlinearity using Kronecker products. (v) This work presents a comparison between real time algorithm and block processing based algorithm. The former has the lesser complexity but, the later provides compression as all the samples are not used for estimation.

Several methods have been presented for state estimation in literature. The Kalman filter (KF) algorithm is widely used for estimation in different applications [90] - [96]. Though it is an optimal estimator, but it can be used for linear systems only. It also assumes that the process and measurement noise are Gaussian in nature and stationarity of the external noise. These assumptions are not followed in various practical applications. For such cases, H_∞ and particle filter (PF) are used. But, most of the literature presents the use of H_∞ filter on linear systems. Implementation of nonlinear version of H_∞ filter leads to instability of the system [97]. PF is also used as an alternative to Gaussian assumption, but its estimation accuracy is affected by particle degradation. The basic method of particle filter is that more weights are given to more probable states for given measurements. It is well suited for Markovian state dynamics [98]. For state estimation of nonlinear systems, version of KF, namely EKF has been used. The EKF applies KF for system dynamics obtained from the linearization of the original nonlinear dynamics around the previous state estimates. EKF has been widely used in various applications [99] - [102]. In [103], the state and measurement models are linear and hence, the KF and its modification works. In [78], the EKF has been applied to state estimation. But in large circuits, there are far more number of state variables to be estimated. In [77], no state dynamics is assumed. Only a nonlinear measurement model is assumed and parameters are estimated by block processing algorithm. We used both, the state dynamics, following KCL applied to a nonlinear circuit along with a measurement model and results are compared with block processing algorithm.

Large inconsistent observations occur in measurements, known as outliers. The

outliers degrade the performance of linear recursive algorithm, if the measurements are assumed to be Gaussian distributed. To overcome this problem, various methods have been proposed [104] - [105]. [104] presented the identification of ARX model with constrained output in the presence of non-Gaussian distribution of measurements. Constraints present an important role in estimation problem as they reduce the degradation of product quality. Optimization also plays an important role in estimation, when several parameters have to be estimated. Various optimization methods have been used in literature for accurate estimation purpose. The main drawback of classical optimization methods is that they are not suitable for complex optimization problems. So, metaheuristic optimization methods have been proposed, which are inspired by natural selection and social adaption. These metaheuristic algorithms make use of the best features of nature and have been applied in various applications such as robotics, power converters etc. [106] - [108].

The Kronecker product has been used for representation of nonlinear system to obtain the more accurate representation of the system dynamics. The O. U. process has been used as an input to consider the both, white noise and the Brownian process. The formal derivation of Brownian motion is white noise, but Îto calculus is preferred as compared to white noise calculus to deal with dynamical systems perturbed by noise. The Kushner Kallainpur filter is an infinite dimensional, real time filter. So, to implement on a computer we expand this equation around the conditional mean and retain up to quadratic order in state estimation errors. This filter is derived by Îto calculus together with Bayes' rule and conditional density. The finite filter, EKF obtained in this way has been used in this chapter for output voltage estimation of MOSFET.

Estimation using the EKF has been compared with wavelet based block processing method. In wavelet representation, the minimum and maximum frequencies are different in various slots. This provides the advantage of using only a portion of wavelet coefficients for estimation by adjusting the resolution in each block. The minimum and maximum indices are different by minimum and maximum frequencies within each time slot. The advantage of wavelet based estimation is that it does not require all the wavelet coefficients for estimation, thus, requires smaller data storage. It is block processing based estimation, so it can not be used for real-time estimation. On the other hand, EKF is real-time estimation and has less complexity as compared to wavelet based estimation

The circuit state space representation using EKV model of MOSFET and Kronecker

product has been derived in Section 4.1. Section 4.2 presents the derivation of WT based system representation using Kronecker product. Section 4.3 presents implementation of EKF to MOS circuit. Simulation results are presented in Section 4.4. Section 4.5 draws the concluding remarks. At the end of this chapter, general remarks are given that discusses the presence of outliers also. The comparison of the computational complexity of both representation is proposed in Table 4.3 and 4.4.

4.1 Modelling of MOSFET Circuit Dynamics Using Kronecker Product

MOSFET circuit is shown in Figure 4.1(a). The EKV model of MOSFET is shown in Figure 4.1(b). Applying KCL and replacing the MOS transistor by EKV model, we have:

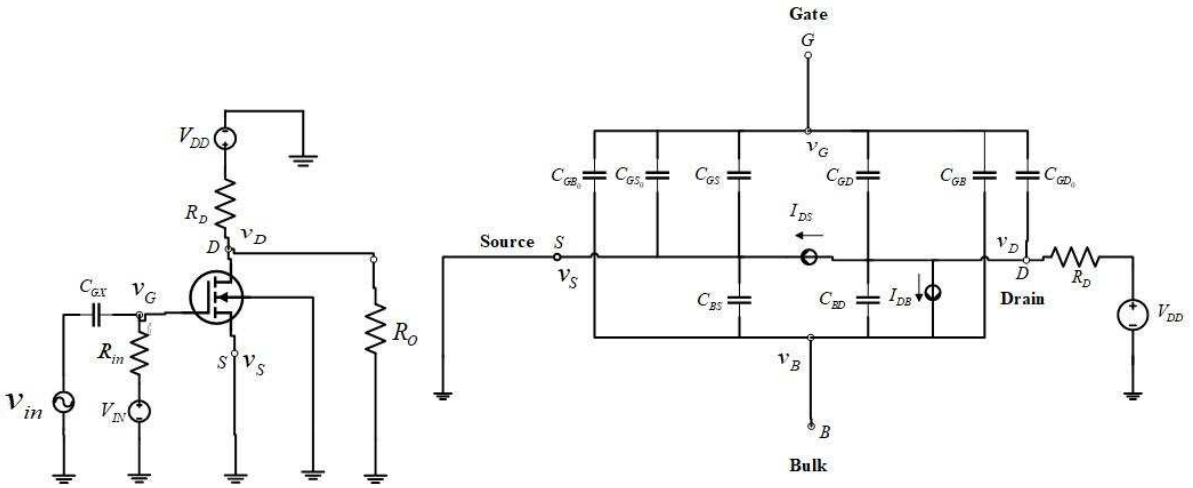

(a) MOSFET circuit diagram (b) EKV equivalent circuit for MOSFET.

Figure 4.1: MOSFET and its EKV equivalent circuit.

$$(C_{GS}+C_{GS_0})\left(\frac{dv_S}{dt}-\frac{dv_G}{dt}\right)+(C_{GD}+C_{GD_0})\left(\frac{dv_D}{dt}-\frac{dv_G}{dt}\right)$$
$$+(C_{GB}+C_{GB_0})\times\left(\frac{dv_B}{dt}-\frac{dv_G}{dt}\right)=0 \tag{4.1}$$

$$(C_{GD}+C_{GD_0})\left(\frac{dv_G}{dt}-\frac{dv_D}{dt}\right)+C_{BD}\left(\frac{dv_B}{dt}-\frac{dv_D}{dt}\right)=I_{DS}+I_{DB} \tag{4.2}$$

$$(C_{GS}+C_{GS_0})\left(\frac{dv_G}{dt}-\frac{dv_S}{dt}\right)+C_{BS}\left(\frac{dv_B}{dt}-\frac{dv_S}{dt}\right)=-I_{DS} \tag{4.3}$$

$$C_{GX}\left(\frac{dv_{in}}{dt}-\frac{dv_G}{dt}\right)+\frac{V_{IN}-v_G}{R_{in}}=0 \tag{4.4}$$

where v_G, v_D, v_S and v_B are the state variables. C_{GD}, C_{GS} and C_{GB} are the drain to channel capacitance, source to channel capacitance and base to channel capacitance respectively. C_{OX} is oxide capacitance. Drain current I_D is

$$I_D = I_{DS}+I_{DB} \tag{4.5}$$

As $I_{DB}\cong 0$, therefore $I_D \cong I_{DS}$. From the EKV model of weak inversion, we have

$$I_D = I_{DS} = I_0\frac{W}{L}e^{\frac{v_{GB}-V_{T_0}}{\eta U_T}}\left(e^{-\frac{v_{SB}}{U_T}}-e^{-\frac{v_{DB}}{U_T}}\right) \tag{4.6}$$

where W is the width and L is the length of the MOSFET channel, $\frac{W}{L}$ is the aspect ratio, V_{T_0} and U_T are the the equilibrium threshold voltage and thermal voltage respectively. I_0 is the unary specific current. η is the subthreshold slope factor.

Expanding (4.6) using Taylor series and retaining up to quadratic terms, we have

$$\begin{aligned} I_D =& \frac{I_0W}{U_TL}\left\{(v_D-v_S)\left(1-\frac{V_{T_0}}{\eta U_T}+\frac{V_{T_0}^2}{2\eta^2U_T^2}-\frac{1}{6}\frac{V_{T_0}^3}{\eta^3U_T^3}\right)\right\}+\frac{I_0W}{2U_T^2L}\left\{\left(v_S^2-v_D^2\right.\right.\\ &\left.\left.-2(v_Sv_B-v_Dv_B)-v_Dv_S+v_Sv_D\right)\times\left(1-\frac{V_{T_0}}{\eta U_T}+\frac{V_{T_0}^2}{2\eta^2U_T^2}-\frac{1}{6}\frac{V_{T_0}^3}{\eta^3U_T^3}\right)\right\}\\ &+\frac{I_0W}{U_TL}\left\{(v_Gv_D-v_Bv_D-v_Gv_S+v_Bv_S)\times\left(\frac{1}{\eta U_T}-\frac{V_{T_0}}{\eta^2U_T^2}+\frac{3V_{T_0}^2}{\eta^3U_T^3}\right)\right\}. \end{aligned} \tag{4.7}$$

Now, modelling the input as O. U. process, to account for both kinds of extreme behaviour namely, the white Gaussian noise process and the Brownian process, we have:

$$\frac{dv_{in}}{dt} = -\gamma v_{in}+\sigma_j\rho_jN_j(t) \tag{4.8}$$

where γ, σ_j and ρ_j are non-negative constants. $N_j(t)$ is white Gaussian noise with zero mean and unit variance.

$$dv_{in}(t) = -\gamma v_{in}dt+\sigma_j\rho_j\,d\beta_j(t) \tag{4.9}$$

where $\beta_j(t)$ is the Brownian motion process. Using $C_{GS}+C_{GS_0}=C_S$, $C_{GD}+C_{GD_0}=C_D$ and $C_{GB}+C_{GB_0}=C_B$ and converting the above differential equations (4.1)-(4.4) to stochastic differential equations (SDE), we have

$$dv_G(t) = -\frac{v_G}{R_{in}C_{GX}}dt + \frac{V_{IN}}{R_{in}C_{GX}}dt - \gamma v_{in}dt + \sigma_1\rho_1\, d\beta_1(t) \tag{4.10}$$

$$\begin{aligned} dv_B(t) = \Bigg[& -\frac{s_2 v_G}{R_{in}C_{GX}} + \frac{I_0}{U_T}\frac{W}{L}s_1 s_7\,(v_D - v_S) - \frac{s_1 s_7}{U_T}v_S v_B + \frac{s_1 s_7}{U_T}v_D v_B \\ & + \frac{s_1 s_7}{2U_T}(-v_D v_S + v_S v_D) + s_1 s_8(v_G v_D - v_G v_S) + s_1 s_8(v_B v_S - v_B v_D) \\ & + \frac{s_1 s_7}{2U_T}(v_S^2 - v_D^2)\Bigg]\, dt + s_4\{-\gamma v_{in}dt + \sigma_2\rho_2\, d\beta_2(t)\} + \frac{s_2 V_{IN}}{R_{in}C_{GX}}dt \end{aligned} \tag{4.11}$$

$$\begin{aligned} dv_S(t) = \Bigg[& -\frac{s_4 v_G}{R_{in}C_{GX}} + \frac{I_0}{U_T}\frac{W}{L}s_3 s_7\,(v_D - v_S) - \frac{s_3 s_7}{U_T}v_S v_B + \frac{s_3 s_7}{U_T}v_D v_B \\ & + \frac{s_3 s_7}{2U_T}(-v_D v_S + v_S v_D) + s_3 s_8(v_G v_D - v_G v_S) + s_3 s_8(v_B v_S - v_B v_D) \\ & + \frac{s_3 s_7}{2U_T}(v_S^2 - v_D^2)\Bigg]\, dt + k_4\{-\gamma v_{in}dt + \sigma_3\rho_3\, d\beta_3(t)\} + \frac{s_4 V_{IN}}{R_{in}C_{GX}}dt \end{aligned} \tag{4.12}$$

$$\begin{aligned} dv_D(t) = \Bigg[& -\frac{s_6 v_G}{R_{in}C_{GX}} + \frac{I_0}{U_T}\frac{W}{L}s_5 s_7\,(v_D - v_S) - \frac{s_5 s_7}{U_T}v_S v_B + \frac{s_5 s_7}{U_T}v_D v_B \\ & + \frac{s_5 s_7}{2U_T}(-v_D v_S + v_S v_D) + s_5 s_8(v_G v_D - v_G v_S) + s_5 s_8(v_B v_S - v_B v_D) \\ & + \frac{s_5 s_7}{2U_T}(v_S^2 - v_D^2)\Bigg]\, dt + s_6\{-\gamma v_{in}dt + \sigma_4\rho_4\, d\beta_4(t)\} + \frac{s_6 V_{IN}}{R_{in}C_{GX}}dt \end{aligned} \tag{4.13}$$

$$\mathbf{z}(t) = v_D(t) \tag{4.14}$$

$s_1 = \frac{C_D(C_S+C_{BS})(C_SC_{BS}+C_SC_{BD})}{C_SC_{BS}(C_{BD}C_S(-C_S-C_{BS})+C_SC_{BS}(-C_D-C_{BD}))} - \frac{1}{C_{BS}}$,

$s_2 = \Bigg[\frac{C_D(C_S+C_{BS})\{-C_SC_DC_{BS}-C_SC_{BD}(C_S+C_{BS})\}}{C_SC_{BS}\{C_SC_{BD}(-C_S-C_{BS})+C_SC_{BS}(-C_D-C_{BD})\}} - \frac{C_S}{C_{BS}} + \frac{(C_S+C_B+C_D)(C_S+C_{BS})}{C_SC_{BS}}$
$+ \frac{C_D(C_S+C_{BS})\{-C_{BD}(C_S+C_D+C_B)(C_S+C_{BS})\}}{C_SC_{BS}\{C_SC_{BD}(-C_S-C_{BS})+C_SC_{BS}(-C_D-C_{BD})\}}\Bigg]$,

$s_3 = \frac{C_D(C_{BS}+C_{BD})}{\{C_SC_{BD}(C_S+C_{BS})+C_SC_{BS}(C_S+C_{BD})\}}$,

$s_4 = \frac{C_D}{C_S}\left\{\frac{C_SC_DC_{BS}-C_S^2C_{BD}+C_{BD}(C_S+C_{BS})(C_S+C_D+C_B)}{C_DC_{BD}(C_S+C_{BS})+C_SC_{BS}(C_D+C_{BD})}\right\} + \frac{C_S+C_D+C_B}{C_S}$,

$s_5 = \frac{C_S(C_{BS}+C_{BD})}{C_DC_{BD}(-C_S-C_{BS})+C_SC_{BS}(-C_D-C_{BD})}$,

$s_6 = \frac{-C_SC_DC_{BS}+C_S^2C_{BD}+C_{BD}(-C_S-C_{BS})(C_S+C_D+C_B)}{C_DC_{BD}(-C_S-C_{BS})+C_SC_{BS}(-C_D-C_{BD})}$,

$s_7 = \frac{I_0}{U_T}\frac{W}{L}\left(1 - \frac{V_{T_0}}{\eta U_T} + \frac{V_{T_0}^2}{2\eta^2U_T^2} - \frac{1}{6}\frac{V_{T_0}^3}{\eta^3U_T^3}\right)$, $s_8 = \frac{I_0}{U_T}\frac{W}{L}\left(\frac{1}{\eta U_T} - \frac{V_{T_0}}{\eta^2U_T^2} + \frac{V_{T_0}^2}{2\eta^3U_T^3}\right)$.

After retaining up to quadratic terms in Taylor series expansion of the function f and

h around the quiescent points, we get a vector of the form

$$\begin{aligned} d\mathbf{x}(t) =& \mathbf{A}_1\mathbf{x}(t) + \mathbf{A}_2(\mathbf{x}(t)\otimes\mathbf{x}(t)) + \mathbf{A}_3\mathbf{u}_1(t) + \mathbf{A}_4\mathbf{u}_2(t) + \mathbf{A}_5(\mathbf{x}(t)\otimes\mathbf{u}(t)) \\ &+ \mathbf{A}_6 d\beta(t) + \mathbf{A}_7(\mathbf{x}(t)\otimes d\beta(t)) \end{aligned} \tag{4.15}$$

$$\mathbf{x}(t) = \begin{bmatrix} v_G(t) & v_B(t) & v_S(t) & v_D(t) \end{bmatrix}^T,$$

$$\mathbf{A}_1 = \begin{bmatrix} -\frac{1}{R_{in}C_{GX}} & 0 & 0 & 0 \\ -\frac{s_2}{R_{in}C_{GX}} & s_1s_7 & -s_1s_7 & 0 \\ -\frac{s_4}{R_{in}C_{GX}} & s_3s_7 & -s_3s_7 & 0 \\ -\frac{s_6}{R_{in}C_{GX}} & s_5s_7 & -s_5s_7 & 0 \end{bmatrix}$$

$$\mathbf{A}_2 = \begin{bmatrix} 0 & 0 & 0 & 0 & 0 & 0 & 0 & 0 & 0 & 0 & 0 & 0 & 0 & 0 & 0 & 0 \\ 0 & s_1s_8 & -s_1s_8 & 0 & 0 & -\frac{s_1s_7}{2U_T} & -\frac{s_1s_7}{2U_T} & \frac{s_1s_7}{U_T} & 0 & \frac{s_1s_7}{2U_T} & \frac{s_1s_7}{2U_T} & -\frac{s_1s_7}{U_T} & 0 & -s_1s_8 & s_1s_8 & 0 \\ 0 & s_3s_8 & -s_3s_8 & 0 & 0 & -\frac{s_3s_7}{2U_T} & -\frac{s_3s_7}{2U_T} & \frac{s_3s_7}{U_T} & 0 & \frac{s_3s_7}{2U_T} & \frac{s_3s_7}{2U_T} & -\frac{s_3s_7}{U_T} & 0 & -s_3s_8 & s_3s_8 & 0 \\ 0 & s_5s_8 & -s_5s_8 & 0 & 0 & -\frac{s_5s_7}{2U_T} & -\frac{s_5s_7}{2U_T} & \frac{s_5s_7}{U_T} & 0 & \frac{s_5s_7}{2U_T} & \frac{s_5s_7}{2U_T} & -\frac{s_5s_7}{U_T} & 0 & -s_5s_8 & s_5s_8 & 0 \end{bmatrix},$$

$$\mathbf{A}_3 = \begin{bmatrix} -\gamma & -\gamma s_2 & -\gamma s_4 & -\gamma s_6 \end{bmatrix}^T,$$

$$\mathbf{A}_4 = \begin{bmatrix} \frac{1}{R_{in}C_{GX}} & \frac{s_2}{R_{in}C_{GX}} & \frac{s_4}{R_{in}C_{GX}} & \frac{s_6}{R_{in}C_{GX}} \end{bmatrix}^T,$$

$\mathbf{A}_5 = 0$,

$$\mathbf{A}_6 = \begin{bmatrix} \rho_1\sigma_1 & 0 & 0 & 0 \\ 0 & \rho_2\sigma_2 & 0 & 0 \\ 0 & 0 & \rho_3\sigma_3 & 0 \\ 0 & 0 & 0 & \rho_4\sigma_4 \end{bmatrix},$$

and $\mathbf{A}_7 = 0$. Input source $\mathbf{u}_1 = v_{in}$, $\mathbf{u}_2 = V_{IN}$.

$$d\beta(t) = \begin{bmatrix} d\beta_1(t) & d\beta_2(t) & d\beta_3(t) & d\beta_4(t) \end{bmatrix}^T.$$

The same method can be applied to the circuit shown in Figure 4.2. Figure 4.2 consists of cascade of two MOSFET amplifiers which is the MOS analogue of the classical bipolar junction transistor (BJT) Darlington pair. The state vector for this circuit is

$$\mathbf{x}^{(2)}(t) = \begin{bmatrix} v_{G_1}(t) & v_{B_1}(t) & v_{S_1}(t) & v_{D_1}(t) & v_{G_2}(t) & v_{B_2}(t) & v_{S_2}(t) & v_{D_2}(t) \end{bmatrix}^T$$

The Kronecker product is applicable to this vector by replacing $\mathbf{x}(t)$ by $\mathbf{x}^{(2)}(t)$. The simulation can be expanded slightly by including the small signal equivalent model

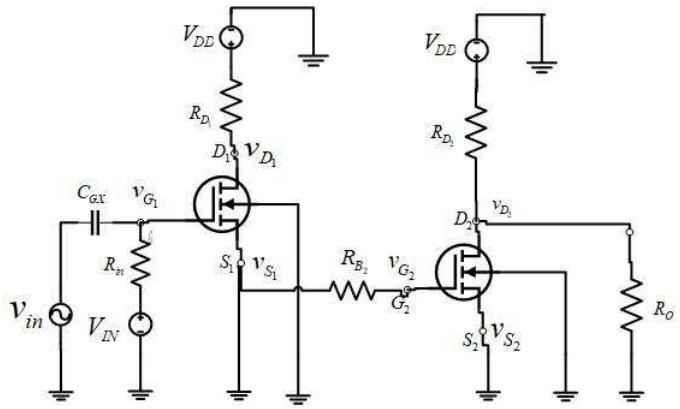

Figure 4.2: Darlington pair circuit using MOSFET.

cascade of the two MOSFET amplifiers, which is the MOS analogue of the BJT Darlington pair amplifier. By enlarging the state vector, the resulting state equation can be put in general form (4.15). The formalism is the same except with $\mathbf{A}_1$, $\mathbf{A}_1$,...,$\mathbf{A}_7$ will be changed to the larger matrices. The source voltage of the first MOSFET amplifier is applied as input to second MOS amplifier i. e. $v_{in_2} = v_{S_1}(t)$, while writing KCL equations.

4.2 System Representation Using Kronecker Product Based Wavelet Transform Method

Representing the measurement model as:

$$d\mathbf{y}(t) = \mathscr{H}\mathbf{x}(t)dt + \sigma_v dw(t) \tag{4.16}$$

where

$$\mathscr{H} = \begin{bmatrix} 1 & 0 & 0 & 0 \\ 0 & 1 & 0 & 0 \\ 0 & 0 & 1 & 0 \\ 0 & 0 & 0 & 1 \end{bmatrix},$$

$w(t)$ is vector valued Brownian motion process. Expanding $\mathbf{x}(t)$ using wavelet basis as

$$\mathbf{x}(t) = \sum_{N_1 \le n \le N_2, k_{\min}(n) \le k \le k_{\max}(n)} c(n,k)\Psi_{n,k}(t)$$

or

$$\mathbf{x}(t) = \sum_{(n,k)\in D} c(n,k)\Psi_{n,k}(t) \tag{4.17}$$

where $\Psi_{n,k}(t)$ is the mother wavelet. Resolution range $[N_1, N_2]$ is chosen appropriately based on characteristic frequency of operation and the time duration of the measurement. Using

$$\Psi_{n,k}(t) = 2^{\frac{n}{2}}\Psi(2^n t - k). \tag{4.18}$$

Let $\Psi(t)$ be concentrated on [a, b] and let w_{min} and w_{max} be the lowest and the highest frequency of operation. Let $[0,T]$ be the time duration of the measurement process. Then, for a given resolution index n, the range of the transition index k must be such that $a \leq 2^n t - k \leq b, t \in [0,T]$. Thus, $2^n t - b \leq k \leq 2^n t - a, t \in [0,T]$ or $-b \leq k \leq 2^n T - a, t \in [0,T]$. Frequency of the wavelet $\Psi_{n,k}(t)$ is

$$\left|\frac{\frac{d\Psi_{n,k}(t)}{dt}}{\Psi_{n,k}(t)}\right| = \frac{2^n\,|\Psi'(2^n t - k)|}{|\Psi(2^n t - k)|} \in [2^n\lambda_{\text{min}}, 2^n\lambda_{\text{max}}] \tag{4.19}$$

where

$$\lambda_{\text{max}} = \max_t \frac{|\Psi'(t)|}{|\Psi(t)|},$$

$$\lambda_{\text{min}} = \min_t \frac{|\Psi'(t)|}{|\Psi(t)|},$$

so the resolution indexes N_1, N_2 must be chosen such that

$$2^{N_2}\lambda_{\text{max}} \approx \frac{w_2}{2\pi},$$

$$2^{N_1}\lambda_{\text{min}} \approx \frac{w_1}{2\pi}$$

or

$$N_1 \approx \log_2\left(\frac{w_1}{2\pi\lambda_{\text{min}}}\right),$$

$$N_2 \approx \log_2\left(\frac{w_2}{2\pi\lambda_{\text{max}}}\right).$$

Choosing the resolution index range in this way enables us to store lesser data for parameter estimation i.e. we have parameter estimation with compression. For the application of wavelet technique, we must either directly measure the entire set of $\mathbf{x}(t)$ of the state variables or else it must be a square non-singular matrix. In the latter

case, we have

$$\mathbf{x}(t) \approx \mathscr{H}^{-1}\frac{d\mathbf{y}(t)}{dt} \tag{4.20}$$

and so

$$\begin{aligned}\frac{d^2\mathbf{y}(t)}{dt^2} &\approx \mathscr{H}\frac{d\mathbf{x}(t)}{dt} \\ &\approx \mathscr{H}\mathbf{A}_1\mathbf{x}(t) + \mathscr{H}\mathbf{A}_2(\mathbf{x}(t)\otimes\mathbf{x}(t)) + \mathscr{H}(\mathbf{A}_3\mathbf{u}_1(t) + \mathbf{A}_4\mathbf{u}_2(t)) + \mathscr{H}\mathbf{A}_5\mathbf{x}(t)\otimes\mathbf{u}(t)\end{aligned} \tag{4.21}$$

Representing the signals $\dot{\mathbf{y}}(t)$ and $\ddot{\mathbf{y}}(t)$ using wavelets as:

$$\dot{\mathbf{y}}(t) \approx \sum_{n,k} c_{\dot{\mathbf{y}}}[n,k]\Psi_{n,k}(t) \tag{4.22}$$

$$\ddot{\mathbf{y}}(t) \approx \sum_{n,k} c_{\ddot{\mathbf{y}}}[n,k]\Psi_{n,k}(t) \tag{4.23}$$

Substituting (4.22) and (4.23) into (4.21) and omitting noise terms, we have

$$\begin{aligned}&\sum_{n,k} c_{\ddot{\mathbf{y}}}[n,k]\Psi_{n,k}(t) \\ &\approx \sum_{n,k}\mathscr{H}\mathbf{A}_1\mathscr{H}^{-1}c_{\dot{\mathbf{y}}}[n,k]\Psi_{n,k}(t) + \sum_{n,k}\mathscr{H}\mathbf{A}_2(\mathscr{H}^{-1}\otimes\mathscr{H}^{-1})(c_{\dot{\mathbf{y}}}[n,k]\otimes c_{\dot{\mathbf{y}}}[n,k]) \\ &\quad\times\Psi_{n,k}(t)\Psi_{m,r}(t) + \mathscr{H}\mathbf{A}_3u_1(t) + \mathscr{H}\mathbf{A}_4u_2(t) + \sum_{n,k}\mathscr{H}\mathbf{A}_5(\mathscr{H}^{-1}\otimes I)(I\otimes\ \mathbf{u}(t)) \\ &\quad\times c_{\dot{\mathbf{y}}}[n,k]\Psi_{n,k}(t)\end{aligned} \tag{4.24}$$

where

$$c_{\dot{\mathbf{y}}}[n,k] \approx \int_0^T \dot{\mathbf{y}}(t)\Psi_{n,k}(t)dt = <\dot{\mathbf{y}},\Psi_{n,k}> = \dot{\mathbf{y}}[n,k]. \tag{4.25}$$

Taking inner product with $\Psi_{p,q}$ on both sides of (4.24) gives

$$\begin{aligned}&\sum_{n,k} c_{\ddot{\mathbf{y}}}[n,k] < \Psi_{n,k},\Psi_{p,q} > \\ &\approx \sum_{n,k}\mathscr{H}\mathbf{A}_1\mathscr{H}^{-1}c_{\dot{\mathbf{y}}}[n,k] < \Psi_{n,k},\Psi_{p,q} > + \sum_{n,k,m,r}\mathscr{H}\mathbf{A}_2(\mathscr{H}^{-1}\otimes\mathscr{H}^{-1}) \\ &c_{\dot{\mathbf{y}}}[n,k]\otimes c_{\dot{\mathbf{y}}}[m,r] < \Psi_{n,k},\Psi_{m,r},\Psi_{p,q} > + \mathscr{H}\mathbf{A}_3u_1[p,q] + \mathscr{H}\mathbf{A}_4u_2[p,q] \\ &+ \sum_{n,k}\mathscr{H}\mathbf{A}_5(\mathscr{H}^{-1}\otimes I)(I\otimes\ \mathbf{u}(t))c_{\dot{\mathbf{y}}}[n,k] < \Psi_{n,k},\Psi_{p,q} >\end{aligned} \tag{4.26}$$

where $\mathbf{u}(t) = \sum\mathbf{u}[n,k]\Psi_{n,k}(t)$, i.e. $\mathbf{u}[n,k] = <\mathbf{u},\Psi_{n,k}>$. Equation (4.26) can be expressed

as

$$c_{\ddot{\mathbf{y}}}[p,q] = \sum_{n,k} m_1[p,q|n,k] c_{\dot{\mathbf{y}}}[n,k] + \delta \sum_{n,k,m,r} m_2[p,q|n,k,m,r](c_{\dot{\mathbf{y}}}[n,k] \otimes c_{\dot{\mathbf{y}}}[m,r]) + \sum_{n,k} m_3[p,q|n,k]\mathbf{u}[n,k] \tag{4.27}$$

where m_1, m_2 and m_3 are expressible in terms of $\mathscr{H}$, $\mathbf{A}_1$,...,$\mathbf{A}_5$. m_1, m_2 depend on Θ, so we write

$$c_{\ddot{\mathbf{y}}}[p,q] = \sum_{n,k} m_1[p,q|n,k,\Theta] c_{\dot{\mathbf{y}}}[n,k] + \delta \sum_{n,k,m,r} m_2[p,q|n,k,m,r,\Theta](c_{\dot{\mathbf{y}}}[n,k] \otimes c_{\dot{\mathbf{y}}}[m,r]) + \sum_{n,k} m_3[p,q|n,k]\mathbf{u}[n,k] \tag{4.28}$$

Applying perturbation theory up to $\mathscr{O}(\delta^2)$ terms

$$c_{\ddot{\mathbf{y}}}[n,k] = c^{(0)}_{\ddot{\mathbf{y}}}[n,k] + \delta c^{(1)}_{\ddot{\mathbf{y}}}[n,k] + \delta^2 c^{(2)}_{\ddot{\mathbf{y}}}[n,k] + \mathscr{O}(\delta^3) \tag{4.29}$$

Equating coefficients of $\delta^{(0)}$, $\delta^{(1)}$, $\delta^{(2)}$ respectively, we have

$$c^{(0)}_{\ddot{\mathbf{y}}}[p,q] = \sum_{n,k} m_1[p,q|n,k,\Theta] c^{(0)}_{\dot{\mathbf{y}}}[n,k] + \sum_{n,k} m_3[p,q|n,k,\Theta]\mathbf{u}[n,k] \tag{4.30}$$

$$\begin{aligned} c^{(1)}_{\ddot{\mathbf{y}}}[p,q] &= \sum_{n,k,m,r} m_2[p,q|n,k,m,r](c^{(0)}_{\dot{\mathbf{y}}}[n,k] \otimes c^{(0)}_{\dot{\mathbf{y}}}[m,r]) + m_1 c^{(1)}_{\dot{\mathbf{y}}}[p,q|n,k] \\ &\stackrel{\Delta}{=} m_2(c^{(0)}_{\dot{\mathbf{y}}} \otimes c^{(0)}_{\dot{\mathbf{y}}})[p,q] + m_1 c^{(1)}_{\dot{\mathbf{y}}}[p,q] \end{aligned} \tag{4.31}$$

$$c^{(2)}_{\ddot{\mathbf{y}}}[p,q] = m_1 c^{(2)}_{\dot{\mathbf{y}}}[p,q] + m_2(c^{(0)}_{\dot{\mathbf{y}}} \otimes c^{(1)}_{\dot{\mathbf{y}}} + c^{(1)}_{\dot{\mathbf{y}}} \otimes c^{(0)}_{\dot{\mathbf{y}}})[p,q] \tag{4.32}$$

where $c^{(0)}_{\dot{\mathbf{y}}}[n,k]$, $c^{(1)}_{\dot{\mathbf{y}}}[n,k]$ and $c^{(2)}_{\dot{\mathbf{y}}}[n,k]$ are obtained from wavelet transform of $\dot{\mathbf{y}}^{(0)}[n,k]$, $\dot{\mathbf{y}}^{(1)}[n,k]$ and $\dot{\mathbf{y}}^{(2)}[n,k]$ respectively by comparing $\mathscr{O}(\delta^0)$, $\mathscr{O}(\delta^1)$ and $\mathscr{O}(\delta^2)$ variations represented in $\mathbf{y}(t)$.

We can retain up to $\mathscr{O}(\delta^0)$ or $\mathscr{O}(\delta^1)$ or $\mathscr{O}(\delta^2)$ terms in expansion of the above equation. Without using perturbation theory, we can estimate Θ plainly by applying the

gradient search algorithm to minimize

$$\xi(\Theta) = \sum_{p,q} ||c_{\dot{\mathbf{y}}}[p,q] - \sum_{n,k} m_1[p,q|n,k,\Theta] c_{\dot{\mathbf{y}}}[n,k] - \sum_{n,k,m,r} m_2[p,q|n,k,m,r,\Theta] \times (c_{\dot{\mathbf{y}}}[n,k] \otimes c_{\dot{\mathbf{y}}}[m,r]) - \sum_{n,k} m_3[p,q|n,k]\mathbf{u}[n,k]||^2. \tag{4.33}$$

The computational burden of WT method is $O(n_x^5)$ per iteration.

4.3 Applying EKF to MOSFET Circuit

Representing equations (4.10)-(4.14) as a state space model

$$\mathbf{x}_k = f_{k-1}(\mathbf{x}_{k-1}, \mathbf{u}_{k-1}, \beta_{k-1}) \tag{4.34}$$

$$\mathbf{z}_k = h_k(\mathbf{x}_k) \tag{4.35}$$

Representing equation (4.34) in terms of Kronecker product, we have :

$$\mathbf{x}_k = \mathbf{F}_{k-1}^{(1)}\mathbf{x}_{k-1} + \mathbf{F}_{k-1}^{(2)}(\mathbf{x}_{k-1} \otimes \mathbf{x}_{k-1}) + \mathbf{B}_{k-1}^{(1)}\mathbf{u}_1 + \mathbf{B}_{k-1}^{(2)}\mathbf{u}_2 + \mathbf{Z}_{k-1}\beta_{k-1} \tag{4.36}$$

where

$$\mathbf{x}_k = \begin{bmatrix} v_G & v_B & v_S & v_D \end{bmatrix}^T$$

$$\mathbf{F}_{k-1}^{(1)} = \frac{\partial f_{k-1}(\hat{\mathbf{x}}_{k-1|k-1}, \mathbf{u}_{k-1})}{\partial \mathbf{x}_{k-1}} \tag{4.37}$$

$$= \begin{bmatrix} 1 - \frac{T_s}{R_{in}C_{GX}} & 0 & 0 & 0 \\ -\frac{s_2 T_s}{R_{in}C_{GX}} & 1 + T_s s_1 s_7 & -T_s s_1 s_7 & 0 \\ -\frac{s_4 T_s}{R_{in}C_{GX}} & T_s s_3 s_7 & 1 - T_s s_3 s_7 & 0 \\ -\frac{s_6 T_s}{R_{in}C_{GX}} & T_s s_5 s_7 & -T_s s_5 s_7 & 1 \end{bmatrix} \tag{4.38}$$

$$\mathbf{F}_{k-1}^{(2)} = \begin{bmatrix} 0 & 0 & 0 & 0 & 0 & 0 & 0 & 0 & 0 & 0 & 0 & 0 & 0 & 0 & 0 & 0 \\ 0 & T_s s_1 s_8 & -T_s s_1 s_8 & 0 & 0 & -\frac{T_s s_1 s_7}{2U_T} & -\frac{T_s s_1 s_7}{2U_T} & \frac{T_s s_1 s_7}{U_T} & 0 & \frac{T_s s_1 s_7}{2U_T} & \frac{T_s s_1 s_7}{2U_T} & -\frac{T_s s_1 s_7}{U_T} & 0 & -T_s s_1 s_8 & T_s s_1 s_8 & 0 \\ 0 & T_s s_3 s_8 & -T_s s_3 s_8 & 0 & 0 & -\frac{T_s s_3 s_7}{2U_T} & -\frac{T_s s_3 s_7}{2U_T} & \frac{T_s s_3 k_7}{U_T} & 0 & \frac{T_s s_3 s_7}{2U_T} & \frac{T_s s_3 s_7}{2U_T} & -\frac{T_s s_3 s_7}{U_T} & 0 & -T_s s_3 s_8 & T_s s_3 s_8 & 0 \\ 0 & T_s s_5 s_8 & -T_s s_5 s_8 & 0 & 0 & -\frac{T_s s_5 s_7}{2U_T} & -\frac{T_s s_5 s_7}{2U_T} & \frac{T_s s_5 s_7}{U_T} & 0 & \frac{T_s s_5 s_7}{2U_T} & \frac{T_s s_5 s_7}{2U_T} & -\frac{T_s s_5 s_7}{U_T} & 0 & -T_s s_5 k_8 & T_s s_5 s_8 & 0 \end{bmatrix} \tag{4.39}$$

$$\mathbf{x}_k \otimes \mathbf{x}_k = \tag{4.40}$$

$$\left[\begin{array}{cccccccccccccccc} v_G v_G & v_G v_B & v_G v_S & v_G v_D & v_B v_G & v_B v_B & v_B v_S & v_B v_D & v_S v_G & v_S v_B & v_S v_S & v_S v_D & v_D v_G & v_D v_B & v_D v_S & v_D v_D \end{array} \right]^T$$

$$\mathbf{B}_{k-1}^{(1)} = \frac{\partial f_{k-1}(\hat{\mathbf{x}}_{k-1|k-1}, \mathbf{u}_{k-1})}{\partial \mathbf{u}_1} \tag{4.41}$$

$$= \left[\begin{array}{cccc} -\gamma T_s & -\gamma s_2 T_s & -\gamma s_4 T_s & -\gamma s_6 T_s \end{array} \right]^T \tag{4.42}$$

$$\mathbf{B}_{k-1}^{(2)} = \frac{\partial f_{k-1}(\hat{\mathbf{x}}_{k-1|k-1}, \mathbf{u}_{k-1})}{\partial \mathbf{u}_2} \tag{4.43}$$

$$= \left[\begin{array}{cccc} \frac{T_s}{R_{in} C_{GX}} & \frac{s_2 T_s}{R_{in} C_{GX}} & \frac{s_4 T_s}{R_{in} C_{GX}} & \frac{s_6 T_s}{R_{in} C_{GX}} \end{array} \right]^T \tag{4.44}$$

$$\mathbf{Z}_{k-1} = \left[\begin{array}{cccc} T_s \rho_1 \sigma_1 & 0 & 0 & 0 \\ 0 & T_s \rho_2 \sigma_2 & 0 & 0 \\ 0 & 0 & T_s \rho_3 \sigma_3 & 0 \\ 0 & 0 & 0 & T_s \rho_4 \sigma_4 \end{array} \right] \tag{4.45}$$

where T_s is sampling period. β_k is the Brownian motion process given by:

$$\beta_k = \left[\begin{array}{cccc} \beta_1 & \beta_2 & \beta_3 & \beta_4 \end{array} \right]^T. \tag{4.46}$$

Measurement model is

$$\mathbf{z}_k = \mathbf{H}_k \mathbf{x}_k \tag{4.47}$$

where

$$\mathbf{H}_k = \frac{\partial h_k(f_{k-1}(\hat{\mathbf{x}}_{k-1|k-1}))}{\partial \mathbf{x}_k} \tag{4.48}$$

$$= \left[\begin{array}{cccc} 0 & 0 & 0 & 1 \end{array} \right] \tag{4.49}$$

EKF algorithm has been implemented to the discrete equations by adding process noise $\mathbf{v}_k$ and measurement noise $\mathbf{w}_k$ to (4.36) and (4.47) respectively.

$$\begin{aligned} \mathbf{x}_k =& \mathbf{F}_{k-1}^{(1)} \mathbf{x}_{k-1} + \mathbf{F}_{k-1}^{(2)} (\mathbf{x}_{k-1} \otimes \mathbf{x}_{k-1}) + \mathbf{B}_{k-1}^{(1)} \mathbf{u}_1 + \mathbf{B}_{k-1}^{(2)} \mathbf{u}_2 \\ &+ \mathbf{Z}_{k-1} \beta_{k-1} + \mathbf{v}_{k-1} \end{aligned} \tag{4.50}$$

$$\mathbf{z}_k = \mathbf{H}_k \mathbf{x}_k + \mathbf{w}_k \tag{4.51}$$

4.4 Simulation Results

We have implemented the proposed estimation method on both (i) data obtained using hardware and (ii) PSPICE simulated data. In both the cases, the estimation has been performed in MATLAB. IRFZ44N IC has been used for hardware implementation to obtain the practical data. Figure 4.3 shows the output estimated data using the practical data and compares the estimated output with measured practical data. Figure 4.4 - Figure 4.7 show the output estimated data using PSPICE simulated for different values of L and W. The MOSFET circuit is represented using Kronecker product. The proposed method has been compared with Kronecker product based WT representation method. The LMS is used for parameter estimation of Kronecker product based WT representation. Peak to peak input voltage is $20mV$. Parameters used for PSPICE simulations are: $U_T = 0.0256V$, $V_{T_0} = 0.5V$, $R_{in} = 3\,k\Omega$, $C_{GX} = 1.0 \times 10^{-11}$, $C_S = 1.5 \times 10^{-10}F$, $C_D = 1.5 \times 10^{-10}F$, $C_B = 4 \times 10^{-10}F$, $C_{BS} = 0.99 \times 10^{-11}F$, $C_{BD} = 1.0 \times 10^{-11}F$, $I_0 = 1.0 \times 10^{-9}A$, $\eta = 1$, $\rho_j = 1$ and $\gamma = 1$. As the EKF performance depends on proper selection of covariance matrices, $\mathbf{Q}_k$, $\mathbf{R}_k$ and $P(0)$ have been selected by trial and error method. To begin the EKF, we require an initial state estimate $\hat{\mathbf{x}}(0|0)$ based on no measurement and initial covariance matrix $P(0|0)$. The covariance of process noise is $\mathbf{Q}_k = \text{diag}[10^{-8}\ \ 10^{-8}\ \ 10^{-8}\ \ 10^{-8}]$. The covariance of measurement noise is $\mathbf{R}_k = 10^{-6}$. If the P_k is singular at any stage, the convergence will be affected. P_k^{-1} should generally replaced with pseudo inverse or generalized inverse of P_k. For hardware implementation the measured output has been taken as actual value. The initialization required for executing EKF are (i) $\hat{\mathbf{x}}(t)$ the initial state estimate and (ii) state estimate covariance matrix $P(t)$ at $t = 0$. The obvious choice of initial condition is

$$\hat{\mathbf{x}}(0) = 0 \tag{4.52}$$

$$\begin{aligned} P(0) &= \text{Cov}(\mathbf{x}(0)) \approx \mathbf{Q}_k \\ &= \text{Process noise covariance} \end{aligned} \tag{4.53}$$

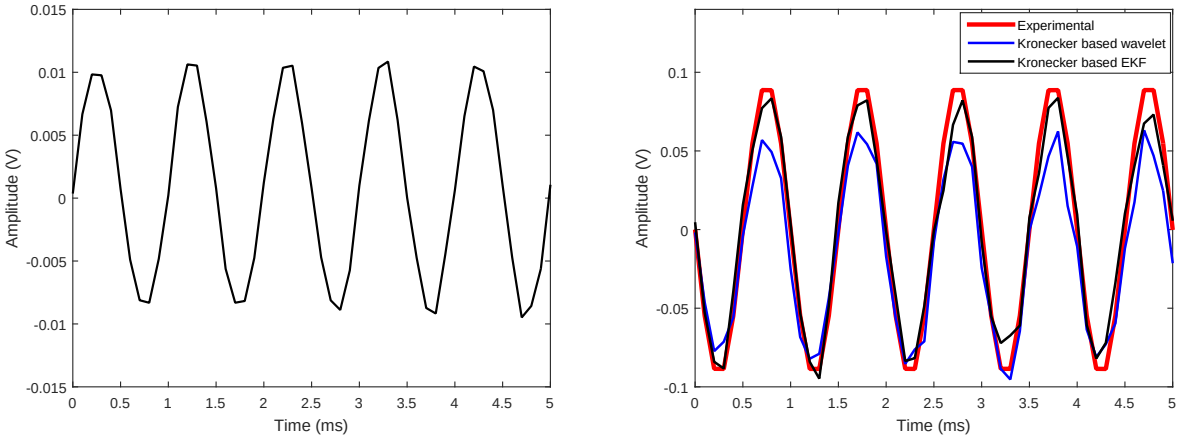

(a) Noisy input to MOSFET.

(b) Estimated MOSFET output voltage.

Figure 4.3: Output voltage estimation for noisy input (white Gaussian noise of zero mean and 0.001 variance) using (i) EKF on Kronecker based system representation (ii) LMS on WT based system representation. Input frequency is 1000 Hz.

The choice of the initial state error covariance may be based on the following logic:-

$$\frac{d\mathbf{x}(t)}{dt} = f(t,\mathbf{x}(t)) + \sigma\frac{d\beta(t)}{dt} \tag{4.54}$$

Using, T as characteristic time scale and where $\Delta = \frac{T}{N}$ is the discretized step size, then

$$\frac{\mathbf{x}(\Delta)-\mathbf{x}(0)}{\Delta} = \sigma\frac{d\beta(t)}{\Delta} \tag{4.55}$$

$$\mathbf{x}(\Delta) = \sigma\, d\beta(t) \tag{4.56}$$

$$\mathrm{Cov}\,(\mathbf{x}(\Delta)) = \sigma^2\Delta I \tag{4.57}$$

since $dt \approx \Delta$

$$\mathrm{Cov}(d\beta(t)) = dt\, I \tag{4.58}$$

$$\approx \Delta I. \tag{4.59}$$

By comparing these figures Figure 4.3 - Figure 4.7, we see that the state estimation based on Kronecker based EKF smoothens out the process noise present in the original dynamical system. The Kronecker based WT also smoothens out the process noise but, not to extend as the EKF. Reason being the WT method is based on neglecting measurement noise unlike the EKF. The estimation have been performed for different process and measurement noise values. Root mean square error (RMSE) is computed using the mathematical expression (3.42). If $\mathbf{x}_k$ is the true state and $\hat{\mathbf{x}}_k$ is

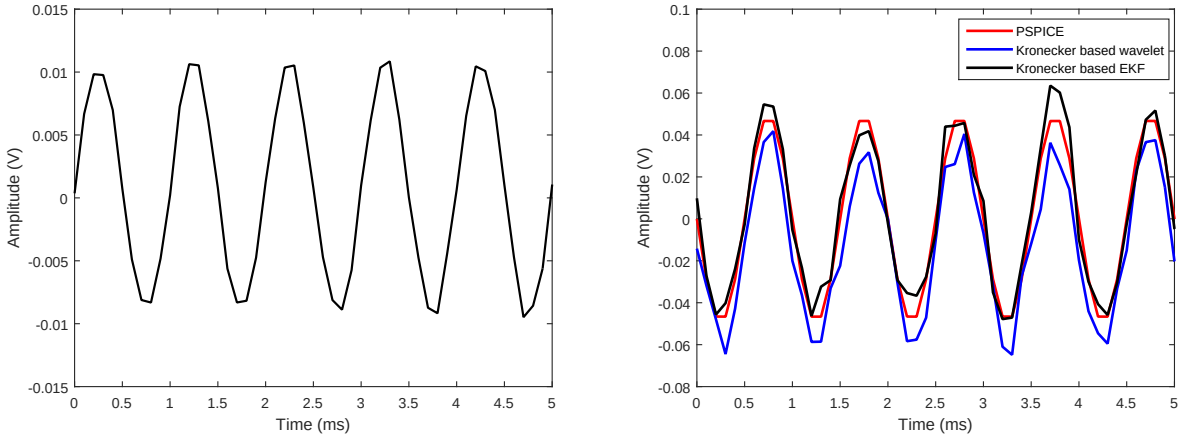

(a) Noisy input to MOSFET. (b) Estimated MOSFET output voltage

Figure 4.4: Output voltage estimation for noisy input (white Gaussian noise of zero mean and 0.001 variance) using (i) EKF on Kronecker based system representation (ii) LMS on WT based system representation. Input frequency is 1000 Hz. W=2μm, L=2μm.

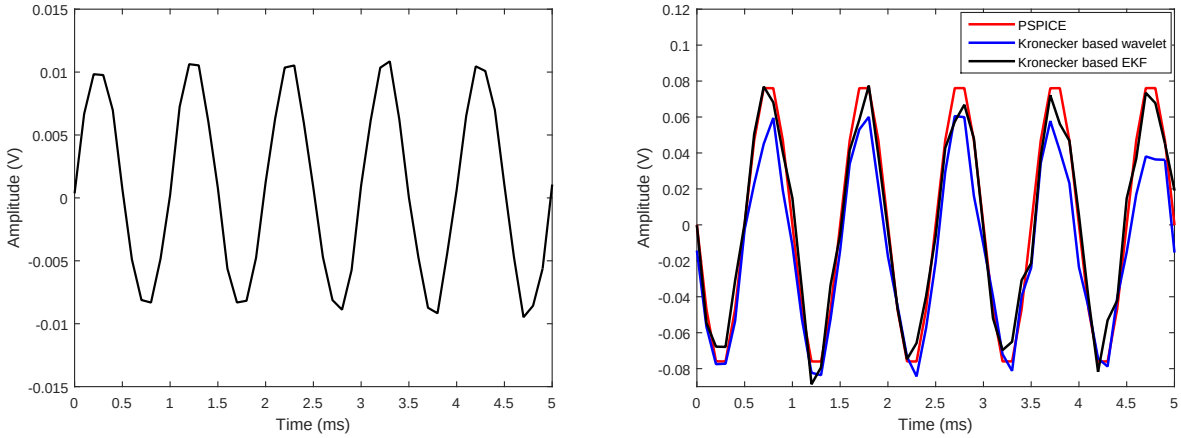

(a) Noisy input to MOSFET. (b) Estimated MOSFET output voltage.

Figure 4.5: Output voltage estimation for noisy input (white Gaussian noise of zero mean and 0.001 variance) using (i) EKF on Kronecker based system representation (ii) LMS on WT based system representation. Input frequency is 1000 Hz. W=20μm, L=20μm.

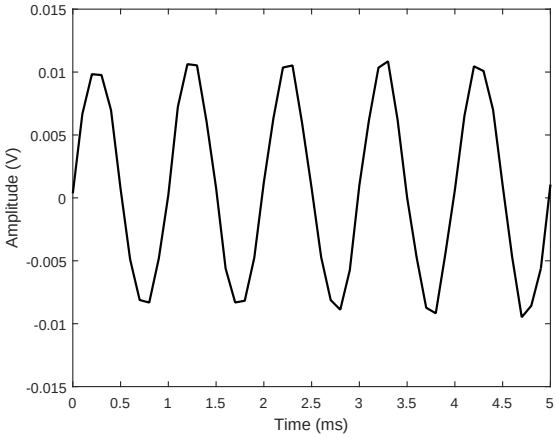

(a) Noisy input to MOSFET.

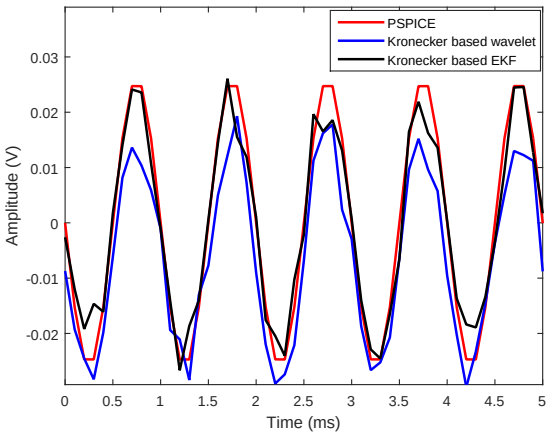

(b) Estimated MOSFET output voltage

Figure 4.6: Output voltage estimation for noisy input (white Gaussian noise of zero mean and 0.001 variance) using (i) EKF on Kronecker based system representation (ii) LMS on WT based system representation. Input frequency is 1000 Hz. W=10μm, L=20μm.

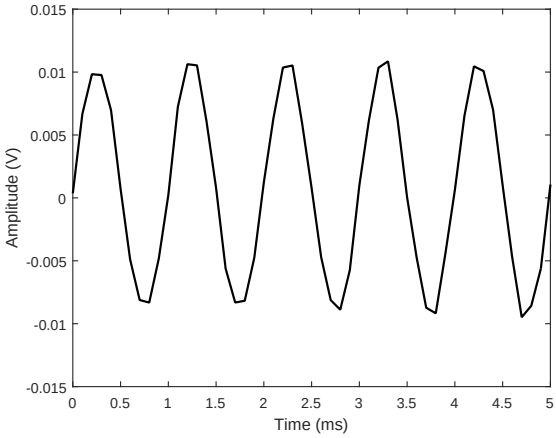

(a) Noisy input to MOSFET.

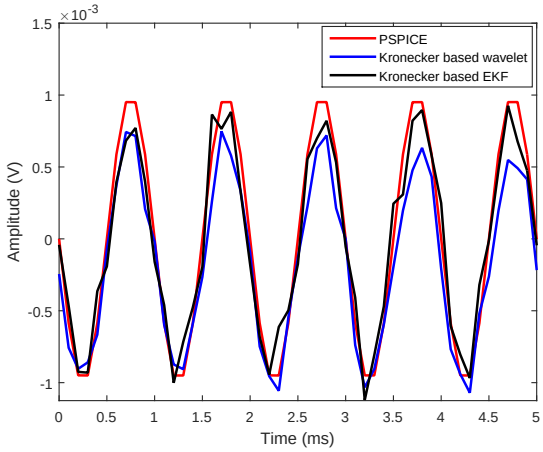

(b) Estimated MOSFET output voltage.

Figure 4.7: Output voltage estimation for noisy input (white Gaussian noise of zero mean and 0.001 variance) using (i) EKF on Kronecker based system representation (ii) LMS on WT based system representation. Input frequency is 1000 Hz. W=10μm, L=2μm.

Table 4.1: RMSE of output voltage estimation using EKF and wavelet transform method when peak to peak MOSFET input is 20mV for practical data.

S. No.	Gaussian noise at input source	Input frequency (Hz)	Estimation using EKF on Kronecker based representation	Estimation using LMS on Kronecker based wavelet representation
1.	$\mu = 0$, $\sigma^2 = 0.001$	100	0.001667	0.002852
2.	$\mu = 0$, $\sigma^2 = 0.001$	1000	0.001683	0.002868
3.	$\mu = 0$, $\sigma^2 = 0.001$	10000	0.001690	0.002866
4.	$\mu = 0$, $\sigma^2 = 0.0025$	100	0.001944	0.003251
5.	$\mu = 0$, $\sigma^2 = 0.0025$	1000	0.001947	0.003260
6.	$\mu = 0$, $\sigma^2 = 0.0025$	10000	0.001956	0.003283

Table 4.2: RMSE of output voltage estimation using EKF and wavelet transform method when peak to peak MOSFET input is 20mV.

S. No.	Gaussian noise at input source	Input frequency (Hz)	Estimation using EKF on Kronecker based representation			Estimation using LMS on Kronecker based wavelet representation		
			$W = 2\mu m$ $L = 2\mu m$	$W = 20\mu m$ $L = 20\mu m$	$W = 10\mu m$ $L = 20\mu m$	$W = 2\mu m$ $L = 2\mu m$	$W = 20\mu m$ $L = 20\mu m$	$W = 10\mu m$ $L = 20\mu m$
1.	$\mu = 0$, $\sigma^2 = 0.001$	100	0.001456	0.001391	0.001424	0.002522	0.002481	0.002492
2.	$\mu = 0$, $\sigma^2 = 0.001$	1000	0.001459	0.001393	0.001426	0.002531	0.002484	0.002495
3.	$\mu = 0$, $\sigma^2 = 0.001$	10000	0.001460	0.001401	0.001430	0.002537	0.002490	0.002501
4.	$\mu = 0$, $\sigma^2 = 0.0025$	100	0.001836	0.001802	0.001812	0.002982	0.002740	0.002823
5.	$\mu = 0$, $\sigma^2 = 0.0025$	1000	0.001838	0.001803	0.001816	0.002985	0.002751	0.002830
6.	$\mu = 0$, $\sigma^2 = 0.0025$	10000	0.001840	0.001807	0.001820	0.002986	0.002755	0.002831

EKF estimate, the e_k =$\mathbf{x}_k - \hat{\mathbf{x}}_k$ for k^{th} realization, so that

$$\frac{1}{N}\sum_{k=1}^{N} e_k^2 \approx \frac{1}{N}\sum_{k=1}^{N} ||\mathbf{x}_k - \hat{\mathbf{x}}_k||^2. \tag{4.60}$$

On the other hand, if $\hat{\Theta}$ is the parameter estimate in the proposed WT approach, $\hat{\mathbf{x}}_k$ is generated using the differential equation

$$\begin{aligned}\frac{d\hat{\mathbf{x}}(t)}{dt} =& \mathbf{A}_1(\hat{\Theta})\hat{\mathbf{x}}(t) + \mathbf{A}_2(\hat{\Theta})(\hat{\mathbf{x}}(t)\otimes\hat{\mathbf{x}}(t)) + \mathbf{A}_3(\hat{\Theta})\mathbf{u}_1(t) + \mathbf{A}_4(\hat{\Theta})\mathbf{u}_2(t) \\ &+ \mathbf{A}_5(\hat{\Theta})(\hat{\mathbf{x}}(t)\otimes\mathbf{u}(t))\end{aligned} \tag{4.61}$$

i. e. we use the state equation (4.15) after setting the noise to zero and replacing the parameters by their estimates.

Table 4.1 shows the RMSE for different noise and different frequencies for both the methods for practical data (hardware implementation). Table 4.2 shows the RMSE for different values of W and L for both the methods for PSPICE simulated data.

General remarks:

1. In the presence of outliers [109], the Gaussian distribution of measurement noise gets perturbed by a small non-Gaussian component. This can be taken care into EKF formalism. As EKF is derived from Kushner nonlinear filter equation, which works, when the state is any Markov process and the measurement noise is white Gaussian. If the measurement noise is non-white Gaussian noise, then also, the nonlinear filter can be developed based on the Bayesian method for computing the conditional probabilities using non-Gaussian probability density functions. The method works mainly because, although the measurement noise is non-Gaussian, it is white and the state process is Markov. First discretize the state model as

$$\mathbf{x}_{n+1} = f(\mathbf{x}_n, \mathbf{u}_{n+1}) + \mathbf{v}_{n+1} \tag{4.62}$$

$$\mathbf{z}(n) = h(\mathbf{x}_n) + \mathbf{w}_n \tag{4.63}$$

$$\mathbf{z}_n = \{\mathbf{z}(n) : \qquad k \leq n\} \tag{4.64}$$

$$p(\mathbf{x}_{n+1}|\mathbf{z}_{n+1}) = \frac{p(\mathbf{x}_{n+1}, \mathbf{z}_{n+1})}{p(\mathbf{z}_{n+1})} = \frac{p(\mathbf{z}(n+1), \mathbf{z}_n, \mathbf{x}_{n+1})}{p(\mathbf{z}_{n+1})} \tag{4.65}$$

$$= \frac{\int p(\mathbf{z}(n+1)|\mathbf{x}_{n+1}) p(\mathbf{x}_{n+1}|\mathbf{x}_n) p(\mathbf{x}_n|\mathbf{z}_n) d\mathbf{x}_n}{\int p(\mathbf{z}(n+1)|\mathbf{x}_{n+1}) p(\mathbf{x}_{n+1}|\mathbf{x}_n) p(\mathbf{x}_n|\mathbf{z}_n) d\mathbf{x}_n d\mathbf{x}_{n+1}} \tag{4.66}$$

$$= \frac{\int p_{w_{n+1}}(\mathbf{z}(n+1) - h(\mathbf{x}_{n+1})) p_{v_{n+1}}(\mathbf{x}_{n+1} - f(\mathbf{x}_n, \mathbf{u}_{n+1})) p(\mathbf{x}_n|\mathbf{z}_n) d\mathbf{x}_n}{\int p_{w_{n+1}}(\mathbf{z}(n+1) - h(\mathbf{x}_{n+1})) p_{v_{n+1}}(\mathbf{x}_{n+1} - f(\mathbf{x}_n, \mathbf{u}_{n+1})) p(\mathbf{x}_n|\mathbf{z}_n) d\mathbf{x}_n d\mathbf{x}_{n+1}} \tag{4.67}$$

$$\hat{\mathbf{x}}_{n+1|n+1} = \underset{\mathbf{x}}{\operatorname{argmax}} \int p_{w_{n+1}}(\mathbf{z}(n+1) - h(\mathbf{x})) p_{v_{n+1}}(\mathbf{x} - f(\mathbf{x}_n, \mathbf{u}_{n+1})) p(\mathbf{x}_n|\mathbf{z}_n) d\mathbf{x}_n. \tag{4.68}$$

   Based on such Bayesian arguments the nonlinear filter can be developed, when state is an arbitrary Markov process and when process or measurement noise are arbitrary non-Gaussian process. Note that in our notation, $\mathbf{z}(n)$ is the instantaneous measurement at the time n, while $\mathbf{z}_n = \{\mathbf{z}_k : k \leq n\}$ is the aggregate of all measurements taken upto time n.

2. Although it may appear that a large measurement noise variance will cause bad estimates, if the measurement noise variance $\mathbf{R}$ is very small with respect to some matrix norm, the $\mathbf{R}^{-1}$ will be very large, causing numerical instability.

3. The main difficulty in the proposed method is obtaining the exact noise variances. However, this can be overcome by blocking the input signal and taking only noise measurements in the circuit and estimating the noise variance by assuming ergodicity after linearizing the circuit. The main computational difficulty in WT method is the application of the gradient algorithm for parameter estimation, since the matrices of $A_j(\Theta),\ j = 1,2,...7$, have the high nonlinear dependence of the parameter Θ.

4. In PSPICE simulation, the leakage current does not appear. When we scale the time and amplitude variables from submicron to a higher scale, the noise effects become small. For example, consider a differential equation

$$\frac{dV(t)}{dt} = f(V(t)) + w(t). \tag{4.69}$$

Suppose we scale time and amplitude $V_1(t) = \lambda V(t)$, $t_1 = \mu t$. Then

$$V(t) = \frac{1}{\lambda} V_1\left(\frac{t_1}{\mu}\right). \tag{4.70}$$

So

$$\frac{dV(t)}{dt} = \frac{1}{\lambda}\frac{dV_1}{dt} = \frac{\mu}{\lambda}\frac{dV_1}{dt_1} \tag{4.71}$$

and then differential equation becomes after scaling

$$\frac{\mu}{\lambda}\frac{dV_1}{dt_1} = f\left(\frac{V_1}{\lambda}\right) + w \tag{4.72}$$

or

$$\frac{dV_1}{dt_1} - \frac{\lambda}{\mu} f\left(\frac{V_1}{\lambda}\right) = \frac{\lambda}{\mu} w. \tag{4.73}$$

Choosing $\frac{\lambda}{\mu} << 1$, we see that noise effects reduce. Whenever we simulate a system defined on a very small scale, we have to scale both amplitude and time so that computer can handle the variables at a classical scale.

5. The idea of scaling both time and amplitude is frequently used in quantum mechanics where time and amplitude are on the Planckian scale and hence to simulate the dynamics of a quantum system, such a scaling is required.

6. Taking $\mathbf{x}_k \in R^{n_x \times 1}$, $\mathbf{F}_k \in R^{n_x \times n_x}$, $\mathbf{u}_1 \in R^{1 \times p}$, $\mathbf{u}_2 \in R^{1 \times p}$, $P \in R^{n_x \times n_x}$, $\mathbf{L}_k \in R^{n_x \times n_x}$, $\mathbf{Q}_k \in$

$R^{n_x \times n_x}$, $\mathbf{H}_k \in R^{d \times n_x}$, $\mathbf{K}_k \in R^{n_x \times d}$, $\mathbf{z}_k \in R^{d \times n_x}$, $\mathbf{A}_1 \in R^{n_x \times n_x}$, $\mathbf{A}_2 \in R^{n_x \times n_x^2}$, $\mathbf{x}_k \otimes \mathbf{x}_k \in R^{n_x^2 \times 1}$, $\mathbf{A}_3 \in R^{n_x \times 1}$, $\mathbf{A}_4 \in R^{n_x \times 1}$, $\mathbf{A}_5 \in R^{n_x \times n_x p}$.

Table 4.3: Computational burden for EKF algorithm.

Equation number	Number of multiplication
(A.12)	$2n_x^2 + n_x p$
(A.13)	$4n_x^3$
(A.14)	$2n_x^2 d + 2n_x d^2$
(A.15)	$2n_x^2 d$
(A.16)	$3n_x^3$
Total multiplication	$7n_x^3 + 4n_x^2 d + 2n_x d^2 + 2n_x^2 + n_x p$
Total multiplication in (4.15)	$n_x^3 + n_x^2 + n_x^2 p + 2n_x p$

Table 4.4: Computational burden for WT method.

Equation number	Number of multiplication
(4.21)	$n_x^4 + 3n_x^3 + 3n_x^2 + 2n_x p + n_x^2 p$
(4.26)	$n_x^5 + n_x^4 + 3n_x^3 + 4n_x^2 + 2n_x^3 p + 2n_x p + n_x^3 p^2$

7. It should be remarked that given any stochastic nonlinear dynamical system with unknown parameters, another way for state estimation is to first estimate the parameters of the systems from the input-output data and then substitute these parameters into the dynamical system differential equations with process noise set equal to zero. That is the approach used in the proposed work for the WT based state estimation technique.

Chapter 5

Stochastic Filtering in Electromagnetics

In the previous chapters, we have developed the extended Kalman filter (EKF) for estimating the states of systems driven by nonlinear ordinary differential equations (ODE's). The prototype examples for that problem were transistor circuits. In this chapter, we develop the Kalman filter (KF) for estimating the state of a linear system driven by a partial differential equation (PDE) with the prototype example being that of the electromagnetic field generated by random charge and current densities of an antenna. In the previous problem, we took noisy measurements on a subset of the states. In this problem, we take noisy measurements on the field of a sparse discrete set of spatial pixels.

This chapter[1] presents the estimation of electric and magnetic fields using the KF. The entire electric and magnetic fields have been estimated using the scalar and vector potential by measurements at a discrete set of spatial pixels. To implement the KF, the state space model has been obtained using the wave equation with sources satisfied by the scalar and vector potential. The proposed method has been implemented on Hertzian dipole antenna. The field estimated using KF has been compared with the recursive least squares (RLS) method. The KF presents better estimation than RLS, as it is an optimal estimator. The proposed method uses the Kronecker product for compact representation of discretized fields in the form of vectors and partial differential operators in the form of matrices. These representations enable effective

[1]This chapter consists the results of research article "Bansal R, Majumdar S, Parthasarthy H. Stochastic filtering in electromagnetics. (Communicated)".

computer simulation. It can be applied for detection of enemy transmitter. Suppose enemy is transmitting signal to his friend. Then by measuring electromagnetic signal at discrete points, then entire field can be estimated using this method. Further it can be used to determine the shape and location of enemy transmitter.

Major contributions of this work are: (i) Wave equation with noisy current source for magnetic vector potential and electric scalar potential have been set up. (ii) Spatial discretization of (i) leads to finite dimensional linear state variable model. (iii) Electric and magnetic fields are expressed in terms of potentials and the measurement model is discretized. (iv) KF is applied to estimate the entire potential from sparse discrete measurements.

Estimation of electric and magnetic fields is important in various applications. Estimation of magnetic field is used for vehicle guidance and motion control applications as positioning is based on the magnetic field sensing. Field estimation is also required for base station antenna used in mobile communication [110]. The electromagnetic devices used for diagnostic and therapeutic applications such as transcranial magnetic simulation (TMS) also need estimation of electric field [111]. Pei *et al.* [112] used field estimation for pedestrian dead reckoning (PDR) algorithm, which calculate the user location. The field estimation is also needed for medical instruments, mine detection, power transmission fields, pipelines, telecommunication lines etc.

Various methods have been used for electric and magnetic field estimation. Belhadj and El-Ferik [113] used artificial neural network for electric and magnetic field estimation of live transmission line workers. Wang *et al.* [114] presented electric field estimation in human body exposed to low frequency magnetic field that uses a boundary element procedure. Zenczak [115] proposed electric and magnetic field estimation in distributed and centralized power systems. Paffi *et al.* [116] proposed a method to calculate the electric field induced inside the brain by a TMS method. The electric field induced by TMS coils inside a brain model is obtained by magnetic resonance imaging (MRI) images. This method is integrated with neuro navigation tools, resulting in efficient application. Puthe *et al.* [117] proposed a method that uses three dimensional (3D) modelling of induction process in the earth and source model obtained by spherical harmonics of observed magnetic data. Petrovic *et al.* [118] proposed a method for estimation of low frequency magnetic field of the overhead power line as these low frequency magnetic field create health risks. To estimate the extremely low frequency fields, Petrovic *et al.* used Biot-Savart law based model that considers the pillar

geometry and conductor mutual position and its catenary shape. [119] proposed the estimation of photospheric electric fields using magnetic field sequence and Doppler measurement. De-Doncker *et al.* [120] proposed statistical approach to deduce the local behaviour of the fields when a set of field values are given. Ekonomou *et al.* [121] presented electric and magnetic field radiated by electrostatic discharges using artificial neural network. This method has the advantage that electromagnetic field can be calculated easily and accurately by measuring the discharge current only. Azpurua and Ramos [122] reviewed the various interpolatory techniques to estimate the average electromagnetic field to represent the continuous dataset over a map of complete plot area. Colak *et al.* [123] developed a visual software, having 3D screening unit using artificial neural network and grid data users can estimate electromagnetic field using in and out of the measurement points using this software.

Sate space derivation of Maxwell's equation in terms of Kronecker product is presented in Section 5.1. This representation of Hertzian dipole antenna is derived in Section 5.2. The KF method as described in appendix Section A.1 is implemented on the state space representation of Hertzian dipole antenna in Section 5.3 for electric and magnetic field estimation. The estimated fields for different noisy cases are shown in figures in Section 5.4.

5.1 Sate Space Representation of Maxwell's Equation

The electromagnetic field is described by two fields namely, the electric field intensity ($\vec{E}$) and magnetic field intensity ($\vec{H}$). Both the quantities depend on the position in space and time. A complete solution of Maxwell's equations results in well known wave equations. In empty space, the scalar potential (Φ), vector potential ($\vec{A}$), electric field ($\vec{E}$), magnetic flux density ($\vec{B}$), all satisfy the wave equation. The Maxwell's equations can also be expressed in terms of differential equations for the scalar and vector potential. Maxwell's equations are the time independent first order differential equations. Though, these equations can be solved simultaneously, but generally, they are reduced to two second order differential equations, known as wave equations. Electric and magnetic fields can be easily evaluated using the scalar and vector potentials. The scalar potential and the vector potential, satisfy the wave equation with the source terms $\frac{\rho}{\varepsilon_0}$ and $\mu_0 J$ respectively, where ρ is the volume charge density, ε_0 is permittivity of free space, μ_0 is vacuum permeability and J is the current density. The wave

equations of $\vec{A}$ and Φ are obtained using the Lorentz gauge condition ($\nabla.\vec{A} = -\frac{1}{c^2}\frac{\partial \Phi}{\partial t}$). The advantage of Lorentz gauge is that the vectorial differential equation for $\vec{A}$ is decoupled into a set of three independent scalar differential equations and there is no mixing of the components i. e. (r, θ, ϕ) so that each vector component ($\vec{A}_i$) or (Φ_i) depends only on the source component (J_i) or (ρ_i). The vector potential at position $\vec{r} = (x, y, z)$ satisfies the wave equation with source:

$$\frac{1}{c^2}\frac{\partial^2 \vec{A}(t,\vec{r})}{\partial t^2} = \nabla^2 \vec{A}(t,\vec{r}) + \mu_0 J(t,\vec{r}) + w_J(t,\vec{r}) \tag{5.1}$$

where c is the velocity of light in free space and w_J is the noise in the current density field.

Similarly, the scalar potential at position $\vec{r}$ satisfies the partial differential equation

$$\frac{1}{c^2}\frac{\partial^2 \Phi(t,\vec{r})}{\partial t^2} = \nabla^2 \Phi(t,\vec{r}) + \frac{\rho(t,\vec{r})}{\varepsilon_0} + w_\rho(t,\vec{r}) \tag{5.2}$$

where w_ρ is the noise in the charge density field. These two equations are derived from the complete set of four Maxwell's equations and then importing the Lorentz gauge condition $div\,\vec{A} + \frac{1}{c^2}\frac{\partial \Phi}{\partial t} = 0$ on the potentials.

We define the state vector matrix as

$$\begin{aligned} \xi(t,\vec{r}) &= \left[\begin{array}{cccc} \vec{A}^T(t,\vec{r}) & \frac{\partial \vec{A}^T(t,\vec{r})}{\partial t} & \Phi(t,\vec{r}) & \frac{\partial \Phi(t,\vec{r})}{\partial t} \end{array} \right]^T \\ &= \left[\begin{array}{cccc} \vec{A}^T(t,\vec{r}) & \vec{V}^T(t,\vec{r}) & \Phi(t,\vec{r}) & \Psi(t,\vec{r}) \end{array} \right]^T. \end{aligned} \tag{5.3}$$

where $\vec{V}(\vec{r},t) = \frac{\partial \vec{A}(t,\vec{r})}{\partial t}$ and $\Psi(t,\vec{r}) = \frac{\partial \Phi(t,\vec{r})}{\partial t}$. Equation (5.1) and (5.2) can be written in the state-space form

$$\frac{\partial \vec{A}(t,\vec{r})}{\partial t} = \vec{V}(t,\vec{r}) \tag{5.4}$$

$$\frac{\partial \vec{V}(t,\vec{r})}{\partial t} = c^2 \nabla^2 \vec{A}(t,\vec{r}) + c^2 \mu_0 J(t,\vec{r}) + c^2 w_J(t,\vec{r}) \tag{5.5}$$

$$\frac{\partial \Phi(t,\vec{r})}{\partial t} = \Psi(t,\vec{r}) \tag{5.6}$$

$$\frac{\partial \Psi(t,\vec{r})}{\partial t} = c^2 \nabla^2 \Phi(t,\vec{r}) + c^2 \frac{\rho(t,\vec{r})}{\varepsilon_0} + c^2 w_\rho(t,\vec{r}). \tag{5.7}$$

On discretizing the spatial variables into N^3 pixels, we represent the above vector and scalar fields at the time t in the form of $N^3 \times 1$ vectors for scalar fields and $3N^3 \times 1$

vectors for vector fields:

$$\vec{A}(t) = \sum_{x,y,z=1}^{N} \vec{A}(t,x,y,z) \otimes e_x \otimes e_y \otimes e_z \tag{5.8}$$

$$\vec{V}(t) = \sum_{x,y,z=1}^{N} \vec{V}(t,x,y,z) \otimes e_x \otimes e_y \otimes e_z \tag{5.9}$$

$$\Phi(t) = \sum_{x,y,z=1}^{N} \Phi_1(t,x,y,z) e_x \otimes e_y \otimes e_z \tag{5.10}$$

$$\Psi(t) = \sum_{x,y,z=1}^{N} \Phi_2(t,x,y,z) e_x \otimes e_y \otimes e_z \tag{5.11}$$

$$J(t) = \sum_{x,y,z=1}^{N} J(t,x,y,z) e_x \otimes e_y \otimes e_z \tag{5.12}$$

$$\rho(t) = \sum_{x,y,z=1}^{N} \rho(t,x,y,z) e_x \otimes e_y \otimes e_z \tag{5.13}$$

where e_x is the $N \times 1$ vector with a one in the x^{th} positions and 0's at all the other positions. We can represent the operator ∇^2 by a $N^3 \times N^3$ matrix D_0, when acting on scalar fields and by a $3N^3 \times 3N^3$ matrix $D = I_3 \otimes D_0$ when acting on vector fields. Specifically,

$$\sum_{x,y,z} \nabla^2 \mathbf{x}(t,x,y,z) \otimes e_x \otimes e_y \otimes e_z = D\mathbf{x} \tag{5.14}$$

where

$$\mathbf{x}(t) = \sum_{x,y,z} \mathbf{x}(t,x,y,z) \otimes e_x \otimes e_y \otimes e_z. \tag{5.15}$$

For example if $\mathbf{x}(t,x,y,z)$ is a vector field, then

$$\begin{aligned} \nabla^2 \mathbf{x} = \sum_{x,y,z=1}^{N} \Bigg[& \frac{\{\mathbf{x}(t,x+1,y,z) + \mathbf{x}(t,x-1,y,z) - 2\mathbf{x}(t,x,y,z)\}}{\Delta^2} \\ & + \frac{\{\mathbf{x}(t,x,y+1,z) + \mathbf{x}(t,x,y-1,z) - 2\mathbf{x}(t,x,y,z)\}}{\Delta^2} \\ & + \frac{\{\mathbf{x}(t,x,y,z+1) + \mathbf{x}(t,x,y,z-1) - 2\mathbf{x}(t,x,y,z)\}}{\Delta^2} \Bigg] \otimes e_x \otimes e_y \otimes e_z \end{aligned} \tag{5.16}$$

$$\begin{aligned} \nabla^2 \mathbf{x} = & \frac{1}{\Delta^2} \sum_{x,y,z} \mathbf{x}(t,x,y,z) \otimes \left[(e_{x+1} + e_{x-1} - 2e_x) \otimes e_y \otimes e_z + e_x \otimes (e_{y+1} + e_{y-1} - 2e_y) \otimes e_z \right. \\ & \left. + e_x \otimes e_y \otimes (e_{z+1} + e_{z-1} - 2e_z) \right]. \end{aligned} \tag{5.17}$$

Using

$$D_1 = \sum_{x,y,z} \left[((e_{x+1} + e_{x-1} - 2e_x) \otimes e_y \otimes e_z)(e_x \otimes e_y \otimes e_z)^T \right] \tag{5.18}$$

and likewise D_2, D_3, we have

$$\begin{aligned} \nabla^2 \mathbf{x} =& \frac{1}{\Delta^2}(I_3 \otimes D_1 + I_3 \otimes D_2 + I_3 \otimes D_3)\mathbf{x}(t) \\ =& \frac{1}{\Delta^2}(I_3 \otimes (D_1 + D_2 + D_3))\mathbf{x}(t) \\ =& I_3 \otimes D_0 \in \mathbb{R}^{3N^3 \times 3N^3} \end{aligned} \tag{5.19}$$

where $D_0 = \frac{1}{\Delta^2} I_3 \otimes (D_1 + D_2 + D_3) \in \mathbb{R}^{N^3 \times N^3}$.

In matrix form (5.4)-(5.7) can be cast as

$$\frac{\partial \xi(t)}{\partial t} = \mathbf{F}(t)\xi(t) + \mathbf{B}^{(1)}(t)J(t) + \mathbf{B}^{(2)}(t)\rho(t) + \mathbf{B}^{(3)}(t)w(t) \tag{5.20}$$

where

$$\xi(t) = \begin{bmatrix} \vec{A}^T(t) & \vec{V}^T(t) & \Phi(t) & \Psi(t) \end{bmatrix}^T \in \mathbb{R}^{N^3 \times 1}$$

$$\mathbf{F}(t,\vec{r}) = \begin{bmatrix} 0 & I & 0 & 0 \\ c^2(I_3 \otimes D_0) & 0 & 0 & 0 \\ 0 & 0 & 0 & I \\ 0 & 0 & c^2 D_0 & 0 \end{bmatrix}$$

$$\mathbf{B}^{(1)}(t,\vec{r}) = \begin{bmatrix} 0 & c^2\mu_0 & 0 & 0 \end{bmatrix}^T$$

$$\mathbf{B}^{(2)}(t,\vec{r}) = \begin{bmatrix} 0 & 0 & 0 & \frac{c^2}{\varepsilon_0} \end{bmatrix}^T$$

$$\mathbf{B}^{(3)}(t,\vec{r}) = \begin{bmatrix} c^2 & 0 \\ 0 & 0 \\ 0 & 0 \\ 0 & c^2 \end{bmatrix}$$

$$w(t) = \begin{bmatrix} w_J & w_\rho \end{bmatrix}^T.$$

After electric and magnetic potentials estimation, electric and magnetic field intensity

can be estimated using the expression

$$\vec{E}(t,x,y,z) = -\nabla\Phi(t,x,y,z) - \frac{\partial\vec{A}(t,x,y,z)}{\partial t}. \tag{5.21}$$

Specifically, the electric field is

$$\vec{E}(t) = \sum_{x,y,z=1}^{N} \vec{E}(t,x,y,z) \otimes e_x \otimes e_y \otimes e_z \tag{5.22}$$

where

$$\vec{E}(t,x,y,z) = -\nabla\Phi(t,x,y,z) - \mathbf{V}(t,x,y,z) \tag{5.23}$$

so

$$\vec{E}(t) = -\frac{1}{\Delta}\sum_{x,y,z}\begin{bmatrix} \Phi(t,x+1,y,z) - \Phi(t,x,y,z) \\ \Phi(t,x,y+1,z) - \Phi(t,x,y,z) \\ \Phi(t,x,y,z+1) - \Phi(t,x,y,z) \end{bmatrix} \otimes e_x \otimes e_y \otimes e_z - \mathbf{V}(t) \tag{5.24}$$

which can be expressed as

$$E(t) = -\mathbb{G}_1\Phi(t) - \mathbf{V}(t) \tag{5.25}$$

where $\mathbb{G}_1$ is a $3N^3 \times N^3$ matrix that represents the gradient operator.

$$\begin{aligned} \nabla\Phi &= \nabla\Phi(t,x,y,z) \otimes e_x \otimes e_y \otimes e_z \\ &= \frac{1}{\Delta}\sum_{x,y,z}\begin{bmatrix} \Phi(t,x+1,y,z) - \Phi(t,x,y,z) \\ \Phi(t,x,y+1,z) - \Phi(t,x,y,z) \\ \Phi(t,x,y,z+1) - \Phi(t,x,y,z) \end{bmatrix} \otimes e_x \otimes e_y \otimes e_z \\ &= \frac{1}{\Delta}\sum_{x,y,z}\begin{bmatrix} ((e_{x+1} - e_x) \otimes e_y \otimes e_z)^T\Phi(t) \\ (e_x \otimes (e_{y+1} - e_y) \otimes e_z)^T\Phi(t) \\ (e_x \otimes e_y \otimes (e_{z+1} - e_z))^T\Phi(t) \end{bmatrix} \otimes e_x \otimes e_y \otimes e_z \\ &= \mathbb{G}_1\Phi(t) \end{aligned} \tag{5.26}$$

where $\mathbb{G}_1 = \frac{1}{\Delta}\sum_{x,y,z}\begin{bmatrix} ((e_{x+1} - e_x) \otimes e_y \otimes e_z)^T \\ (e_x \otimes (e_{y+1} - e_y) \otimes e_z)^T \\ (e_x \otimes e_y \otimes (e_{z+1} - e_z))^T \end{bmatrix} \otimes e_x \otimes e_y \otimes e_z \in \mathbb{R}^{3N^3 \times N^3}$.

Likewise the magnetic flux is

$$\vec{B}(t,x,y,z) = \nabla \times \vec{A}(t,x,y,z) \tag{5.27}$$

i. e.

$$\vec{B}(t) = \sum_{x,y,z=1}^{N} \vec{B}(t,x,y,z) \otimes e_x \otimes e_y \otimes e_z \tag{5.28}$$

$$= C\vec{A}(t) \tag{5.29}$$

where $\vec{A}(t) = \sum_{x,y,z=1}^{N} \vec{A}(t,x,y,z) \otimes e_x \otimes e_y \otimes e_z$. C is a $3N^3 \times 3N^3$ matrix that represents the curl operator. Let $M \in \mathbb{R}^{p \times 6N^3}$ represent the measurement matrix of the electromagnetic field of p pixels ($p << N^3$). M is a sparse matrix of ones and zeros. The measurement model is then

$$\mathbf{z}(t) = M \begin{bmatrix} \vec{E}(t) \\ \vec{B}(t) \end{bmatrix} \tag{5.30}$$

$$= M \begin{bmatrix} -\mathbb{G}_1 \Phi(t) - \mathbf{V}(t) \\ C\vec{A}(t) \end{bmatrix} + \varepsilon_v(t) \tag{5.31}$$

It is interesting for the reader to write down the explicit form of the sparse matrix M where the told number of pixels is $2^3 = 8$ and measurements of the electromagnetic field on the $(1,1,1)$ and $(2,2,2)$ pixels are made.

$$\mathbf{z}(t) = M \begin{bmatrix} 0 & -I & -\mathbb{G}_1 & 0 \\ C & 0 & 0 & 0 \end{bmatrix} \begin{bmatrix} \vec{A}(t) \\ \vec{V}(t) \\ \vec{\phi}(t) \\ \vec{\psi}(t) \end{bmatrix} + \varepsilon_v(t) = \mathbf{H}\xi(t) + \varepsilon_v(t) \tag{5.32}$$

where $\varepsilon_v(t)$ is the measurement noise.

5.2 State Space Modelling of Hertzian Dipole Antenna

Estimation of electric and magnetic field in the space surrounding the antenna is important in antenna analysis. Given an antenna structure together with input excitation, the establishment of current distribution on the antenna structure satisfies the Maxwell's equations everywhere at all times. The antenna analysis has two parts: -

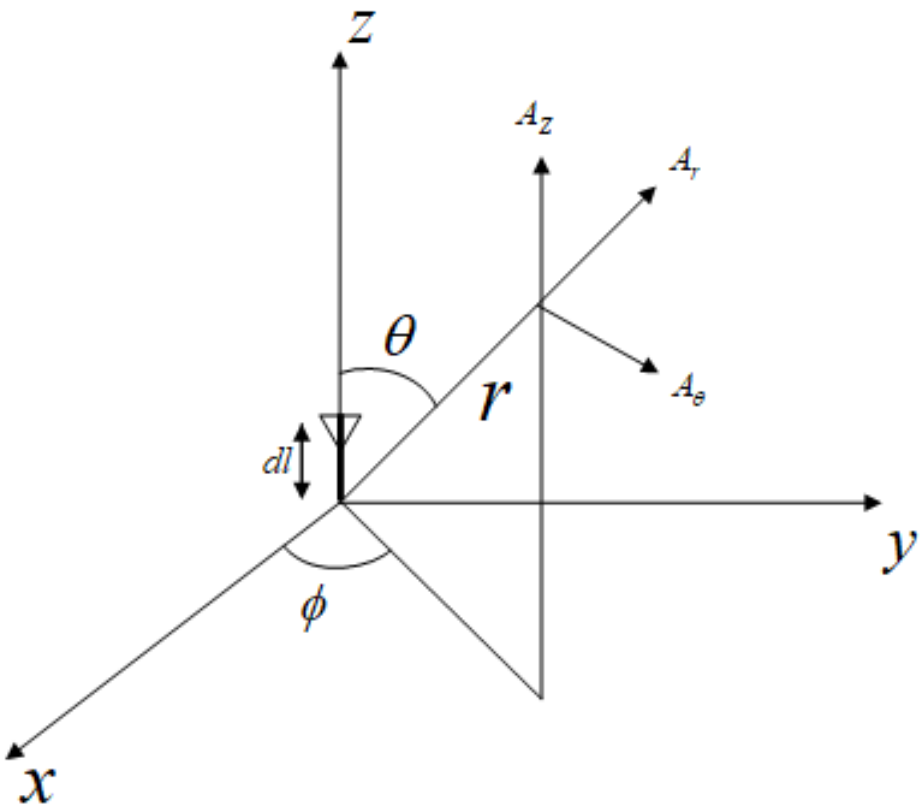

Figure 5.1: Hertzian dipole antenna.

1. Determination of current distribution due to excitation

2. Field evaluation due to this current distribution in the surrounding space of the antenna.

Hertzian dipole is the most basic antenna element. It is an elemental antenna consisting of an infinitesimally long wire carrying an alternating current ($I(t)$). Consider a Hertzian dipole antenna of dl length oriented along z-axis and carrying current $I_0 e^{jwt}$ as shown in Figure 5.1. This dipole antenna is driven by time dependent current charge

$$J = -S\,\varepsilon_0 \cos(\omega t) \tag{5.33}$$

and volume charge density

$$\rho = -\frac{S}{\mu_0}\cos(\omega t) \tag{5.34}$$

where S is the shape function. Consider a point $P(r,\theta,\phi)$ in spherical coordinate system. The magnetic vector potential components at point $P(r,\theta,\phi)$ are as given by

Green's function

$$A_r = \frac{\mu_0}{4\pi} I_0 \, dl \; e^{j(\omega t - \beta r)} \cos(\theta) \;\; \hat{a}_r \tag{5.35}$$

$$A_\theta = -\frac{\mu_0}{4\pi} I_0 \, dl \; e^{j(\omega t - \beta r)} \sin(\theta) \;\; \hat{a}_\theta \tag{5.36}$$

$$A_\phi = 0. \tag{5.37}$$

The state space equations are

$$\frac{\partial \vec{A}(t,\vec{r})}{\partial t} = \vec{V}(t,\vec{r}) \tag{5.38}$$

$$\begin{aligned}\frac{\partial \vec{V}(t,\vec{r})}{\partial t} =& c^2 \left\{ \frac{\mu_0}{4\pi} I_0 \, dl \; e^{j(\omega t - \beta r)} \cos(\theta) \left(\frac{j\beta}{r^2} - \frac{\beta^2}{r} + \frac{1}{r^3} \right) \right\} \;\; \hat{a}_r \\ &+ c^2 \left\{ \frac{\mu_0}{4\pi} I_0 \, dl \; e^{j(\omega t - \beta r)} \sin(\theta) \;\; \left(\frac{\beta}{r^2} \right) \right\} \;\; \hat{a}_\theta + c^2 \mu_0 \{ -S \, \varepsilon_0 \cos(\omega t) \} + c^2 w_J(t)\end{aligned} \tag{5.39}$$

$$\frac{\partial \Phi(t,\vec{r})}{\partial t} = \Psi(t,\vec{r}) \tag{5.40}$$

$$\frac{\partial \Psi(t,\vec{r})}{\partial t} = c^2 \left\{ \frac{\omega}{4\pi\varepsilon_0} I_0 \, dl \; e^{j(\omega t - \beta r)} \cos(\theta) \left(-\frac{\beta}{r} + \frac{j}{r^2} \right) \right\} + c^2 \frac{\left\{ -\frac{S}{\mu_0} \cos(\omega t) \right\}}{\varepsilon_0} + c^2 w_\rho(t). \tag{5.41}$$

We used Euler-Maruyama method to obtain discrete time state space matrix. Mathematically, $t_k - t_{k-1} = T_s$ and $\mathbf{F}_k = e^{\mathbf{F}(t_k - t_{k-1})} \approx I + \mathbf{F}T_s$ and $\mathbf{B}_k = \sum_{t_k}^{t_{k-1}} e^{\mathbf{F}(t_k - \tau)} \mathbf{B} d\tau \approx \mathbf{B}T_s$, where T_s is the sampling time. I is the identity matrix.

5.3 Applying KF to Hertzian Dipole

Differential equation (5.38)-(5.41) can be expressed in terms of discrete time state space equation as

$$\mathbf{x}_k = \mathbf{F}_{k-1}\mathbf{x}_{k-1} + \mathbf{B}_{k-1}^{(1)}\mathbf{u}_1 + \mathbf{B}_{k-1}^{(2)}\mathbf{u}_2 + \mathbf{B}_{k-1}^{(3)} w_{k-1} + \mathbf{Z}_k \tag{5.42}$$

$$\mathbf{z}_k^{(1)} = \mathbf{H}_k^{(1)}\mathbf{x}_k \tag{5.43}$$

$$\mathbf{z}_k^{(2)} = \mathbf{H}_k^{(2)}\mathbf{x}_k \tag{5.44}$$

where

$$\mathbf{x}_k = \begin{bmatrix} \vec{A} & \vec{V} & \Phi & \Psi \end{bmatrix}^T,$$

$$\mathbf{F}_{k-1} = \begin{bmatrix} 1 & T_s & 0 & 0 \\ 0 & 1 & 0 & 0 \\ 0 & 0 & 1 & T_s \\ 0 & 0 & 0 & 1 \end{bmatrix},$$

$$\mathbf{B}_{k-1}^{(1)} = \begin{bmatrix} 0 & T_s c^2 \mu_0 & 0 & 0 \end{bmatrix}^T,$$

$$\mathbf{u}_1 = -S\,\varepsilon_0 \cos(\omega t),$$

$$\mathbf{B}_{k-1}^{(2)} = \begin{bmatrix} 0 & 0 & 0 & \frac{T_s c^2}{\varepsilon_0} \end{bmatrix}^T,$$

$$\mathbf{u}_2 = -\frac{S}{\mu_0} \cos(\omega t).$$

$$\mathbf{B}_{k-1}^{(3)} = \begin{bmatrix} T_s c^2 & 0 \\ 0 & 0 \\ 0 & 0 \\ 0 & T_s c^2 \end{bmatrix}$$

$$w_{k-1} = \begin{bmatrix} w_J & w_\rho \end{bmatrix}^T.$$

$$\mathbf{Z}_k = \begin{bmatrix} Z_{k_1} & Z_{k_2} & Z_{k_3} & Z_{k_4} \end{bmatrix}^T$$

where

$Z_{k_1} = 0,$

$$Z_{k_2} = T_s c^2 \left\{ \frac{\mu_0}{4\pi} I_0\, dl\, e^{j(\omega t - \beta r)} \cos(\theta) \left(\frac{j\beta}{r^2} - \frac{\beta^2}{r} + \frac{1}{r^3} \right) \right\} \hat{a}_r + T_s c^2 \left\{ \frac{\mu_0}{4\pi} I_0\, dl\, e^{j(\omega t - \beta r)} \sin(\theta) \left(\frac{\beta}{r^2} \right) \right\} \hat{a}_\theta,$$

$Z_{k_3} = 0,$

$$Z_{k_4} = T_s c^2 \left\{ \frac{\omega}{4\pi\varepsilon_0} I_0\, dl\, e^{j(\omega t - \beta r)} \cos(\theta) \left(-\frac{\beta}{r} + \frac{j}{r^2} \right) \right\}$$

$$\mathbf{H}_k^{(1)} = \begin{bmatrix} 0 & 0 & 1 & 0 \end{bmatrix}$$

$$\mathbf{H}_k^{(2)} = \begin{bmatrix} 1 & 0 & 0 & 0 \end{bmatrix}.$$

State space representation for Hertzian dipole antenna is

$$\begin{bmatrix} \vec{A}_k \\ \vec{V}_k \\ \vec{\phi}_k \\ \vec{\psi}_k \end{bmatrix} = \begin{bmatrix} 1 & T_s & 0 & 0 \\ 0 & 1 & 0 & 0 \\ 0 & 0 & 1 & T_s \\ 0 & 0 & 0 & 1 \end{bmatrix} \begin{bmatrix} \vec{A}_{k-1} \\ \vec{V}_{k-1} \\ \vec{\phi}_{k-1} \\ \vec{\psi}_{k-1} \end{bmatrix} + \begin{bmatrix} 0 \\ T_s c^2 \mu_0 \\ 0 \\ 0 \end{bmatrix} \mathbf{u}_1 + \begin{bmatrix} 0 \\ 0 \\ 0 \\ \frac{T_s c^2}{\varepsilon_0} \end{bmatrix} \mathbf{u}_2$$
$$+ \begin{bmatrix} T_s c^2 & 0 \\ 0 & 0 \\ 0 & 0 \\ 0 & T_s c^2 \end{bmatrix} \begin{bmatrix} w_J \\ w_\rho \end{bmatrix} + \begin{bmatrix} Z_{k_1} \\ Z_{k_2} \\ Z_{k_3} \\ Z_{k_4} \end{bmatrix}.$$

Implementation of KF algorithm on the discrete equations is done by adding process noise $\mathbf{v}_k$ to (5.42) and measurement noise $\mathbf{w}_k$ to (5.43) and (5.44).

$$\mathbf{x}_k = \mathbf{F}_{k-1}\mathbf{x}_{k-1} + \mathbf{B}_{k-1}^{(1)}\mathbf{u}_1 + \mathbf{B}_{k-1}^{(2)}\mathbf{u}_2 + \mathbf{B}_{k-1}^{(3)}w_{k-1} + \mathbf{Z}_k + \mathbf{v}_k \tag{5.45}$$

$$\mathbf{z}_k^{(1)} = \mathbf{H}_k^{(1)}\mathbf{x}_k + \mathbf{w}_k \tag{5.46}$$

$$\mathbf{z}_k^{(2)} = \mathbf{H}_k^{(2)}\mathbf{x}_k + \mathbf{w}_k \tag{5.47}$$

KF algorithm, as given in Chapter 2, is applied to the above equations (5.45)-(5.47). Time update and measurement update has been done iteratively after initialization. After estimating the scalar potential and vector potential, electric and magnetic field intensity is computed using (5.25) and (5.27) respectively.

Remark

A more direct way to apply the KF on the Hertzian model is to use the partial differential equations

$$\frac{\partial^2 \vec{A}(t,x,y,z)}{\partial t^2} = c^2 \nabla^2 \vec{A}(t,x,y,z) + c^2 \mu_0 J(t,x,y,z) + c^2 w_J(t,x,y,z) \tag{5.48}$$

$$\frac{\partial^2\Phi(t,x,y,z)}{\partial t^2} = c^2\nabla^2\Phi(t,x,y,z) + c^2\frac{\rho(t,x,y,z)}{\varepsilon_0} + c^2 w_\rho(t,x,y,z) \tag{5.49}$$

where

$$J(t,x,y,z) = I_0\, cos(\omega t)\,\delta(x)\,\delta(y)\,\Theta\left(\frac{z}{\delta l}\right)\begin{bmatrix}0\\0\\1\end{bmatrix}$$

and

$$\begin{aligned}\rho(t,x,y,z) &= -\int_0^t div J\, dt \\ &= \frac{I_0}{\omega} sin(\omega t)\left(\delta\left(z-\frac{dl}{2}\right) - \delta\left(z+\frac{dl}{2}\right)\right)\delta(x)\,\delta(y)\end{aligned}$$

and use smooth approximation for the δ-function.

5.4 Simulation Results

The derived expressions have been implemented in MATLAB software. Figure 5.2 to Figure 5.3 and Figure 5.5 to Figure 5.6 show the electric field estimation of (r,θ,ϕ) components for various noise for near field and far field respectively. Figure 6.4 and Figure 5.7 show the magnetic field estimation of (r,θ,ϕ) components for various noise for near field and far field respectively. Figure 5.8 and Figure 5.10 show the 3-dimensional estimation of electric field for various noise for near field and far field respectively. Figure 5.9 and Figure 5.11 show the 3-dimensional estimation of magnetic field for various noise for near field and far field respectively. Initial values assigned to the KF are: The covariance of process noise, $\mathbf{Q}_k = \text{diag}[0.0001 \;\; 0.001 \;\; 0.0001 \;\; 0.01]$. The covariance of measurement noise, $\mathbf{R}_k = 0.01$. The predicted covariance, $P(0) = \text{diag}[0.0001 \;\; 0.0001 \;\; 0.0001 \;\; 0.0001]$. RMSE is computed using the expression given in (3.42).

Table 5.1-Table 5.12 show the RMSE for electric and magnetic field estimation using KF and compares the result with RLS and theoretical value. The KF presents better accuracy as compared to the RLS method as it is an optimal estimator that minimizes the mean square of the estimation error.

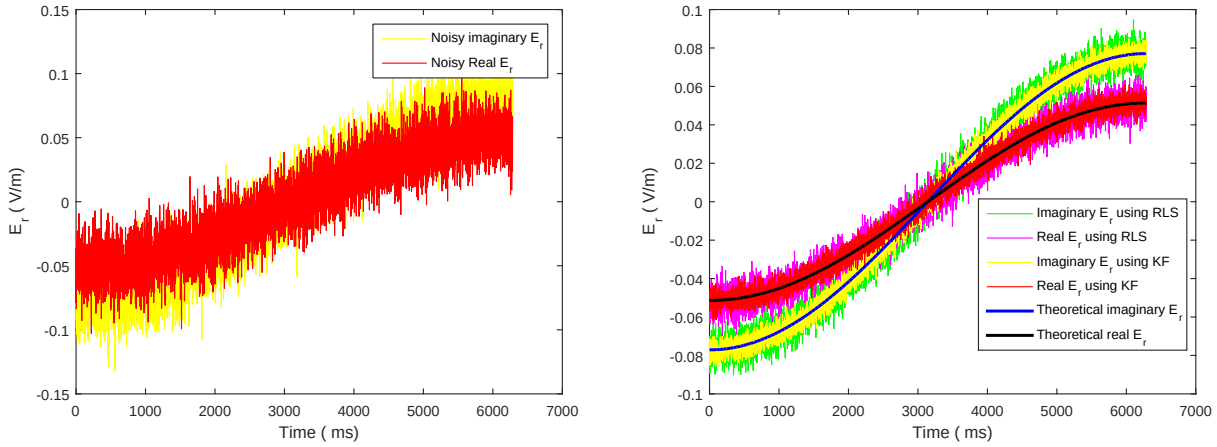

(a) Noisy electric field intensity (E_r). (b) Estimated electric field intensity (E_r).

Figure 5.2: Electric field intensity (E_r) for noisy driving source (white Gaussian noise of zero mean and 0.00025 variance) for near-field.

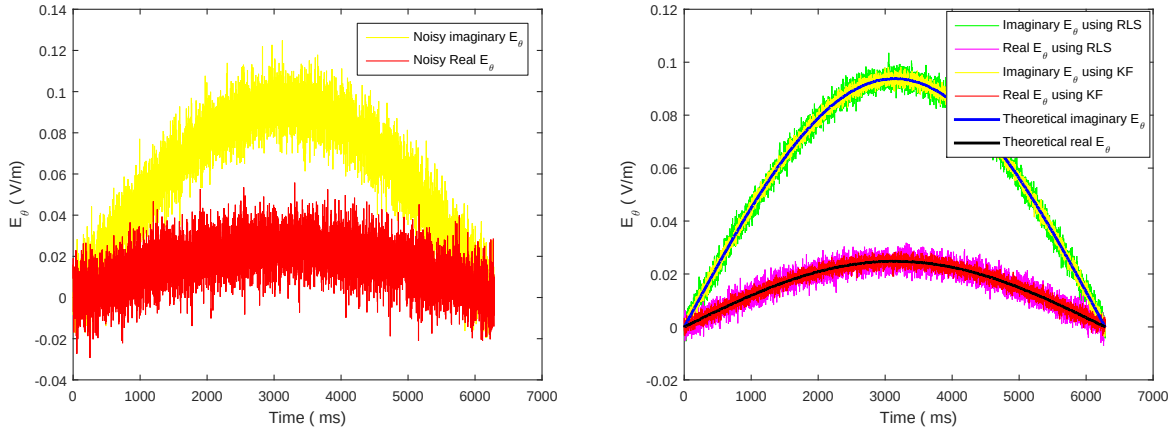

(a) Noisy electric field intensity (E_θ). (b) Estimated electric field intensity (E_θ).

Figure 5.3: Electric field intensity (E_θ) for noisy driving source (white Gaussian noise of zero mean and 0.00025 variance) for near-field.

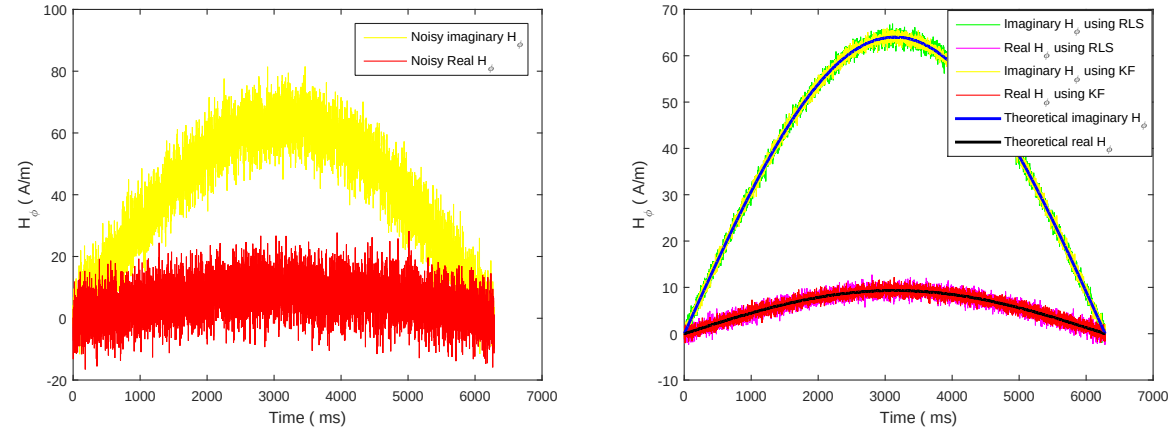

(a) Noisy magnetic field intensity (H_ϕ). (b) Estimated magnetic field intensity (H_ϕ).

Figure 5.4: Magnetic field intensity (H_ϕ) for noisy driving source (white Gaussian noise of zero mean and 0.00025 variance) for near-field.

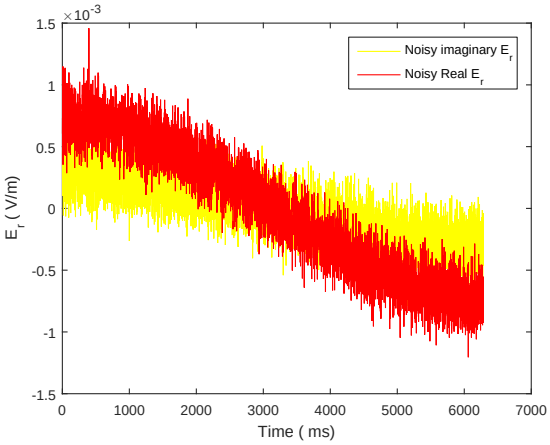

(a) Noisy electric field intensity (E_r).

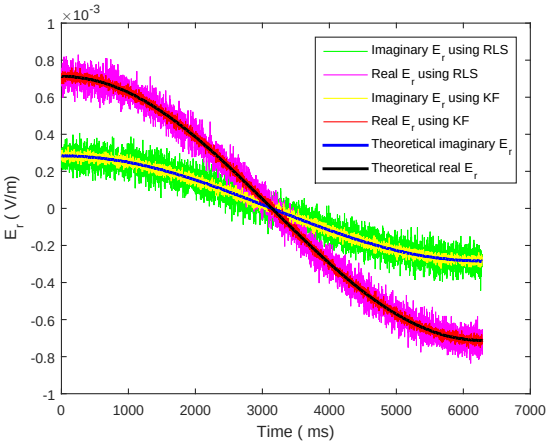

(b) Estimated electric field intensity (E_r).

Figure 5.5: Electric field intensity (E_r) for noisy driving source (white Gaussian noise of zero mean and 0.00025 variance) for far-field.

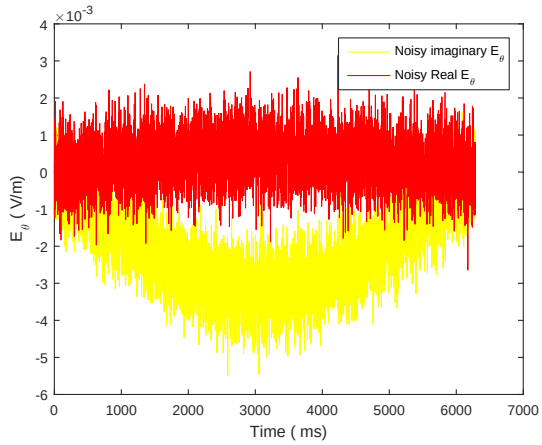

(a) Noisy electric field intensity (E_θ).

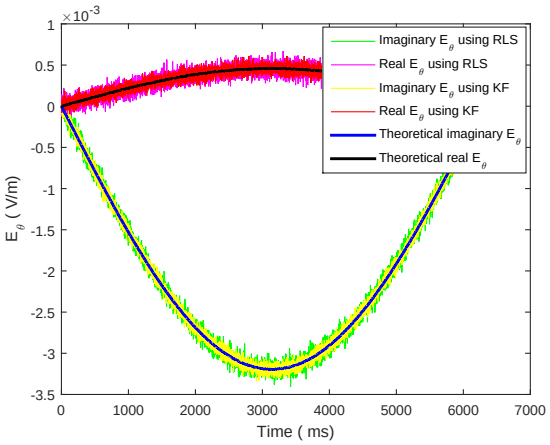

(b) Estimated electric field intensity (E_θ).

Figure 5.6: Electric field intensity (E_θ) for noisy driving source (white Gaussian noise of zero mean and 0.00025 variance)for far-field.

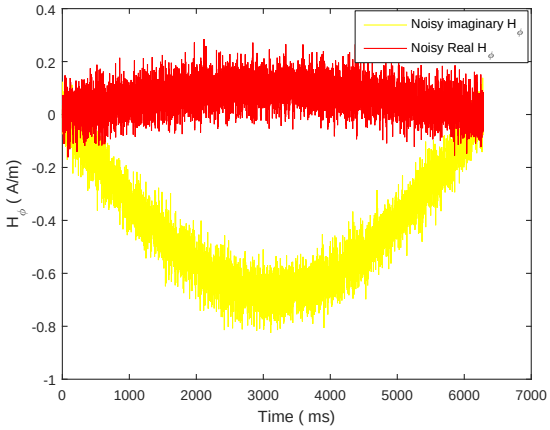

(a) Noisy magnetic field intensity (H_ϕ).

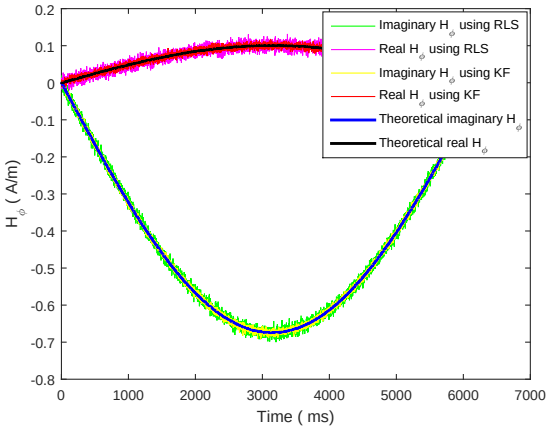

(b) Estimated magnetic field intensity (H_ϕ).

Figure 5.7: Magnetic field intensity (H_ϕ) for noisy driving source (white Gaussian noise of zero mean and 0.00025 variance) for far-field.

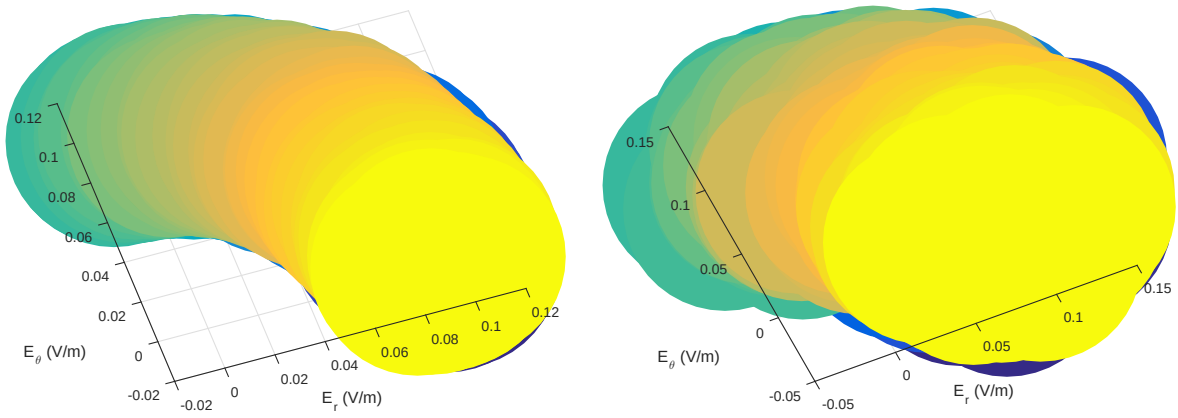

(a) (b)

Figure 5.8: (a): Estimated E-field using KF for near field. (b): Estimated E-field using RLS for near field.

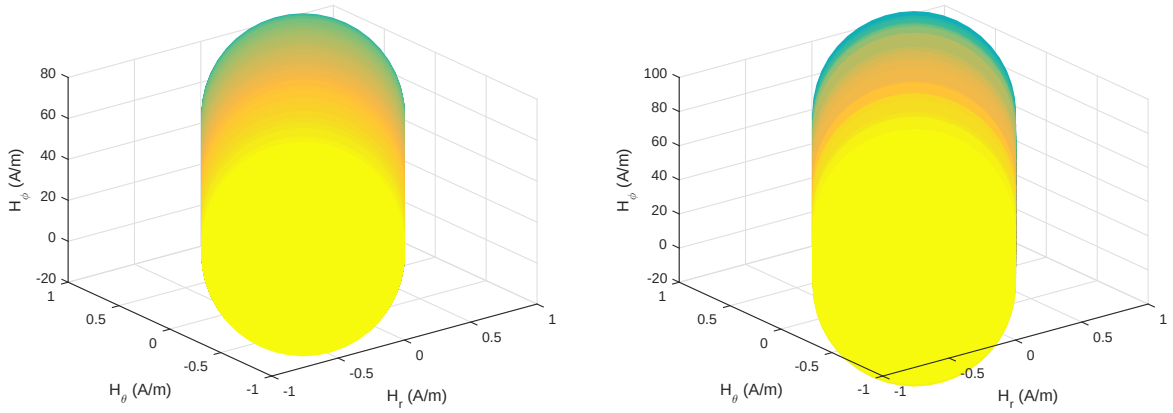

(a) (b)

Figure 5.9: (a): Estimated H-field using KF for near field. (b): Estimated H-field using RLS for near field.

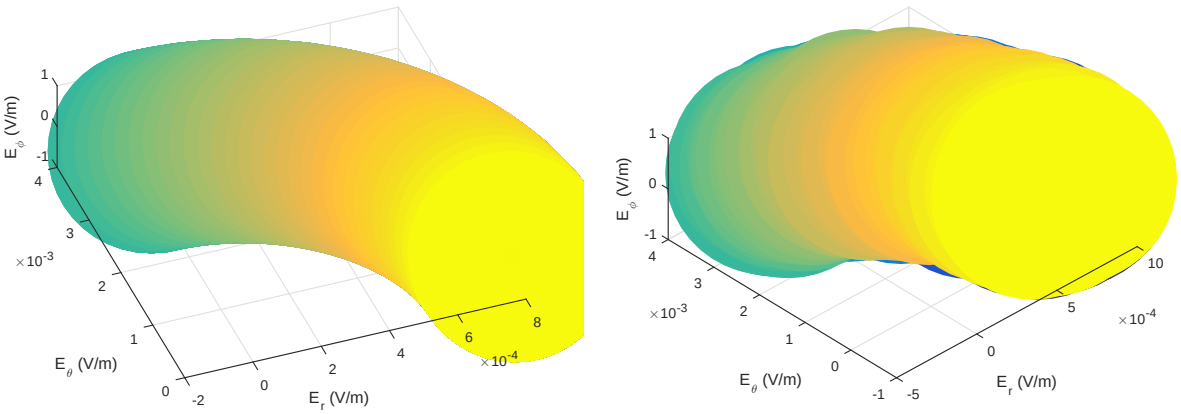

(a) (b)

Figure 5.10: (a): Estimated E-field using KF for far field. (b): Estimated E-field using RLS for far field.

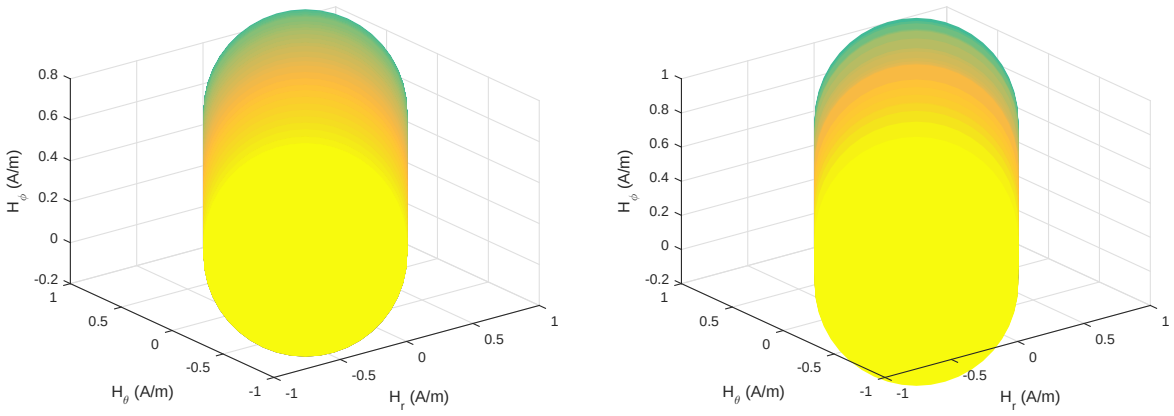

(a) (b)

Figure 5.11: (a): Estimated H-field using KF for far field. (b): Estimated H-field using RLS for far field.

Table 5.1: RMSE of electric field (E_r) estimation using KF for near-field.

S. No.	Gaussian noise at driving source	Imag(E_r) estimation using KF	Real(E_r) estimation using KF	Absolute E-field estimation using KF
1.	$\mu = 0, \sigma = 0.00025$	1.91×10^{-5}	1.98×10^{-5}	1.92×10^{-5}
2.	$\mu = 0, \sigma = 0.00050$	5.10×10^{-5}	5.14×10^{-5}	5.23×10^{-5}

Table 5.2: RMSE of electric field (E_θ) estimation using KF for near-field.

S. No.	Gaussian noise at driving source	Imag(E_θ) estimation using KF	Real (E_θ) estimation using KF	Absolute E-field estimation using KF
1.	$\mu = 0, \sigma = 0.00025$	4.573×10^{-7}	4.671×10^{-7}	4.708×10^{-7}
2.	$\mu = 0, \sigma = 0.00050$	6.802×10^{-7}	6.824×10^{-7}	7.027×10^{-7}

Table 5.3: RMSE of magnetic field (H_ϕ) estimation using KF for near-field.

S. No.	Gaussian noise at driving source	Imag(H_ϕ) estimation using KF	Real (H_ϕ) estimation using KF	Absolute H-field estimation using KF
1.	$\mu = 0, \sigma = 0.00025$	0.0102	0.0101	0.0102
2.	$\mu = 0, \sigma = 0.00050$	0.0124	0.0122	0.0124

Table 5.4: RMSE of electric field (E_r) estimation using RLS for near-field.

S. No.	Gaussian noise at driving source	Imag(E_r) estimation using RLS	Real(E_r) estimation using RLS	Absolute E-field estimation using RLS
1.	$\mu = 0$, $\sigma = 0.00025$	3.46×10^{-5}	3.44×10^{-5}	3.41×10^{-5}
2.	$\mu = 0$, $\sigma = 0.00050$	5.56×10^{-5}	5.59×10^{-5}	5.65×10^{-5}

Table 5.5: RMSE of electric field (E_θ) estimation using RLS for near-field.

S. No.	Gaussian noise at driving source	Imag(E_θ) estimation using RLS	Real (E_θ) estimation using RLS	Absolute E-field estimation using RLS
1.	$\mu = 0$, $\sigma = 0.00025$	8.963×10^{-7}	8.998×10^{-7}	9.212×10^{-7}
2.	$\mu = 0$, $\sigma = 0.00050$	1.127×10^{-6}	1.634×10^{-6}	1.886×10^{-6}

Table 5.6: RMSE of magnetic field (H_ϕ) estimation using RLS for near-field.

S. No.	Gaussian noise at driving source	Imag(H_ϕ) estimation using RLS	Real (H_ϕ) estimation using RLS	Absolute H-field estimation using RLS
1.	$\mu = 0$, $\sigma = 0.00025$	0.0108	0.0109	0.0109
2.	$\mu = 0$, $\sigma = 0.00050$	0.0141	0.0146	0.0146

Table 5.7: RMSE of electric field (E_r) estimation using KF for far-field.

S. No.	Gaussian noise at driving source	Imag(E_r) estimation using KF	Real(E_r) estimation using KF	Absolute E-field estimation using KF
1.	$\mu = 0$, $\sigma = 0.00025$	1.95×10^{-7}	1.94×10^{-7}	1.92×10^{-7}
2.	$\mu = 0$, $\sigma = 0.00050$	4.29×10^{-7}	4.32×10^{-7}	4.45×10^{-7}

Table 5.8: RMSE of electric field (E_θ) estimation using KF for far-field.

S. No.	Gaussian noise at driving source	Imag(E_θ) estimation using KF	Real (E_θ) estimation using KF	Absolute E-field estimation using KF
1.	$\mu = 0$, $\sigma = 0.00025$	6.82×10^{-7}	6.92×10^{-7}	6.84×10^{-7}
2.	$\mu = 0$, $\sigma = 0.00050$	8.10×10^{-7}	8.19×10^{-7}	8.12×10^{-7}

Table 5.9: RMSE of magnetic field (H_ϕ) estimation using KF for far-field.

S. No.	Gaussian noise at driving source	Imag(H_ϕ) estimation using KF	Real (H_ϕ) estimation using KF	Absolute H-field estimation using KF
1.	$\mu = 0$, $\sigma = 0.00025$	7.03×10^{-4}	7.05×10^{-4}	7.06×10^{-4}
2.	$\mu = 0$, $\sigma = 0.00050$	7.26×10^{-4}	7.28×10^{-4}	7.29×10^{-4}

Table 5.10: RMSE of electric field (E_r) estimation using RLS for far-field.

S. No.	Gaussian noise at driving source	Imag(E_r) estimation using RLS	Real(E_r) estimation using RLS	Absolute E-field estimation using RLS
1.	$\mu = 0$, $\sigma = 0.00025$	7.84×10^{-7}	7.74×10^{-7}	7.75×10^{-7}
2.	$\mu = 0$, $\sigma = 0.00050$	9.56×10^{-7}	9.64×10^{-7}	9.61×10^{-7}

Table 5.11: RMSE of electric field (E_θ) estimation using RLS for far-field.

S. No.	Gaussian noise at driving source	Imag(E_θ) estimation using RLS	Real (E_θ) estimation using RLS	Absolute E-field estimation using RLS
1.	$\mu = 0$, $\sigma = 0.00025$	9.56×10^{-7}	9.54×10^{-7}	9.58×10^{-7}
2.	$\mu = 0$, $\sigma = 0.00050$	1.37×10^{-6}	1.35×10^{-6}	1.54×10^{-6}

Table 5.12: RMSE of magnetic field (H_ϕ) estimation using RLS for far-field.

S. No.	Gaussian noise at driving source	Imag(H_ϕ) estimation using RLS	Real (H_ϕ) estimation using RLS	Absolute H-field estimation using RLS
1.	$\mu = 0$, $\sigma = 0.00025$	1.22×10^{-3}	1.22×10^{-3}	1.23×10^{-3}
2.	$\mu = 0$, $\sigma = 0.00050$	1.46×10^{-3}	1.48×10^{-3}	1.49×10^{-3}

Chapter 6

Conclusions and Future Scope

6.1 Conclusions

We have studied the state estimation of linear and nonlinear systems described by ordinary differential equations and partial differential equations using Kalman filter (KF) and extended Kalman filter (EKF). We recapitulate the salient features of this investigation study and results obtained for state estimation in the following points:-

1. As a first problem, we derived the closed form linear and nonlinear expressions of following three circuits:-
   (i) Bipolar junction transistor (BJT) based cross coupled oscillator circuit.
   (ii) BJT based differential amplifier circuit.
   (iii) MOSFET circuit.
   The main advantage of the method is that the use of nonlinear expressions obtained using perturbation theory instead of using the linear expression represents distortion which shows the importance of nonlinear expression. Percentage distortion for CCO circuit is approximately 0.428 %. Percentage distortion for DA circuit using perturbation theory is approximately 0.60 % and for MOSFET is 0.07 %.

2. As a second problem, we estimated the states of following two nonlinear circuits using EKF:-
   (i) BJT based differential amplifier circuit.
   (ii) MOSFET circuit.
   It also compares the estimation results with recursive least square (RLS) method.

The EKF method presents better estimate than RLS as the EKF accounts for measurement noise. Also, the maximal precision of simulation requires the modeling of circuit in terms of device parameters and circuit elements, so the method is able to provide good estimation. The proposed method has also the advantage that it can be used for any mode of MOSFET operation besides quiescent point region. It can also be used for large input amplitude. The method presents the real-time estimation. RMSE for MOSFET circuit using EKF is 0.32 and using RLS is 0.62 approximately. RMSE for DA circuit using EKF and RLS are 0.0005 and 0.0009 respectively.

3. The third problem presents the state estimation using EKF, where the circuit dynamics is represented using Kronecker product and compares the result with implementation of least mean square (LMS) on Kronecker based wavelet transformation of the circuit.

   The method has the following advantages:-
   (i) It can be used for any mode of transistor operation besides near the quiescent point region. The nonlinearity in saturation can be considered in the proposed method.
   (ii) The method can be used for large amplitude input signal. For small amplitude input signal, KF can be used, which results in inaccurate estimation due to linearization of nonlinear system.
   (iii) The method presents real time parameter estimation, as EKF has been used for nonlinear system. It is able to track the parameters, when they are slowly changing with time.
   (iv) Use of Kronecker product presents more accurate representation of nonlinear system.
   (v) The final outcome of the wavelet based estimation is that although it is block processing based estimation and not the real time processing based estimation, but we are able to estimate using the lesser data storage, i.e. having compression. EKF is a real time estimation and has been compared with wavelet transform based block processing as regards, complexity, real time estimation and compression as all the samples are not used for estimation. The RMSE for EKF based estimation using Kronecker product based system representation is 0.00195 whereas using LMS on Kronecker product based wavelet representation is 0.00328.

4. The fourth problem presents the field estimation of Hertzian antenna using KF and discrete set of measurements. The formulation uses Kronecker product for compact representation of fields. The method compares the KF estimation with RLS estimation. The KF presents better estimate than RLS as the process and measurement noise is taken into account by it. The main advantage of applying KF for estimating the electromagnetic field in space time is that the KF is a real-time estimation and moreover it takes advantage of apriori dynamics of the field in the entire space time zone to provide estimation over this entire zone by only taking measurements over a sparse zone. The RMSE using KF for near field electric (E_r) is 3.41×10^{-5} whereas using RLS is 3.91×10^{-5}. The RMSE for near field (E_θ) using KF is 1.6×10^{-6} whereas using RLS is 1.88×10^{-6}.

6.2 Scope for Future Work

1. The EKF can be developed for estimating the electromagnetic field within a waveguide or cavity resonator when the probes contain noisy currents. The electromagnetic fields satisfy 2-dimensional Helmholtz equations at a given frequency with boundary conditions.

2. The EKF can be developed to estimate the line voltage and current along a transmission line in the presence of noisy sources and random line voltage and current loading. The line voltage and current satisfy first order partial differential equations (PDE's) in space and time.

3. The EKF can be developed for estimating the wave function of a quantum mechanical system defined by a noisy Shrödinger equation with noisy measurements taken on set of observations. The additional condition to be accounted for this is collapse of the wave function following a measurement.

4. The EKF can be developed to estimate a quantum field like the quantum electromagnetic field or the quantum Dirac field of electron and positron from noisy measurements of the average value of the quantum fields in a given state.

5. The EKF has been extended by V. P. Belavkin to quantum filtering theory involving estimating states and observations of quantum systems evolving according to the Hudson-Parthasarthy noisy Shrödinger equation based on non-demolition

measurements. This scheme can be applied to estimate states and observations obtained via canonical quantization of classical noisy quantum system.

References

[1] Rigatos, G.G., 2011. A derivative-free Kalman filtering approach to state estimation-based control of nonlinear systems. IEEE Transactions on Industrial Electronics, 59(10), pp.3987-3997.

[2] Vadigepalli, R. and Doyle, F.J., 2003. A distributed state estimation and control algorithm for plantwide processes. IEEE Transactions on Control Systems Technology, 11(1), pp.119-127.

[3] Parsa, K., Angeles, J. and Misra, A.K., 2002. Linearized kinematics for state estimation in robotics. In Advances in Robot Kinematics (pp. 39-48). Springer, Dordrecht.

[4] Jun, M., Roumeliotis, S.I. and Sukhatme, G.S., 1999, October. State estimation of an autonomous helicopter using Kalman filtering. In IROS (pp. 1346-1353).

[5] Barfoot, T.D., 2017. State Estimation for Robotics. Cambridge University Press.

[6] Gomez-Exposito, A. and Abur, A., 2004. Power system state estimation: theory and implementation. CRC press.

[7] Wu, F.F., 1990. Power system state estimation: a survey. International Journal of Electrical Power and Energy Systems, 12(2), pp.80-87.

[8] Monticelli, A., 2000. Electric power system state estimation. Proceedings of the IEEE, 88(2), pp.262-282.

[9] Houlian, W. and Gongbo, Z., 2018. State of charge prediction of supercapacitors via combination of Kalman filtering and backpropagation neural network. IET Electric Power Applications, 12(4), pp.588-594.

[10] Awasthi, V. and Raj, K., 2011. A comparison of Kalman filter and extended Kalman filter in State estimation. Int. J. Electron. Eng, 3(1), pp.67-71.

[11] Xiong, R., Yu, Q., Wang, L.Y. and Lin, C., 2017. A novel method to obtain the open circuit voltage for the state of charge of lithium ion batteries in electric vehicles by using H infinity filter. Applied energy, 207, pp.346-353.

[12] Rusnak, I., 2017. H_∞ Based Estimation of Nonlinear Systems. IEEE control systems letters, 1(2), pp.358-363.

[13] Emami, K., Fernando, T., Iu, H.H.C., Trinh, H. and Wong, K.P., 2014. Particle filter approach to dynamic state estimation of generators in power systems. IEEE Transactions on Power Systems, 30(5), pp.2665-2675.

[14] Yu, Y., Wang, Z. and Lu, C., 2018. An extended Kalman particle filter for power system dynamic state estimation. COMPEL-The international journal for computation and mathematics in electrical and electronic engineering, 37(6), pp.1993-2005.

[15] Zuo, J., Guo, Q. and Ling, Z., 2017. Particle filter for estimating multi-sensor systems using one-or two-step delayed measurements. AEU-International Journal of Electronics and Communications, 82, pp.265-271.

[16] Zhou, W., Liu, L. and Hou, J., 2019. Firefly Algorithm-Based Particle Filter for Nonlinear Systems. Circuits, Systems, and Signal Processing, 38(4), pp.1583-1595.

[17] Zhang, J., Welch, G., Ramakrishnan, N. and Rahman, S., 2015. Kalman filters for dynamic and secure smart grid state estimation. Intelligent Industrial Systems, 1(1), pp.29-36.

[18] Zupanski, M., 2005. Maximum likelihood ensemble filter: Theoretical aspects. Monthly Weather Review, 133(6), pp.1710-1726.

[19] Gandhi, M.A. and Mili, L., 2010. Robust Kalman filter based on a generalized maximum-likelihood-type estimator. IEEE Transactions on Signal Processing, 58(5), pp.2509-2520.

[20] Uzunoglu, B. and Ulker, M.A., 2018. Maximum likelihood ensemble filter state estimation for power systems. IEEE Transactions on Instrumentation and Measurement, 67(9), pp.2097-2106.

[21] Zhou, N., Meng, D., Huang, Z. and Welch, G., 2014. Dynamic state estimation of a synchronous machine using PMU data: A comparative study. IEEE Transactions on Smart Grid, 6(1), pp.450-460.

[22] Li, Y., Huang, Z., Zhou, N., Lee, B., Diao, R. and Du, P., 2012, May. Application of ensemble Kalman filter in power system state tracking and sensitivity analysis. In PES T and D 2012 (pp. 1-8).

[23] Ray, P.K. and Subudhi, B., 2012. Ensemble-Kalman-filter-based power system harmonic estimation. IEEE transactions on instrumentation and measurement, 61(12), pp.3216-3224.

[24] Naseri, F., Kazemi, Z., Farjah, E. and Ghanbari, T., 2019. Fast detection and compensation of current transformer saturation using extended Kalman Filter. IEEE Transactions on Power Delivery, 34(3), pp. 1087-1097.

[25] Chen, X., Lei, H. and Xiong, R., 2018. A bias correction based state-of-charge estimation method for multi-cell battery pack under different working conditions. IEEE Access, 6, pp. 78184-78192.

[26] Cevallos, H., Intriago, G., Plaza, D. and Idrovo, R., 2018. The Extended Kalman filter in the dynamic state estimation of electrical power systems. Enfoque UTE, 9(4), pp. 120-130.

[27] Liao, F. and Lou, X., 2016. State and parameter estimations of chaotic memristive systems based on extended Kalman filter. In 2016 35th Chinese Control Conference (CCC) pp. 865-868.

[28] Lee, K.T., Dai, M.J. and Chuang, C.C., 2018. Temperature-compensated model for lithium-ion polymer batteries with extended Kalman filter state-of-charge estimation for an implantable charger. IEEE Transactions on Industrial Electronics, 65(1), pp. 589-596.

[29] Raissi, T., Ramdani, N. and Candau, Y., 2004. Set membership state and parameter estimation for systems described by nonlinear differential equations. Automatica, 40(10), pp.1771-1777.

[30] Zhang, H., Basin, M.V. and Skliar, M., 2005, June. Optimal state estimation of the general linear ODE with multiplicative and additive Wiener noises. In Proceedings of the 2005, American Control Conference, 2005. (pp. 3441-3446). IEEE.

[31] Mandela, R.K., Rengaswamy, R., Narasimhan, S. and Sridhar, L.N., 2010. Recursive state estimation techniques for nonlinear differential algebraic systems. Chemical engineering science, 65(16), pp.4548-4556.

[32] Mobed, P., Munusamy, S., Bhattacharyya, D. and Rengaswamy, R., 2016. State and parameter estimation in distributed constrained systems. 1. extended Kalman filtering of a special class of differential-algebraic equation systems. Industrial and Engineering Chemistry Research, 56(1), pp.206-215.

[33] Buonomo, A. and Schiavo, A.L., 2005. Perturbation analysis of nonlinear distortion in analog integrated circuits. IEEE Transactions on Circuits and Systems I: Regular Papers, 52(8), pp.1620-1631.

[34] Majumdar, S. and Parthasarathy, H., 2010. Perturbation approach to Ebers-Moll equations for transistor circuit analysis. Circuits, Systems and Signal Processing, 29(3), pp.431-448.

[35] Rathee, A. and Parthasarathy, H., 2012. Perturbation-Based Fourier Series Analysis of Transistor Amplifier. Circuits, Systems, and Signal Processing, 31(1), pp.313-328.

[36] Rathee, A. and Parthasarathy, H., 2013. Perturbation-based stochastic modeling of nonlinear circuits. Circuits, Systems, and Signal Processing, 32(1), pp.123-141.

[37] Dang, Y., Liang, Y., Bie, B., Ding, J. and Zhang, Y., 2018. A Range Perturbation Approach for Correcting Spatially Variant Range Envelope in Diving Highly Squinted SAR With Nonlinear Trajectory. IEEE Geoscience and Remote Sensing Letters, 15(6), pp.858-862.

[38] Bulow, H., Aref, V. and Schmalen, L., 2018. Modulation on discrete nonlinear spectrum: Perturbation sensitivity and achievable rates. IEEE Photonics Technology Letters, 30(5), pp.423-426.

[39] Benchabane, F., Guettaf, A., Yahia, K. and Sahraoui, M., 2018. Experimental investigation on induction motors inter-turns short-circuit and broken rotor bars faults diagnosis through the discrete wavelet transform. e & i Elektrotechnik und Informationstechnik, 135(2), pp. 187-194.

[40] Zhang, Z.L., Cheng, X., Lu, Z.Y. and Gu, D.J., 2016. SOC estimation of lithium-ion batteries with AEKF and wavelet transform matrix. IEEE Transactions on Power Electronics, 32(10), pp. 7626-7634.

[41] Avdakovic, S., Nuhanovic, A., Kusljugic, M. and Music, M., 2012. Wavelet transform applications in power system dynamics. Electric Power Systems Research, 83(1), pp. 237-245.

[42] Wang, Y., Pan, R., Liu, C., Chen, Z. and Ling, Q., 2018. Power capability evaluation for lithium iron phosphate batteries based on multi-parameter constraints estimation. Journal of Power Sources, 374, pp. 12-23.

[43] Fridholm, B., Wik, T., Kuusisto, H. and Klintberg, A., 2018. Estimating power capability of aged lithium-ion batteries in presence of communication delays. Journal of Power Sources, 383, pp. 24-33.

[44] Wei, Z., Meng, S., Tseng, K.J., Lim, T.M., Soong, B.H. and Skyllas-Kazacos, M., 2017. An adaptive model for vanadium redox flow battery and its application for online peak power estimation. Journal of Power Sources, 344, pp. 195-207.

[45] Xiong, R., Sun, F., He, H. and Nguyen, T.D., 2013. A data-driven adaptive state of charge and power capability joint estimator of lithium-ion polymer battery used in electric vehicles. Energy, 63, pp. 295-308.

[46] Haykin, S. (1991), Adaptive filter theory.

[47] Brewer, J., 1978. Kronecker products and matrix calculus in system theory. IEEE Transactions on circuits and systems, 25(9), pp.772-781.

[48] Barnett, S., 1973. Matrix differential equations and Kronecker products. SIAM Journal on Applied Mathematics, 24(1), pp.1-5.

[49] Kuntman, H., 1983. Application of modified Ebers Moll model to nonlinear distortion analysis of transistor amplifier. Electronics Letters, 19(4), pp. 126–127.

[50] Fong K. L. and Meyer, R. G., 1998. High frequency nonlinear analysis of common emitter and differential pair transconductance stages. IEEE Journal of Solid State circuits, 33(4), pp. 548–555.

[51] Song, B., He, S., Peng J. and Zhao, Y., 2017. Dynamic deviation memory polynomial model for digital predistortion. Electronics Letters, 53(9), pp. 606-607.

[52] Wu, X., Grassi, F. Manfredi P. and Ginste, D. V., 2018. Perturbative analysis of differential-to-common mode conversion in asymmetric nonuniform interconnects. IEEE Transactions on Electromagnetic Compatibility, 60(1), pp. 7-15.

[53] Afifi S. and Dusseaux, R., 2018. Scattering from 2-D perfect electromagnetic conductor rough surface: analysis with the small perturbation method and the small-slope approximation. IEEE Transactions on Antennas and Propagation, 66(1), pp. 340-346.

[54] Mishra, S. and Yadava, R. D. S., 2017. A method for chaotic self-modulation in nonlinear colpitts oscillator and its potential applications. Circuits, Systems, and Signal Processing, pp. 1-21.

[55] Liu, W. Q., Wang X. M. and Deng, Z. L., 2017. Robust centralized and weighted measurement fusion Kalman predictors with multiplicative noises, uncertain noise variances, and missing measurements. Circuits, Systems, and Signal Processing, pp. 1-40.

[56] Thuan M. V. and Huong, D. C., 2017. New Results on Exponential Stability and Passivity Analysis of Delayed Switched Systems with Nonlinear Perturbations. Circuits, Systems, and Signal Processing, pp. 1-24.

[57] Buonomo A. and Schiavo, A. L., 2013. Predicting nonlinear distortion in multistage amplifiers and gm-C filters. Analog Integrated Circuits and Signal Processing, 77(3), pp. 483-493, 2013.

[58] Wang, H., Qi M. and Wang, B., 2017. PPV modeling of memristor-based oscillators and application to ONN pattern recognition. IEEE Transactions on Circuits and Systems II: Express Briefs, 64(6), pp. 610-614.

[59] Bernardini, A., Werner, K.J., Sarti, A. and Smith III, J.O., 2016. Modeling nonlinear wave digital elements using the Lambert function. IEEE Transactions on Circuits and Systems I: Regular Papers, 63(8), pp.1231-1242.

[60] Bennour, A., Moutier, F., Polleux, J.L., Algani, C. and Mazer, S., 2017. A distributed extended Ebers-Moll model topology for SiGe heterojunction bipolar phototransistors based on Drift-Diffusion hydrodynamic behavior. IEEE Transactions on Electron Devices, 64(5), pp.2267-2274.

[61] Wang, W., Nguang, S. K., Zhong S. and Liu, H. Y. 2014. New delay-dependent stability criteria for uncertain neutral system with time-varying delays and nonlinear perturbations", *Circuits, Systems, and Signal Processing*, 33(9) pp. 2719-2740.

[62] Lakshmanan, S., Park J. H. and Jung, H. Y., 2013. Robust delay-dependent stability criteria for dynamic systems with nonlinear perturbations and leakage delayCircuits, systems, and signal processing, 32(4), pp. 1637-1657.

[63] Enz C.C., Krummenacher F., Vittoz E.A., 1995. An analytical MOS transistor model valid in all regions of operation and dedicated to low-voltage and low-current applications. Analog int circuits signal process, 8(1), pp. 83-114.

[64] Enz, C.C. and Vittoz, E.A., 2006. Charge-based MOS transistor modeling. John Wiely & Sons Inc, 68.

[65] Kamas, L.A. and Sanders, S.R. (1993), Parameter and state estimation in power electronic circuits. IEEE Transactions on Circuits and Systems I: Fundamental Theory and Applications, Vol. 40, No. 12, pp. 920-928.

[66] Beadle, E.R. and Djuric, P.M. (1997), A fast-weighted Bayesian bootstrap filter for nonlinear model state estimation, IEEE Transactions on Aerospace and Electronic Systems, Vol. 33 No. 1, pp. 338-343.

[67] Chen, Y., Liu, F., Mei, S. and Ma, J. (2015), A robust WLAV state estimation using optimal transformations, IEEE Transactions on Power Systems, Vol. 30 No. 4, pp. 2190-2191.

[68] Yu, K.K., Watson, N. and Arrillaga, J. (2005), An adaptive Kalman filter for dynamic harmonic state estimation and harmonic injection tracking, IEEE Transactions on Power Delivery, Vol. 20 No. 2, pp. 1577-1584.

[69] Kyriakides, E., Suryanarayanan, S. and Heydt, G.T. (2005), State estimation in power engineering using the huber robust regression technique, IEEE Transactions on Power Systems,Vol. 20 No. 2, pp. 1183-1184.

[70] Zhao, J., Zhang, G., Dong, Z.Y. and La Scala, M., 2018. Robust forecasting aided power system state estimation considering state correlations. IEEE Transactions on Smart Grid, 9(4), pp.2658-2666.

[71] Rana, M.M., Xiang, W. and Wang, E., 2018. Iot-based state estimation for microgrids. IEEE Internet of Things Journal, 5(2), pp.1345-1346.

[72] Kong, X., Yan, Z., Guo, R., Xu, X. and Fang, C., 2018. Three-stage distributed state estimation for ac-dc hybrid distribution network under mixed measurement environment. IEEE Access, 6, pp.39027-39036.

[73] Sutivong, A., Chiang, M., Cover, T.M. and Kim, Y.H., 2005. Channel capacity and state estimation for state-dependent Gaussian channels. IEEE Transactions on Information Theory, 51(4), pp.1486-1495.

[74] Zhao, J., Zhang, G., Dong, Z.Y. and Wong, K.P., 2016. Forecasting-aided imperfect false data injection attacks against power system nonlinear state estimation. IEEE Transactions on Smart Grid, 7(1), pp.6-8.

[75] Netto, M. and Mili, L., 2018. A robust data-driven Koopman Kalman filter for power systems dynamic state estimation. IEEE Transactions on Power Systems, 33(6), pp.7228-7237.

[76] Zhao, J., 2018. Dynamic state estimation with model uncertainties using H_∞ extended Kalman filter. IEEE Transactions on Power Systems, 33(1), pp.1099-1100.

[77] Zheng, W., Wu, W., Gomez-Exposito, A., Zhang, B. and Guo, Y., 2017. Distributed robust bilinear state estimation for power systems with nonlinear measurements. IEEE Transactions on Power Systems, 32(1), pp.499-509.

[78] Yu, Y., Wang, Z. and Lu, C., 2018. A joint filter approach for reliable power system state estimation. IEEE Transactions on Instrumentation and Measurement, (99), pp.1-8.

[79] Wang, L.Y., Lin, F. and Chen, W., 2018. Controllability, Observability, and Integrated State Estimation and Control of Networked Battery Systems. IEEE Transactions on Control Systems Technology, 26(5), pp.1699-1710.

[80] Cao, X., Cheng, P., Chen, J., Ge, S.S., Cheng, Y. and Sun, Y., 2014. Cognitive radio based state estimation in cyber-physical systems. IEEE Journal on Selected Areas in Communications, 32(3), pp.489-502.

[81] Li, L., Chen, X. and Zhang, L., 2014. Multimodel ensemble for freeway traffic state estimations. IEEE Transactions on Intelligent Transportation Systems, 15(3), pp.1323-1336.

[82] Farnoosh R, Nabati P, Hajirajabi A., 2012. Parameters estimation for RL electrical circuits based on least square and Bayesian approach. COMPEL, 31(6), pp. 1711-1725.

[83] Yin Z, Li G, Zhang Y, Liu, J., Sun, X. and Zhong, Y., 2017. A speed and flux observer of induction motor based on extended Kalman filter and Markov chain. IEEE T Power Electr, 2017, 32(9), pp. 7096-7117.

[84] Gautam A K and Majumdar S., 2018. Parameter estimation of RC circuits using extended Kalman filter. Int J Adv Man Tech Eng Sci, 2018, 8, pp. 83-91.

[85] Kazakov L N, Shakhtarin B I, Khodunin A V., 2015. Recovery of an information sequence with the help of the extended Kalman filter included in the variable-symbol-frequency modem. J Commun Technol El, 2015, 60(6), pp. 611-618.

[86] Shakhtarin B I, Shen K, Neusypin K A., 2016. Modification of the nonlinear kalman filter in a correction scheme of aircraft navigation systems. J Commun Technol El, 2016, 61(11), pp.1252-1258.

[87] Hu Z, Gallacher B., 2016. Extended Kalman filtering based parameter estimation and drift compensation for a MEMS rate integrating gyroscope. Sensor Actuat A-Phys, 250, pp. 96-105.

[88] Paschero M, Storti G L, Rizzi A, Mascioli, F. M. and Rizzoni, G., 2016. A novel mechanical analogy-based battery model for SoC estimation using a multicell EKF. IEEE T Sustain Energ, 2016, 7(4), pp. 1695-1702.

[89] Xiong, B., Zhao, J., Wei, Z., Skyllas-Kazacos, M. 2014, Extended Kalman filter method for state of charge estimation of vanadium redox flow battery using thermal-dependent electrical model, Journal of Power Sources, 262, pp. 50-61.

[90] Ermolova N.Y., 2003. Kalman filter application for mitigation of nonlinear effects in multicarrier communication systems. IEE Proceedings-Communications ; 150(4), pp. 265-2658.

[91] Schneebeli M., Matzler C., 2009. A calibration scheme for microwave radiometers using tipping curves and Kalman filtering. IEEE Trans Geosci Remote Sens, 47(12): pp. 42001-42019.

[92] Xie, J., Kumar, B.V., 2007. Dropout compensation by equalizer selection and Kalman filter-based timing recovery. IEEE trans magn, 43(5), pp. 2045-2053.

[93] Liu N., Zhang L.R., Zhang J., Shen D. Direction finding of MIMO radar through ESPRIT and Kalman filter. Electronics letters 2009; 45(17): pp. 908-910.

[94] Shi L. Kalman filtering over graphs: Theory and applications. IEEE Trans Autom Control 2009 54(9): 2230-2234.

[95] Balakumar B., Shahbazpanahi S., Kirubarajan T. Joint MIMO channel tracking and symbol decoding using Kalman filtering. IEEE Trans Signal Process 2007; 55(12): 5873-5879.

[96] Chaloupka Z., Alsindi N., Aweya J. Clock skew estimation using Kalman filter and IEEE 1588v2 PTP for telecom networks. IEEE Commun Lett 2015; 19(7): 1181-1184.

[97] Rusnak I. H_∞ based estimation of nonlinear systems. IEEE Control Syst Letters 2017; 1(2): pp. 358-363.

[98] Zhou, W., Liu L., Hou, J. Firefly algorithm-based particle filter for nonlinear systems. Circ Syst Signal Process. 2018: doi.org/10.1007/s00034-018-0927-0.

[99] Olama, M.M., Djouadi, S.M., Papageorgiou I.G., Charalambous C.D., 2008. Position and velocity tracking in mobile networks using particle and Kalman filtering with comparison. IEEE Trans Veh Technol, 57(2), pp. 1001-1010.

[100] Do, D.V., Forgez C., Benkara K.E., Friedrich G., 2009. Impedance observer for a Li-ion battery using Kalman filter. IEEE Trans Veh Technol, 58(8): pp. 3930-3937.

[101] Leung, H., Zhu Z., 2001. Performance evaluation of EKF-based chaotic synchronization. IEEE Trans. Circuits Syst I: Fundam Theory Appl, 48(9): pp. 1118-1125.

[102] Hugues-Salas O., Shore, K.A., 2010. An extended Kalman filtering approach to nonlinear time-delay systems: Application to chaotic secure communications. IEEE Trans Circuits Systems I, 57(9): pp. 2520-2530.

[103] Xu, D., Wu, Z., Huang, Y., 2019, A new adaptive Kalman filter with inaccurate noise statistics. Cir Syst Signal Process, doi.org/10.1007/s00034-019-01053-w.

[104] Stojanovic, V., Nedic, N., Prsic, D., Dubonjic L., 2016. Optimal experiment design for identification of ARX models with constrained output in non-Gaussian noise. Appl Math Modelling, 40, pp. 6676-6689.

[105] Stojanovic, V., Filipovic V., 2014. Adaptive input design for identification of output error model with constrained output. Cir Syst Signal Process, 33(1), pp. 97-113.

[106] Stojanovic V., Nedic, N., 2016 A nature inspired parameter tuning approach to cascade control for hydraulically driven parallel robot platform. J Optimiz Theory App, 168(1), pp. 332-347.

[107] Nedic, N., Prsic, D., Dubonjic, L., Stojanovic V., Djordjevic V., 2014. Optimal cascade hydraulic control for a parallel robot platform by PSO. Int J Adv Manuf Tech, 72, pp. 1085-1098.

[108] De Leon-Aldaco, S.E., Calleja, H., Alquicira J.A., 2015, Metaheuristic optimization methods applied to power converters: A review. IEEE Trans Power Electr, 30(12), pp. 6791-6803.

[109] Stojanovic, V, Nedic, N. Robust Kalman filtering for nonlinear multivariable stochastic systems in the presence of non-Gaussian noise. Int J Robust Nonlinear Control 2016; 26(3), 445-460.

[110] Sugimoto, Y., Arai, H., Maruyama, T., Nasuno, M., Hirose, M. and Kurokawa, S., 2018. Fast Far-Field Estimation Method by Compact Single Cut Near-Field Measurements for Electrically Long Antenna Array. IEEE Transactions on Antennas and Propagation, 66(11), pp. 5859-5868.

[111] Arduino, A., Bottauscio, O., Chiampi, M., Laakso, I. and Zilberti, L., 2018. Computational Low-Frequency Electromagnetic Dosimetry Based on Magnetic Field Measurements. IEEE Journal of Electromagnetics, RF and Microwaves in Medicine and Biology, 2(4), pp. 302-309.

[112] Pei, L., Liu, D., Zou, D., Choy, R.L.F., Chen, Y. and He, Z., 2018. Optimal heading estimation based multidimensional particle filter for pedestrian indoor positioning. IEEE Access, 6, pp. 49705-49720.

[113] Belhadj, C.A. and El-Ferik, S., 2009. Electric and magnetic fields estimation for live transmission line right of way workers using artificial neural network. In 2009 15th International Conference on Intelligent System Applications to Power Systems (pp. 1-6).

[114] Wang, W., Bottauscio, O., Chiampi, M., Giordano, D. and Zilberti, L., 2012. A procedure to estimate the electric field induced in human body exposed to unknown magnetic sources. Radiation protection dosimetry, 154(2), pp. 157-163.

[115] Zenczak, M., 2016. Method of estimating the exposure of the natural environment to 50 Hz electric and magnetic fields in power systems with distributed and centralized generations. Archives of electrical engineering, 65(2), pp. 295-304.

[116] Paffi, A., Camera, F., Carducci, F., Rubino, G., Tampieri, P., Liberti, M. and Apollonio, F., 2015. A computational model for real-time calculation of electric field due to transcranial magnetic stimulation in clinics. International Journal of Antennas and Propagation, http://dx.doi.org/10.1155/2015/976854.

[117] Puthe, C., Manoj, C. and Kuvshinov, A., 2014. Reproducing electric field observations during magnetic storms by means of rigorous 3-D modelling and distortion matrix co-estimation. Earth, Planets and Space, 66(1), p. 162.

[118] Petrovic, G., Kilic, T. and Garma, T., 2013. Measurements and estimation of the extremely low frequency magnetic field of the overhead power lines. Elektronika ir Elektrotechnika, 19(7), pp. 33-37.

[119] Kazachenko, M.D., Fisher, G.H. and Welsch, B.T., 2014. A comprehensive method of estimating electric fields from vector magnetic field and Doppler measurements. The Astrophysical Journal, 795(1), pp. 1-19.

[120] De Doncker, P.H., Dricot, J.M., Meys, R., Helier, M. and Tabbara, W., 2006. Electromagnetic fields estimation using spatial statistics. Electromagnetics, 26(2), pp. 111-122.

[121] Ekonomou, L., Fotis, G.P., Maris, T.I. and Liatsis, P., 2007. Estimation of the electromagnetic field radiating by electrostatic discharges using artificial neural networks. Simulation modelling practice and theory, 15(9), pp. 1089-1102.

[122] Azpurua, M. and Ramos, K.D., 2010. A comparison of spatial interpolation methods for estimation of average electromagnetic field magnitude. Progress In Electromagnetics Research M, 14(2010), pp. 135-145.

[123] Colak, I., Kosalay, I. and Inan, A., 2007. Estimation of magnetic field distributions in substation centers using artificial neural networks. 15, pp. 1089-1102

Appendix A

A.1 Kalman Filter

KF algorithm is the most widely used state and parameter estimation technique to optimize the states taking measurement noise and process noise into consideration for better accuracy. Its main advantage is that it is a real time algorithm and is therefore computationally cheap. Discrete state and measurement model for the KF model is

$$\mathbf{x}_k = \mathbf{A}_{k-1}\mathbf{x}_{k-1} + \mathbf{B}_{k-1}\mathbf{u}_{k-1} + \mathbf{v}_{k-1} \tag{A.1}$$

$$\mathbf{y}_k = \mathbf{C}_k\mathbf{x}_k + \mathbf{w}_k \tag{A.2}$$

where $\mathbf{x}_k$ is the state vector, $\mathbf{A}_k$ is the state matrix. $\mathbf{B}_k$ is the coefficient matrix. $\mathbf{u}_k$ is the known input. $\mathbf{y}_k$ is the measurement vector. $\mathbf{C}_k$ is the observation matrix. $\mathbf{v}_k$ and $\mathbf{w}_k$ are process and measurement noise. These are Gaussian noise with zero mean and covariance matrices $\mathbf{Q}_k$ and $\mathbf{R}_k$ respectively.

KF algorithm consists of following steps:

1. *Initialization:-* This step initialize the following parameters: $P^K_{k-1|k-1}$, $\hat{\mathbf{x}}_{k-1|k-1}$, $\mathbf{Q}_{k-1}$ and $\mathbf{R}_k$.

2. *Time update:-* It consists of following steps:-

   (a) *Prediction of state time update:-*

$$\hat{\mathbf{x}}_{k|k-1} = \mathbf{A}_{k-1}\hat{\mathbf{x}}_{k-1|k-1} + \mathbf{B}_{k-1}\mathbf{u}_k. \tag{A.3}$$

(b) *Error covariance time update:-*

$$P^K_{k|k-1} = \mathbf{A}_{k-1} P^K_{k-1|k-1} \mathbf{A}^T_{k-1} + \mathbf{Q}_{k-1} \tag{A.4}$$

3. *Measurement update:-* It consists of following steps:-

(a) *Kalman gain is calculated as:-*

$$K^K_k = P^K_{k|k-1} \mathbf{C}^T_k \left[\mathbf{C}_k P^K_{k|k-1} \mathbf{C}^T_k + \mathbf{R}_k \right]^{-1} \tag{A.5}$$

(b) *State estimate measurement is updated using:-*

$$\hat{\mathbf{x}}_{k|k} = \hat{\mathbf{x}}_{k|k-1} + K^K_k [\mathbf{y}_k - \mathbf{C}_k \hat{\mathbf{x}}_{k|k-1}] \tag{A.6}$$

(c) *Error covariance measurement is updated as:-*

$$P^K_{k|k} = \left[I - K^K_k \mathbf{C}_k \right] P^K_{k|k-1} \tag{A.7}$$

where $(k|k-1)$ and $(k|k)$ represents a prior estimate and post estimate respectively. I is the identity matrix.

A.2 Extended Kalman Filter

In general, a nonlinear system can be represented using following equations :

$$\mathbf{x}_k = f_{k-1}(\mathbf{x}_{k-1}, \mathbf{u}_{k-1}, \mathbf{v}_{k-1}) \tag{A.8}$$

$$\mathbf{z}_k = h_k(\mathbf{x}_k, \mathbf{w}_k) \tag{A.9}$$

where $\mathbf{x}_k$ is the state vector, $f_k(.)$ and $h_k(.)$ are the nonlinear functions. $\mathbf{u}_k$ is the known input. $\mathbf{z}_k$ is the measurement vector. $\mathbf{v}_k$ and $\mathbf{w}_k$ are the process noise and measurement noise respectively. They are zero mean white Gaussian noise with covariance $\mathbf{Q}_k$ and $\mathbf{R}_k$ respectively.

Expanding (A.8) and (A.9) using Taylor series expansion, we have

$$\mathbf{x}_k \approx f_{k-1}(\hat{\mathbf{x}}_{k-1|k-1}) + \mathbf{F}_{k-1} \tilde{\mathbf{x}}_{k-1} + \Delta f(\tilde{\mathbf{x}}^2_{k-1}) + \mathbf{v}_{k-1} \tag{A.10}$$

$$\mathbf{z}_k \approx h_k(f_{k-1}(\hat{\mathbf{x}}_{k-1|k-1})) + \mathbf{H}_k\tilde{\mathbf{x}}_k + \Delta h(\tilde{\mathbf{x}}_{k-1}^2) + \mathbf{w}_k \tag{A.11}$$

where $\tilde{\mathbf{x}}_k = \mathbf{x}_k - \hat{\mathbf{x}}_{k-1}$. $\Delta f(\tilde{\mathbf{x}}_{k-1}^2)$ and $\Delta h(\tilde{\mathbf{x}}_{k-1}^2)$ are the higher order terms in Taylor series expansion.

$$\mathbf{F}_{k-1} = \frac{\partial f_{k-1}(\hat{\mathbf{x}}_{k-1|k-1})}{\partial \mathbf{x}_{k-1}},$$

$$\mathbf{L}_{k-1} = \frac{\partial f_{k-1}(\hat{\mathbf{x}}_{k-1|k-1})}{\partial \mathbf{v}_{k-1}},$$

$$\mathbf{H}_k = \frac{\partial h_k(f_{k-1}(\hat{\mathbf{x}}_{k-1|k-1}))}{\partial \mathbf{x}_k},$$

$$\mathbf{M}_k = \frac{\partial h_k(f_{k-1}(\hat{\mathbf{x}}_{k-1|k-1}))}{\partial \mathbf{w}_k}.$$

EKF method consists of following steps:

1. *Initialization:-* This step initializes the following parameters: $P^E_{k-1|k-1}$, $\hat{\mathbf{x}}_{k-1|k-1}$, $\mathbf{Q}_{k-1}$ and $\mathbf{R}_k$.

2. *Time update:-* It consists of following steps:-

   (a) *Prediction of state time update:-*

$$\hat{\mathbf{x}}_{k|k-1} = f_{k-1}(\hat{\mathbf{x}}_{k-1|k-1}, \mathbf{u}_{k-1}). \tag{A.12}$$

   (b) *Error covariance time update:-*

$$P^E_{k|k-1} = \mathbf{F}_{k-1}P^E_{k-1|k-1}\mathbf{F}^T_{k-1} + \mathbf{L}_{k-1}\mathbf{Q}_{k-1}\mathbf{L}^T_{k-1} \tag{A.13}$$

3. *Measurement update:-* It consists of following steps:-

   (a) *Kalman gain is calculated as:-*

$$K^E_k = P^E_{k|k-1}\mathbf{H}^T_k \left[\mathbf{H}_k P^E_{k|k-1}\mathbf{H}^T_k + \mathbf{M}_k\mathbf{R}_k\mathbf{M}^T_k\right]^{-1} \tag{A.14}$$

   (b) *State estimate measurement is updated using:-*

$$\hat{\mathbf{x}}_{k|k} = \hat{\mathbf{x}}_{k|k-1} + K^E_k[\mathbf{z}_k - h_k(\hat{\mathbf{x}}_{k|k-1})]. \tag{A.15}$$

(c) *Error covariance measurement is updated as:-*

$$P^E_{k|k} = \left[I - K^E_k \mathbf{H}_k\right] P^E_{k|k-1} \tag{A.16}$$

where $(k|k-1)$ and $(k|k)$ represent a prior estimate and post estimate respectively. I is the identity matrix. The time prediction step consists of computing the state projection and error covariance estimation. Measurement update step is also known as the correction step, which consists of computing the Kalman gain, state correction and covariance update. Kalman gain is used to correct the expected state. In this step, observed measurements and expected values are compared for state correction and covariance estimation. The flowchart of EKF algorithm is shown in Figure A.1.

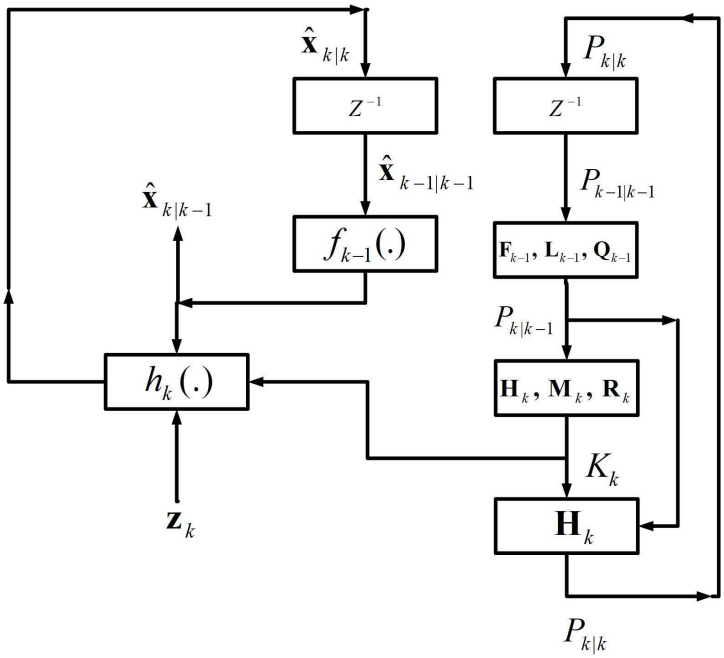

Figure A.1: EKF algorithm flowchart.